



Marine Biology Section  
Department of Biology  
Faculty of Science  
University of Copenhagen



## PhD-Thesis

Nicolas Tarik Bekkouche

# Evolution and structure of neuromuscular systems in spiralian meiofauna

Principal supervisor: Katrine Worsaae

Co-supervisor: Andreas Hejnol

Submission: 02/05/2016

This thesis has been submitted to the PhD School of The Faculty of Science, University of Copenhagen



Academic supervisor:

**Associated Professor Katrine Worsaae, PhD**

Marine Biology Section, Department of Biology, University of Copenhagen  
Copenhagen, Denmark

Co-supervisor:

**Group leader Andreas Hejnol, PhD**

Sars International Centre for Marine Molecular Biology, University of Bergen  
Bergen, Norway

Reviewed by:

**Professor Ulf Jondelius, PhD**

Swedish Museum of Natural History  
Stockholm, Sweden

**Professor Dr. Andreas Schmidt-Rhaesa**

Centrum für Naturkunde (CeNak)  
Hamburg, Germany

Faculty opponent:

**Associate Professor Anders Garm, PhD**

Marine Biology Section, Department of Biology, University of Copenhagen  
Copenhagen, Denmark

Submitted:

May, 2<sup>nd</sup>, 2016



# Table of Contents

<b>ACKNOWLEDGEMENTS .....</b>	<b>1</b>
<b>ABSTRACT .....</b>	<b>4</b>
Abstract .....	4
Resumé.....	5
<b>I) BACKGROUND AND JUSTIFICATION OF THE STUDY .....</b>	<b>6</b>
<b>II) AIMS.....</b>	<b>7</b>
<b>III) SCIENTIFIC JUSTIFICATION.....</b>	<b>8</b>
<b>IV) METHODS OF INVESTIGATION.....</b>	<b>10</b>
A) Collection of material .....	10
B) Confocal Laser Scanning Microscopy (CLSM).....	10
C) Transmission electron microscopy (TEM) .....	11
D) Phylogenetic reconstruction.....	12
<b>V) FILLING THE INTERSTITIAL GAPS OF THE SPIRALIAN PHYLOGENY .....</b>	<b>12</b>
A) Results and implications of the new phylogeny of Spiralia .....	12
B) Impact of the study on subsequent studies .....	14
<b>VI) THE “RESURRECTION” OF <i>LOBATOCEREBRUM</i>: THE ENIGMATIC SPIRALIA IS NOW AN ENIGMATIC ANNELIDA .....</b>	<b>15</b>
A) Introduction and studies on <i>Lobatocerebrum</i> .....	15
B) Further possible researches around Lobatocerebridae .....	16
<b>VII) MICROGNATHOZOA, THE THIRD MEMBER OF GNATHIFERA .....</b>	<b>18</b>
A) Introduction: the importance of Micrognathozoa .....	18
B) The musculature of Micrognathozoa (Bekkouche et al 2014).....	19

C) Nervous system, ciliation and glandular system of Micrognathozoa (Bekkouche and Worsaae, submitted) ... 22

D) Conclusion, opening and further studies on Gnathifera ..... 23

**VIII) THE MORPHOLOGY OF *DIURONOTUS ASPETOS*, AN INTERESTING GASTROTRICH AND ITS IMPLICATION IN THE UNDERSTANDING OF GASTROTRICH EVOLUTION.....25**

A) Introduction: the Gastrotricha, an understudied, yet important taxon ..... 25

B) Results and discussion: the morphology of *Diuronotus aspetos* ..... 26

C) Conclusion: opening and further researches on Gastrotricha..... 27

i) On the evolution of the ventral ciliary pattern in Gastrotricha ..... 28

ii) On the fine evolution of the nervous system of Gastrotricha ..... 29

**IX) CONCLUSION .....30**

**X) REFERENCES.....31**

**ARTICLES AND MANUSCRIPTS.....37**

**Manuscript I: Spiralian Phylogeny Informs the Evolution of Microscopic Lineages.** Laumer, C. E., Bekkouche, N., Kerbl, A., Goetz, F., Neves, R. C., Sørensen, M. V., Kristensen, R. M., Hejnol, Dunn C. W., Giribet G. and Worsaae K. (published)

**Manuscript II: Detailed reconstruction of the nervous and muscular system of Lobatocerebridae with an evaluation of its annelid affinity.** Kerbl A., Bekkouche N., Sterrer W., and Worsaae K. (published)

**Manuscript III: Detailed reconstruction of the musculature in *Limnognathia maerski* (Micrognathozoa) and comparison with other Gnathifera.** Bekkouche N., Kristensen R. M., Hejnol A., Sørensen M. V., and Worsaae, K. (published)

**Manuscript IV: Nervous system and ciliary structures of Micrognathozoa (Gnathifera) – evolutionary insight from an early branch in Spiralia.** Bekkouche N., and Worsaae K. (submitted)

**Manuscript V: Neuromuscular study of early branching *Diuronotus aspetos* (Paucitubulatina) gives insight on the evolution of organs system within Gastrotricha.** Bekkouche N., and Worsaae K. (submitted)

# Acknowledgements

First of all, thanks a lot Katrine to give me the incredible chance to work on all these amazing “worms”. You provided the perfect environment. Zoologically, I have never been limited taxonomically. Humanly, as busy as you are, you always found the time to help, and even worry about us, wondering if you should better “kick me in the a\*\* or pet me on the shoulder” (that’s your words!), actually finding the right balance! You also built up an amazing team, creating a real lab life. Scientifically it has also been an awesome chance to do this thesis, with many insightful and inspirational meetings, and some very entertaining time in front of the scans. We also had, thanks to you, the opportunity to do some field work, from Denmark to Israel (I try to forget the customs) and even Greenland, where we had some very nice adventures and where you gave me the opportunity to see some of the rarest animals, which I had not even dreamt to see before beginning this thesis. I think it is hard to express how grateful I am and how much I have learnt during all this time in Denmark. I really hope that we will continue to work together many times.

I have to thank Andi a lot as well to teach me, together with Kevin and Chema, the beauty of in-situ hybridization, you have been incredible teachers even when I was repetitively lamely failing, always encouraging me, and explaining me how to solve the problem with pedagogy! Well Andi, of course, you will also always be a model (organism) when it comes to jokes. But obviously, this rainy time in Bergen would not have been so enjoyable without the other people of the SARS with whom the ambiance was always fun in the lab, or sometime, drinking shots in the bars. So thank also to Carmen, Daniel, Antonio, Bruno, Aina, Annie, Julia and Clemens, and I will remember for long the zombie time.

Then I have to thank my Ger... Austrian co-worker, and lab-mate: Alexandra. This thesis would had never been the same without all the lab time spent together in the lab (happy *Lobatocerebrum* scanning or grumpy in-situs), the plates drawing, the endless discussions on *Lobatocerebrum*, phylogeny or in-situs, the courses taken together, the field work, the “procrastination time” etc. (the list is endless, but I have to mention saving my life helping me to carry my bed to the rooftops of Frederiksberg). But in overall, and I will not be the first to mention it, what has been the most significant for all of us, is your kindness. You never say “no” and any trouble we have can be solved even before we ask for your help. So thanks again for all this help.

I also have to thank all the other people of the lab. Ale for being such a great help scientifically, but also when it concerns fun (whether it exists or not), during the thesis, and mostly, and more crucially, at the beginning, when I just moved to Helsingør. Now I know what can possibly go wrong. Brett, my office mate in Copenhagen, thanks for all these nights in the lab, at the Irish Rover, or even these romantic times in Ikea. Ludwik, thanks for all these stimulating conversations on Gnathostomulids in the lab or philosophy of science in Lumksebuksen, you are an awesome student. Lisa, for the back and forth English vs French jokes. Always remember, you are as French as me. Maikon, for your cheering mood, it was a pleasure to have you in the lab, and to the top, for this adventure in Greenland. Benedikt, even though we couldn’t catch up for a beer during my

first year, we corrected it later on, and had some good time. Hannah for all these nice moments in Helsingør and UP4, and your nice mood. Demeng, also for these nice times and beer between Helsingør and Copenhagen. And now after citing the four latter persons, I have to recall a certain trip in Rostock. "Day one!", is long over but I hope we will have more of them. Sachia for your sometimes nice mood, when you don't want to kill me, I definitely prefer drink shots with you than mess with your computer. Ellie, as one of the first person I supervised: you are a student full of curiosity. Marion, for your passion on Jellyfish, it was nice to have a French fellow/friend around and I wish you all the best for your time in Bergen! Cecilie, for your energetic company and, well, thanks to you I have a home now, and a Danish abstract! Kevin for the nice beers, from Axelhus to the Moose, from 6 to 6. Nadya, to be such an energetic person to enjoy, and I'm sure that we will sing Irish songs in many towns. And the list could go on for long so, I am very sorry to get shorter now. Anyway, I have to thank all the nice people who surrounded me, for the beers, the good mood, or both: Nikolaï, Irene, Jiseon, Vibe, Kirsten, Kevin, Terje, Karin, Natia, Elene, Martin, and Martin, Maria, Tobias, Julie, Pernille etc. I am so sorry if I forget people, and I have to thank all people of UP4 and the Marine biological section.

A special thank for the people who taught me science and without whom I would have never done this thesis:

I guess my wandering zoological journey began with my second year of master where I had the chance to be formed by Michaël and Muriel. If you would have not given me the incredible chance to work on the morphology and evolution of ctenophores, I guess I would never have ended up in Denmark doing this thesis. Thank again to both of you for your pedagogy and to have opened me the path to Zoology!

Also, I have to thank all the teaching team of my master in Paris, for giving me the love of phylogenetics and organisms biology.

Then I began my Scandinavian wandering, continuing the zoological one, having the chance to work with one of the kindest and inspiring person I know on the Oligo-cutes. Thanks a lot Christer to have offered me, with open arm, the chance to work with you in Göteborg, and scientifically grow up before I had to work on even smaller critters.

Lis thank you with your technical support and your good mood with the animal sectioning. Thomas and Jakob for your help with the boat.

Reinhardt, thanks for this beautiful time in Greenland, the Inuit stories, and most of all, seeing the legendary Micrognathozoa with you in Qeqertasuaq!

Wolfgang, thanks for your awesome presence in Israel where we found nine specimens of *Lobatocerebrum* and in Arcachon where we found... Well, not that much, but that was some very good time anyway.

I also have to thank all my French friends, part of the Cladist crew, with who I always had some fun coming back in France and who kept me in the loop of the passionate phylogenetic and epistemological conversation and thoughts, but also always here for a beer (or three) every time I came back. I wish I could name you all, but well, we have a mailing list for that. V.A.V.E.

I cannot forget my other friends who supported me from France. My dear old friends from Colombes where I grew up: Nicolas, Jacques, Flavien and Mathieu, and of course Sophie and Karen. Céline, who always kept contact even when I did not give news for weeks, take care of your veliger. And Sophie-mou, the first person who told me about Micrognathozoa, who would have thought that it would bring us to such friendship and bring me to work on this topic? Eli, Lucas, Viktorche, Mich-mich, my old friends for master, it is so nice to continue to see you, with beers and cladistics. And the “youngsters” joining the group afterward Donald, Boris, Ninon, Mathilde, Lucie, Malcolm, Charles (for the arrangeoir time on Skype, you have seen things that you shouldn't), Jeremy, Laetitia, Marc, Tifenn, Wahid and the people I forget but will find themselves in the cladist crew (see above). Without all these people around me all of this wouldn't have been so enjoyable.

Thanks also for the blog team, it helped me to keep my passion and keep interested in other topics than my PhD only, so thanks Boris, Battle, Aurélide, Sophie (and not Donald!).

Thanks also for my two lovely roommates, Sarah and Irene and there support on the last days of the thesis; with tea and toilette paper shouting at me on the door!

All the people who visited me, keeping me in contact with the rest of the world: The French: Laetitia, Donald, Lili, Maeva, Lucas, Jacques, Mathieu, Marilyn; The Swedes: Ida and Ida, Anna, Linn, Simon; The Belgians: Kathleen and Esther; and even a Greek from Norway: Carmen.

Laetitia for the gorgeous cover, you scientific help with the phylogenetic analysis, inspiring conversations on feminism, when I didn't love my Micrognathozoa ladies enough, and of course your unconditional support. Your help and our relation were crucial for me, and a constant source of inspiration for the thesis or other things in life.

Et bien sûr ma famille: Rabia, Adda, Yasmine, Félix, Georges, Apolline, Katrine, David et Alexandre. Rabia, Adda, Yasmine et Félix, un grand merci pour vos visites ! Et Adda, Rabia, Yasmine et Georges, merci pour vos encouragements soutenus, tout cela n'aurait pas été possible sans savoir que j'ai une famille tenant fort à moi (et s'inquiétant dès que je bois la moindre bière) à l'autre bout de l'Europe.

# Abstract

## Abstract

Spiralia is a vast clade of Metazoa comprising large and well-known organisms, e.g., Annelida and Mollusca, but also many microscopic animals such as Gastrotricha or Gnathifera (including, Rotifera) of the often overlooked meiofauna. To date, the phylogeny and morphology of Spiralia have been difficult to resolve and understand. The present thesis focuses on spiralian meiofauna to i) reconstruct the phylogeny of this clade using transcriptomics and place enigmatic meiofaunal taxa and ii) resolve the morphology of three important taxa, mainly employing confocal laser scanning microscopy and immunohistochemistry: the spiralian incertae sedis, *Lobatocerebrum*, the recently described monospecific phylum Micrognathozoa (Gnathifera), and an early branching Gastrotricha, *Diuronotus aspetos*.

The new spiralian phylogeny reveals with high support that the deepest branches of Spiralia consist of meiofaunal representatives, that Gnathifera is the sister group of remaining Spiralia, that Gastrotricha+Platyhelminthes branches off next and that *Lobatocerebrum* is an Annelida. The morphological surveys of the musculature, nervous system, glands, and ciliation on three phylogenetically distinct taxa yield more insight into their evolution: *Lobatocerebrum* is an aberrant annelid showing only few common traits with Annelida, yet, our detailed studies unravel putative resemblances of muscular, nervous and glandular system to previous findings in annelids. Micrognathozoa shows more resemblances with Rotifera than Gnathostomulida (these three taxa together forming Gnathifera). Furthermore, we could infer possible plesiomorphic states of Gnathifera such as the paired ventro-lateral nerve chords (shared with many Spiralia) as well as recover putative Gnathifera apomorphies such as the pharyngeal ganglion; all adding new information on the evolution of this group. *Diuronotus aspetos* shows a unique combination of muscular traits not easily traceable, but in contrast the nervous system traits can be compared in high details, hereby bridging to other Chaetonotida (Gastrotricha). Moreover, we describe new gastrotrich characters such as the ciliary pattern or a system of pharyngeal canals of possible importance for future comparative approaches.

These different studies show that information on rare and phylogenetically isolated animals with their unique combination of neural and muscular characters are necessary to understand the evolution of Spiralia. Also, several organ systems should be considered for systematic comparisons, here emphasized with ciliary and glandular systems in Micrognathozoa, Gastrotricha and *Lobatocerebrum* showing potential phylogenetic information.

## Resumé

Spiralia er en stor klade af metazoer bestående af både store og kendte organismer som eksempelvis Annelida og Mollusca, men også af mange mikroskopiske dyr såsom Gastrotricha eller Gnathifera (herunder f.eks. Rotifera), der er repræsentanter for den ofte oversete såkaldte meiofauna. Til dato har Spiralias fylogeni og morfologi været svær at løse og forstå. Denne afhandling fokuserer på meiofaunal Spiralia til i) at rekonstruere en fylogeni af denne klade ved hjælp transcriptomics og placering af kryptiske meiofauna taksa, ii) klarlægge morfologien for tre vigtige taksa hovedsageligt ved hjælp af konfokal laser scannings mikroskopi og immunohistokemi, med udgangspunkt i den tidligere incertae sedis, *Lobatocerebrum*, det nyligt beskrevne monospecifikke "phylum" Micrognathozoa (Gnathifera), og en tidlig forgrening af Gastrotricha, *Diuronotus aspetos*.

De betydeligste resultater af den nye Spiralia fylogeni er, at de dybeste grene af Spiralia består af meiofaunale repræsentanter, at Gnathifera er søster gruppe af de resterende Spiralia, og at *Lobatocerebrum* er placeret i Annelida. De morfologiske undersøgelser af muskulatur, nervesystemer, kirtler, og ciliering på de tre fylogenetisk adskilte taksa giver yderligere indsigt i deres udvikling: *Lobatocerebrum* er en afvigende annelid, og viser kun få fælles træk med Annelida. Micrognathozoa viser flere ligheder med Rotifera end Gnathostomulida (disse tre taksa danner tilsammen Gnathifera). Desuden kunne vi udlede mulige plesiomorfiske tilstande i Gnathifera, såsom de parrede ventrolaterale nervefibre (delt med mange Spiralia) eller tilstedeværelsen af et svælgganglie, hvilket tilføjer ny information om evolutionen af denne gruppe. *Diuronotus aspetos* viser en enestående kombination af gastrotrich træk, især kan nervesystemet nemt sammenlignes med andre Chaetonotida (Gastrotricha), desuden beskriver vi nye karakterer såsom de ciliære mønstre, og et system af svælgkanaler der har mulig betydning for fremtidige komparative studier.

Disse studier viser, at sjældne og fylogenetisk isolerede dyr, med deres unikke kombination af neurale og muskulære træk, er nødvendige for at forstå udviklingen af Spiralia. Ydermere, bør hvert organsystem tages i betragtning ved systematiske sammenligninger, da ciliemønstre og kirtelsystemer i Micrognathozoa, Gastrotricha og *Lobatocerebrum* viser potentiel fylogenetisk information. Endelig, er denne afhandling med til at opklare en række manglende viden om nogle centrale meiofaunale taksa, tilførende sammenligneligt materiale til yderligere forskning.

## I) Background and justification of the study

In the past few years, our picture and understanding of the phylogenetic relationships of animals have been greatly changed and improved thanks to the advances in large-scale molecular phylogenies, e.g. (Edgecombe et al. 2011, Dunn et al. 2014, Telford et al. 2015, Halanych 2016). Yet, the evolution of specific organs systems is still far from being understood and explaining their evolution between all the subgroups of animals is still challenging. Although evolutionary developmental biology (evo-devo) e.g. (Arendt et al. 2008, Manuel 2009, Lauri et al. 2014, Marlow et al. 2014, Hejnal and Martin-Duran 2015) and descriptive morphology e.g. (Schmidt-Rhaesa 2007, Brusca et al. 2016, Schmidt-Rhaesa et al. 2016) have done great advances in describing and understanding the body patterning and the organization of specific organs systems of many taxa, the overall picture of how these structures are related is still unclear (Hejnal and Lowe 2015).

One of the main questions still left is the size and complexity of the first Bilateria. During the last decades, studies on complex model organisms (e.g. mouse, zebrafish, fruit fly) showed that the genetic underlying mechanisms patterning complex organs and their arrangement are similar, and thus thought to be inherited from a common ancestor, e.g. (Prud'homme et al. 2003, Arendt et al. 2008). However, many groups of animals of smaller size are still unstudied when it comes to evo-devo, phylogenetic sampling or morphology (Hejnal et al. 2015). This inequality in the study of different groups of animals can lead to a bias in the reconstruction of animal evolution, and these gaps need to be filled.

Meiofauna, or meiobenthos, consists of animals passing through a 1mm sieve and retained by a 42µm sieve (Higgins and Thiel 1988). This very practical and arbitrary definition with limited zoological information includes taxonomically and ecologically diverse animals, e.g. exclusively meiofaunal Gastrotricha; marine, freshwater or inland like Rotifera; sessile animals such as urochordates; non-vermiform forms like Cnidarians. Therefore, many animals belong to meiofauna, and – due to the difficulty to collect and manipulate them – they are still understudied. However, their size is not proportional to their evolutionary relevance, and many groups with a crucial phylogenetic position belong to meiofauna (Rundell and Leander 2010). Spiralia, one of the three largest groups of Bilateria next to Ecdysozoa (e.g. insects, nematodes) and Deuterostomia (e.g. vertebrates, echinoderms) counts several primitively meiofaunal clades,

such as the Gastrotricha and the three Gnathifera taxa: Gnathostomulida, Micrognathozoa (including one species: *Limnognathia maerski* Kristensen and Funch, 2000 and Rotifera. Additionally, phylogenies of Platyhelminthes indicated a meiofaunal origin of this group comprising many secondarily large sized animals (Egger et al. 2015, Laumer et al. 2015) (but see Ax, 1956, showing that this was long suspected). Gnathifera, Gastrotricha and Platyhelminthes together form the disputed group “Platyzoa” (Cavalier-Smith 1998), a taxon found by molecular phylogenies but with no morphological justification, and many authors have questioned its relevance e.g. (Zrzavý 2003, Dunn et al. 2008, Giribet 2008). Furthermore, two other genera of special interest in this thesis, *Diurodrilus* and *Lobatocerebrum*, so far had a disputed position within Spiralia (Rieger 1980, Jenner and Littlewood 2008, Worsaae and Rouse 2008). Even though they have originally been supposed to belong to Annelida, further studies have questioned their annelid affinities. In this context, understanding the phylogenetic position of these groups as well as describing their morphology is necessary.

## II) Aims

The purpose of this work is to describe the morphology of some of these animals to enhance our knowledge on animal evolution as well as to integrate them in a phylogenetic context, therefore focusing on:

-A large transcriptomic data set which was analyzed in order to position *Diurodrilus*, *Lobatocerebrum* and Micrognathozoa within the Spiralian phylogeny, as well as to resolve the platyzoan relationships (Laumer et al. 2015), and assess the importance of meiofauna in the evolution of this group (manuscript I).

-*Lobatocerebrum*, a former *incertae sedis* not studied for more than 30 years since its discovery (Rieger 1980, Rieger 1981), and the description of its muscular, nervous and glandular system in order to better understand its annelids affinities (Kerbl et al. 2015) (manuscript II).

-the recently described Micrognathozoa (Kristensen et al. 2000) and still unknown internal anatomy with study of its musculature (Bekkouche et al. 2014) (manuscript III), nervous system and ciliation (manuscript IV), aiming to shed new light on the evolution of Gnathifera, as it is the sister group of other Spiralia.

-the gastrotrich key taxon *Diuronotus*, and its detailed morphology in order to have a better understanding of the evolution and diversity of the internal organ systems of Gastrotricha with the study of an important taxon in the morphologically poorly known Chaetonotida (manuscript V).

While the first manuscript provides the phylogenetic framework of this thesis, the studied organisms show three distinct examples of the diversity of meiofauna within Spiralia: i) *Lobatocerebrum riegeri* Kerbl et al., 2015 shows a case of a highly divergent meiofaunal animal among a well defined group of mainly macrofaunal animals, Annelida), ii) *Limnognathia maerski* is an example of a meiofaunal species so distinct from other groups that it justified (according to some authors) the erection of a supra-specific rank (Kristensen et al. 2000, Giribet et al. 2004), iii) *Diuronotus aspetos* Todaro et al., 2005, one species within the relatively well known meiofaunal group Gastrotricha. These three case studies illustrate our lack of knowledge on spiralian meiofauna and their internal anatomy, and the here presented thesis aims to elucidate the anatomy of each of these taxa in order to evaluate if their morphology can be of comparative relevance at their very different phylogenetic levels. It also aims to offer comprehensive descriptions in order to provide relevant comparative information for further studies on closely related organisms.

### **III) Scientific justification**

The introduction of systematic phylogenetics (cf cladistics) by Willi Hennig in 1966 (Hennig 1966), led to a scientific Khunian revolution (Kuhn 1962) in the domain of systematics and evolutionary biology. This theory did not only initiate deep conceptual changes in the interpretation of the phylogenetic relationship between organisms, but also in the use and interpretation of the characters themselves. Cladistics proposed a method where characters could be discussed and used in a transparent way for phylogenetic reconstruction, contrasting with the previously employed evolutionary systematics. However, soon after e.g. (Field et al. 1988), the field of molecular systematics has undergone a rapid increase until today, and consequently, the discipline of morphology has been in a “crisis”. Indeed, the increasing availability of molecular data seemed to have very quickly outcompete the use of morphological data for phylogenetic reconstruction, sometimes consigning morphology to a simple descriptive discipline, e.g. (Mooi and Gill 2010, Jenner 2011). This replacement however, was not the consequence of theoretical justifications,

but only of technical advances. Therefore morphology has no philosophical reasons to be excluded and should not be forgotten.

In this context, morphology is an important ontological tool. Indeed a mandatory descriptive step/process is necessary in order to define the entities zoologists are discussing in evolution, and the evolutionary interpretation of morphological structures comes in three steps:

-The first step is to understand and describe these structures in a formal way in order to make them comparable with other structures of the same organism and of other organisms.

-The second step is to actually compare these structures with other organisms/taxa and state hypotheses about homology relationships.

-The third step is to interpret the relationship of these structures; are they homologous as supposed in the second step or not?

If these three steps are not necessarily well segregated in the scientific process, the first one corresponds to the field of descriptive morphology, the central point of the present thesis. The two subsequent steps belong to the field of phylogenetic reconstruction and interpretation, but depend directly on the first step.

The recent description of new so-called “phyla” (Ax 1956, Kristensen 1983, Funch and Kristensen 1995, Kristensen et al. 2000, Kristensen 2002) resulted in more questions about the understanding of animal evolution than expected, mainly because both comprehensive molecular and morphological datasets were not available at the time. Although the aim of this thesis is partly to gather and provide new molecular data on these taxa (i.e. transcriptomes), its main goal is to morphologically describe these various lesser known animals to also supplement the morphological dataset. For this purpose, we mostly applied Confocal Laser Scanning Microscopy (CLSM) and widely used fluorescent histochemical stainings to label and investigate the nervous system and the musculature (DAPI, phalloidin, antibodies directed against tyrosinated  $\alpha$ -tubulin, acetylated  $\alpha$ -tubulin, serotonin and FMRF-amide). Indeed, these two organ systems have been widely studied and included in phylogenetic discussions (see for instance, among other textbooks, “The evolution of organ systems” (Schmidt-Rhaesa 2007), and the “Handbook of Zoology: Gastrotricha and Gnathifera” (Schmidt-Rhaesa 2015), or “Structure and evolution of Invertebrates

nervous systems” (Schmidt-Rhaesa et al. 2016)). It is not to say that these organ systems are always straightforward to compare and homologize between different animals, but that the large available literature, on top of their crucial biological function, make them very suitable organ systems for morphological comparison across phylogenetically diverse animals.

## **IV) Methods of investigation**

### **A) Collection of material**

First of all, animals are collected and fixed for the needed studies. Most material is collected via magnesium chloride narcotization and decantation (Higgins et al. 1988), i.e. the animals in the sediment are anesthetized with isotonic  $MgCl_2$ , suspended by agitation with the surrounding organic matter, and concentrated. Thereafter, the extract is deposited on a sieve after washing the  $MgCl_2$ , to allow the animals to crawl through the mesh and get separated from the retained organic matter. Then animals are collected individually and fixed in the appropriate manner (Glutaraldehyde/trialdehyde for electron-microscopy, paraformaldehyde for confocal microscopy, ethanol for molecular analysis, etc.). One of the major limitations of meiofauna studies is the accessibility and difficulty to manipulate animals. Indeed, some animals: i) have remote locations such as *Limnognathia maerski* and *Diuronotus aspetos* found in Greenland, ii) have very strict seasonality as *Limnognathia maerski* found only in summer, iii) have patchy distribution e.g. the fortunate finding of many *Diurodrilus subterraneus* Remane, 1934 in few spots on a beach in Sweden (Ystad) allowed us to collect sufficient material for transcriptomics (Laumer et al. 2015), or iv) are extremely rare as the finding of nine specimens of *Lobatocerebrum riegeri* in Israel was only permitted through the joint effort of four people over the course of two weeks (Kerbl et al. 2015). Furthermore, the size of these animals makes them easy to lose and break during manipulation, and difficult to mount for high-magnification microscopy.

### **B) Confocal Laser Scanning Microscopy (CLSM)**

Morphological characters in this thesis are mainly described with the use of CLSM with immunohistochemistry and fluorescent stainings. The main organs targeted will be musculature, nervous system and ciliation (locomotory, sensory, etc.). The size of meiofaunal animals is especially suitable for CLSM (Wanninger 2007, Leasi and Todaro 2008), indeed, the high resolution

of this technique allows us to reconstruct details of the animal at the cellular level. Additionally, entire animals can be mounted and scanned. The transparency and the thinness of these animals also permit the light to go through the animals with low to virtually no loss of signal. The output is a 3D reconstruction of the targeted organ systems, giving an overall picture of the organic arrangement. Data are then interpreted with 3D imaging software.

It is necessary to emphasize that CLSM only reveals the 3D repartition of a specific fluorescence within the animal, which carries several limitations, as for instance i) an overlapping of different fluorochrome fluorescence leading to a limited segregation of the different stainings, ii) the auto-fluorescence of non-targeted structures, iii) the non-specificity of the antibodies iv) the non-extensiveness of some stainings only revealing a subpart of an organ system.

On the other hand, some of these limitations can be used in a positive way. Auto-fluorescence and non-specificity can lead to the recognition and the characterization of additional and unexpected structures, and the non-extensiveness of staining can lead to specific characterization of some structure, as for instance the recognition of very nerve cells.

### **C) Transmission electron microscopy (TEM)**

Before the use of CLSM, TEM was one of the most widely used method of comparative biology of meiofauna and a profusion of work illustrates this statement, e.g. (Harrison and Ruppert 1991, Ahrichs 1993, Wiedermann 1995, Kristensen et al. 2000). Indeed, thanks to its very high resolution, TEM offers the accessibility of a wide variety of characters that the size and simplicity of meiofauna does not offer at the dimensions of conventional light microscopy. Therefore, a great amount of details has been collected on the ultrastructure of many organs of meiofaunal animals. Unfortunately, these data often neglect the 3D arrangement of large organ systems throughout the body of these animals. This emphasizes how TEM is complementing CLSM, each technique providing information at a specific level. However, it is easy to overlook structures on TEM as illustrated by the examples of the specific pharyngeal cilia in *Limnognathia maerski* (manuscript IV), or of a canal system in the pharynx of *Diuronotus aspetos* (manuscript V), although visible in the previous publications (Ruppert 1991, Kristensen et al. 2000). On the other hand, a clear demarcation between *Lobatocerebrum psammicola* Rieger, 1980 and

*Lobatocerebrum riegeri* due to the difference of the glandular system would not have been possible without TEM.

#### **D) Phylogenetic reconstruction**

Two phylogenetic analyses using molecular data have been conducted in this thesis, each with quite different objectives. The first one, a transcriptomic analysis involving hundreds of genes, acquired through transcriptome sequencing, aimed at resolving the interrelation of Spiralia and placing several taxon of zoological importance (Laumer et al. 2015). The second one, more humble, aimed at confirming the morphological placement of a genus into a recently erected family of Gastrotricha (Leasi et al. 2008) via target sequencing and the use of only three loci (manuscript V). However, these two approaches offer an important framework for the interpretation of morphological evolution within the studied groups.

### **V) Filling the interstitial gaps of the spiralian phylogeny**

#### **Manuscript I: Spiralian Phylogeny Informs the Evolution of Microscopic Lineages**

Laumer, C. E., Bekkouche, N., Kerbl, A., Goetz, F., Neves, R. C., Sørensen, M. V., Kristensen, R. M., Hejnol., Dunn C. W., Giribet G. and Worsaae K.

#### **A) Results and implications of the new phylogeny of Spiralia**

So far phylogenomics reconstruction of the spiralian phylogeny with high support was difficult (Giribet 2008, Hejnol et al. 2009, Kocot 2016), hampering the understanding of animal evolution. However, the sampling has previously been heavily biased toward macroscopic animals. The here presented study focused on the placement of several enigmatic taxa, but also on proposing the most comprehensive sampling of microscopic animals ever used in a phylogenomic study of Spiralia. This sampling comprised the three taxa Micrognathozoa, *Lobatocerebrum* and *Diurodrilus* previously unplaced with molecular data. Besides, it also included already previously considered taxa as two representatives of Gnathostomulida, *Diuronotus aspetos* as a key taxon in Gastrotricha, and a representative of Catenulida, the sister group of the remaining

Platyhelminthes (Larsson and Jondelius 2008, Egger et al. 2015, Laumer et al. 2015). The results showed that Gnathifera represent the sister group of other Spiralia, and that Rousphozoa (Platyhelminthes + Gastrotricha) is the sister group to the remaining Spiralia. This confirms the results by Struck et al. in 2014 (Struck et al. 2014) who found a similar topology. However, Struck et al. could not recover the monophyly of Gastrotricha (only when removing *Lepidodermella*, and *Dactylopodola*) and their study did not include Micrognathozoa. The stronger support for the topology of our study has important consequences since it points to a meiofaunal origin of Spiralia (Vinther 2015) (Fig. 1) and questions the evolution of many central characters. Indeed, under this topology, it is unclear if the plesiomorphic conditions of Spiralia involve the presence of: a coelom (body cavity), an anus, spiral cleavage in the early developmental stages, or two separated ventro-lateral nerve cords (Hejnol et al. 2015, Kocot 2016). Therefore, it is very plausible that the ancestor of Spiralia, and maybe Bilateria, was a small acoelomate animal lacking an anus and having direct development. However, this can only be confirmed with the resolution of i) the placement of Cycliophora, ii) the placement of Chaetognatha, iii) the resolution of the phylogeny of Ecdysozoa, to reconstruct the ancestral meiofaunal or macrofaunal state of this group.

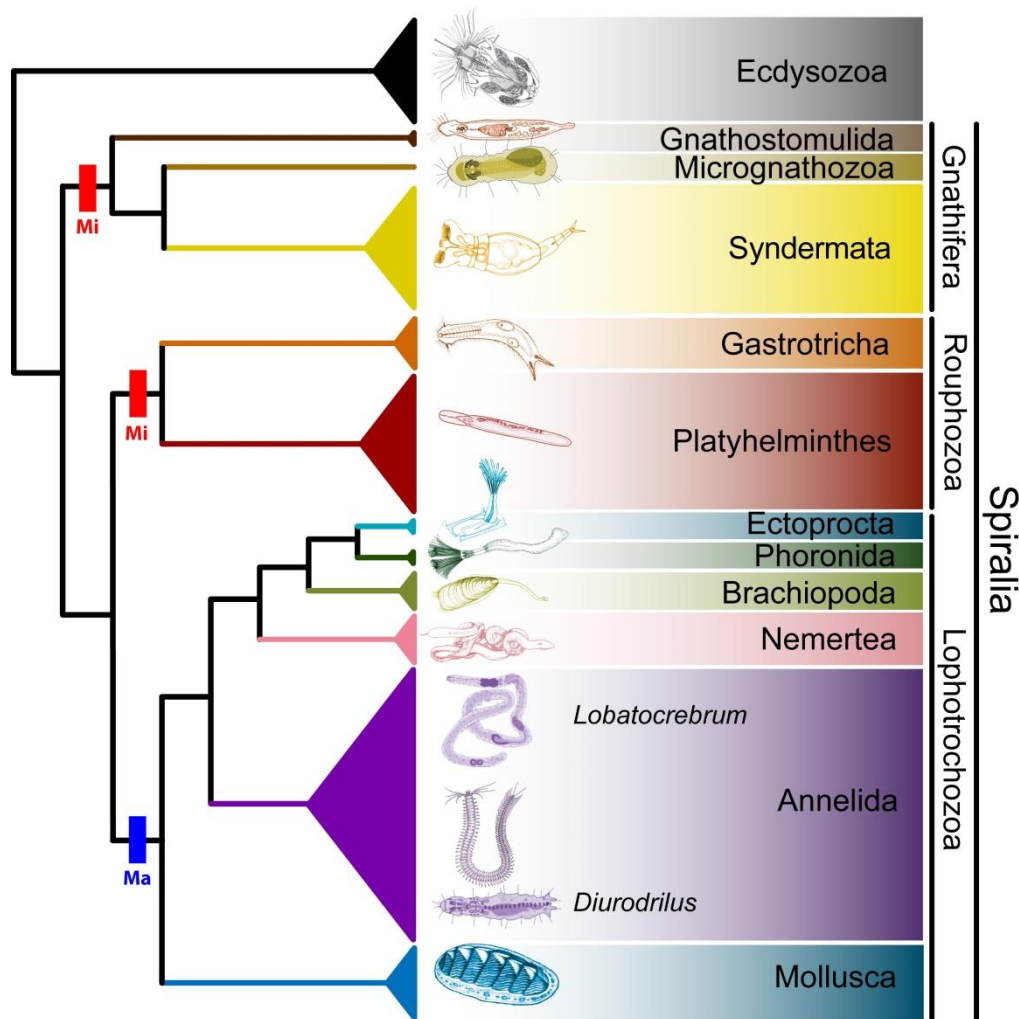


Figure 1: Summary of the phylogenetic tree of Laumer et al. 2015 (Laumer et al. 2015). **Mi** and **Ma** show groups with primitively assumed “Microscopic” or “Macroscopic” condition, respectively.

## B) Impact of the study on subsequent studies

Adding to these general results, more specific relations have to be mentioned here since they have implications on the other parts of this thesis presented below:

-The phylogenetic position of *Lobatocerebrum* as an annelid and sister group to Sipuncula, another taxon of very peculiar unsegmented annelids. This refutes the idea that *Lobatocerebrum* represents its own group within Spiralia and shows a case study of loss of characters related to miniaturization.

-The sister group relationship between Micrognathozoa and Rotifera as already strongly suggested by some authors (Ahlrichs 1997, Kristensen et al. 2000, De Smet 2002, Wulfken and Ahlrichs 2012),

but not yet confirmed with molecular data (Giribet et al. 2004, Worsaae et al. 2008), reinforcing the monophyly of Gnathifera.

-The sister group relationship between Gastrotricha and Platyhelminthes. Although this relationship is still difficult to interpret and has little implication on the present studies of Gastrotricha, it is worth mentioning that the inclusion of *Diuronotus aspetos* in this phylogenomic study seems to stabilize the position of *Lepidodermella squamata*, leading to the recovery of the monophyly of Gastrotricha.

## **VI) The “resurrection” of *Lobatocerebrum*: the enigmatic Spiralia is now an enigmatic Annelida**

**Manuscript II: Detailed reconstruction of the nervous and muscular system of Lobatocerebridae with an evaluation of its annelid affinity.** Kerbl A., Bekkouche N., Sterrer W., and Worsaae K.

### **A) Introduction and studies on *Lobatocerebrum***

Lobatocerebridae is a family of Annelida described in 1980 (Rieger 1980), originally comprising one species, and now one new described species in the manuscript presented in this study (Kerbl et al. 2015). This family of very long and slender, worm-like, completely ciliated, and very elusive animals has puzzled zoologists for a long time (Rieger 1980, Rieger 1981, Haszprunar et al. 1991, Zrzavý et al. 2001, Zrzavý 2003, Jenner et al. 2008), and could not be previously placed in the Metazoan phylogeny. Despite the cosmopolitan repartition of these animals (Rieger 1980, Kristensen 1983, Kerbl et al. 2015, Laumer et al. 2015), they are so rare and discrete that studies on their morphology have been scarce since their discovery (as shown by the collection of “only” nine specimens by four persons over the course of two weeks (Kerbl et al. 2015)). However, one of the manuscripts of the presented thesis (manuscript I) confirmed, with the use of transcriptomics, the previously suspected inclusion of *Lobatocerebrum* within Annelida. This phylogenetic placement warranted a re-assessment of the morphology of *Lobatocerebrum* with modern techniques. Therefore we described the musculature, nervous system and glandular system of *Lobatocerebrum* with CLSM, complemented with TEM and live observations. The results mostly

confirmed the findings of Rieger, 1980 (Rieger 1980), but CLSM permitted a better three-dimensional understanding of these animals and allowed us to describe the internal anatomy with more details as well as to find previously undescribed structures. The study of the musculature confirmed the inner position of the circular muscles relative to the longitudinal muscles, with the circular muscles actually being “transverse muscular ring complexes”, consisting of individual diagonal fibers originating from one longitudinal muscle and extending to the next one on the transversal section. Several of these muscles are giving together the impression of a continuous circular muscle. Similar muscles, though crossing each other, give a star appearance and are only found in the rostrum. The nervous system investigation confirmed the presence of a prominent lobular brain, a pair of ventro-lateral nerve cords extending along the entire body length, and a pair of subpharyngeal ganglia supplying a pair of commissures. Additionally, details of the brain and anterior nerves were given, and we documented the presence of a previously undescribed unpaired median longitudinal nerve as well as two trunk commissures without associated ganglia. The presence of the median nerve and of additional commissures weakly corroborates an annelid affinity see (Kerbl et al. 2015) for a full review. Finally, a new species of *Lobatocerebrum*, *Lobatocerebrum riegeri*, was described due to its different proportions, glandular system and geographical position differing from the previously assessed *Lobatocerebrum psammicola*. To summarize, the detailed morphological re-description of *Lobatocerebrum* does not show any unambiguous trait relating it to Annelida, but the combination of characters such as the complex brain with numerous commissures, the median nerve cord and the ganglionated commissures, corroborates, without confirming, its relation with annelids. Finally, the present phylogenomic (Laumer et al. 2015) and morphological (Kerbl et al. 2015) studies indicate that *Lobatocerebrum* is another aberrant annelid, extending the already long list, e.g. (Zrzavý et al. 2009, Weigert 2016).

## **B) Further possible researches around Lobatocerebridae**

Unfortunately, the extremely divergent morphology of *Lobatocerebrum* does not give many insights on its origin within Annelida. Furthermore, developmental and in-situ hybridization researches on Lobatocerebridae appear so far unrealistic due to the extreme elusiveness of this animal. This suggests that further morphological investigations of *Lobatocerebrum psammicola* and *L. riegeri* are unlikely to shed light on its evolution. On the other hand, further researches on the phylogenetic placement of interstitial annelids could lead to a better understanding of the

origin of *Lobatocerebrum*, and of the numerous other interstitial annelids (Westheide 1990). Fortunately, recent studies appear to move toward a better phylogenetic placement of the different interstitial families of annelids (Andrade et al. 2015, Laumer et al. 2015, Struck et al. 2015). One of these studies (Struck et al. 2015) indicates that there might have been two large interstitial radiations in Annelida (not including *Lobatocerebrum*), comprising among others, Protodrilidae and Dinophilidae, respectively. However, these studies do not include e.g. Psammodrilidae, Parergodrilidae, Aelosomatidae and *Hrabeiella*, which are still to place. Furthermore, Problematica still exist around Annelida, namely *Jennaria pulchra* Rieger, 1991, or the parasitic Orthonectida. *Jennaria pulchra* demonstrates a similar case to *Lobatocerebrum* in being an interstitial vermiform animal with no apparent segmentation, and it was suggested to be related to Annelida in its original description (Rieger 1991). Unfortunately, this animal has never been reported after its description despite intensive researches (Worsaae personal communication). Although Rieger (1991) rejected a sister group relationship with Lobatocerebridae, molecular and morphological studies with recent methods could confirm or reject this hypothesis. Ultrastructural studies on Orthonectida have suggested that they may be related to Annelida (Slyusarev and Kristensen 2003), and molecular phylogeny could not reject this hypothesis (Petrov et al. 2010). Interestingly, a recent study by Slyusarev and Starunov (2016) reconstructed details of the musculature of one species of Orthonectida, thereby showing circular muscles inside the longitudinal musculature, with the circular ones seemingly originating from the longitudinal fibres – an intriguing configuration very similar to what is found in *Lobatocerebrum*. Last but not least, more species of Lobatocerebridae are suspected (Rieger 1980, Kristensen 1983), which could potentially offer a broader morphological diversity of the family, and give more elements to understand their evolution. Finally, the resolution of one or several mentioned lacks in the knowledge of aberrant annelids could help to better understand the evolution of *Lobatocerebrum* and divergent annelids. In conclusion, although our current understanding of the morphology of *Lobatocerebrum* is of limited use to unravel annelid evolution, the thorough morphological description provided in this thesis was necessary to give a comparative framework for all possible further research approaches mentioned above.

## **VII) Micrognathozoa, the third member of Gnathifera**

**Manuscript III: Detailed reconstruction of the musculature in *Limnognathia maerski* (Micrognathozoa) and comparison with other Gnathifera.** Bekkouche N., Kristensen R. M., Hejnol A., Sørensen M. V., and Worsaae, K.

**Manuscript IV: Nervous system and ciliary structures of Micrognathozoa (Gnathifera) – evolutionary insight from an early branch in Spiralia.** Bekkouche N., and Worsaae K. (submitted)

### **A) Introduction: the importance of Micrognathozoa**

In 1994, Kristensen and Funch found a small ciliated organism bearing jaws in a fresh water pond in Greenland, with all found specimens apparently being female (Kristensen et al. 2000). The presence of complex jaws in this animal allowed the authors to immediately relate this new organism to the well-known rotifers. However, it possessed ventral ciliation and lacked the ciliated corona, contrary to Rotifera. In 1995, Rieger and Tyler (Rieger and Tyler 1995) proposed a sister group relationship between the jawed Gnathostomulida and Rotifera (including Acanthocephala) due to the similar ultrastructure of the jaws consisting of parallel rods with an electrodense core and an electroluscent cortex. At the same time, Ahlrich in 1995 (Ahlrichs 1995) proposed the name Gnathifera for this clade. The unification of Gnathostomulida and Rotifera has been encouraged by the discovery of the new animal, which was not formally described at this time, but only informally discussed between zoologists. The proposed character unifying Gnathifera was again the ultrastructure of the jaws (Rieger et al. 1995). This close relationship between Rotifera and Gnathostomulida finally permitted to relate together two “aschelminthes” of previously uncertain phylogenetic placement. Indeed, many interrelationships between Rotifera, Gnathostomulida and other taxa were proposed, as for instance, Rotifera + Platyhelminthes (Markevich 1993) or Gnathostomulida + Gastrotricha (Rieger 1976, Zrzavý et al. 2001) or Gnathostomulida + Platyhelminthes (Ax 1956, Ax 1996). Finally, in 2000, the new taxon was formally described as *Limnognathia maerski* Kristensen and Funch, 2000 (Kristensen et al. 2000), belonging to the monospecific class Micrognathozoa within the phylum Gnathifera. Later on, in 2004, Giribet et al.

(Giribet et al. 2004) attempted to place Micrognathozoa in the animal phylogeny using four different genes, but the results had very low support. Additionally, this study introduced Micrognathozoa as its own phylum. Ranks relevance can be discussed (see Giribet (2016) for recent discussions on this matter), but whether Micrognathozoa are a class, a phylum or only one species does not matter much in this discussion. In any case, this ranking emphasizes the interest of zoologist for this singular animal.

The original description of Micrognathozoa (Kristensen et al. 2000) provided numerous details of the jaws anatomy as well as some information on the inner anatomy and the ultrastructure of the animal. However the discussion of this manuscript was more focused on the phylogenetic implication of *Limnognathia maerski* than on its internal morphology. The complexity of the jaws of Micrognathozoa continued to attract the curiosity of zoologists and the two following morphological works were fully focused on the details of the jaws (De Smet 2002, Sørensen 2003). Interestingly, De Smet found some animals in subantarctic islands (Crozet Island), and the detailed study of the jaws did not show any difference to the Greenlandic animals, leading to the conclusion that Micrognathozoa from Greenland and Crozet Island belong to the same species.

Until the present study, these few works constituted almost the totality of the knowledge we have on Micrognathozoa. Additionally, molecular studies supported the monophyly of Gnathifera, without placing the Micrognathozoa (Witek et al. 2009, Struck et al. 2014). Furthermore, recent phylogenies showed the importance of Gnathifera since they seem to be the sister group to all the other Spiralia (Struck et al. 2014, Laumer et al. 2015). This stresses two important needs: resolving the internal relationships inside the Gnathifera, which today appears to be attained, and acquiring more information on the morphology of different Gnathifera. The very rare information on the internal anatomy of Micrognathozoa and their systematic interest makes them a crucial target of this study.

## **B) The musculature of Micrognathozoa (Bekkouche et al 2014)**

The muscular reconstruction of *Limnognathia maerski* reveals a quite peculiar arrangement difficult to relate to other Gnathifera (Bekkouche et al. 2014). The body wall musculature consists of seven major longitudinal muscles in the trunk and 13 pairs of dorso ventral muscles. This organization in discrete and well separated muscles bundles is more similar to the musculature

found in Rotifera, e.g. (Sørensen 2005, Leasi and Ricci 2010, Leasi et al. 2012), than the one found in Gnathostomulida (Tyler and Hooge 2001, Müller and Sterrer 2004). Additionally, some longitudinal muscles of *L. maerski* do not extend throughout the entire body, compartmentalizing the body in different regions similar to what is observed in Rotifera, e.g. (Leasi et al. 2010, Leasi et al. 2012). Moreover, the dorso-ventral muscles of *L. maerski* resemble the dorso-ventral or semi-circular muscles found in many Rotifera. However, there also are differences since the dorso-ventral muscles of *L. maerski* are positioned inside the longitudinal musculature, while they are positioned outside in Rotifera (Leasi et al. 2010) (this is also the case in Gnathostomulida (Müller et al. 2004))(Fig. 2). It is therefore likely that the dorso-ventral musculature of *L. maerski* is not homologous to the circular muscles of Gnathostomulida and the dorso-ventral muscles of Rotifera.

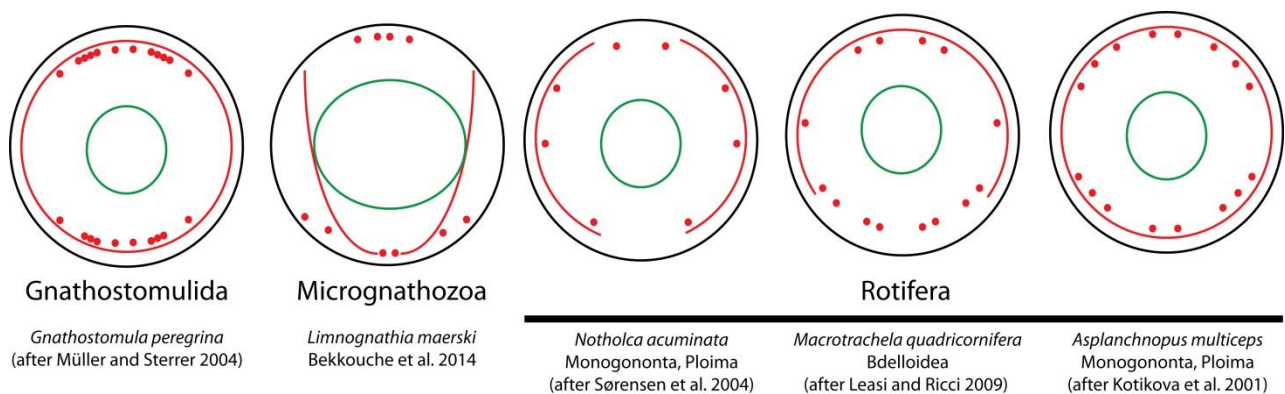


**Figure 2: The muscular arrangement in five species of Gnathifera in the transversal section of the trunk (based on (Kotikova et al. 2001, Sørensen et al. 2003, Müller et al. 2004, Leasi et al. 2010, Bekkouche et al. 2014))**

The pharyngeal musculature of *Limnognathia maerski* is complex and consists of six paired and two unpaired muscles, articulating the different sclerites of the trophi with each other. In this respect, it resembles the muscular organization of the mastax of Rotifera, e.g. (Riemann and Ahlrichs 2008, Wulfken et al. 2010), probably constrained by the similarity in the arrangement of the jaw system of *L. maerski* and Rotifera in contrast to Gnathostomulida (Sørensen et al. 2003, Müller et al. 2004). However, specific homologies between the pharyngeal muscles described in Rotifera and *L. maerski* are not possible since a consensus has not been reached on the homologies of the different sclerites of *L. maerski* with the sclerites of Rotifera (Fig. 3). Since only the incus of Rotifera can be homologized with the jaw sclerites of Gnathostomulida and *L. maerski*, the so called “musculus fulcro ramicus” found in many Rotifera (e.g. (Wilts et al. 2010, Wilts et al. 2012)) is the only muscle which could be homologized with the “caudal muscle” of *L. maerski*. Furthermore, a ventral pharyngeal muscle is present, forming a muscular plate under the trophi,

and is probably involved in the movement of the entire pharynx. However, no equivalent has been found in other Gnathifera. Interestingly, this muscle is similar to an important pharyngeal muscle found in *Diurodrilus* (Worsaae et al. 2008), with which *L. maerski* has been extensively compared.

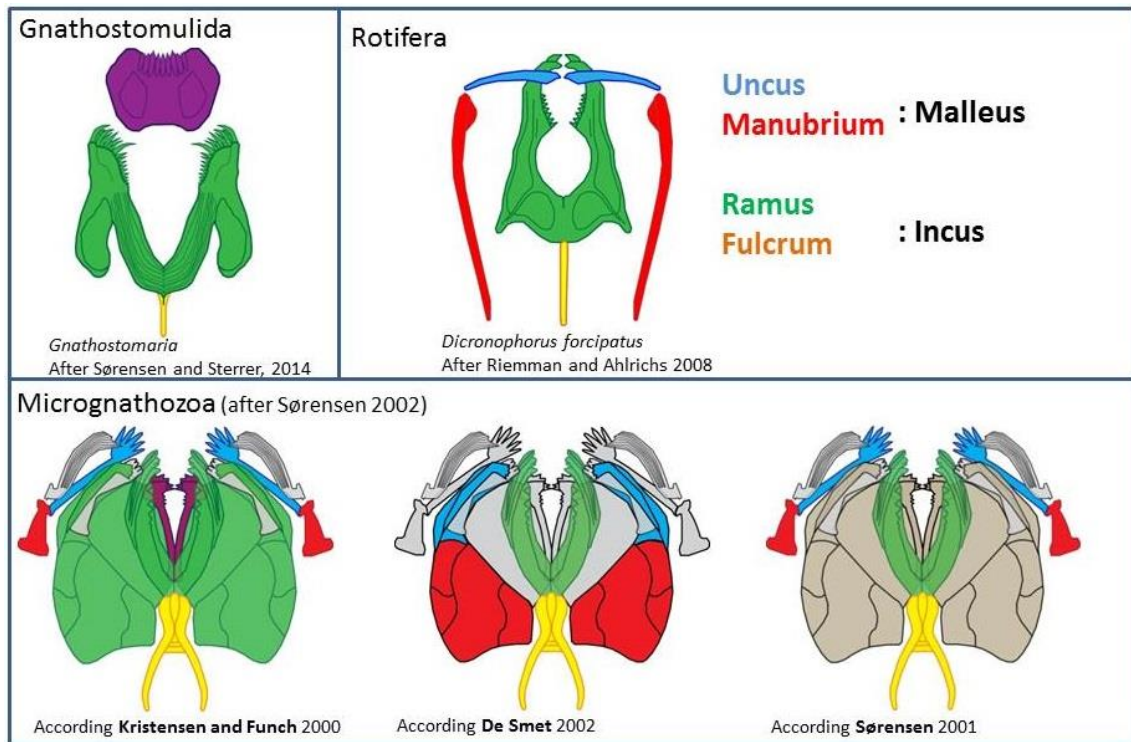


**Figure 3: Different hypothesis of homology between the jaw sclerites of Micrognathozoa and other Gnathifera according different authors (Kristensen et al. 2000, De Smet 2002, Sørensen 2003, Riemann et al. 2008, Sterrer and Sørensen 2015)**

Furthermore, the detailed morphological description of the pharyngeal musculature of *Limnognathia maerski*, together with reports of behavior observed in the living animal permitted assumptions about the jaw movements. Kristensen and Funch (2000) described the existence of fast snapping movement of the main jaws during foraging, and the extrusion of the ventral jaws grasping food, moving independently to the rest of the jaws (also described by De Smet, 2002), which contrasts the movement of the malleus of Rotifera relative to the incus (both being linked e.g. Riemann et al., 2008). In a similar fashion than Riemann et al., 2008, a jaw movement sequence of Micrognathozoa has been inferred (Fig. 4 and (Bekkouche et al. 2015)). This of course has to be confirmed by further behavior studies and high speed imaging, but shows the value of morphological studies in understanding and interpreting how such small and intricate structures can function.

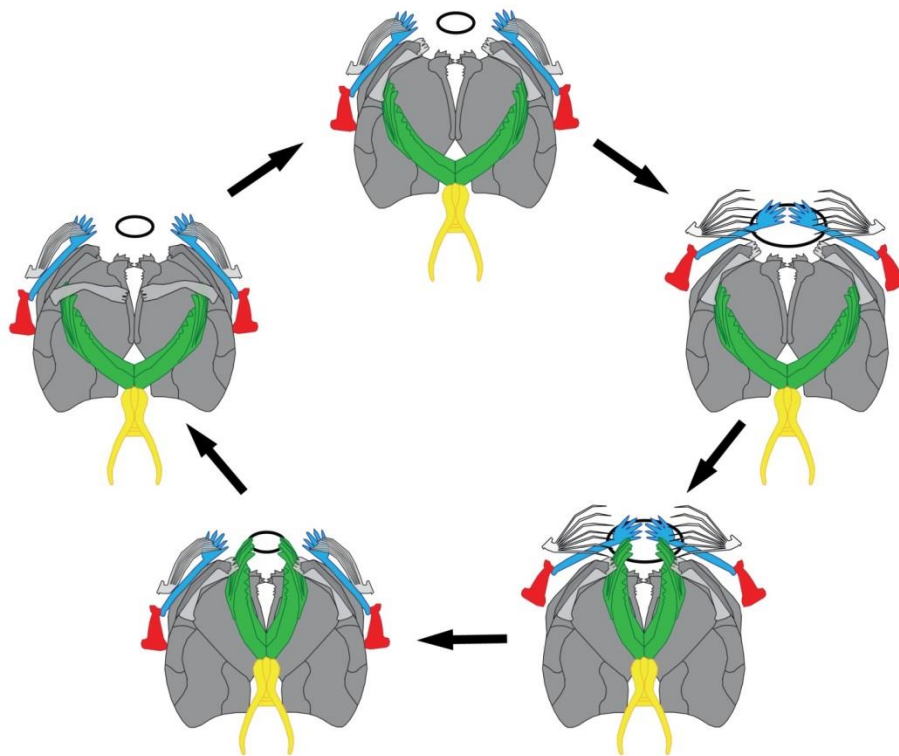


Figure 4: Assumed jaw movement sequence of *Limnognathia maerski* according to behavioral observations and studies on the pharyngeal musculature (Bekkouche et al. 2015). Color coding after Sørensen (Sørensen 2003) interpretation of Fig. 3.

### C) Nervous system, ciliation and glandular system of Micrognathozoa (Bekkouche and Worsaae, submitted)

The nervous system of *Limnognathia maerski* is quite simple and consists of an anterior brain, a pair of ventro-lateral nerve cords and a pharyngeal ganglion. Few other structures are described as, for example, an anterior and posterior commissure, a peripheral nervous system and a pair of thin ventro-median nerves. Interestingly, a peripheral nervous system innervating different sensory structures is also found in Rotifera (Hochberg 2006, Fontaneto and De Smet 2015). On the other hand, the ciliation of *L. maerski* shows a previously unsuspected complexity with more than one pair of ciliophores anteriorly and the presence of pharyngeal cilia very similar to the ciliary receptor of Rotifera (Clement and Wurdak 1991). Additionally, CLSM could confirm the presence of anterior and posterior nephridia, and of a multiciliated collecting duct, which is also reported from Rotifera (Ahlrichs 1993, Ahlrichs 1993) but absent in Gnathostomulida (Lammert 1985). Furthermore, a set of two glands, one unpaired and one paired, is found dorsally in the head

opening dorso-apically, and these glands are similar to the retrocerebral organ of Rotifera (Fontaneto et al. 2015). Surprisingly, these results show that – although the nervous system is of limited use to confirm the relationship between Micrognathozoa and Rotifera – some glands and specific ciliary structures are. This study also confirms that the paired ventro-lateral nerve cords and the pharyngeal ganglion are common traits of Gnathifera, the first one being a plesiomorphy (Hejnol et al. 2015), and the second one a synapomorphy of the group.

#### **D) Conclusion, opening and further studies on Gnathifera**

Although the muscular and nervous system of *Limnognathia maerski* show quite superficial, but numerous, resemblances to Rotifera, the ciliary and glandular systems show more convincing shared characters with Rotifera. Together with the ultrastructure of the tegument (Ahlrichs 1997, Kristensen et al. 2000), the organization of the jaws (De Smet 2002, Wulfken et al. 2012), the shared presence of a specific arrangement of the pharyngeal cilia, the structure of the nephridia and the possible retrocerebral organs furthermore support the sister group relationship between Rotifera and Micrognathozoa. However, nervous system investigations on the early branching rotifer Seisonidae (Rotifera) are lacking, and the inner anatomy of Gnathostomulida is still largely unexplored. Indeed, very few studies on their nervous system and musculature are available. Fortunately, our ignorance on the structure and diversity of the nervous system of Gnathostomulida should not last for long since a collaborative ongoing project carried out by Ludwik Gąsiorowski (Gąsiorowski, Bekkouche and Worsaae, unpublished) aims to solve this problem. The forthcoming study investigates the nervous system of several Gnathostomulida by means of CLSM and should shed more light onto the evolution of the nervous system of Gnathifera (Fig. 5). Preliminary results show substantial variation in the number of longitudinal nerves and brain morphology, and also shows e.g. the presence of pharyngeal cilia related to the buccal ganglion (though more scarce than in Rotifera and Micrognathozoa).

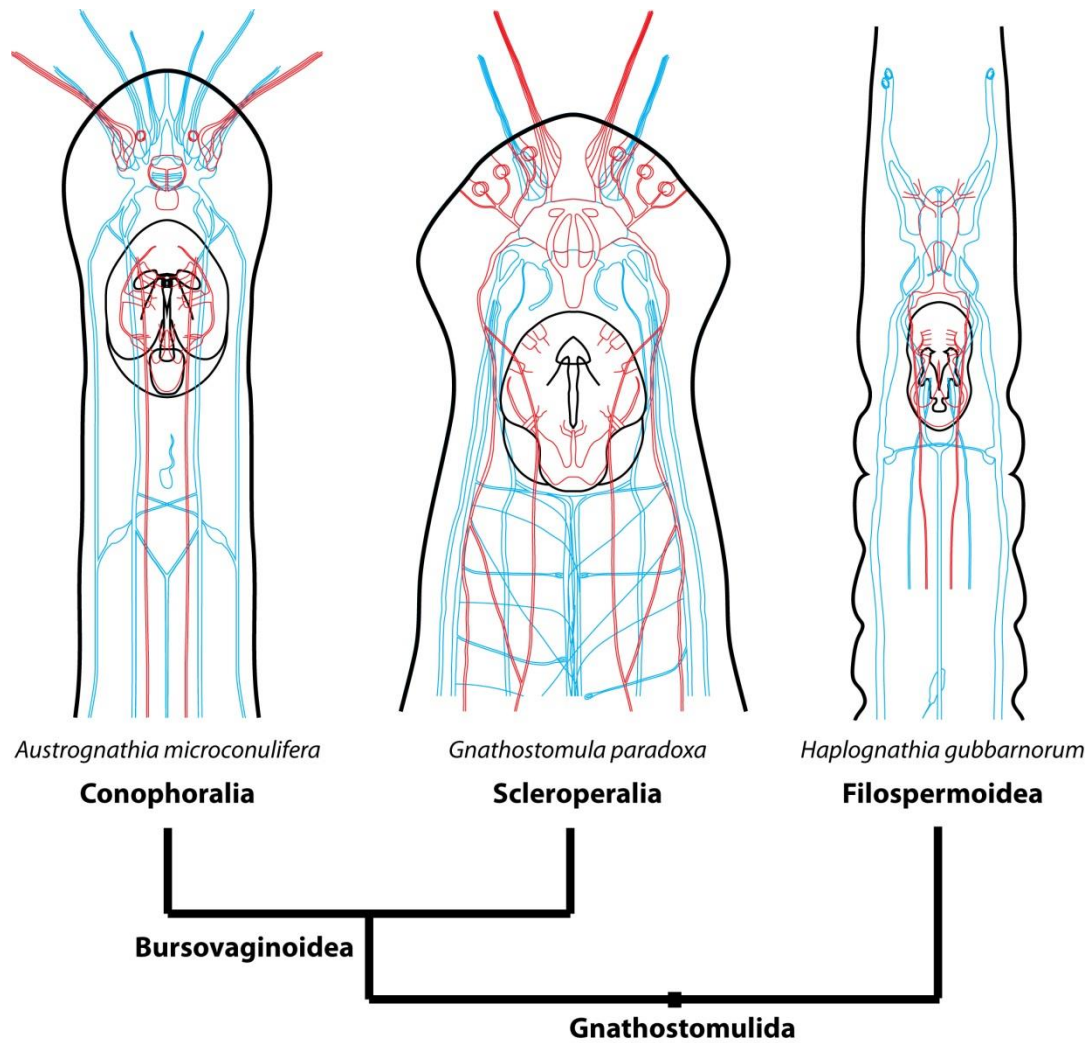


Figure 5: Comparison of the anterior nervous system of three species of Gnathostomulida, representing its three main clades. Ventral nervous system in blue, dorsal nervous system in red. Unpublished results from Gąsiorowski et al.

Finally, with the thorough description of the inner anatomy of Micrognathozoa, one point can be raised: the surprising consistency of the morphology of Gnathifera and their seemingly straightforward relationships. Indeed, for this phylogenetic depth, and the morphological simplicity of these animals, such phylogenetic resolution (including the monophyly of subgroups of Gnathostomulida (Sørensen et al. 2006) and Rotifera (Sørensen and Giribet 2006, Wey-Fabrizius et al. 2014, Sielaff et al. 2016)), supported by both molecular data and morphology (Rieger et al. 1995, Ahlrichs 1997, Kristensen et al. 2000, De Smet 2002, Zrzavý 2003, Witek et al. 2009, Wulfken et al. 2012, Struck et al. 2014, Laumer et al. 2015), may represent a unique case in zoology.

## **VIII) The morphology of *Diuronotus aspetos*, an interesting gastrotrich and its implication in the understanding of gastrotrich evolution**

**Manuscript V: Neuromuscular study of early branching *Diuronotus aspetos* (Paucitubulatina) gives insight on the evolution of organs system within Gastrotricha.** Bekkouche N., and Worsaae K. (submitted)

### **A) Introduction: the Gastrotricha, an understudied, yet important taxon**

Gastrotricha are small and ventrally ciliated animals. These “turbellariform worms” have an extensive cuticle covering the cilia, an organization unique in Metazoa (Ruppert 1991, Kieneke et al. 2008). Rather understudied, they are found in most aquatic environments, from any sandy beach, oceanic bottom, freshwater environment or even humid soil. They are divided into two large groups: the often elongated and marine Macrodasysida possessing multiple adhesive glands, pharyngeal pores and an inverted “Y” cross section of the pharyngeal lumen, and the often fresh water and tenpin shaped Chaetonotida, Paucitubulatina, with only two adhesive posterior glands, no pharyngeal pores and a “Y” cross section of the pharynx lumen. A third taxon, *Neodasys*, belongs to Chaetonotida (Multitubulatina), is characterized by multiple adhesive glands and a peculiar adhesive system, and has a disputed phylogenetic position (Rothe et al. 2011, Kieneke and Schmidt-Rhaesa 2015).

Not only are members of Gastrotricha cosmopolitan and often play a very important part of the microscopic fauna, but they also have a disputed phylogenetic position. Originally supposed to be close to rotifers due to their superficial resemblance (Hyman 1951), ultrastructural studies suggested that they could be the sister group to or even nested within Ecdysozoa, the clade of molting animals comprising arthropods and nematodes. This was proposed on the base of three characteristics: the complex multilayered extensive cuticle, the “myoglanduloepithelial” pharynx very similar to the one found in Nematoda (Ruppert 1982), and the circumpharyngeal brain found also in Nematoda and various other Ecdysozoa (see Schmidt-Rhaesa, 2007 and Kieneke et al., 2015, for discussion). Although some morphological evidences pointed to an ecdysozoan

relationship, molecular phylogenies supported a Spiralian relationship supported only by few morphological data. Gastrotricha were then often placed into the disputed “Platyzoa” (Cavalier-Smith 1998, Giribet et al. 2000, Halanych 2004, Hejnol et al. 2009). Subsequently, recent studies on phylogenomics suggested for the first time a quite robust position of Gastrotricha as a sister group of Platyhelminthes in the clade Rousphozoa (Struck et al. 2014, Laumer et al. 2015). As explained above, this puts gastrotrichs forward as a group of high interest for animal evolution. Prior to such conclusions, however, a better understanding of the inner evolution of Gastrotricha is needed. Although knowledge about gastrotrich evolution has notably increased recently with the implementation of CLSM (Hochberg and Litvaitis 2001, Hochberg and Litvaitis 2001, Leasi et al. 2008, Rothe et al. 2011, Rothe et al. 2011), a lot of work is still needed to better understand the variability of the inner anatomy of Gastrotricha. In order to increase this knowledge and further understand the evolution of Gastrotricha, we studied one of the key taxon: *Diuronotus aspetos*.

## **B) Results and discussion: the morphology of *Diuronotus aspetos***

*Diuronotus aspetos*, a large member of Chaetonotida, has been recently described (2005) (Todaro et al. 2005) and justified the erection of a new genus within Gastrotricha. Its morphological similarities with the rare and enigmatic *Musellifer* have been recognized from the original description and further confirmed (Balsamo et al. 2010), consequently leading to the erection of a new family, Muselliferidae (Leasi et al. 2008). The study presented in this thesis, as well as previous morphological and molecular investigations (Kieneke et al. 2008, Leasi et al. 2008, Kånneby et al. 2014), suggest that indeed, Muselliferidae belongs to the deep nodes of the phylogenetic tree of Paucitubulatina, emphasizing the importance of this family for understanding the evolution of Gastrotricha. Muselliferidae are especially rare: *Musellifer* is occasionally reported in very low abundance (Hummon 1969, Kånneby et al. 2014) (sometimes only one (Kånneby et al. 2014)) and *Diuronotus* is found in few locations (Denmark and Greenland (Todaro et al. 2005), Germany (Kieneke 2015), and informally mentioned in North America (Ruppert 1982)).

First, we placed *D. aspetos* into the phylogeny of Paucitubulatina, confirming with molecular data that it is the sister group of *Musellifer*. Additionally, we studied *D. aspetos* with CLSM, supporting the peculiarity of this gastrotrich. The musculature, for instance, shows only few longitudinal muscles, but numerous pairs of dorso-ventral muscles in the transversal section (up to five), a

configuration not found in other Paucitubulatina (Leasi et al. 2008). We also described the musculature of the furca in detail, showing the presence of circular muscles around the adhesive glands, and some semi-circular muscles in the posterior region of the trunk. These special traits make the specific muscles of *Diuronotus aspetos* difficult to homologize with other Paucitubulatina. The nervous system is also described in great detail, giving valuable information, since so far *Xenotrichula* was the only other Paucitubulatina for which the nervous system was carefully assessed (Rothe et al. 2011). We found the common gastrotrich arrangement of one dumbbell shaped brain and a pair of ventro-lateral nerve cords (Kieneke et al. 2015), but also described some specific nervous structures such as i) additional ventro-median cords ventral to the pharynx, ii) a ventral commissure of the brain shifted anteriorly, associated to a dorsal commissure forming an anterior nerve ring, and the presence of iii) post-pharyngeal and iv) anal ganglia. Interestingly, some of these characters can be homologized with *Xenotrichula* (Rothe et al. 2011), and even specific perikarya of the brain can be compared *Neodasys* (Rothe et al. 2011) and *Xenotrichula*. The pharynx is also comprehensively described, including its nervous system, showing pharyngeal cilia in the pharynx of Paucitubulatina with CLSM for the first time, but also demonstrating the existence of a system of seemingly hollow canals in the pharynx. These canals are of unknown function and have never been described in other Gastrotricha previously. Finally, the ciliary system is studied, showing for the first time the presence of two pairs of protonephridia in Paucitubulatina (Kieneke et al. 2008, Kieneke and Hochberg 2012), and resolving the detailed pattern of the repartition of the ventral multiciliated cells. This detailed study shows the presence of previously undescribed structures (additional muscles, nerves or the pharyngeal canal system), and furthermore demonstrates that the nervous system might be easily comparable across Paucitubulatina. We therefore emphasize that this investigation will serve as a basis for future descriptions in other Paucitubulatina or other Gastrotricha.

### **C) Conclusion: opening and further researches on Gastrotricha**

This study on *Diuronotus aspetos* shows the necessity to study even (apparently) minor characters (such as ciliary patterns and glands) to understand the evolution and diversity of Gastrotricha. It also shows that extensive descriptive studies such as conducted in the presented thesis and in e.g. (Wiedermann 1995, Rothe et al. 2011, Rothe et al. 2011, Todaro et al. 2015), are mandatory to facilitate a comparative and evolutionary database. To illustrate that, two examples of future

researches on Gastrotricha either inspired by, or broadening, the present study on *D. aspetos* are presented here.

**i) On the evolution of the ventral ciliary pattern in Gastrotricha**

The presented study on *Diuronotus aspetos*, together with the investigation of ciliation patterns of *Limnognathia maerski* (manuscript IV) indicate the value of CLSM for detailed descriptions of the ciliary system of meiofaunal animal. This led to the description of fine and unexpected details such as the presence of pharyngeal cilia in *D. aspetos*, and the mosaic-pattern of ventral multiciliated cells in *L. maerski*. This potential new type of characters could possibly be of systematic importance and we hope that it will be more exploited in the future. During the course of this thesis, acetylated  $\alpha$ -tubulin immunoreactivity have been studied in a range of gastrotrichs, especially Thaumastodermatidae, which are known to possess multiciliated locomotory cells (Todaro et al. 2011). Together with DAPI, these data showed that variability exists between the ciliary pattern of different members of Thaumastodermatidae (Fig. 6) and we hope that further analysis will reveal the systematic relevance of this character.

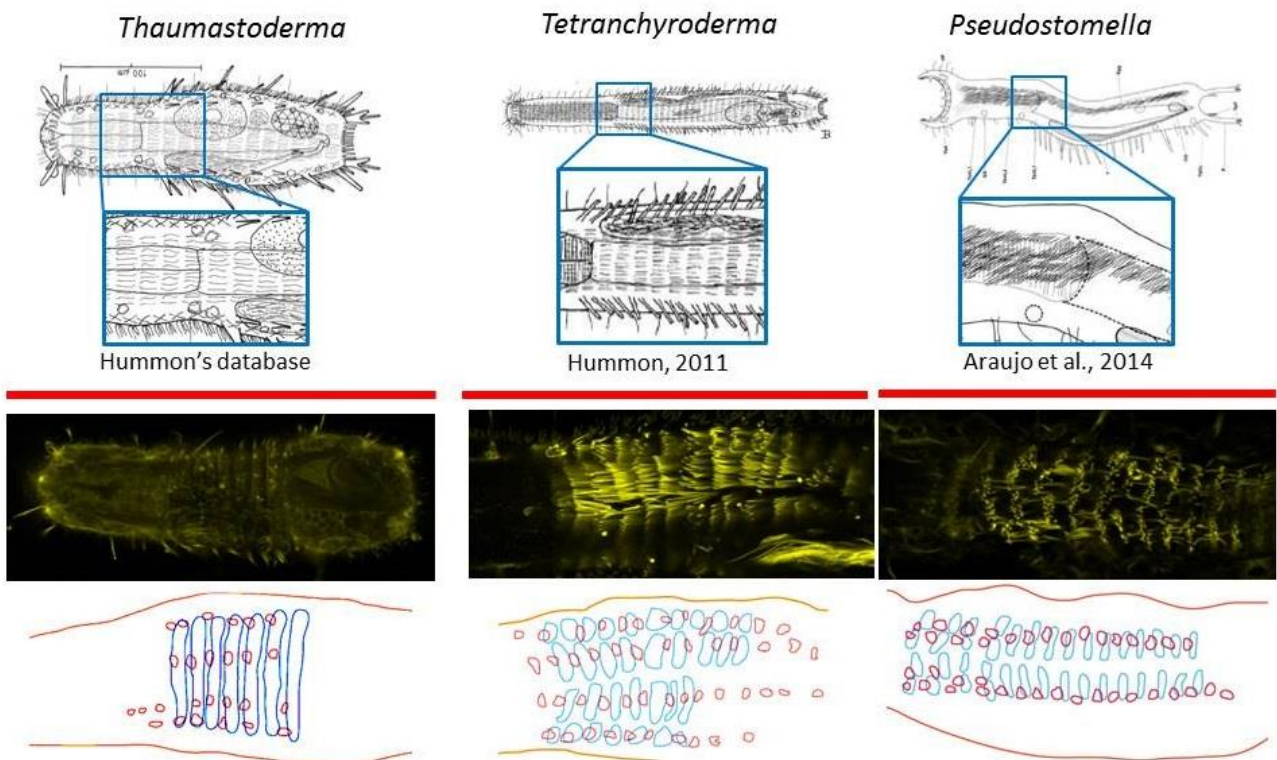


**Figure 6: Comparative representation of the ventral ciliation of various Thaumastodermatidae based on literature (Hummon 2011, Araujo et al. 2014) and own CLSM interpretation, displaying variation in the precise pattern of multiciliated cells. Interpretation from Eleonor Sharples.**

## ii) On the fine evolution of the nervous system of Gastrotricha

A range of nervous systems of various members of Gastrotricha was analyzed during the course of this thesis, which could unfortunately not be integrated in the presented work. However, several interesting observations could be made. Among those, Synapsin-I-like immunoreactivity showed the presence of an anterior nerve ring (Fig. 7) consisting of the already described ventral commissure of the brain, always associated to a dorso-anterior brain commissure, with the entire ring usually being isolated from the main neuropil of the brain in several Gastrotricha (Schmidt-Rhaesa 2007). Interestingly, an anterior nerve ring, also showing Synapsin-I-like immunoreactivity, was found in the brain of *Diuronotus aspetos* (manuscript V). These observations showed that the addition of Synapsin-I-like immunoreactivity aids the frequent recovering of the dorsal and ventral brain commissure, which might be a shared character of all Gastrotricha. Additionally, more variation of the brain and nerve cord was found, as illustrated in the Fig. 7, with serotonin-like immunoreactivity among Gastrotricha. If the general morphology of the nervous system of Gastrotricha seems to be conserved, we hope and expect that the variation of the “minor” nerves will be of systematic importance, and will shed new light on the evolution of the nervous system within this group.

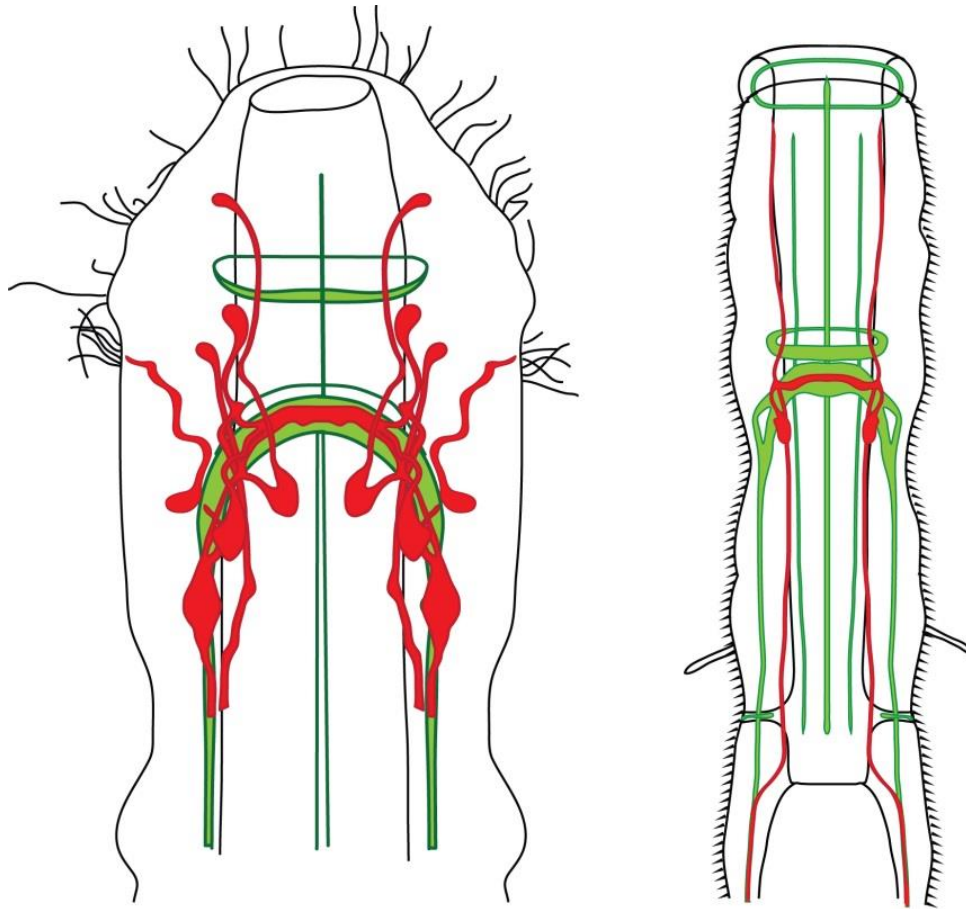


Figure 7: Schematic drawing of the anterior nervous system of two species of Macrodasyida interpreted from CLSM: *Paradasys subterraneus* on the left and *Acanthodasys* sp. on the right. Serotonin-like immunoreactivity in red and synapsin-I-like immunoreactivity in green. Note the association of the ventral commissure with a dorsal commissure, forming an anterior nerve ring, set anteriorly and apart from the brain neuropil.

## IX) Conclusion

The reconstruction of the morphology of the animals studied in this thesis shows that careful investigation of meiofaunal animals is necessary to give a comprehensible framework for understanding Spiralian evolution. Furthermore, the inclusion of several organ systems as presented in this thesis revealed the potential of exhaustive studies as compared to investigations of only a specific subset of organ systems. For instance, some new possible homologies between Rotifera and Micrognathozoa concern glands and ciliation patterns, organ systems rarely considered when it involves this phylogenetic depth (but see (Rieger 1976, Rieger 1981)). Yet, nervous system shows its potential for comparative studies as the assessment of the pharyngeal ganglion as a shared character of Gnathifera. Also, *Diuronotus* offers further illustration of the need of comprehensive descriptions: the nervous system appears to show some degrees of

conservation, making it easy to compare, with *Xenotrichula* (Rothe et al. 2011) or *Neodasys* (Rothe et al. 2011), which contrasts findings of the muscular system, more difficult to compare ( but see (Leasi et al. 2008)). Finally, the present work offers the phylogenetic placement and morphological description of *Lobatocerebrum* and Micrognathozoa, also giving new insights within Gastrotricha, filling a previously important knowledge gap in the incredibly diverse and still poorly understood Spiralia.

## X) References

- Ahlrichs, W. (1993). Ultrastructure of the protonephridia of *Seison annulatus* (Rotifera). *Zoomorphology* **113**(4): 245-251.
- Ahlrichs, W.H. (1993). On the protonephridial system of the brackish-water rotifer *Proales reinhardti* (Rotifera, Monogononta). *Microfauna Marina* **8**: 39-53.
- Ahlrichs, W.H. (1995). Ultrastruktur und Phylogenie von *Seison nebaliae* (Grube 1859) und *Seison annulatus* (Claus 1876), Göttingen. 310p.
- Ahlrichs, W.H. (1997). Epidermal ultrastructure of *Seison nebaliae* and *Seison annulatus*, and a comparison of epidermal structures within the Gnathifera. *Zoomorphology* **117**(1): 41-48.
- Andrade, S.C.S., Novo, M., Kawachi, G.Y., Worsaae, K., Pleijel, F., Giribet, G. and Rouse, G.W. (2015). Articulating 'Archiannelids': Phylogenomics and Annelid Relationships, with Emphasis on Meiofaunal Taxa. *Molecular Biology and Evolution* **32**(11): 2860-2875.
- Araujo, T.Q., Balsamo, M. and Garraffoni, A.R.S. (2014). A new species of *Pseudostomodella* (Gastrotricha, Thaumastodermatidae) from Brazil. *Marine Biodiversity* **44**(3): 243-248.
- Arendt, D., Denes, A.S., Jekely, G. and Tessmar-Raible, K. (2008). The evolution of nervous system centralization. *Royal Society Philosophical Transactions Biological Sciences* **363**(1496): 1523-1528.
- Ax, P. (1956). Die Gnathostomulida, eine rätselhafte Wurmgruppe aus dem Meeressand. Mainz,, Verlag der Akademie der Wissenschaften und der Literatur; in Kommission bei F. Steiner. 32p.
- Ax, P. (1996). Multicellular animals. A new approach to the phylogenetic order in nature. Volume 1. Berlin, Heidelberg etc., Springer-Verlag. 1-225p.
- Balsamo, M., Guidi, L., Ferraguti, M., Pierboni, L. and Kristensen, R.M. (2010). *Diuronotus aspetos* (Gastrotricha): new morphological data and description of the spermatozoon. *Helgoland Marine Research* **64**(1): 27-34.
- Bekkouche, N., Kristensen, R.M., Hejnol, A., Sørensen, M.V. and Worsaae, K. (2014). Detailed reconstruction of the musculature in *Limnognathia maerski* (Micrognathozoa) and comparison with other Gnathifera. *Frontiers in Zoology* **11**.
- Bekkouche, N., Kristensen, R.M., Hejnol, A., Sørensen, M.V. and Worsaae, K. (2015). The jaw musculature of Micrognathozoa, function and evolution. *Integrative and Comparative Biology* **55**: E13-E13.
- Brusca, R.C., Moore, W. and Shuster, M. (2016). Invertebrates, third edition. Massachusetts, USA, Sinauer Associates, Inc. 1103p.
- Cavalier-Smith, T. (1998). A revised six-kingdom system of life. *Biological Reviews (Cambridge)* **73**(3): 203-266.
- Clement, P. and Wurdak, E. (1991). Rotifera. *Microscopic anatomy of invertebrates. Volume 4: Aschelminthes*. Harrison, F. W. and Ruppert, E. E. New York, Chichester etc., Wiley-Liss: 219-297.
- De Smet, W.H. (2002). A new record of *Limnognathia maerski* Kristensen & Funch, 2000 (Micrognathozoa) from the subantarctic Crozet Islands, with redescription of the trophi. *Journal of Zoology (London)* **258**(3): 381-393.

- Dunn, C.W., Giribet, G., Edgecombe, G.D. and Hejnal, A. (2014). Animal Phylogeny and Its Evolutionary Implications. *Annual Review of Ecology Evolution and Systematics* **45**: 371-395.
- Dunn, C.W., Hejnal, A., Matus, D.Q., Pang, K., Browne, W.E., Smith, S.A., Seaver, E., Rouse, G.W., Obst, M., Edgecombe, G.D., Sorensen, M.V., Haddock, S.H.D., Schmidt-Rhaesa, A., Okusu, A., Kristensen, R.M., Wheeler, W.C., Martindale, M.Q. and Giribet, G. (2008). Broad phylogenomic sampling improves resolution of the animal tree of life. *Nature (London)* **452**(7188): 745-750.
- Edgecombe, G.D., Giribet, G., Dunn, C.W., Hejnal, A., Kristensen, R.M., Neves, R.C., Rouse, G.W., Worsaae, K. and Sørensen, M.V. (2011). Higher-level metazoan relationships: recent progress and remaining questions. *Organisms Diversity & Evolution* **11**(2): 151-172.
- Egger, B., Lapraz, F., Tomiczek, B., Mueller, S., Dessimoz, C., Girstmair, J., Skunca, N., Rawlinson, K.A., Cameron, C.B., Beli, E., Todaro, M.A., Gammoudi, M., Norena, C. and Telford, M.J. (2015). A Transcriptomic-Phylogenomic Analysis of the Evolutionary Relationships of Flatworms. *Current Biology* **25**(10): 1347-1353.
- Field, K.G., Olsen, G.J., Lane, D.J., Giovannoni, S.J., Ghiselin, M.T., Raff, E.C., Pace, N.R. and Raff, R.A. (1988). Molecular Phylogeny of the Animal Kingdom. *Science* **239**(4841): 748-753.
- Fontaneto, D. and De Smet, W. (2015). 4. Rotifera. *Handbook of Zoology, Gastrotricha and Gnathifera*. Schmidt-Rhaesa, A., De Gruyer. **3**.
- Funch, P. and Kristensen, R.M. (1995). Cycliophora is a new phylum with affinities to Entoprocta and Ectoprocta. *Nature (London)* **378**(6558): 711-714.
- Giribet, G. (2008). Assembling the lophotrochozoan (=spiralian) tree of life. *Royal Society Philosophical Transactions Biological Sciences* **363**(1496): 1513-1522.
- Giribet, G., Distel, D.L., Polz, M., Sterrer, W. and Wheeler, W.C. (2000). Triploblastic relationships with emphasis on the acoelomates and the position of Gnathostomulida, Cycliophora, Plathelminthes, and Chaetognatha: a combined approach of 18S rDNA sequences and morphology. *Systematic Biology* **49**(3): 539-562.
- Giribet, G., Hormiga, G. and Edgecombe, G.E. (2016). The meaning of categorical ranks in evolutionary biology. *Organisms Diversity & Evolution*.
- Giribet, G., Sørensen, M.V., Funch, P., Kristensen, R.M. and Sterrer, W. (2004). Investigations into the phylogenetic position of Micrognathozoa using four molecular loci. *Cladistics* **20**(1): 1-13.
- Halanych, K.M. (2004). The new view of animal phylogeny. *Annual Review of Ecology Evolution and Systematics* **35**: 229-256.
- Halanych, K.M. (2016). How our view of animal phylogeny was reshaped by molecular approaches: lessons learned. *Organisms Diversity & Evolution*(Special issue: The new animal phylogeny: The first 20 years).
- Harrison, F.W. and Ruppert, E.E. (1991). Microscopic anatomy of invertebrates. Volume 4. Aschelminthes, Wiley-Liss, New York, Chichester etc. i-xiv, 1-424p.
- Haszprunar, G., Rieger, R.M. and Schuchert, P. (1991). Extant 'Problematica' within or near the Metazoa. *The early evolution of Metazoa and the significance of problematic taxa. Proceedings of an International Symposium held at the University of Camerino 27- 31 March 1989*. Simonetta, A. M. and Conway Morris, S. Cambridge, New York etc., Cambridge University Press: 99-105.
- Hejnal, A. and Lowe, C.J. (2015). Embracing the comparative approach: how robust phylogenies and broader developmental sampling impacts the understanding of nervous system evolution. *Royal Society Philosophical Transactions Biological Sciences* **370**(1684): 20150045.
- Hejnal, A. and Martin-Duran, J.M. (2015). Getting to the bottom of anal evolution. *Zoologischer Anzeiger* **256**: 61-74.
- Hejnal, A., Obst, M., Stamatakis, A., Ott, M., Rouse, G.W., Edgecombe, G.D., Martinez, P., Baguna, J., Bailly, X., Jondelius, U., Wiens, M., Mueller, W.E.G., Seaver, E., Wheeler, W.C., Martindale, M.Q., Giribet, G. and Dunn, C.W. (2009). Assessing the root of bilaterian animals with scalable phylogenomic methods. *Proceedings of the Royal Society Biological Sciences Series B* **276**(1677): 4261-4270.
- Hennig, W. (1966). Phylogenetic systematics. Urbana ; London, University of Illinois Press. 263p.
- Higgins, R.P. and Thiel, H. (1988). Introduction to the study of meiofauna, Smithsonian Institution Press, Washington, D.C. 1-488p.

- Hochberg, R. (2006). On the serotonergic nervous system of two planktonic rotifers, *Conochilus coenobasis* and *C. dossuarius* (Monogononta, Flosculariacea, Conochilidae). *Zoologischer Anzeiger* **245**(1): 53-62.
- Hochberg, R. and Litvaitis, M.K. (2001). A muscular double helix in gastrotricha. *Zoologischer Anzeiger* **240**(1): 61-68.
- Hochberg, R. and Litvaitis, M.K. (2001). The musculature of *Draculiciteria tessalata* (Chaetonotida, Paucitubulatina): implications for the evolution of dorsoventral muscles in Gastrotricha. *Hydrobiologia* **452**(1-3): 155-161.
- Hummon, W.D. (1969). *Musellifer Sublitoralis* a New Genus and Species of Gastrotricha from San Juan Archipelago Washington. *Transactions of the American Microscopical Society* **88**(2): 282-286.
- Hummon, W.D. (2011). Marine Gastrotricha of the Near East: 1. Fourteen new species of Macrodasysida and a redescription of *Dactylopodola agadasys* Hochberg, 2003. *Zookeys*(94): 1-59.
- Hyman, L.H. (1951). The Invertebrates. Vol. 3, Acanthocephala, aschelminthes, and entoprocta : the pseudocoelomate bilateria. New York etc., McGraw-Hill Book Company. VII, 572p.
- Jenner, R.A. (2011). Use of Morphology in Criticizing Molecular Trees. *Journal of Crustacean Biology* **31**(2): 373-377.
- Jenner, R.A. and Littlewood, D.T.J. (2008). Problematica old and new. *Royal Society Philosophical Transactions Biological Sciences* **363**(1496): 1503-1512.
- Kånneby, T., Atherton, S. and Hochberg, R. (2014). Two new species of *Musellifer* (Gastrotricha: Chaetonotida) from Florida and Tobago and the systematic placement of the genus within Paucitubulatina. *Marine Biology Research* **10**(10): 983-995.
- Kerbl, A., Bekkouche, N., Sterrer, W. and Worsaae, K. (2015). Detailed reconstruction of the nervous and muscular system of Lobatocerebridae with an evaluation of its annelid affinity. *Bmc Evolutionary Biology* **15**.
- Kieneke, A. (2015). Record of the 'Arctic' marine gastrotrich *Diuronotus aspetos* (Paucitubulatina) from the southern North Sea. *Marine Biodiversity* **45**(4): 615-616.
- Kieneke, A., Ahlrichs, W.H., Arbizu, P.M. and Bartolomeaus, T. (2008). Ultrastructure of protonephridia in *Xenotrichula carolinensis syltensis* and *Chaetonotus maximus* (Gastrotricha: Chaetonotida): comparative evaluation of the gastrotrich excretory organs. *Zoomorphology* **127**(1): 1-20.
- Kieneke, A. and Hochberg, R. (2012). Ultrastructural observations of the protonephridia of *Polymerurus nodicaudus* (Gastrotricha: Paucitubulatina). *Acta Zoologica* **93**(1): 115-124.
- Kieneke, A., Riemann, O. and Ahlrichs, W.H. (2008). Novel implications for the basal internal relationships of Gastrotricha revealed by an analysis of morphological characters. *Zoologica Scripta* **37**(4): 429-460.
- Kieneke, A. and Schmidt-Rhaesa, A. (2015). 1. Gastrotricha. *Handbook of Zoology, Gastrotricha and Gnathifera*. Schmidt-Rhaesa, A., De Gruyer. **3**.
- Kocot, K.M. (2016). On 20 years of Lophotrochozoa. *Organisms Diversity & Evolution*(Special Issue: The new animal phylogeny: The first 20 years).
- Kotikova, E.A., Raikova, O.I., Flyatchinskaya, L.P., Reuter, M. and Gustafsson, M.K.S. (2001). Rotifer muscles as revealed by phalloidin-TRITC staining and confocal scanning laser microscopy. *Acta Zoologica* **82**(1): 1-9.
- Kristensen, R.M. (1983). Loricifera, a new phylum with Aschelminthes characters from the meiobenthos. *Journal of Zoological Systematics and Evolutionary Research* **21**(3): 163-180.
- Kristensen, R.M. (2002). An introduction to Loricifera, Cyclophora, and Micrognathozoa. *Integrative and Comparative Biology* **42**(3): 641-651.
- Kristensen, R.M. and Funch, P. (2000). Micrognathozoa: A new class with complicated jaws like those of Rotifera and gnathostomulida. *Journal of Morphology* **246**(1): 1-49.
- Kuhn, T.S. (1962). The structure of scientific revolutions. Chicago, University of Chicago Press. 172 pagesp.
- Lammert, V. (1985). The fine structure of protonephridia in Gnathostomulida and their comparison within Bilateria. *Zoomorphology* **105**(5): 308-316.
- Larsson, K. and Jondelius, U. (2008). Phylogeny of Catenulida and support for Platyhelminthes. *Organisms Diversity & Evolution* **8**(5): 378-387.

- Laumer, C.E., Bekkouche, N., Kerbl, A., Goetz, F., Neves, R.C., Sørensen, M.V., Kristensen, R.M., Hejno, A., Dunn, C.W., Giribet, G. and Worsaae, K. (2015). Spiralian Phylogeny Informs the Evolution of Microscopic Lineages. *Current Biology* **25**(15): 2000-2006.
- Laumer, C.E., Hejnol, A. and Giribet, G. (2015). Nuclear genomic signals of the "microturbellarian" roots of platyhelminth evolutionary innovation. *Elife* **4**.
- Lauri, A., Brunet, T., Handberg-Thorsager, M., Fischer, A.H.L., Simakov, O., Steinmetz, P.R.H., Tomer, R., Keller, P.J. and Arendt, D. (2014). Development of the annelid axochord: Insights into notochord evolution. *Science* **345**(6202): 1365-1368.
- Leasi, F., Neves, R.C., Worsaae, K. and Sørensen, M.V. (2012). Musculature of *Seison nebaliae* Grube, 1861 and *Paraseison annulatus* (Claus, 1876) revealed with CLSM: a comparative study of the gnathiferan key taxon Seisonacea (Rotifera). *Zoomorphology (Berlin)* **131**(3): 185-195.
- Leasi, F. and Ricci, C. (2010). Musculature of two bdelloid rotifers, *Adineta ricciae* and *Macrotrachela quadricornifera*: organization in a functional and evolutionary perspective. *Journal of Zoological Systematics and Evolutionary Research* **48**(1): 33-39.
- Leasi, F. and Todaro, M.A. (2008). The muscular system of *Musellifer delamarei* (Renaud-Mornant, 1968) and other chaetonotidans with implications for the phylogeny and systematization of the Paucitubulatina (Gastrotricha). *Biological Journal of the Linnean Society* **94**(2): 379-398.
- Manuel, M. (2009). Early evolution of symmetry and polarity in metazoan body plans. *Comptes Rendus Biologies* **332**(2-3): 184-209.
- Markevich, G.I. (1993). Phylogenetic-Relationships of Rotifera to Other Veriform Taxa. *Hydrobiologia* **255**: 521-526.
- Marlow, H., Tosches, M.A., Tomer, R., Steinmetz, P.R., Lauri, A., Larsson, T. and Arendt, D. (2014). Larval body patterning and apical organs are conserved in animal evolution. *BMC Biology* **12**: 7, 1-17.
- Mooi, R.D. and Gill, A.C. (2010). Phylogenies without Synapomorphies-A Crisis in Fish Systematics: Time to Show Some Character. *Zootaxa*(2450): 26-40.
- Müller, M.C.M. and Sterrer, W. (2004). Musculature and nervous system of *Gnathostomula peregrina* (Gnathostomulida) shown by phalloidin labeling, immunohistochemistry, and cLSM, and their phylogenetic significance. *Zoomorphology (Berlin)* **123**(3): 169-177.
- Petrov, N.B., Aleshin, V.V., Pegova, A.N., Ophitserov, M.V. and Slyusarev, G.S. (2010). New insight into phylogeny of Mesozoa: evidence from 18 and 28S rRNA genes. *Vestnik Moskovskogo Universiteta Seriya XVI Biologiya* **4**: 42-45.
- Prud'homme, B., de Rosa, R., Arendt, D., Julien, J.-F., Pajaziti, R., Dorresteijn, A.W.C., Adoutte, A., Wittbrodt, J. and Balavoine, G. (2003). Arthropod-like expression patterns of engrailed and wingless in the annelid *Platynereis dumerilii* suggest a role in segment formation. *Current Biology* **13**(21): 1876-1881.
- Remane, A. (1934). *Diurodrilus subterraneus* nov. spec., ein Archannelide aus dem Küstengrundwasser. *Schriften der Naturwissenschaftlichen Vereins für Schleswig-Holstein* **20**(2): 249.
- Rieger, R.M. (1976). Monociliated epidermal cells in Gastrotricha; significance for concepts of early metazoan evolution. *Zeitschrift Zool Syst EvolForsch* **14**(3): 198-226.
- Rieger, R.M. (1980). A new group of interstitial worms, Lobatocerebridae nov. fam. (Annelida) and its significance for metazoan phylogeny. *Zoomorphologie* **95**(1): 41-84.
- Rieger, R.M. (1981). Fine structure of the body wall, nervous system, and digestive tract in the Lobatocerebridae Rieger and the organization of the gliointerstitial system in Annelida. *Journal of Morphology* **167**(2): 139-165.
- Rieger, R.M. (1991). *Jennaria pulchra*, nov. gen. nov. spec., eine den psammobionten Anneliden nahestehende Gattung aus dem Küstengrundwasser von North Carolina. *Berichte des Naturwissenschaftlich-Medizinischen Vereins in Innsbruck* **78**: 203-215.
- Rieger, R.M. and Tyler, S. (1995). Sister-group relationship of Gnathostomulida and Rotifera-Acanthocephala. *Invertebrate Biology* **114**(2): 186-188.
- Riemann, O. and Ahlrichs, W.H. (2008). Ultrastructure and function of the mastax in *Dicranophorus forcipatus* (Rotifera: Monogononta). *Journal of Morphology* **269**(6): 698-712.

- Rothe, B.H., Kieneke, A. and Schmidt-Rhaesa, A. (2011). The nervous system of *Xenotrichula intermedia* and *X. velox* (Gastrotricha: Paucitubulatina) by means of immunohistochemistry (IHC) and TEM. *Meiofauna Marina* **19**: 71-88.
- Rothe, B.H., Schmidt-Rhaesa, A. and Kieneke, A. (2011). The nervous system of *Neodasys chaetonotoideus* (Gastrotricha: *Neodasys*) revealed by combining confocal laserscanning and transmission electron microscopy: evolutionary comparison of neuroanatomy within the Gastrotricha and basal Protostomia. *Zoomorphology* **130**(1): 51-84.
- Rundell, R.J. and Leander, B.S. (2010). Masters of miniaturization: Convergent evolution among interstitial eukaryotes. *Bioessays* **32**(5): 430-437.
- Ruppert, E.E. (1982). Comparative ultrastructure of the gastrotrich pharynx and the evolution of myoepithelial foreguts in Aschelminthes. *Zoomorphology (Berlin)* **99**(3): 181-220.
- Ruppert, E.E. (1991). Gastrotricha. *Microscopic anatomy of invertebrates. Volume 4: Aschelminthes*. Harrison, F. W. and Ruppert, E. E. New York, Chichester etc., Wiley-Liss: 41-109.
- Schmidt-Rhaesa, A. (2007). The evolution of organ systems. Oxford & New York, Oxford University Press. i-x, 1-385p.
- Schmidt-Rhaesa, A. (2015). Handbook of Zoology, Gastrotricha and Gnathifera, De Gruyer. 354p.
- Schmidt-Rhaesa, A., Harzsch, S. and Purschke, G. (2016). Structure and Evolution of Invertebrate Nervous Systems. Oxford, United Kingdom, Oxford University Press. 748p.
- Sielaff, M., Schmidt, H., Struck, T.H., Rosenkranz, D., Mark Welch, D.B., Hankeln, T. and Herlyn, H. (2016). Phylogeny of Syndermata (syn. Rotifera): Mitochondrial gene order verifies epizoic Seisonidea as sister to endoparasitic Acanthocephala within monophyletic Hemirotoifera. *Mol Phylogenet Evol* **96**: 79-92.
- Slyusarev, G.S. and Kristensen, R.M. (2003). Fine structure of the ciliated cells and ciliary rootlets of *Intoshia variabilis* (Orthonectida). *Zoomorphology (Berlin)* **122**(1): 33-39.
- Slyusarev, G.S. and Starunov, V.V. (2016). The structure of the muscular and nervous systems of the female *Intoshia linei* (Orthonectida). *Organisms Diversity & Evolution* **16**(1): 65-71.
- Sørensen, M.V. (2003). Further structures in the jaw apparatus of *Limnognathia maerski* (Micrognathozoa), with notes on the phylogeny of the Gnathifera. *Journal of Morphology* **255**(2): 131-145.
- Sørensen, M.V. (2005). Musculature in three species of *Proales* (Monogononta, Rotifera) stained with phalloidin-labeled fluorescent dye. *Zoomorphology* **124**(1): 47-55.
- Sørensen, M.V., Funch, P., Hooge, M. and Tyler, S. (2003). Musculature of *Notholca acuminata* (Rotifera: Ploima: Brachionidae) revealed by confocal scanning laser microscopy. *Invertebrate Biology* **122**(3): 223-230.
- Sørensen, M.V. and Giribet, G. (2006). A modern approach to rotiferan phylogeny: combining morphological and molecular data. *Molecular Phylogenetics and Evolution* **40**(2): 585-608.
- Sørensen, M.V., Sterrer, W. and Giribet, G. (2006). Gnathostomulid phylogeny inferred from a combined approach of four molecular loci and morphology. *Cladistics* **22**(1): 32-58.
- Sørensen, M.V., Tyler, S., Hooge, M.D. and Funch, P. (2003). Organization of pharyngeal hard parts and musculature in *Gnathostomula armata* (Gnathostomulida: Gnathostomulidae). *Canadian Journal of Zoology* **81**(9): 1463-1470.
- Sterrer, W. and Sørensen, M.V. (2015). 2. Phylum Gnathostomulida. *Handbook of Zoology, Gastrotricha and Gnathifera*. Schmidt-Rhaesa, A., De Gruyer. **3**.
- Struck, T.H., Golombek, A., Weigert, A., Franke, F.A., Westheide, W., Purschke, G., Bleidorn, C. and Halanych, K.M. (2015). The Evolution of Annelids Reveals Two Adaptive Routes to the Interstitial Realm. *Current Biology* **25**(15): 1993-1999.
- Struck, T.H., Wey-Fabrizius, A.R., Golombek, A., Hering, L., Weigert, A., Bleidorn, C., Klebow, S., Iakovenko, N., Hausdorf, B., Petersen, M., Kueck, P., Herlyn, H. and Hankeln, T. (2014). Platyzoan Paraphyly Based on Phylogenomic Data Supports a Noncoelomate Ancestry of Spiralia. *Molecular Biology and Evolution* **31**(7): 1833-1849.
- Telford, M.J., Budd, G.E. and Philippe, H. (2015). Phylogenomic Insights into Animal Evolution. *Current Biology* **25**(19): R876-R887.

- Todaro, M.A., Balsamo, M. and Kristensen, R.M. (2005). A new genus of marine chaetonotids (Gastrotricha), with a description of two new species from Greenland and Denmark. *Journal of the Marine Biological Association of the United Kingdom* **85**(6): 1391-1400.
- Todaro, M.A., Dal Zotto, M. and Leasi, F. (2015). An Integrated Morphological and Molecular Approach to the Description and Systematisation of a Novel Genus and Species of Macrodasysida (Gastrotricha). *PLoS ONE* **10**(7): e0130278.
- Todaro, M.A., Kanneby, T., Dal Zotto, M. and Jondelius, U. (2011). Phylogeny of Thaumastodermatidae (Gastrotricha: Macrodasysida) Inferred from Nuclear and Mitochondrial Sequence Data. *PLoS ONE* **6**(3): e17892, 17891-17813.
- Tyler, S. and Hooge, M.D. (2001). Musculature of *Gnathostomula armata* Riedl 1971 and its ecological significance. *Marine Ecology* **22**(1-2): 71-83.
- Vinther, J. (2015). Animal Evolution: When Small Worms Cast Long Phylogenetic Shadows. *Current Biology* **25**(17): R762-R764.
- Wanninger, A. (2007). The application of confocal microscopy and 3D imaging software in Functional, Evolutionary, and Developmental Zoology: reconstructing myo- and neurogenesis in space and time. *Modern Research and Educational Topics in Microscopy*. Mendez-Vilas, A. D., J. Bardajoz (Spain), Formatex: 353-361.
- Weigert, A.B., C. (2016). Current status of annelid phylogeny. *Organisms Diversity & Evolution*(Special Issue. The new animal phylogeny: The first 20 years).
- Westheide, W. (1990). Polychaetes: interstitial families. Keys and notes for the identification of the species. *Synopses of the British Fauna New Series*: 1-152.
- Wey-Fabrizius, A.R., Herlyn, H., Rieger, B., Rosenkranz, D., Witek, A., Welch, D.B.M., Ebersberger, I. and Hankeln, T. (2014). Transcriptome Data Reveal Syndermatan Relationships and Suggest the Evolution of Endoparasitism in Acanthocephala via an Epizotic Stage. *PLoS ONE* **9**(2): e88618, 88611-88611.
- Wiedermann, A. (1995). On the ultrastructure of the nervous system in *Cephalodasys maximus* (Macrodasysida, Gastrotricha). Zur Ultrastruktur des Nervensystems bei *Cephalodasys maximus* (Macrodasysida, Gastrotricha). *Microfauna Marina* **10**: 173-233.
- Wilts, E.F., Wulfken, D. and Ahlrichs, W.H. (2010). Combining confocal laser scanning and transmission electron microscopy for revealing the mastax musculature in *Bryceella stylata* (Milne, 1886) (Rotifera: Monogononta). *Zoologischer Anzeiger* **248**(4): 285-298.
- Wilts, E.F., Wulfken, D., Ahlrichs, W.H. and Arbizu, P.M. (2012). The musculature of *Squatinella rostrum* (Milne, 1886) (Rotifera: Lepadellidae) as revealed by confocal laser scanning microscopy with additional new data on its trophi and overall morphology. *Acta Zoologica* **93**(1): 14-27.
- Witek, A., Herlyn, H., Ebersberger, I., Welch, D.B.M. and Hankeln, T. (2009). Support for the monophyletic origin of Gnathifera from phylogenomics. *Molecular Phylogenetics and Evolution* **53**(3): 1037-1041.
- Worsaae, K. and Rouse, G.W. (2008). Is *Diurodrilus* an annelid? *Journal of Morphology* **269**(12): 1426-1455.
- Wulfken, D. and Ahlrichs, W.H. (2012). The ultrastructure of the mastax of *Filinia longiseta* (Flosculariaceae, Rotifera): Informational value of the trophi structure and mastax musculature. *Zoologischer Anzeiger* **251**(4): 270-278.
- Wulfken, D., Wilts, E.F., Martinez-Arbizu, P. and Ahlrichs, W.H. (2010). Comparative analysis of the mastax musculature of the rotifer species *Pleurotrocha petromyzon* (Notommatidae) and *Proales tillyensis* (Proalidae) with notes on the virgate mastax type. *Zoologischer Anzeiger* **249**(3-4): 181-194.
- Zrzavý, J. (2003). Gastrotricha and metazoan phylogeny. *Zoologica Scripta* **32**(1): 61-82.
- Zrzavý, J., Hypsa, V. and Tietz, D.F. (2001). Myzostomida are not annelids: molecular and morphological support for a clade of animals with anterior sperm flagella. *Cladistics* **17**(2): 170-198.
- Zrzavý, J., Riha, P., Pialek, L. and Janouskovec, J. (2009). Phylogeny of annelida (Lophotrochozoa): total-evidence analysis of morphology and six genes. *BMC Evolutionary Biology* **9**: 14.

## Articles and manuscripts

**Manuscript I: Spiralian Phylogeny Informs the Evolution of Microscopic Lineages.**

Laumer, C. E., Bekkouche, N., Kerbl, A., Goetz, F., Neves, R. C., Sørensen, M. V., Kristensen, R. M., Hejnol, Dunn C. W., Giribet G. and Worsaae K. (published)

**Manuscript II: Detailed reconstruction of the nervous and muscular system of Lobatocerebridae with an evaluation of its annelid affinity.** Kerbl A., Bekkouche N.,

Sterreri W., and Worsaae K. (published)

**Manuscript III: Detailed reconstruction of the musculature in *Limnognathia maerski* (Micrognathozoa) and comparison with other Gnathifera.** Bekkouche N.,

Kristensen R. M., Hejnol A., Sørensen M. V., and Worsaae, K. (published)

**Manuscript IV: Nervous system and ciliary structures of Micrognathozoa (Gnathifera) – evolutionary insight from an early branch in Spiralia.** Bekkouche N.,

and Worsaae K. (submitted)

**Manuscript V: Neuromuscular study of early branching *Diuronotus aspetos* (Paucitubulatina) gives insight on the evolution of organs system within**

**Gastrotricha.** Bekkouche N., and Worsaae K. (submitted)



**Manuscript I:**

**Spiralian Phylogeny Informs the Evolution of Microscopic Lineages**

Laumer, C. E., Bekkouche, N., Kerbl, A., Goetz, F., Neves, R. C., Sørensen, M. V., Kristensen, R. M., Hejnol., Dunn C. W., Giribet G. and Worsaae K.

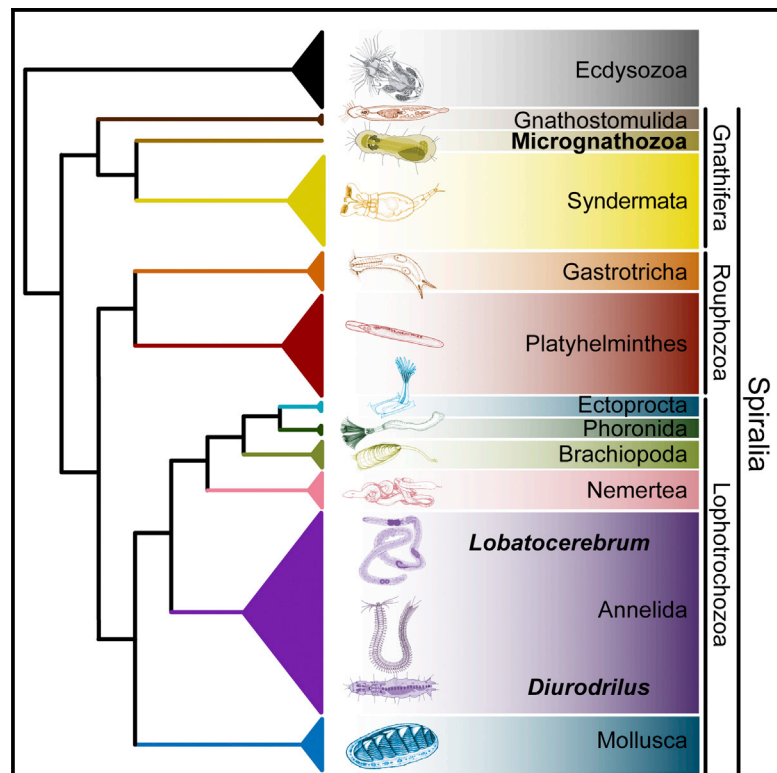
Current Biology, Volume 25, issue 15, Pages 2000-2006



# Current Biology

## Spiralian Phylogeny Informs the Evolution of Microscopic Lineages

### Graphical Abstract



### Authors

Christopher E. Laumer, Nicolas Bekkouche, Alexandra Kerbl, ..., Casey W. Dunn, Gonzalo Giribet, Katrine Worsaae

### Correspondence

claumer@ebi.ac.uk

### In Brief

Laumer et al. reconstruct the phylogeny of Spiralia, the animal group including molluscs, annelids, flatworms, and many microscopic worms. The new tree suggests that some previously unsampled, interstitial Problematica originated through miniaturization from large-bodied ancestors but also implies a primarily interstitial origin for many lineages.

### Highlights

- *Diurodrilus* and *Lobatocerebrum*, two problematic meiofauna, are miniaturized annelids
- Micrognathozoa, the newest-described animal phylum, is the sister group of Rotifera
- Bayesian mixture models recover strong support for deep spiralian relationships
- Two clades comprising Platyzoa form separate early branches in Spiralia



# Spiralian Phylogeny Informs the Evolution of Microscopic Lineages

Christopher E. Laumer,<sup>1,7,\*</sup> Nicolas Bekkouche,<sup>2</sup> Alexandra Kerbl,<sup>2</sup> Freya Goetz,<sup>3</sup> Ricardo C. Neves,<sup>4</sup> Martin V. Sørensen,<sup>5</sup> Reinhardt M. Kristensen,<sup>5</sup> Andreas Hejnol,<sup>6</sup> Casey W. Dunn,<sup>3</sup> Gonzalo Giribet,<sup>1</sup> and Katrine Worsaae<sup>2</sup>

<sup>1</sup>Department of Organismic and Evolutionary Biology, Museum of Comparative Zoology, Harvard University, 26 Oxford Street, Cambridge, MA 02138, USA

<sup>2</sup>Marine Biological Section, Department of Biology, University of Copenhagen, Universitetsparken 4, 2100 Copenhagen Ø, Denmark

<sup>3</sup>Department of Ecology and Evolutionary Biology, Brown University, Providence, RI 02906, USA

<sup>4</sup>Biozentrum, University of Basel, Klingelbergstrasse 50, 4056 Basel, Switzerland

<sup>5</sup>Natural History Museum of Denmark, Universitetsparken 15, 2100 Copenhagen Ø, Denmark

<sup>6</sup>Sars International Centre for Marine Molecular Biology, University of Bergen, Thormøhlensgate 55, 5008 Bergen, Norway

<sup>7</sup>Present address: The EMBL European Bioinformatics Institute (EMBL-EBI) and the Wellcome Trust Sanger Institute (WTSI), Wellcome Trust Genome Campus, Hinxton, Cambridgeshire CB10 1SD, UK

\*Correspondence: [claumer@ebi.ac.uk](mailto:claumer@ebi.ac.uk)

<http://dx.doi.org/10.1016/j.cub.2015.06.068>

## SUMMARY

Despite rapid advances in the study of metazoan evolutionary history [1], phylogenomic analyses have so far neglected a number of microscopic lineages that possess a unique combination of characters and are thus informative for our understanding of morphological evolution. Chief among these lineages are the recently described animal groups Micrognathozoa and Loricifera, as well as the two interstitial “Problematica” *Diurodrilus* and *Lobatocerebrum* [2]. These genera show a certain resemblance to Annelida in their cuticle and gut [3, 4]; however, both lack primary annelid characters such as segmentation and chaetae [5]. Moreover, they show unique features such as an inverted body-wall musculature or a novel pharyngeal organ. This and their ciliated epidermis have led some to propose relationships with other microscopic spiralian, namely Platyhelminthes, Gastrotricha, and in the case of *Diurodrilus*, with Micrognathozoa [6, 7]—lineages that are grouped by some analyses into “Platyzoa,” a clade whose status remains uncertain [1, 8–11]. Here, we assess the interrelationships among the meiofaunal and macrofaunal members of Spiralia using 402 orthologs mined from genome and transcriptome assemblies of 90 taxa. *Lobatocerebrum* and *Diurodrilus* are found to be deeply nested members of Annelida, and unequivocal support is found for Micrognathozoa as the sister group of Rotifera. Analyses using site-heterogeneous substitution models further recover a lophophorate clade and position Loricifera + Priapulida as sister group to the remaining Ecdysozoa. Finally, with several meiofaunal lineages branching off early in the diversification of Spiralia, the emerging concept of a microscopic,

acoelomate, direct-developing ancestor of Spiralia is reviewed.

## RESULTS

Understanding metazoan evolutionary history requires resolving the phylogenetic positions of not only the major animal groups but also of more obscure lineages showing unique character combinations. Examples of such important “Problematica” are Lobatocerebromorpha [3, 12, 13], Diurodrilida [4, 5], Micrognathozoa [6, 7], and Loricifera [14], representing among the smallest animals ever discovered, which have received phylum-level affiliations or remain of uncertain position within Protostomia. We present here the first nuclear protein-coding data from representatives of all four clades, incorporating these and other new and published protein-coding surveys into a 402-ortholog, 90-taxon supermatrix comprising all free-living lineages of Spiralia (Table S1). Phylogenetic analyses of this matrix were performed using maximum likelihood (ML; Figures 1 and S1), with partitioned analyses of the full-size matrix (Figure 1A) and unpartitioned analyses of two submatrices constructed to investigate putative long-branch attraction (LBA) artifacts (Figures 1B and 1C). To further control for other potential systematic artifacts, we also undertook analyses using Bayesian inference (BI) under a site-heterogeneous mixture model (CAT + GTR +  $\Gamma$ 4; [15]), using a matrix groomed of unstable taxa and sites showing evidence of compositional non-stationarity (Figure 2). Bayesian analyses of the complete matrix were also performed (Figure S2).

The ML and BI analyses differ, at least superficially, in the topology they present for deep spiralian interrelationships. Our ML trees from partitioned analyses of the full matrix (Figure 1A) and from analyses of a slow-evolving subset of the full matrix (Figure 1B) are nearly identical and recapitulate results found in previous large-scale ML investigations of spiralian phylogeny [10, 11], e.g., monophyly of Trochozoa, Platyzoa, and Polyzoa [1, 15]. In contrast, analyses of a fast-evolving subset (Figure 1C) of this matrix do not recover the monophyly of Platyzoa, Polyzoa, or even Ecdysozoa. In general, however, few relevant clades

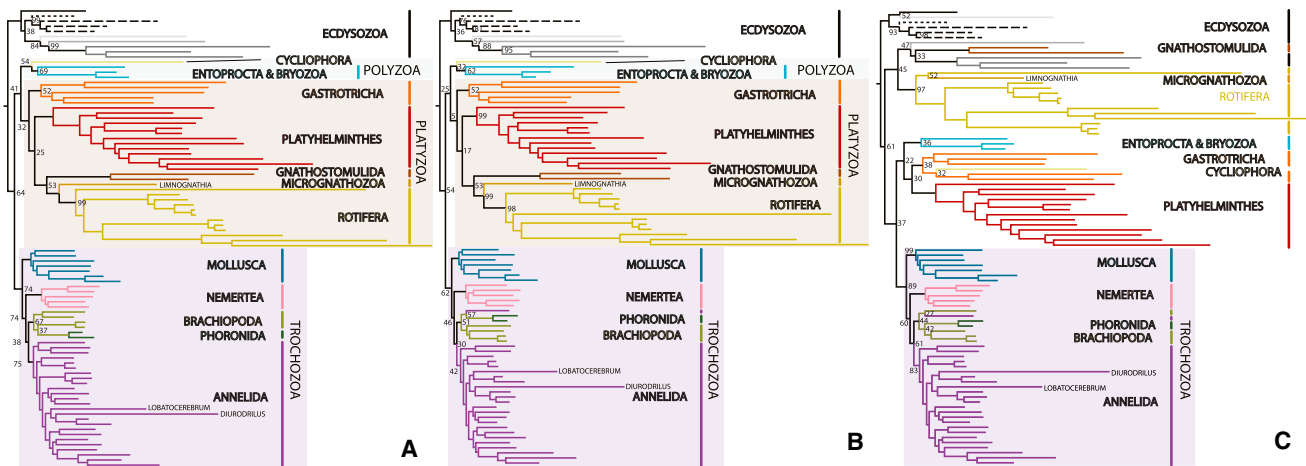


**Figure 1. Maximum Likelihood Inference of Spiralian Interrelationships from the Complete Matrix and Two Submatrices Stratified by Evolutionary Rate**

Maximum likelihood (ExaML v.3.0.0) phylograms inferred from the 402-gene, 79,954-amino-acid (aa) supermatrix (57.57% missing data).

(A) Partitioned analysis (from PartitionFinderProtein v.1.1.1) inferred from the total matrix.

(B) LG4M + F analysis from a submatrix comprising all but the fastest-evolving quartile of variable sites (20,167 aa).

(C) LG4M + F analysis from a submatrix comprising all but the slowest-evolving quartile of variable sites (20,293 aa).

Nodal values (given only to show support for the monophyly and interrelationships of the labeled major clades, i.e., not depicting support for intra-phylum relationships) reflect frequency of clades in a set of 100 bootstrap trees; clades with full support are not labeled. For labeled terminal taxa and full support values, refer to Figure S1 and the data Dryad accession.

find strong support in any ML analysis, with even several uncontroversially monophyletic taxa (e.g., Annelida, Gastrotricha) failing to see strong support (Figure 1). In contrast, the BI analyses under a site-heterogeneous model (CAT + GTR +  $\Gamma$ 4) find strong support for many spiralian clades, including all those that are also supported in the ML analyses, but also for Spiralia, Gnathifera, and Lophotrochozoa, among others (Figure 2). Thus, while the ML trees and BI consensus phylograms topologically differ, there is no evidence of strongly supported incongruence between ML and BI. Most importantly, BI places both *Diurodrilus* and *Lobatocerebrum* as deeply nested members of Annelida (as does ML, although with lesser support). Finally, BI also finds strong support for the non-monophyly of “Platyzoa,” with Gnathifera forming the earliest-diverging branch (Figures 2 and S2). Platyzoan non-monophyly is also recovered under ML in our fastest-evolving matrix subset (Figure 1C), but support for basal relationships is poor in this analysis.

The BI analyses of the trimmed (Figure 2) and untrimmed (Figure S2) matrices differ in only few respects. Platyhelminthes + Gastrotricha (called Rousphozoa in [11]) and Lophotrochozoa (in the sense of its original definition by [16] and not the looser common usage introduced by [17]) are supported in the trimmed matrix, but not the untrimmed matrix. Mixture model inference on both matrices, in sharp contrast to our ML analyses, also recovers the monophyly of the lophophorate phyla with high support, with Phoronida (here as in [18]) forming the sister group of Bryozoa. Mollusca was recovered as the sister group to the other Lophotrochozoa (in marked contrast to recent studies [11, 18]), albeit with weak support in the complete matrix (Figure S2). Indeed, the only strongly supported deep topological difference observed between analyses of the trimmed versus complete matrix concerns the position of Nemertea, which forms the sister

taxon of Annelida in the untrimmed matrix (Figure S2), or of the lophophorate clade in the trimmed matrix (Figure 2). Remarkably, in the complete matrix, we see no support for the hypothesis previously suggested by both molecules and morphology [18–20] of a sister-group relationship between Cyclophora and Entoprocta (the latter being instead recovered as sister group to Bryozoa; [21]); here, Cyclophora falls, but with low posterior probability (pp; pp = 0.5), as the sister group of Lophotrochozoa (Figure S2), a result perhaps related to the poor sequencing depth of this transcriptome.

Within Ecdysozoa, we find strong support under BI analysis of the untrimmed matrix (Figure S2) only for Onychophora + Arthropoda and Tardigrada + Nematoda, as found in a recent study focused on Ecdysozoa [22]. However, in the trimmed matrix (Figure 2), support (pp = 0.98) also emerges for a scenario in which the meiofaunal Loricifera fall together with our other scalidophoran representative, Priapulida, as the sister group to other members of Ecdysozoa. Although evidence for Scalidophora itself is poor (pp = 0.78), and we lack a representative of Kinorhyncha, this is the first time molecular data have recovered a clade of Loricifera + Priapulida, two taxa that share many common morphological traits [23].

## DISCUSSION

### *Diurodrilus* and *Lobatocerebrum* Are Miniaturized Annelids

The deeply nested positions of *Diurodrilus* and *Lobatocerebrum* within Annelida suggest independent miniaturizations of these lineages from an indirect-developing, macrofaunal annelid ancestor. *Diurodrilus* has traditionally been considered a member of Archannelida [4, 24], a taxon of morphologically simple

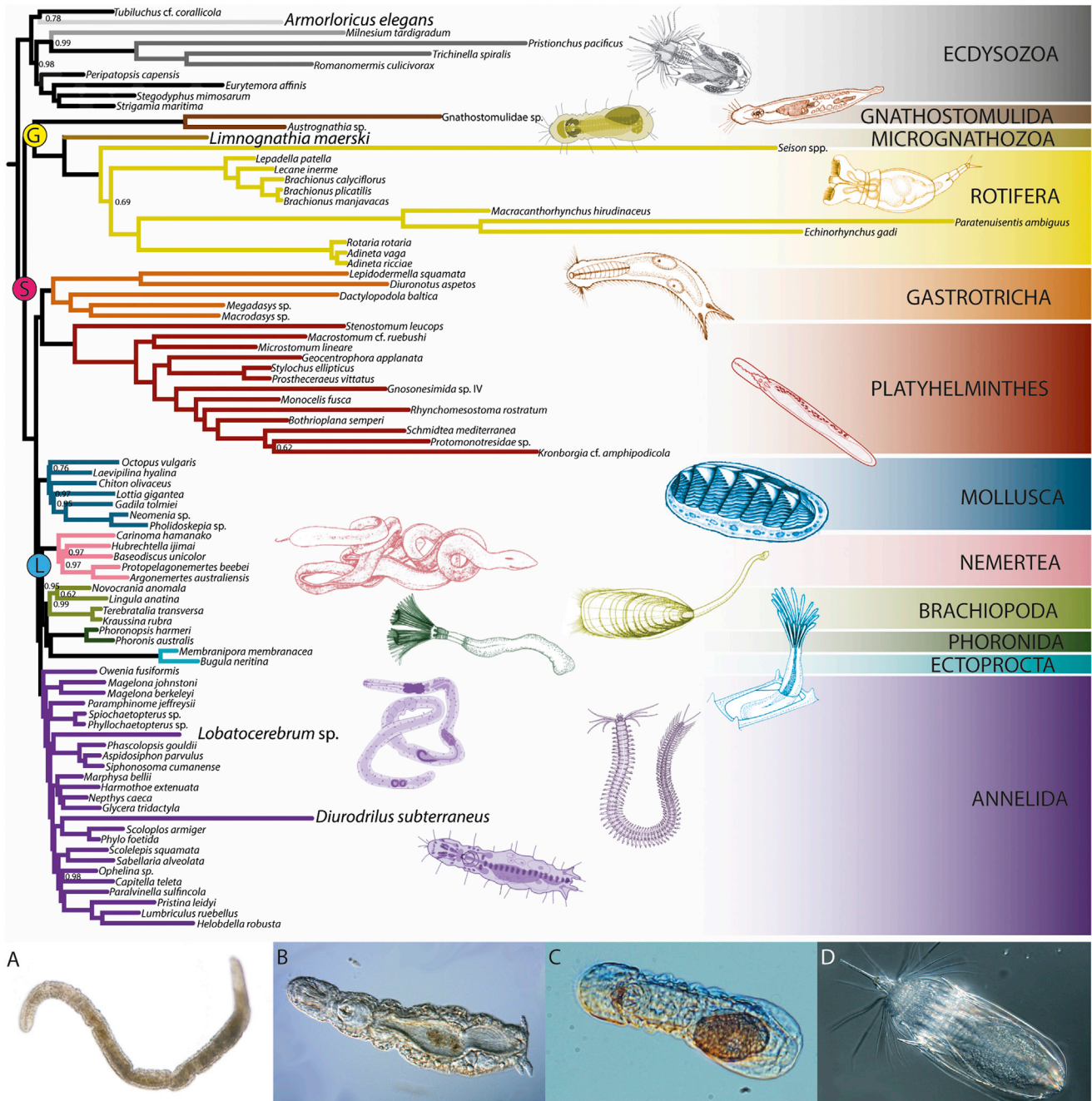


**Figure 2. Bayesian Mixture Model Inference of Spiralian Interrelationships, with Special Reference to the Placement of Problematic Interstitial Taxa**

Bayesian inference of the interrelationships among taxa of Spiralia in the 88-taxon “trimmed” matrix (72,243 aa, 58.17% missing data), made by PhyloBayes-MPI v.1.4e, under the CAT + GTR +  $\Gamma$ 4 mixture model. Nodal support values represent posterior probability; completely supported nodes are unlabeled. G, Gnathifera; L, Lophotrochozoa; S, Spiralia. Inset at lower right: selected images of problematic interstitial meiofauna placed in this phylogenetic analysis.

- (A) Adult *Lobatocerebrum* sp. from Bird Island, Bocas del Toro, Panama; differential interference contrast (DIC) optics.
- (B) Adult *Diurodrilus* sp. from Bailey’s Rock, Nahant, Massachusetts; DIC optics.
- (C) Adult *Limnognathia maerski* with egg from Isunngua Spring, Disko Island, Greenland; DIC optics.
- (D) Adult of *Armorialicus elegans* from Roscoff, France; DIC optics.

interstitial annelids originally considered “ancestral” to the other annelid taxa [25, 26], other members of which have recently been shown to be non-monophyletic and derived from macrofaunal ancestors [27, 28]. However, for *Diurodrilus*, several authors have also proposed a relationship outside of Annelida, specifically to the recently discovered Micrognathozoa, with which

they share, e.g., characteristic mid-ventral trunk ciliophores and a ventral muscular plate of the pharynx [5–7]. Equally complicated is the case of *Lobatocerebrum*, originally described as “a turbellariomorph member of the annelid line of evolution” [3], i.e., an intermediate between Platyhelminthes and Annelida—a position maintained by Rieger [12] and Hazprunar et al. [2] (who erected for it the phylum Lobatocerebromorpha), which we aimed to test here.

None of these hypotheses are supported in the present study. The precise position in which we recovered *Diurodrilus* within Annelida—as sister taxon to the macrofaunal Orbiniidae—has also been supported by ML analysis of mitogenomic data (although curiously, orbiniids appear more distant in gene order analyses) [29]. Remarkably, in previous rRNA-based phylogenetic studies orbiniids have been recovered as relatives of Parerodrilidae, another meiofaunal annelid lineage [30]. However, *Diurodrilus* shows with its apomorphic pharyngeal organ, adhesive toes, and ventral ciliophores no close resemblance to any known orbiniid, adult, larval or juvenile [29, 31]. Indeed, it represents the most “reduced” annelid to date, both sexes being of microscopic size and lacking all common annelid traits such as segmentation, coelomic cavities, chaetae, and nuchal organ [26]. With respect to *Lobatocerebrum*, we find it strongly supported as the sister group of Sipuncula [32], constituting an intriguing clade of unsegmented annelids; however, there are no other obvious synapomorphies for the two groups.

*Lobatocerebrum* and *Diurodrilus* share gross anatomical characteristics with many interstitial annelids, most prominent among these being an acoelomate or pseudocoelomate condition (with coincident protonephridia and absence of a vascular system). This organization may be related to small body size and can arise homoplastically as the consequence of diverse processes, such as an enlarged peritoneal lining and/or endoderm, or lack of cavity formation within the mesoderm [26, 33–35]. These different manifestations of an acoelomate condition, as well as the apparent independent origin of *Lobatocerebrum*, *Diurodrilus*, and most other interstitial annelid families [26, 28, 31] indicate that their miniaturizations do not follow a predictable pattern. Accordingly, it cannot easily be explained by the popular theory of progenesis [31], especially considering their lack of specific resemblance to larval or juvenile stages of macrofaunal relatives (e.g., Orbiniidae). Regardless of the mechanism of their reduction, however, our recovered placement of *Diurodrilus* and *Lobatocerebrum* within Annelida contributes to the enormous morphological disparity of this taxon, together with the recent positioning of other aberrant annelids such as Sipuncula, Echiura, Myzostomida, and Pogonophora [27].

### Micrognathozoa Is Sister Group to Rotifera within Gnathifera

All our analyses supported monophyletic Gnathifera—a clade composed of protostomes with a special type of cuticular jaws—with Micrognathozoa as the sister group of Rotifera, both constituting the sister group of Gnathostomulida (Figures 1 and 2). Despite the microscopic size and understudied biology of most gnathiferan lineages (e.g., male micrognathozoans having not been observed), this topology has been supported previously with morphological data [6, 36, 37], albeit not using conventional molecular markers [38]. The main synapomorphies of

Rotifera + Micrognathozoa have been uncovered in ultrastructural studies of the epidermis [39] and of the jaw apparatus composed of rod-like structures [37], with Rotifera + Micrognathozoa having some common supporting musculature [7].

### “Platyzoa” Is Likely a Systematic Artifact

Our mixture model analyses reject the monophyly of Platyzoa [8], a grouping of mainly interstitial taxa whose only shared characteristics, such as minute size (excepting some secondarily large Platyhelminthes and the acanthocephalan Rotifera; [40]), direct development, external ciliation, and an acoelomate or pseudocoelomate condition, are features also found in many other animals. The poorly supported division between Platyzoa/Polyzoa and Trochozoa, which we recover only under ML (Figure 1), neatly correlates (with the exceptions of *Diurodrilus* and *Lobatocerebrum*) with a division between fast-evolving and slow-evolving spiralian, suggesting the possibility of an LBA artifact [11]. Further, even though under both phylogenetic methods the problematic *Diurodrilus* and *Lobatocerebrum* are recovered as deeply nested annelids, the positions of these taxa within Annelida differ between reconstruction methods, with ML (Figure 1) placing these fast-evolving lineages in close proximity, consistent also with an LBA effect. It is remarkable that even the use of a statistically well-justified partitioning scheme, as provided by the PartitionFinder algorithm [41], groups the fast-evolving interstitial taxa into a clade (Figure 1). Only under the CAT + GTR +  $\Gamma$ 4 mixture model do we recover non-monophyly of this long-branched assemblage, consistent with previous observations that such flexible models better fit the substitution-pattern heterogeneity characteristic of such large matrices, thereby rendering them more robust to model misspecification and subsequent LBA [42]. Apparently the relevant substitution process heterogeneities in such data may be occurring not between genes but between sites within genes (at, e.g., the domain level; [43]).

Interestingly, a similar resolution of “Platyzoa” as non-monophyletic has also been proposed in another recent study [11], also using RNA sequencing libraries as a source of phylogenetic evidence (several of which we reanalyze here with distinct assembly and orthology assignment algorithms). However, in this study, such a topology only emerged under consideration of specific gene and taxon subsets, and even then, no single analysis offered strong resampling support for all newly introduced clades (i.e., “Rouphozoa” and “Platytrchozoa”). Indeed, choosing to exclude specific data subsets may at times prove positively misleading: for instance, ML analysis of our fastest-evolving submatrix recovers a topology (albeit with low support) similar to our BI analyses (Figure 1C). This may thus be seen as an argument in favor of a “total evidence” approach to phylogenetics even at this scale of inference; although fast-evolving sites and genes may indeed mislead simple reconstruction methods, they may also retain valuable phylogenetic signal [44].

### Was the Spiralian Ancestor a Microscopic, Acoelomate, Direct-Developing Worm?

The colonization of the interstices of marine sediments is among the most successful modes of life employed by metazoans, with nearly every major animal clade having at least some interstitial representatives and some being known exclusively from this habitat [45–47]. Animals that have adapted to such lifestyles,

sometimes known as meiofauna, bear a common set of characteristics, being generally of microscopic size, direct developing, with limited reproductive output and lifespan, and showing, relative to larger metazoans, a simplified, often acoelomate body design. Phylogenetic discussions regarding such meiofauna, including the members of “Platyzoa” [34], interstitial Annelida [3, 31], and other taxa such as the acoelomorph flatworms [48], have centered on the question of whether these morphologically “simple” taxa have originated via miniaturization from a macrofaunal ancestor, or have instead inherited their simple morphology from ancestors with similarly microscopic adults.

In this contribution, we aimed to address these themes within the major metazoan clade Spiralia, by resolving the interrelationships between the meiofaunal and macrofaunal members of this clade, including genome and transcriptome sampling of a range of previously sparsely sampled (Gnathostomulida) or unsampled microscopic taxa (Catenulida, Micrognathozoa, Chaetonotida, Lobatocerebridae, Diurodrilidae). Under a phylogenetic mixture model (Figure 2), we find uniformly strong support for a topology in which a monophyletic Gnathifera forms the sister group to all other spiralian, with the remaining members of Spiralia split between a clade of, on the one hand, Platyhelminthes and Gastrotricha, and on the other, Lophotrochozoa. A parsimonious reading of this topology posits the common features of these interstitial worms as plesiomorphies, implying an interstitial, direct developing, unsegmented, acoelomate or pseudocoelomate condition for the spiralian ancestor. This further implies multiple independent origins of, e.g., segmentation, coelomic cavities, planktotrophic larvae, and other morphological structures across Bilateria.

However, under the topology recovered here, only two separate reductions in body size (miniaturizations) and transitions to an acoelomate condition—perhaps, though not necessarily, via progenesis—are required to derive Gnathifera and Rousphozoa from a macrofaunal, coelomate spiralian ancestor. If miniaturized taxa such as *Lobatocerebrum* and *Diurodrilus* have separate origins within Annelida, might not Gnathifera and Rousphozoa, clades that evince rather distinct manifestations of the acoelomate condition [17], therefore also be the remaining survivors of two ancient miniaturization events [13, 48, 49]? The principle of parsimony casts doubt on this scenario, as it posits the existence and independent extinction of two separate macrofaunal lineages related to both branches of “Platyzoa,” a suggestion for which there is no fossil evidence, despite the widespread availability of exceptionally preserved Cambrian fossils of most other soft-bodied macrofaunal bilaterian lineages. This being recognized, there are continued arguments from comparative developmental genetic studies (reviewed by [50]) for homology across Bilateria in traits seemingly specific to macrofaunal animals, most recently extending to larval apical organs [51], a complex, tripartite forebrain [52], and collagenous midline supportive structures [53]. Unfortunately, the interpretation of such studies remains biased by the absence of data on the expression and function of developmental genes during the embryogenesis of gnathiferans, platyhelminths, and gastrotrichs.

Comparisons to outgroup taxa are critical to understanding the nature of the ancestor of Spiralia and earlier branches (Protostomia, and Bilateria). Ecdysozoa, one of two possible out-

groups to Spiralia [1], encompasses substantial body plan diversity, and the relationships within this clade remain incompletely understood. However, it is possibly suggestive in this context that in this analysis as well as others [22], the members of Scaliophora, a clade of primarily interstitial, largely acoelomate or pseudocoelomate animals, are supported as sister taxon to other ecdysozoans. The precise placement of two other extant vermiform taxa—the enigmatic chaetognaths, representing a likely distinct branch of protostomes in their own right [54], and the acoelomorph flatworms (with or without *Xenoturbella*), representing either early-branching bilaterians or deuterostomes of uncertain precise placement [1]—may also provide some additional signal required to test the homology of the traits common to the “platyzoan” taxa. With the continued availability of genomic and genome-informed datasets from representatives of problematic taxa such as those presented here, we are approaching a clearer picture of the relationships, limits, and shared derived characteristics of not only these microscopic groups but also the most familiar branches of the metazoan tree. The evidence presented here has yielded the first well-resolved spiralian phylogeny inclusive of all free-living groups and hence provides clear hypotheses for future investigations to test, not least among which is the supposition that the ancestor of Spiralia was most probably a meiofaunal animal, as this is the predominant lifestyle of the two earliest-branching lineages within this diverse clade.

#### ACCESSION NUMBERS

See Table S1 for a full list of SRA accession numbers for previously unreported data.

#### SUPPLEMENTAL INFORMATION

Supplemental Information includes Supplemental Experimental Procedures, two figures, and one table and can be found with this article online at <http://dx.doi.org/10.1016/j.cub.2015.06.068>.

#### AUTHOR CONTRIBUTIONS

C.E.L., K.W., and G.G. conceived the study. K.W., N.B., A.K., M.V.S. R.C.N., R.M.K., and A.H. collected specimens for RNA sequencing. A.H., C.E.L., C.W.D., K.W., and F.G. produced and sequenced cDNA libraries. A.K., A.H., C.E.L., N.B., and K.W. produced and improved all figures.

#### ACKNOWLEDGMENTS

We thank Yale Passamaneck for contributing samples used to sequence *Phoronopsis harmeri*; Sónia Andrade and Felipe Zapata for providing Trinity assemblies for our other represented Nemertea, Phoronida, and Mollusca; Chong Wang for providing a multisource assembly for *Milnesium tardigradum*; Tors-ten Struck for providing unfiltered raw data from numerous platyzoan taxa; Greg Edgecombe, Greg Rouse, and Wolfgang Sterrer for collecting with many of us in a Greenland expedition, before techniques for sequencing transcriptomes of such small animals were optimized; Aina Børve, Bruno Vellutini, and Chema Martin-Duran for the collection of *Membranipora membranacea* and *Terebratalia transversa*; Bob Freeman and Paul Edmon from the Research Computing staff at Harvard University for providing support on the Odyssey 2 cluster; and Claire Reardon and Christian Daly for offering a free MiSeq run used to provide data for *Symbion americanus*. Sequencing costs at Harvard were supported by internal funds from The Museum of Comparative Zoology to G.G. Additional sequencing costs and salaries of A.K. and N.B. were supported by the Villum Foundation (grant no. 102544). The fieldwork in Greenland

was supported by the Carlsberg Foundation (grant no. 2009\_01\_0053, grant no. 2012\_01\_0123, and grant no. 2010\_01\_0802) and the Villum Foundation (grant no. 102544).

Received: March 30, 2015

Revised: June 2, 2015

Accepted: June 26, 2015

Published: July 23, 2015

## REFERENCES

- Dunn, C.W., Giribet, G., Edgecombe, G.D., and Hejnal, A. (2014). Animal phylogeny and its evolutionary implications. *Annu. Rev. Ecol. Evol. Syst.* **45**, 371–395.
- Haszprunar, G., Rieger, R.M., and Schuchert, P. (1991). Extant “Problematica” within or near the Metazoa. In *The Early evolution of Metazoa and the Significance of Problematic Taxa*, A.M. Simonetta, and S. Conway Morris, eds. (Cambridge: Oxford University Press), pp. 99–105.
- Rieger, R.M. (1980). A new group of interstitial worms, Lobatocerebridae nov. fam. (Annelida) and its significance for metazoan phylogeny. *Zoomorphologie* **95**, 41–84.
- Kristensen, R.M., and Niilonen, T. (1982). Structural studies on *Diurodrilus* Remane (Diurodrilidae fam.n.), with description of *Diurodrilus westheidei* sp.n. from the Arctic interstitial meiobenthos, W. Greenland. *Zool. Scr.* **11**, 1–12.
- Worsaae, K., and Rouse, G.W. (2008). Is *Diurodrilus* an annelid? *J. Morphol.* **269**, 1426–1455.
- Kristensen, R.M., and Funch, P. (2000). Micrognathozoa: a new class with complicated jaws like those of Rotifera and Gnathostomulida. *J. Morphol.* **246**, 1–49.
- Bekkouche, N., Kristensen, R.M., Hejnal, A., Sørensen, M.V., and Worsaae, K. (2014). Detailed reconstruction of the musculature in *Limnognathia maerski* (Micrognathozoa) and comparison with other Gnathifera. *Front. Zool.* **11**, 71.
- Cavalier-Smith, T. (1998). A revised six-kingdom system of life. *Biol. Rev. Camb. Philos. Soc.* **73**, 203–266.
- Giribet, G., Distel, D.L., Polz, M., Sterrer, W., and Wheeler, W.C. (2000). Triploblastic relationships with emphasis on the acoelomates and the position of Gnathostomulida, Cycliophora, Plathelminthes, and Chaetognatha: a combined approach of 18S rDNA sequences and morphology. *Syst. Biol.* **49**, 539–562.
- Hejnal, A., Obst, M., Stamatakis, A., Ott, M., Rouse, G.W., Edgecombe, G.D., Martinez, P., Baguñà, J., Bailly, X., Jondelius, U., et al. (2009). Assessing the root of bilaterian animals with scalable phylogenomic methods. *Proc. R. Soc. B Biol. Sci.* **276**, 4261–4270.
- Struck, T.H., Wey-Fabrizius, A.R., Golombek, A., Hering, L., Weigert, A., Bleidorn, C., Klebow, S., Iakovenko, N., Hausdorf, B., Petersen, M., et al. (2014). Platyzoan paraphyly based on phylogenomic data supports a noncoelomate ancestry of spiralia. *Mol. Biol. Evol.* **31**, 1833–1849.
- Rieger, R.M. (1988). Comparative ultrastructure and the Lobatocerebridae: keys to understand the phylogenetic relationship of Annelida and the acoelomates. In *Microfauna Marina, Volume 4*, P. Ax, ed. (Gustav Fischer Verlag), pp. 373–382.
- Rieger, R.M. (1991). Neue Organisationstypen aus der Sandlückenraumfauna: Die Lobatocerebriden und *Jennaria pulchra*. *Verh. Dtsch. Zool. Ges.* **84**, 247–259.
- Kristensen, R.M. (1983). Loricifera, a new phylum with Aschelminthes characters from the meiobenthos. *J. Zoolog. Syst. Evol. Res.* **21**, 163–180.
- Dunn, C.W., Hejnal, A., Matus, D.Q., Pang, K., Browne, W.E., Smith, S.A., Seaver, E., Rouse, G.W., Obst, M., Edgecombe, G.D., et al. (2008). Broad phylogenomic sampling improves resolution of the animal tree of life. *Nature* **452**, 745–749.
- Halanych, K.M., Bacheller, J.D., Aguinaldo, A.M., Liva, S.M., Hillis, D.M., and Lake, J.A. (1995). Evidence from 18S ribosomal DNA that the lophophorates are protostome animals. *Science* **267**, 1641–1643.
- Aguinaldo, A.M.A., Turbeville, J.M., Linford, L.S., Rivera, M.C., Garey, J.R., Raff, R.A., and Lake, J.A. (1997). Evidence for a clade of nematodes, arthropods and other moulting animals. *Nature* **387**, 489–493.
- Nesnidal, M.P., Helmkampf, M., Meyer, A., Witek, A., Bruchhaus, I., Ebersberger, I., Hankeln, T., Lieb, B., Struck, T.H., and Hausdorf, B. (2013). New phylogenomic data support the monophyly of Lophophorata and an Ectoproct-Phoronid clade and indicate that Polyzoa and Kryptozoa are caused by systematic bias. *BMC Evol. Biol.* **13**, 253.
- Funch, P., and Kristensen, R.M. (1995). Cycliophora is a new phylum with affinities to Entoprocta and Ectoprocta. *Nature* **378**, 711–714.
- Giribet, G., Dunn, C.W., Edgecombe, G.D., Hejnal, A., Martindale, M.Q., and Rouse, G.W. (2009). Assembling the spiralian tree of life. In *Animal Evolution: Genes, Genomes, Fossils and Trees*, M.J. Telford, and D.T.J. Littlewood, eds. (Oxford: Oxford University Press), pp. 52–64.
- Nielsen, C. (2012). *Animal Evolution - Interrelationships of the Living Phyla* (Oxford: Oxford University Press).
- Borner, J., Rehm, P., Schill, R.O., Ebersberger, I., and Burmester, T. (2014). A transcriptome approach to ecdysozoan phylogeny. *Mol. Phylogenet. Evol.* **80**, 79–87.
- Lemburg, C. (1995). Ultrastructure of the sense organs and receptor cells of the neck and lorica of *Halicryptus spinulosus* larva (Priapulida). In *Microfauna Marina, Volume 10*, P. Ax, ed. (Gustav Fischer Verlag), pp. 7–30.
- Remane, A. (1925). Diagnosen neuer Archanneliden (zugleich 3. Beitrag zur Fauna der Kieler Bucht). *Zool. Anz.* **65**, 15–17.
- Hermans, C.O. (1969). The systematic position of the Archannelida. *Syst. Biol.* **18**, 85–102.
- Worsaae, K., and Kristensen, R.M. (2005). Evolution of interstitial Polychaeta (Annelida). *Hydrobiologia* **179**, 319–340.
- Weigert, A., Helm, C., Meyer, M., Nickel, B., Arendt, D., Hausdorf, B., Santos, S.R., Halanych, K.M., Purschke, G., Bleidorn, C., and Struck, T.H. (2014). Illuminating the base of the annelid tree using transcriptomics. *Mol. Biol. Evol.* **31**, 1391–1401.
- Andrade, S., Novo, M., Kawauchi, G., Pleijel, F., Giribet, G., and Rouse, G. Articulating the “archannelids”: a phylogenomic approach to annelid relationships with emphasis on meiofaunal taxa. *Mol. Biol. Evol.* Published online July 30, 2015. <http://dx.doi.org/10.1093/molbev/msv157>.
- Golombek, A., Tobergte, S., Nesnidal, M.P., Purschke, G., and Struck, T.H. (2013). Mitochondrial genomes to the rescue—Diurodrilidae in the myzostomid trap. *Mol. Phylogenet. Evol.* **68**, 312–326.
- Bleidorn, C. (2005). Phylogenetic relationships and evolution of Orbiniidae (Annelida, Polychaeta) based on molecular data. *Zool. J. Linn. Soc.* **144**, 59–73.
- Westheide, W. (1987). Progenesis as a principle in meiofauna evolution. *J. Nat. Hist.* **21**, 843–854.
- Boyle, M.J., and Rice, M.E. (2014). Sipuncula: an emerging model of spiralian development and evolution. *Int. J. Dev. Biol.* **58**, 485–499.
- Fransen, M.E. (1980). Ultrastructure of coelomic organization in annelids. *Zoomorphologie* **95**, 235–249.
- Rieger, R.M. (1985). The phylogenetic status of the acoelomate organization within the Bilateria: a histological perspective. In *The Origins and Relationships of Lower Invertebrates Systematics Association Special Volumes*, S. Conway-Morris, J.D. George, R. Gibson, and H.M. Platt, eds. (Oxford: Oxford University Press), pp. 101–122.
- Koch, M., Quast, B., and Bartolomeaus, T. (2014). Coeloms and nephridia in annelids and arthropods. In *Deep Metazoan Phylogeny: the Backbone of the Tree of Life; New Insights from Analyses of Molecules, Morphology, and Theory of Data Analysis*, J.W. Waagele, and T. Bartolomeaus, eds. (Berlin: De Gruyter), pp. 173–284.

36. Sørensen, M.V. (2002). Phylogeny and jaw evolution in Gnathostomulida, with a cladistic analysis of the genera. *Zool. Scr.* **31**, 461–480.
37. Sørensen, M.V. (2003). Further structures in the jaw apparatus of *Limnognathia maerski* (Micrognathozoa), with notes on the phylogeny of the Gnathifera. *J. Morphol.* **255**, 131–145.
38. Giribet, G., Sørensen, M.V., Funch, P., Kristensen, R.M., and Sterrer, W. (2004). Investigations into the phylogenetic position of Micrognathozoa using four molecular loci. *Cladistics* **20**, 1–13.
39. Ahlrichs, W.H. (1997). Epidermal ultrastructure of *Seison nebaliae* and *Seison annulatus*, and a comparison of epidermal structures within the Gnathifera. *Zoomorphology* **117**, 41–48.
40. Laumer, C.E., Hejnol, A., and Giribet, G. (2015). Nuclear genomic signals of the 'microturbellarian' roots of platyhelminth evolutionary innovation. *eLife* **4**, 05503.
41. Lanfear, R., Calcott, B., Ho, S.Y.W., and Guindon, S. (2012). Partitionfinder: combined selection of partitioning schemes and substitution models for phylogenetic analyses. *Mol. Biol. Evol.* **29**, 1695–1701.
42. Lartillot, N., Brinkmann, H., and Philippe, H. (2007). Suppression of long-branch attraction artefacts in the animal phylogeny using a site-heterogeneous model. *BMC Evol. Biol.* **7** (1), S4.
43. Misof, B., Liu, S., Meusemann, K., Peters, R.S., Donath, A., Mayer, C., Frandsen, P.B., Ware, J., Flouri, T., Beutel, R.G., et al. (2014). Phylogenomics resolves the timing and pattern of insect evolution. *Science* **346**, 763–767.
44. Gatesy, J., and Baker, R.H. (2005). Hidden likelihood support in genomic data: can forty-five wrongs make a right? *Syst. Biol.* **54**, 483–492.
45. Swedmark, B. (1964). The interstitial fauna of marine sand. *Biol. Rev. Camb. Philos. Soc.* **39**, 1–42.
46. Higgins, R.P., and Thiel, H. (1988). Introduction to the Study of Meiofauna (Washington, D.C.: Smithsonian Institution Press).
47. Curini-Galletti, M., Artois, T., Delogu, V., De Smet, W.H., Fontaneto, D., Jondelius, U., Leasi, F., Martínez, A., Meyer-Wachsmuth, I., Nilsson, K.S., et al. (2012). Patterns of diversity in soft-bodied meiofauna: dispersal ability and body size matter. *PLoS ONE* **7**, e33801.
48. Tyler, S. (2001). The early worm—origins and relationships of the lower flatworms. In *Interrelationships of the Platyhelminthes Systematics Association Special, Volume D*, T.J. Littlewood, and R.A. Bray, eds. (London: Taylor and Francis), pp. 3–12.
49. Rieger, R.M. (1994). The biphasic life cycle—a central theme of metazoan evolution. *Am. Zool.* **34**, 484–491.
50. Hejnol, A., and Martindale, M.Q. (2008). Acoel development supports a simple planula-like urbilaterian. *Philos. Trans. R. Soc. Lond. B Biol. Sci.* **363**, 1493–1501.
51. Marlow, H., Tosches, M.A., Tomer, R., Steinmetz, P.R., Lauri, A., Larsson, T., and Arendt, D. (2014). Larval body patterning and apical organs are conserved in animal evolution. *BMC Biol.* **12**, 7.
52. Strausfeld, N.J., and Hirth, F. (2013). Deep homology of arthropod central complex and vertebrate basal ganglia. *Science* **340**, 157–161.
53. Lauri, A., Brunet, T., Handberg-Thorsager, M., Fischer, A.H.L., Simakov, O., Steinmetz, P.R.H., Tomer, R., Keller, P.J., and Arendt, D. (2014). Development of the annelid axochord: insights into notochord evolution. *Science* **345**, 1365–1368.
54. Marlétaz, F., Martin, E., Perez, Y., Papillon, D., Caubit, X., Lowe, C.J., Freeman, B., Fasano, L., Dossat, C., Wincker, P., et al. (2006). Chaetognath phylogenomics: a protostome with deuterostome-like development. *Curr. Biol.* **16**, R577–R578.

**Current Biology**

**Supplemental Information**

# **Spiralian Phylogeny Informs the Evolution of Microscopic Lineages**

**Christopher E. Laumer, Nicolas Bekkouche, Alexandra Kerbl, Freya Goetz, Ricardo C. Neves, Martin V. Sørensen, Reinhardt M. Kristensen, Andreas Hejnol, Casey W. Dunn, Gonzalo Giribet, and Katrine Worsaae**

**Figure S1** – Partitioned maximum likelihood phylogram schematized in Figure 1, with full terminal taxon names given. Support values represent a proportion of 100 bootstrap replicates.

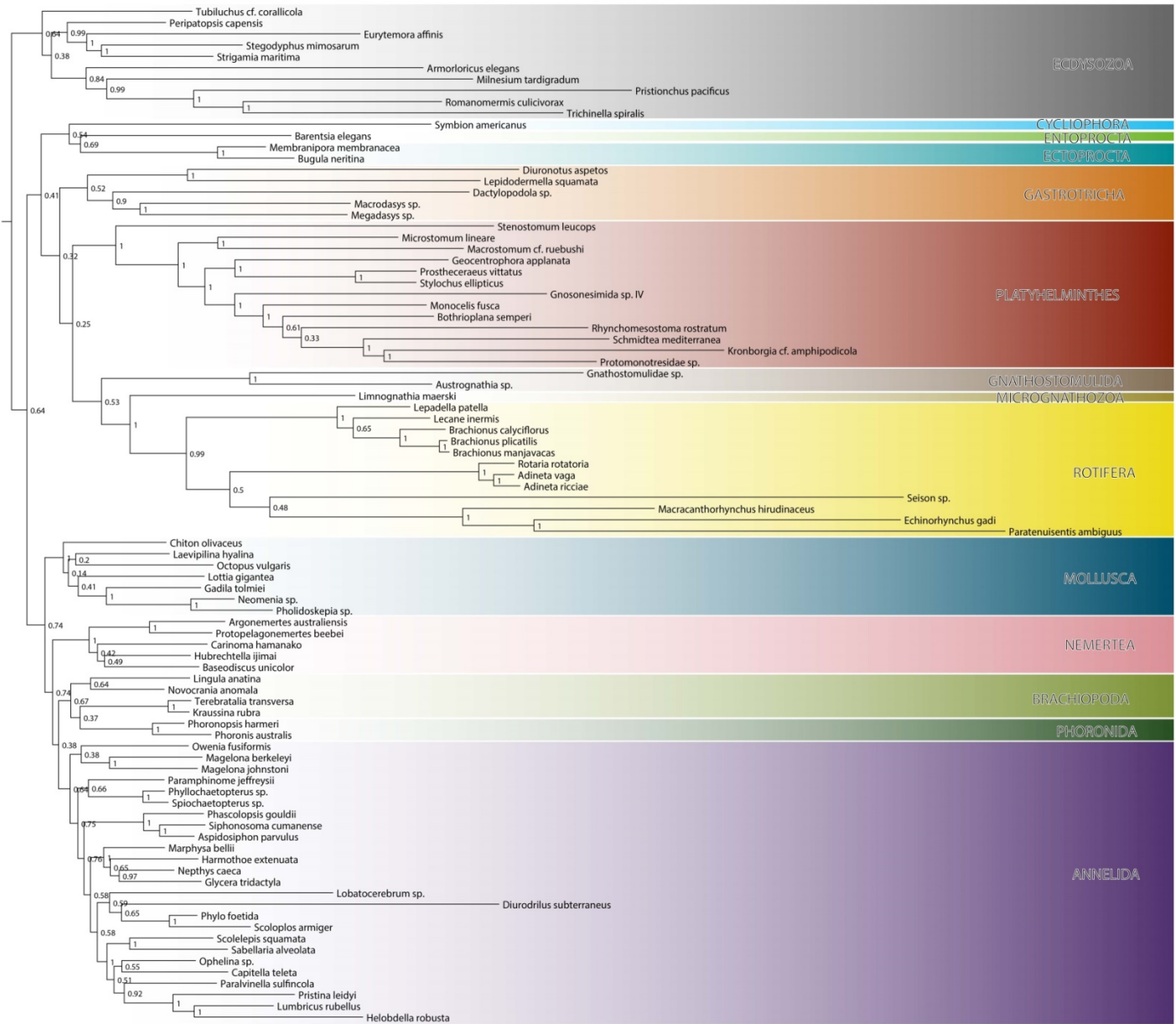


**Figure S2** – Bayesian inference of spiralian phylogeny from PhyloBayes-MPI v1.4e analysis of the untrimmed matrix (90 taxa, 79,954 amino acids, 57.57% missing data). Nodal support values represent posterior probability.

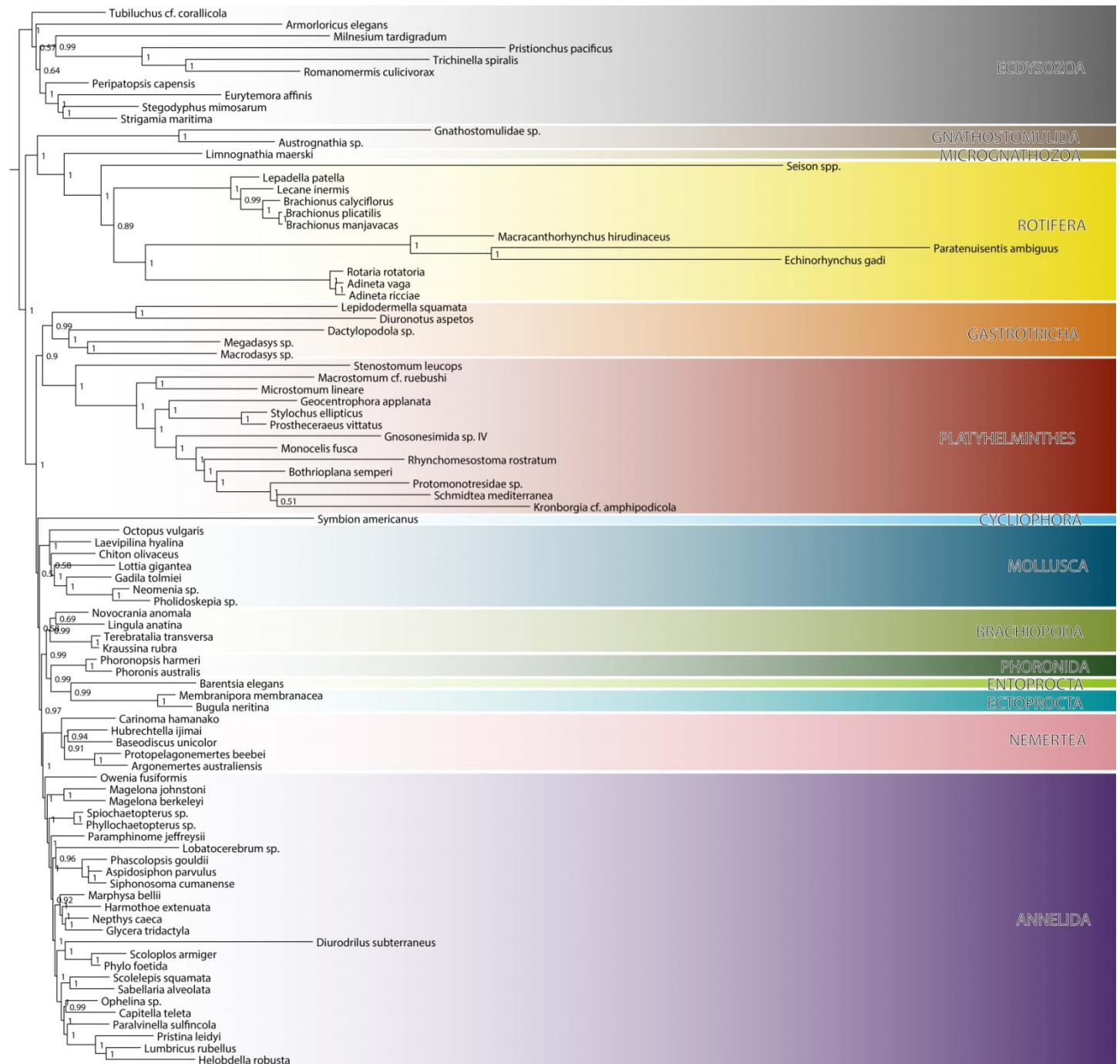


**Table S1** – Summary statistics describing genome and transcriptome assemblies and availability from the 90 taxa used in this study. Newly sequenced species are labeled in bold. Statistics were calculated with scripts provided within Trinity r20140413 or using the fastq-stats program in the ea-utils package. Species with a ‘??’ in read-level cells were provided to us as assemblies only. Peptide counts are for isoform-filtered peptides.

Higher Taxon	Species name	Orthologs used (of 402)	Contigs	N50 bp	GC%	SRA accessions	Seq. tech	read length	N reads post QC	N read 2 post QC	%dup	QC'd read length	N peptides	N50 peptides	
Rotifera (Monogononta)	Brachionus calyciflorus		129	32604	824	30.6	SRR611718,SRR611719,SRR611720,SRR620051,SRR620163	illumina	1x76	-	-	-	21255	267	
	Brachionus manjavacas		168	12782	1222	38.59	SRR801079		454	-	642611	51.7855	428.6357	9893	335
	Brachionus plicatilis		221	9843	841	35.12	-	Sanger	-	-	-	-	7796	240	
	Lecane inermis		51	1546	412	40.08	ERR538168		454	-	42257	69.8511	373.8784	662	132
Rotifera (Bdelloidea)	Lepadella patella		52	4794	350	45.51	SRR1976570	illumina	2x100	28960839	25006533	85.2665	96.4364	896	157
	Adineta ricciae		133	16363	448	38.85	ERR106424, ERR106425		1x76	2219710	-	23.5749	74.19	8062	175
	Adineta vaga		300	-	-	-	-	Genome peptide predicti	-	-	-	-	49300	513	
Rotifera (Acanthocephala)	Rotaria rotatoria		206	37801	600	34.99	ERR454505	illumina	2x101	11719523	8416935	44.6275	90.4427	18130	210
	Echinorhynchus gadi		183	19844	1272	34.62	PRJNA289343 (BioProject)	illumina	2x100	26001112	24684658	52.1093	96.7653	7911	488
	Macracanthorhynchus hirudinaceus		218	40159	1067	38.64	ERR454503,ERR454504	illumina	2x151	61148545	41317798	37.85	97.0097	9214	534
	Paratenisientis ambiguus		72	4590	410	40.13	ERR238747,ERR238748		454	105625	-	61.8054	346.304	2189	136
Rotifera (Seisonidea)	Seison spp.		40	3811	628	38.16	ERR245083,ERR245084		454	107659	-	70.7781	301.3726	2177	178
	Barentsia elegans		29	1065	523	47.29	LIBEST_027828	Sanger	-	-	-	-	511	158	
Entoprocta	Symbion americanus		44	6930	866	40.42	PRJNA289346 (BioProject)	illumina	2x250	1563570	940720	52.1787	127.5406	2060	243
Cycloprocta	Bugula neritina		83	4703	529	43.39	SRR034781		454	138851	-	55.2808	354.7924	2454	158
Ectoprocta	Membranipora membranacea		217	59525	1948	41.13	PRJNA289347 (BioProject)	illumina	2x101	??	??	??	??	16262	667
	Kraussina rubra		158	67800	505	34.77	PRJNA289348 (BioProject)	illumina	2x100	22273199	20867617	56.2537	96.7919	12424	209
Brachiopoda	Lingula anatina		88	4545	608	40.65	SRR330440		454	70218	-	41.7186	382.0747	1792	165
	Novocrania anomala		39	1744	571	44.48	LIBEST_028289	Sanger	-	-	-	-	1058	177	
	Terebratalia transversa		253	80500	1590	37.21	SRR2005824	illumina	2x101	??	??	??	16543	512	
	Phoronis australis		205	48760	779	41.53	SRR2018856	illumina	2x101	???	???	???	10665	250	
Phoronida	Phoronopsis harmeri		134	221814	511	39.5	PRJNA289349 (BioProject)	illumina	2x100	31183424	28203012	22.4423	92.9718	26791	228
	Dactylopodola baltica		167	27382	468	43.6	SRR1273672,SRR1273673,SRR1275388,SRR1275389	illumina	1x76	5237767	-	27.9676	73.2472	8863	167
	Diuronotus aspetos		279	43932	1768	46.57	PRJNA289341 (BioProject)	illumina	2x101	223317375	196873642	30.2696	92.4609	16044	485
	Lepidodermella squamata		214	65976	1502	45.2	SRR1982110	illumina	2x50	-	-	30.952	25909	446	
Gastrotricha	Macrodasya sp.		215	24844	752	38.02	SRR1271706,SRR1271707,SRR1271708,SRR1275393	illumina	1x76	10661270	-	35.9984	73.9785	11217	279
	Megadasya sp.		156	49893	482	43.58	SRR1273711,SRR1273712,SRR1275394,SRR1275397	illumina	1x76	11462311	-	23.304	72.7681	13779	201
	Austrorhynchia sp.		81	29042	396	48.4	SRR1976176	illumina	2x100	20377447	18327483	82.9648	98.3212	9859	168
	Gnathostomulida		184	66671	526	44.66	SRR1271607,SRR1271608,SRR1271613,SRR1275390	illumina	2x76	26680556	21567750	49.4162	74.0475	24294	191
Nemertea	Gnathostomulidae sp. (Gnathostomula paradoxa in Struck et al 2014)		130	84309	547	43.57	SRR1506999,SRR1507000,SRR1507001	illumina	??	??	??	??	16484	231	
	Argonemertes australiensis		101	320035	483	41.1	SRR1505175	illumina	??	??	??	??	24137	219	
	Baseodiscus unicolor		125	158584	411	38.76	SRR1505092, SRR1505094	illumina	??	??	??	??	19728	191	
	Carinoma hamanako		132	168493	393	41.94	SRR1505099, SRR1505100	illumina	??	??	??	??	17521	178	
	Hubrechtella ijimai		122	33168	496	46.26	SRR1507060	illumina	??	??	??	??	9701	203	
	Protopelagoneurtes beebii		211	86426	674	48.66	SRR1955240, SRR1796356	illumina	2x100	25818779	25818770	52.1932	100.4869	19364	325
	Geocentrophora applanata		245	115616	1032	34.79	SRR1955490	illumina	2x100	9147419	9147419	2.6755	100.2318	31359	446
	Gnosonemida sp. IV		239	59282	935	43.5	SRR1976178, SRR1976442	illumina	2x100	45303696	41236359	28.4711	102.5083	17711	428
	Kronborgia cf. amphipodica		219	50691	915	37.65	SRR1976457	illumina	2x100	40648076	35845841	59.856	98.3981	12321	486
	Macrostromum cf. ruebushi		152	70620	399	52.56	SRR1979670	illumina	2x100	3714012	3714012	23.8276	98.6725	14460	163
	Microstromum lineare		245	121725	753	39.03	SRR1980039	illumina	2x100	15828839	14164740	39.5581	106.9272	28253	320
	Monocelis fusca		209	72335	1028	37.53	SRR1979673	illumina	2x100	8655212	8655212	17.6753	106.0273	21570	416
Prostheceraea vittatus		266	522247	618	38.43	SRR2000268	illumina	2x100	54190643	54190643	11.0032	99.1496	37209	471	
Protomonotresidae sp.		164	41570	582	39.14	SRR1980045	illumina	2x100	22449452	20621232	61.5313	106.7998	15242	227	
Rhynchomesostoma rostratum		186	75386	563	39.02	SRR1980143	illumina	2x100	5229794	5229794	17.0893	105.2568	25492	248	
Schmidtea mediterranea		238	104779	1362	33.29	-	illumina	2x100	??	??	??	??	17400	577	
Stenostomum leucops		209	66953	1699	48.52	SRR1910423	illumina	2x100	23216077	23216077	29.4315	100.2308	21396	513	
Stylochus ellipticus		246	121448	1309	47.62	SRR1980704, SRR1980690	illumina	2x100	61471878	61471878	39.8519	99.7003	20392	526	
Mollusca	Chiton olivaceus		128	70271	588	42.84	SRR618506	illumina	??	??	??	??	18249	194	
	Gadila tolmiei		281	120740	793	40.28	SRR331897	illumina	??	??	??	??	54018	295	
	Laevipilina hyalina		150	84890	717	42.03	SRR1505115	illumina	??	??	??	??	23080	271	
	Lottia gigantea		312	-	-	-	-	Genome peptide predicti	-	-	-	-	23842	490	
	Neomenia megatrapezata		274	48977	1418	42.05	SRR331899	illumina	??	??	??	??	15710	449	
	Octopus vulgaris		163	52440	767	38.31	SRR331946	illumina	??	??	??	??	15702	323	
	Pholidoskepia sp. (previously identified as Chaetoderma sp.)		49	11580	479	45.17	SRR1505105	illumina	??	??	??	??	5170	166	
	Aspidosiphon parvulus		210	98877	435	39.11	SRR1646391	illumina	??	??	??	??	14376	185	
	Diurodrilus subterraneus		208	101952	760	46.99	PRJNA289340 (BioProject)	illumina	2x100	36042142	32576752	45.6607	99.3184	26379	311
	Capitella teleta		300	-	-	-	-	Genome peptide predicti	-	-	-	-	32415	450	
	Glycera tridactyla		189	94622	518	42.24	SRR1237833, SRR1237870, SRR1237831, SRR1237869, SRR1237830, SRR1237868, SRR1237838	illumina	2x101	25611706	21990173	39.4977	89.9966	10394	232
	Harmothoe extenuata		150	21100	437	44.19	SRR1237766, SRR1237765	illumina	2x76	176521	1623453	26.4265	72.4482	3639	198
Helobdella robusta		283	-	-	-	-	Genome peptide predicti	-	-	-	-	23432	507		
Lobateleutherozoa	Lobateleutherozoa sp.		111	60713	420	47.99	PRJNA289338 (BioProject)	illumina	2x100	23678507	21868291	56.8513	98.8947	11657	189
	Lumbricus rubellus		254	92033	1170	43.7	SRR923752	illumina	2x51	46622983	43820981	17.4688	50.8498	27141	400
	Magelona berkeleyi		69	35795	312	42.86	SRR1257638,SRR1257639	illumina	2x100	19844585	11545217	85.5419	86.6335	4320	141
	Magelona johnstoni		182	55698	439	42.84	SRR1222290	illumina	2x76	4567874	4439922	26.8992	75.9942	10652	219
	Marphysa bellii		211	56551	558	39.7	SRR1232821,SRR1232833	illumina	2x76	7303586	6813609	35.2149	74.7354	10943	248
	Nephtys caeca		283	81625	774	39.83	SRR1232685,SRR1232795	illumina	2x76	12376520	11661192	21.4305	74.8405	15828	353
	Ophelina sp.		147	19087	459	42.79	SRR328399,SRR328400	illumina	454	647028	-	61.8927	368.5492	5656	153
	Owenia fusiformis		137	29361	453	39.57	SRR1222288	illumina	2x77	1850839	1781292	19.3198	76.0699	8256	205
	Paralvinella sulfincola		218	31733	992	39.94	SRR172997,SRR172998,SRR172999,SRR173000	illumina	454	2579170	-	54.2136	339.0098	11405	253
	Paramphinoe jeffreysii		262	109952	589	42.03	SRR1257731,SRR1257732	illumina	2x100	27726184	21854311	49.6886	92.9264	23893	266
	Phascolopsis gouldii		160	125915	457	38.68	SRR1654498	illumina	??	??	??	??	19968	200	
	Phyllochaetopterus sp.		303	125511	880	35.47	SRR1257898,SRR1257899	illumina	2x100	27964145	23401001	44.7501	96.036	29179	346
Phylo foetida		197	40687	483	37.54	SRR1222216	illumina	2x77	5204464	4915759	46.1485	76.7036	8296	221	
Pristina leidy		182	65767	768	44.37	SRR387799,SRR387801,SRR387803	illumina	454	1548723	-	47.8724	382.7167	22277	206	
Sabellaria alveolata		73	11265	363	37.04	SRR1232634	illumina	2x76	1505872	-	37.3362	73.7567	1510	203	

## Supplemental Experimental Procedures

Peptide predictions used for grouping into orthologous sets were derived from a mixture of publically available gene models from well-annotated genome assemblies, and transcriptome assemblies derived from mainly Illumina, 454, and in a few cases Sanger, cDNA sequencing projects accessioned in NCBI's SRA or EST databases; 13 Illumina cDNA libraries were also newly sequenced for this project. Illumina reads were quality-controlled while maintaining parity using Trimmomatic v0.32 [S1], trimming to a minimum Phred33 score of 20 (in a 4-bp sliding window), and removing all reads with a post-trimmed length of <36 bp; relevant adapter sequences (including SMART cDNA amplification adapters, in the case of libraries produced using this method; [S2]) were removed. 454 libraries were trimmed to a minimum Phred score of 30, and reads with post-trimmed length <30 were removed, using the fastq\_quality\_trimmer tool from the FASTX toolkit. Illumina and 454 cDNA libraries (following [S3]) were both assembled using the Trinity RNA-seq de novo assembler, r20140413 [S4]. Sanger EST libraries were processed using SeqClean and TGICL-2.1, as described in [S5]. Libraries were screened for metazoan-origin contamination by screening the *de novo* assemblies against the SILVA 18S rRNA database using BLASTn at an e-value of 1e-100. All transcriptome assemblies were redundancy-reduced using cd-hit-est at c=0.95, and likely ORFs were predicted using TransDecoder r20131117; the longest peptide per retained Trinity subcomponent (i.e. putative unigene) was then selected with a custom Python script (choose\_longest\_v3.py; [S5]). Further details of data source, library preparation, and several key summary statistics describing properties of raw sequence data, finished assemblies, and predicted peptides, are described in Table S1.

Predicted peptides were grouped into putative orthologous clusters with a single peptide per species using the OMA-standalone algorithm, v0.99x [S6]. We retained all OMA groups with 6 or more members, of which there were 17,066, and performed multiple sequence alignment on this set using the L-INS-i algorithm from MAFFT v7.149 [S7], quantifying alignment errors using ZORRO [S8], and trimming columns assigned an alignment uncertainty score of  $<0.5$  [S5]. From these aligned, sequence-masked orthogroups, we selected 402 orthologs to use for phylogenetic analysis using the matrix reduction (MARE) tool v0.1.2rc, with  $d=1$  and  $t=1000$ , to select for an information-dense matrix without the loss of any taxa [S9]. This yielded a matrix of 79,954 AA with a completeness of 42.43%. From this matrix we also prepared a trimmed matrix using BMGE-1.11 [S10], with ‘-g 1 -n BLOSUM30 -s FAST’, so as to retain gappy regions and trim entropic sequences using the least stringent substitution matrix possible, while removing sites that show evidence of non-stationarity: this yielded 72,243 AA with a completeness of 41.83%. *Symbion americanus* and *Barentsia elegans* were deleted from this matrix after inspection of a preliminary PhyloBayes run showed these taxa to be highly unstable during MCMC.

Maximum likelihood phylogenetic inference was performed in parallel on the Harvard FAS Division of Science Odyssey 2 research cluster using ExaML v3.0.0 [S11], with 100 bootstrap replicates calculated manually to measure nodal support, as described in the RAxML-Light manual. For the tree presented in Figure 1A, likelihood was calculated under a partitioning scheme selected by PartitionFinderProtein v1.1.1 [S12], calculating likelihoods with the provided RAxML binary and using with heuristic clustering (‘-rcluster-percent 10’). This selected 62 partitions (beginning from a 402-partition per-ortholog scheme), most of which were assigned the PROTGAMMALG model. Unfortunately BMGE does not take into account the

boundaries between partitions while trimming, so only the untrimmed matrix was considered for partitioned maximum likelihood inference. For the submatrices analyzed in Figures 1B and 1C, we used TIGER v1.2 to rank sites by relative evolutionary rate [S13], writing the scaled rates to an output file using the ‘-rl’ command. We then used a custom python script to parse these rates, defining for the variable sites (those with a rate value less than 1.0) the first and third quartiles, and using the PyCogent library [S14] to retain new submatrices composed of the upper and lower three fastest quartiles, respectively. These matrices were then analyzed under the LG4M+F substitution matrix in ExaML v3.0.0 [S11]. Nodal support from the 100 bootstrap replicates was summarized onto the best-found tree from ExaML using the sumtrees.py program of DendroPy [S15].

Bayesian mixture model inference under the CAT+GTR model was conducted in PhyloBayes-MPI v1.4e [S16], removing constant sites (“-dc”) and running four independent chains each for, in the case of the untrimmed matrix, a minimum of 14,000 generations (maximum 21,784), or in the case of the trimmed matrix, a minimum of 16,000 generations (maximum 21,056). Runs were considered to have converged adequately when the maximum proportion of bipartition differences dropped below  $<0.3$  for at least 3 pairs of chains. The posterior summaries interpreted here were generated from a single pair of chains per matrix, with a burn-in of 5000 generations from the complete matrix (maxdiff= 0.179) and of 3000 generations from the trimmed matrix (maxdiff= 0.143).

### **Supplemental References**

S1. Bolger, A. M., Lohse, M., and Usadel, B. (2014). Trimmomatic: a flexible trimmer for Illumina sequence data. *Bioinformatics* 30, 2114–2120.

- S2. Struck, T. H., Wey-Fabrizius, A. R., Golombek, A., Hering, L., Weigert, A., Bleidorn, C., Klebow, S., Iakovenko, N., Hausdorf, B., Petersen, M., et al. (2014). Platyzoan paraphyly based on phylogenomic data supports a noncoelomate ancestry of Spiralia. *Mol. Biol. Evol.* *31*, 1833–1849.
- S3. Ren, X., Liu, T., Dong, J., Sun, L., Yang, J., Zhu, Y., and Jin, Q. (2012). Evaluating de Bruijn graph assemblers on 454 transcriptomic data. *PLoS ONE* *7*, e51188.
- S4. Haas, B. J., Papanicolaou, A., Yassour, M., Grabherr, M., Blood, P. D., Bowden, J., Couger, M. B., Eccles, D., Li, B., Lieber, M., et al. (2013). *De novo* transcript sequence reconstruction from RNA-seq using the Trinity platform for reference generation and analysis. *Nat. Protoc.* *8*, 1494–1512.
- S5. Laumer, C. E., Hejnal, A., and Giribet, G. (2015). Nuclear genomic signals of the “microturbellarian” roots of platyhelminth evolutionary innovation. *eLife*, e05503.
- S6. Roth, A., Gonnet, G., and Dessimoz, C. (2008). Algorithm of OMA for large-scale orthology inference. *BMC Bioinformatics* *9*, 518.
- S7. Katoh, K., and Toh, H. (2008). Recent developments in the MAFFT multiple sequence alignment program. *Brief. Bioinform.* *9*, 286–298.
- S8. Wu, M., Chatterji, S., and Eisen, J. A. (2012). Accounting for alignment uncertainty in phylogenomics. *PLoS ONE* *7*, e30288.
- S9. Misof, B., Meyer, B., Reumont, B. M. von, Kück, P., Misof, K., and Meusemann, K. (2013). Selecting informative subsets of sparse supermatrices increases the chance to find correct trees. *BMC Bioinformatics* *14*, 348.
- S10. Criscuolo, A., and Gribaldo, S. (2010). BMGE (Block Mapping and Gathering with Entropy): a new software for selection of phylogenetic informative regions from multiple sequence alignments. *BMC Evol. Biol.* *10*, 210.
- S11. Kozlov, A. M., Aberer, A. J., and Stamatakis, A. (2015). ExaML version 3: a tool for phylogenomic analyses on supercomputers. *Bioinformatics*, btv184.
- S12. Lanfear, R., Calcott, B., Ho, S. Y. W., and Guindon, S. (2012). PartitionFinder: combined selection of partitioning schemes and substitution models for phylogenetic analyses. *Mol. Biol. Evol.* *29*, 1695–1701.
- S13. Cummins, C. A., and McInerney, J. O. (2011). A method for inferring the rate of evolution of homologous characters that can potentially improve phylogenetic inference, resolve deep divergence and correct systematic biases. *Syst. Biol.* *60*, 833–844.
- S14. Knight, R., Maxwell, P., Birmingham, A., Carnes, J., Caporaso, J. G., Easton, B. C., Eaton, M., Hamady, M., Lindsay, H., Liu, Z., et al. (2007). PyCogent: a toolkit for making sense from sequence. *Genome Biol.* *8*, R171.

S15. Sukumaran, J., and Holder, M. T. (2010). DendroPy: a Python library for phylogenetic computing. *Bioinformatics* 26, 1569–1571.

S16. Lartillot, N., Rodrigue, N., Stubbs, D., and Richer, J. (2013). PhyloBayes MPI. Phylogenetic reconstruction with infinite mixtures of profiles in a parallel environment. *Syst. Biol.* 62, 611–615.

**Manuscript II:**

**Detailed reconstruction of the nervous and muscular system of  
Lobatocerebridae with an evaluation of its annelid affinity**

Kerbl A., Bekkouche N., Sterrer W., and Worsaae K.

BMC Evolutionary Biology, Volume 15, issue 227



RESEARCH ARTICLE

Open Access



# Detailed reconstruction of the nervous and muscular system of Lobatocerebridae with an evaluation of its annelid affinity

Alexandra Kerbl<sup>1</sup>, Nicolas Bekkouche<sup>1</sup>, Wolfgang Sterrer<sup>2</sup> and Katrine Worsaae<sup>1\*</sup>

## Abstract

**Background:** The microscopic worm group Lobatocerebridae has been regarded a ‘problematicum’, with the systematic relationship being highly debated until a recent phylogenomic study placed them within annelids (Curr Biol 25: 2000-2006, 2015). To date, a morphological comparison with other spiralian taxa lacks detailed information on the nervous and muscular system, which is here presented for *Lobatocerebrum riegeri* n. sp. based on immunohistochemistry and confocal laser scanning microscopy, supported by TEM and live observations.

**Results:** The musculature is organized as a grid of longitudinal muscles and transverse muscular ring complexes in the trunk. The rostrum is supplied by longitudinal muscles and only a few transverse muscles. The intraepidermal central nervous system consists of a big, multi-lobed brain, nine major nerve bundles extending anteriorly into the rostrum and two lateral and one median cord extending posteriorly to the anus, connected by five commissures. The glandular epidermis has at least three types of mucus secreting glands and one type of adhesive unicellular glands.

**Conclusions:** No exclusive “annelid characters” could be found in the neuromuscular system of Lobatocerebridae, except for perhaps the mid-ventral nerve. However, none of the observed structures disputes its position within this group. The neuromuscular and glandular system of *L. riegeri* n. sp. shows similarities to those of meiofaunal annelids such as Dinophilidae and Protodrilidae, yet likewise to Gnathostomulida and catenulid Platyhelminthes, all living in the restrictive interstitial environment among sand grains. It therefore suggests an extreme evolutionary plasticity of annelid nervous and muscular architecture, previously regarded as highly conservative organ systems throughout metazoan evolution.

**Keywords:** Nervous system, Musculature, Glandular system, Meiofauna, Annelida, Spiralia, CLSM, Immunohistochemistry, Ultrastructure

## Background

Although phylogenomic studies have increased our knowledge of metazoan phylogeny significantly [1–4], a few ‘Problematica’ [5, 6] remain unplaced. Chief among those is the interstitial family Lobatocerebridae, which a recent phylogenetic study based on transcriptomic data positioned within Annelida, as sister group to Sipuncula, albeit with moderate support [7]. This enigmatic group of microscopic, thread-like, fully ciliated animals with glandular epidermis, living interstitially between sand

grains in the subtidal sandy sea-floor, was described as its own family, Lobatocerebridae, with one species, *Lobatocerebrum psammicola* [8]. The morphological data available have never indicated a relationship to Sipuncula, although affinities to Annelida as well as to Platyhelminthes have been debated [8, 9]. Due to the ambiguity of the morphological features pointed out by Rieger [8–11], this group was suggested to be its own phylum Lobatocerebromorpha in 1991, alongside annelids, platyhelminthes, molluscs and other spiralian [6, 12]; a status now denied by the recent phylogenomic analyses [7].

*Lobatocerebrum psammicola* was described from the shallow waters off the Coast of North Carolina, USA, based on TEM and LM section series [8–11]. The same

\* Correspondence: kworsaae@bio.ku.dk

<sup>1</sup>Marine Biological Section, Department of Biology, University of Copenhagen, Universitetsparken 4, 1st floor, 2100 Copenhagen E, Denmark  
Full list of author information is available at the end of the article

articles mention two additional undescribed species from the deep waters off North Carolina and from Eilat, Israel, respectively [8–10]. Additional specimens have been recorded by various authors from marine localities in the Atlantic (for example in Denmark [13], Gran Canaria (Spain) and Elba (Italy, W. Sterrer unpublished), and the Atlantic coast of Panama [7]), but the detailed morphology or taxonomy of these animals (besides *L. psammicola*) has never been investigated. Lobatocerebridae are found in subtidal marine habitats with coarse sand mixed with fine silt, but with limited organic and terrestrial matter. Although found at shallow depths, they are never abundant, and may be mistaken for platyhelminthes, juvenile nemerteans or gnathostomulids, which might explain their understudied nature and lack of additional records. Due to the inaccessibility of material, the explicit descriptions given by R. Rieger in his series of articles [8–11] have remained the only source for systematic and evolutionary discussions for decades [5, 6, 12, 14].

Lobatocerebrids have been described by Rieger [8–10] as having a thin, elongated body with circular cross section and complete ciliation. The epidermis is furthermore interspersed with a high number of unicellular glands. The ventral mouth opening is located one-third of the length from the tip (delineating the rostrum from the trunk), the dorsal male gonopore is positioned two-thirds of the length from the tip, followed by one to several lateral openings of the seminal receptacles in the posterior end of the body and the subterminal dorsal anus. The most prominent and also eponymous character of the animal is the large, multi-lobed brain, which is located anterior to the mouth opening, nearly taking up the entire cross section of the animal. The intraepidermal, ventral nervous system is reported to consist of two lateral nerve cords and two postpharyngeal commissures. The body wall musculature was described as outer longitudinal and inner circular muscles. The animals are simultaneous hermaphrodites [8–10]. Still, none of these morphological characteristics have made a clear classification into or next to one of the existing nominal phyla possible at the end of the 20<sup>th</sup> century since the identification of common traits has been ambiguous. However, especially Annelida, Gastrotricha, Gnathostomulida, Mollusca, Nemertea, and Platyhelminthes have been discussed as most likely relatives [6, 8, 11, 12]. Details of the epidermis and other characters were examined by Rieger [8–11] with ultrathin (40–70 nm) sections and transmission electron microscopy (TEM), providing information of great ultrastructural detail. However, a detailed cohesive analysis of several organ systems throughout the entire body, including the complete nervous and muscular system mapped with immunostaining and confocal microscopy is still warranted. This will not only enhance our understanding

of their morphology but also facilitate a comparison with morphological data on other interstitial groups gathered within the last two decades [15–17].

Both muscular and nervous systems have been assumed to represent rather conserved organ systems when it comes to their general architecture [18]. Annelids, however, have been found to be highly diverse in their morphological characters, and the ancestral states of musculature [19, 20] and nervous system [21] are still debated. The muscular layout in Lobatocerebridae has been described as internal circular and external longitudinal muscles [8, 10], which contradicts the arrangement found in the majority of annelids [22, 23]. However, cases are known where external circular muscles are reduced [24, 25] and several other muscle sets such as transverse, dorsoventral or bracing muscles have been proposed to functionally represent the circular muscles [22]. Nervous system organization has been suggested to be of high systematic importance, revealing synapomorphies of larger clades within e.g., Crustacea [26], which may be undetectable within other organ systems [21, 27, 28]. However, the nervous system in Annelida varies between being intraepidermal to subepidermal [29], in the number of commissures in the brain (2–4, [29]), the number of circumesophageal commissures (1–2, [29]), the number and arrangement of ventral nerve cords (1–7, medio- to lateroventral [15, 21, 29]) and the number and arrangement of commissures in the ventral nervous system (regularly and mid-segmental to irregularly spread along the entire ventral nervous system [15, 21, 29]). Based on the previously available information [8, 10] none of the few characteristics of the musculature or nervous system of Lobatocerebridae could be ascribed to annelids only, since they also show similarities to the pattern described especially from interstitial Gnathostomulida, Platyhelminthes, and Mollusca [6, 8–10].

Lobatocerebridae belongs to the meiofauna (animals between 2 mm and 0.06 mm in size [16]), together with exclusively microscopic lineages such as Gastrotricha, Acoelomorpha, Rotifera, Gnathostomulida, Platyhelminthes (except for parasitic forms), Tardigrada, Loricifera, Kinorhyncha, as well as miniaturized forms of macrofaunal lineages such as Annelida, Mollusca and Crustacea [16, 30, 31]. The apparent lack of distinct morphological synapomorphies with other clades, the presence of many autapomorphies, and the inaccessibility of material are the main reasons for why the phylogenetic positioning of these interstitial lineages has been so challenging; and why we only most recently have obtained more information on their evolution [7, 32, 33]. Interstitial fauna (living in the interstices between sand grains) all have a microscopic diameter size and most forms are also categorized as meiofaunal. Besides their small size, these interstitial animals often display simple-looking,

worm-like, highly ciliated and glandular, acoelomate bodies with no or few appendages; traits that generally seem to be favored in their confined interstitial environment [16, 34–36]. Several of these seemingly shared traits of interstitial fauna may either have originated as convergent adaptations to their restrictive environment and size, or reflect the recently proposed ancestral meio-faunal condition of Spiralia [7]. Hence, new detailed anatomical investigations of Lobatocerebridae should be evaluated in comparison not only with Annelida, discussing heritage and character evolution, but also with other relevant interstitial metazoans, in order to uncover possible convergent anatomical adaptations to the interstitial space-restricted environment.

The present study will evaluate the recent molecular placement of Lobatocerebridae within Annelida [7], in the light of detailed morphological investigation of nervous, muscular and glandular system with state-of-the-art immunohistochemistry in combination with confocal laser scanning microscopy (CLSM) and transmission electron microscopy (TEM). Hereby, we attempt to unravel and discuss possible resemblances with relevant interstitial spiralian, and whether these common traits may represent annelid synapomorphies, annelid or spiralian plesiomorphies, or convergent adaptations to the space restricted interstitial environment. Furthermore, with the description of *Lobatocerebrum riegeri* n. sp., we are adding another species to this enigmatic, otherwise monotypic group.

## Results

Specimens of *Lobatocerebrum riegeri* n. sp. overall resemble the body plan described by Rieger [8] for *Lobatocerebrum psammicola*. More details of the nervous, muscular and glandular systems could be detected in this study, as described in the following (Figs. 1, 2, 3, 4, 5, 6, 7, 8, 9).

### Musculature

*Examined in live and preserved specimens in LM; with phalloidin staining in CLSM and ultrathin sections in TEM; Figs. 1, 2.*

### Body wall

**Longitudinal musculature** As observed by Rieger [8, 10], all muscles of Lobatocerebridae are smooth muscles (confirmed by both CLSM and TEM); no striated musculature was detected in the present study. The longitudinal musculature is organized in six pairs of loose bundles, extending from the rostral tip to the posteriormost end of the body (Figs. 1, 2a–h). Five pairs of these, the dorsal (dlm), dorsolateral (dllm), two pairs of lateral (llm) and one pair of ventrolateral muscle bundles (vllm), lie dorsal to the

two prominent ventral nerve cords, whereas the ventral longitudinal muscles are located ventral to those (Fig. 1a–g). Each of these muscle bundles consists of three to five muscle fibres (Fig. 2a–f) and has a diameter of 1.2–2.4  $\mu\text{m}$  (measurements based on: number of specimens ( $n$ ) = 3, region of body ( $r$ ) = 1–4, measurements ( $m$ ) = 5), deeply embedded into the epidermal cells distal to the transverse muscular ring complexes (see below, tmr). The twelve bundles are regularly distributed along the entire body length (spaced 7.2–10.1  $\mu\text{m}$  apart,  $n$  = 3,  $r$  = 1–4,  $m$  = 5, Figs. 1b–g, 2a–e), except around the mouth opening, where the ventralmost pair (vlm) is shifted closer to the adjacent ventrolateral pair (vllm). The male gonopore or the openings of the seminal receptacles do not cause any similar distortions. All twelve longitudinal muscle bundles extend to the posterior end of the body, inserting subterminally around the anus. While the dorsal, dorsolateral and lateral muscles insert directly, the ventrolateral and ventral bundles first trace the epidermis to the terminal end, before bending antero-dorsally and inserting subterminally around the anus (Fig. 2c).

**Transverse muscular ring complexes** Transverse muscular ring complexes (tmr) are distributed in a regular pattern (spaced 14.5–16.9  $\mu\text{m}$  apart) from the pharynx to the ovary (Fig. 2a), and spaced 6.8–8.9  $\mu\text{m}$  apart posterior of the ovary to the sixth sphincter ( $n$  = 3,  $r$  = 2, 3,  $m$  = 5, Figs. 1, 2b–c). They have previously been misidentified as internal circular musculature [8]. This study, however, could detect that each muscular ring is formed by a series of individual transverse muscle fibres (diameter 0.8–1.3  $\mu\text{m}$ ,  $n$  = 3,  $r$  = 2, 3,  $m$  = 5); each of them only spanning the distance between one to three longitudinal bundles (7.6–35.7  $\mu\text{m}$ ,  $n$  = 3,  $r$  = 2, 3,  $m$  = 5, Fig. 2j). Up to nine individual transverse fibres are found to constitute one transverse muscular ring complex between all 12 longitudinal muscles (Fig. 2i–j).

Transverse muscles do not form transverse muscular ring complexes in the rostrum, but instead appear as contralateral fibres between longitudinal muscle bundles of opposite sides of the body, hereby creating a star-like structure of individual fibres (star-shaped muscles, ssm, diameter of individual fibres 0.5–1.1  $\mu\text{m}$ , length 10.5–45.2  $\mu\text{m}$ ,  $n$  = 3,  $r$  = 1,  $m$  = 5, Fig. 2d, g–h). Their abundance is highest close to the rostral tip (spaced 2.4–5.7  $\mu\text{m}$  apart,  $n$  = 2,  $r$  = 1,  $m$  = 5), where the ducts of the posterior frontal glands are ramifying, and farther separated towards the middle region of the rostrum (spaced 10.3–20.6  $\mu\text{m}$  apart,  $n$  = 2,  $r$  = 1,  $m$  = 5, Fig. 2g–h). The glandular ducts are not muscularized and no closing or constricting mechanism could be detected in this or previous studies [8, 9, 11]. The transverse muscles might therefore be involved in regulating the flow of

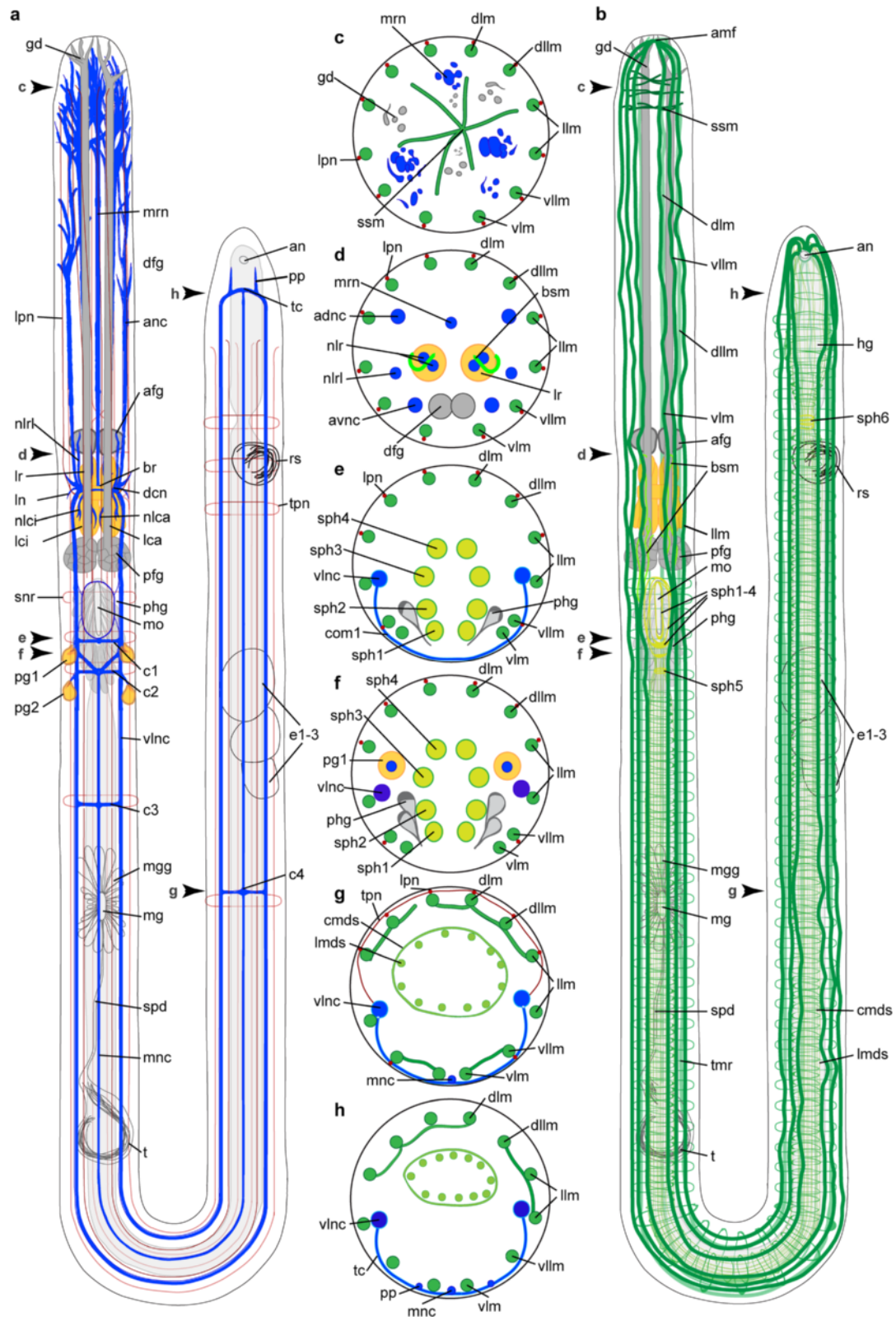


Fig. 1 (See legend on next page.)

(See figure on previous page.)

**Fig. 1** Anatomy of *Lobatocerebrum riegeri* n. sp. as inferred from immunohistochemistry and CLSM. Information is based on all specimens investigated and all antibodies used. **a** Nervous system **b** Musculature, **c–g** cross sections in the middle of the rostrum (**c**), at the level of the anterior end of the rostral lobes (**d**), at the level of the first commissure posterior to the pharynx of *L. riegeri* n. sp. (**e**), between the first and the second commissure (**f**), at the level of the fourth commissure (**g**) and the level of the subrectal commissure (**h**). Abbreviations: adnc: anterior dorsal nerve cord, afg: anterior frontal gland, amf: anterior point of muscle fusion, an: anus, anc: anterior nerve cord, br: brain, bsm: brain supporting muscle, c1–4: commissures 1–4, cmds: circular muscle of the digestive system, dcn: dorso-anterior commissure of the central neuropil, dfg: frontal gland ducts, dllm: dorsolateral longitudinal muscle, dlm: dorsal longitudinal muscle, e1–3: egg 1–3, gd: opening of the frontal glands, hg: hindgut, lca: major caudal lobe, lci: minor caudal lobe, llm: lateral longitudinal muscle, lmds: longitudinal muscle of the digestive system, ln: lateral nerve, lpn: lateral peripheral nerve, lr: rostral lobe, lrl: lateral rostral lobe, mg: male gonopore, mgg: male gonopore gland, mnc: median nerve cord, mo: mouth opening, mrn: median rostral nerve, nlca: nerve of the major caudal lobe, nlci: nerve of the minor caudal lobe, nlr: nerve of the lateral rostral lobe, nlr: nerve of the major rostral lobe, pfg: posterior frontal gland, pg1–2: postpharyngeal ganglion 1–2, phg: pharyngeal gland, pp: posterior projection, rs: seminal receptacles, snr: stomatogastric nerve ring, spd: spermiduct, sph1–6: sphincter 1–6, ssm: star-shaped muscle, t: testis, tc: terminal commissure, tmr: transverse muscle ring complex, tpn: transverse ring of the peripheral nervous system, vllm: ventrolateral longitudinal muscle, vlm: ventral longitudinal muscle, vln: ventral longitudinal nerve cord

secretion, in addition to enhancing the flexibility of the rostral tip as observed by behavioral observations (Additional file 1).

**Additional minor body muscles** Specific musculature is formed around the brain, emerging from the ventral and ventrolateral muscles around the pharynx and extending towards the anterior. The lateral pair of these muscles extends lateroventral to the brain, where the fibres branch off around or into the frontal lobe complex (Figs. 1b, 2e–f). The median pair extends to the caudal lobes, where they branch off into more individual fibres and lead to the major, minor and lateral caudal lobes (Figs. 1b, 2e). Due to the intricate network hereby formed around the anterior and posterior regions of the brain, we suggest these muscles to be a supportive structure for the brain, which is probably necessary due to a lack of other structures securing its position in the rostrum.

#### Intestinal musculature

**Pharynx** Although lacking a ventral or axial muscle bulb as found in most annelids, the pharynx is still the most prominent muscular structure in the body, showing five sphincter muscles as already defined by Rieger [8] in addition to the longitudinal body and gut musculature. The first four sphincter muscles of the pharynx surround the mouth opening and mouth cavity (sph1–sph4, adapted from Rieger's sph0–3 [8]), while the fifth sphincter constricts the digestive tract in the transversal plane, as a short esophagus delineating the pharynx from the midgut (sph5, Figs. 1b, 2a, i–j). Sphincters 1–4 consist of two to three fibres each (diameter 0.7–1.6  $\mu\text{m}$ ), which are always external to the longitudinal muscles of the digestive tract (Fig. 2j). The fifth sphincter (sph5), however, consists of up to eight thin, serially aligned, muscle fibres (diameter 1.2–1.5  $\mu\text{m}$ ,  $n = 3$ ,  $r = 2$ ,  $m = 5$ ). It marks the border to the midgut through an elongated constriction to a diameter of

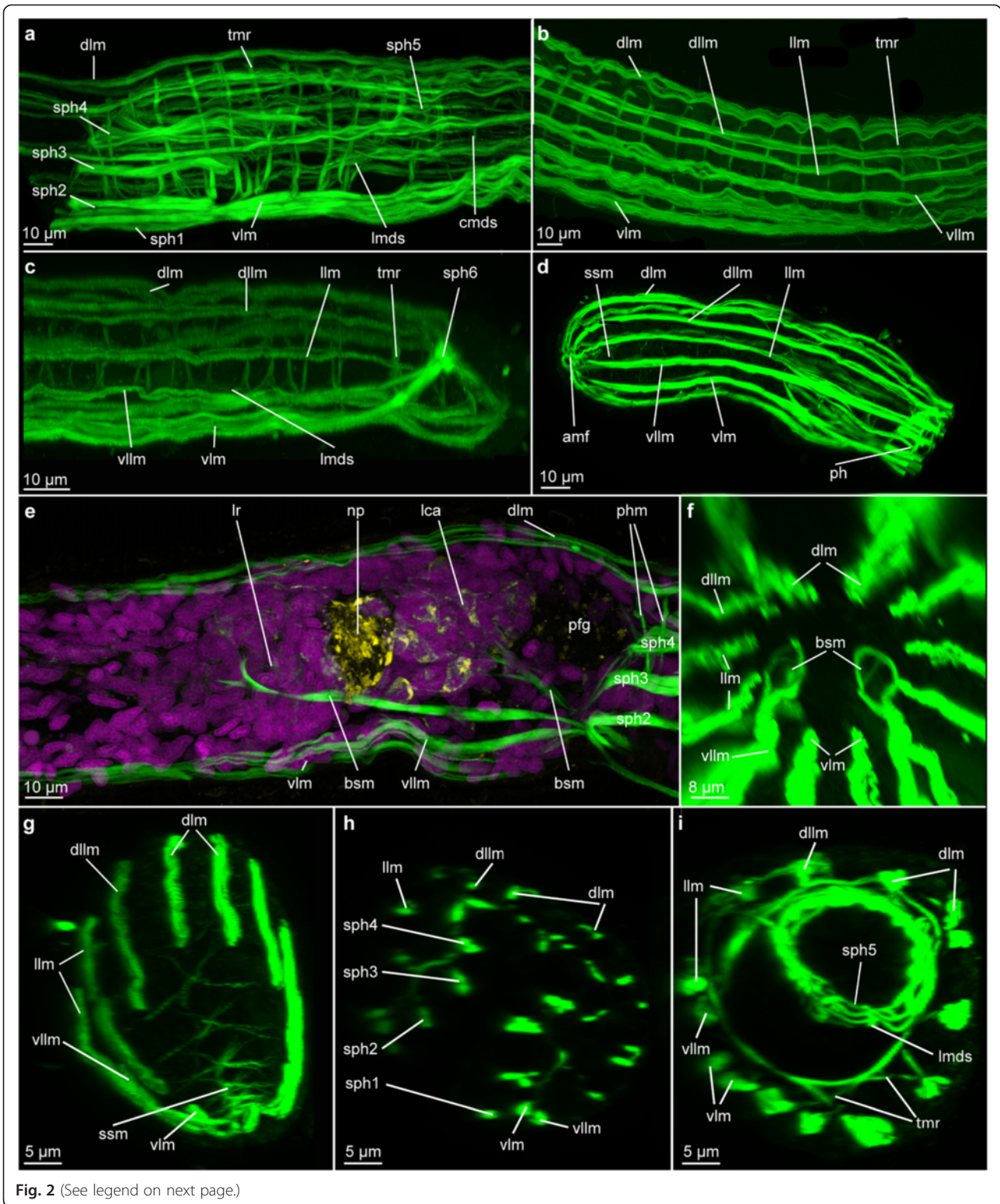
4.5–4.98  $\mu\text{m}$  when relaxed ( $n = 3$ ,  $r = 2$ ,  $m = 5$ , Figs. 1b, 2a, j). Additionally, the individual fibres are interwoven with the longitudinal gut muscles, rather than being located externally of these (Fig. 2j).

**Digestive tract** The intestinal musculature consists of 12 to 16 individual longitudinal fibres (lmds, diameter 0.66–0.74  $\mu\text{m}$ ,  $n = 3$ ,  $r = 2$ , 3, 4,  $m = 5$ ) arranged in equal distance from each other (spaced 1.5–3.1  $\mu\text{m}$  apart,  $n = 3$ ,  $r = 2$ , 3, 4,  $m = 5$ ), and therefore resembling the muscular pattern of the body wall musculature (Fig. 2a, i). The circular muscles of the digestive system (cmds), however, are arranged external to the longitudinal muscles of the gut (Fig. 2a, j), as is typical for gut musculature. These true circular muscles (as compared to the transverse muscular ring complexes) are very thin (diameter 0.5–0.6  $\mu\text{m}$ , spaced 3.1–5.8  $\mu\text{m}$  apart,  $n = 3$ ,  $r = 2$ , 3, 4,  $m = 5$ ) and most consistent in the pharyngeal region anterior and posterior to the fifth sphincter. In the posterior part of the body the longitudinal muscle fibres are embraced by the sixth, last sphincter, which consists of two short circular fibres (diameter 1.35–2.1  $\mu\text{m}$ ,  $n = 3$ ,  $r = 4$ ,  $m = 3$ ) and constricts the digestive tract to 6.4–6.6  $\mu\text{m}$  when relaxed ( $n = 3$ ,  $r = 4$ ,  $m = 4$ , Fig. 2c). The longitudinal muscles of the digestive system fuse with the longitudinal muscles posterior to this constriction (Fig. 2c).

#### Nervous system

Visualized with acetylated  $\alpha$ -tubulin IR, serotonin IR, FMRFamide-like IR, DAPI for cell nuclei and CLSM, Figs. 1, 2, 3, 4, 5, 6, 7.

The brain in the rostrum of *Lobatocerebrum riegeri* n. sp. is the most conspicuous part of the central nervous system. A series of both anterior rostral and posterior trunk nerve cords emerges from the central neuropil, and some additional nerve bundles are found branching off laterally to the brain (Fig. 4). The brain was described as having one pair of lobes anterior to the neuropil (rostral lobes) and two pairs of lobes (major and minor caudal



(See figure on previous page.)

**Fig. 2** Muscular architecture in *Lobatocerebrum riegeri* n. sp. as seen with CLSM. Musculature (actin-filaments) in green, DAPI in purple, acetylated alpha-tubulin in yellow. **a, d, g** and **h**) Maximum intensity projections of a juvenile specimen, **b, c, e, f** and **i**) Maximum intensity projections of adult specimens. If not indicated otherwise, anterior is to the left and dorsal is up. **a** Lateral view of the body wall and digestive system musculature in pharyngeal area with sphincters, **b** Lateral view of the body wall musculature in the median region (between the male gonopore and the female ovary), **c** Lateral view of the body wall and digestive system musculature in the posterior tip of the animal, **d** Lateral view of the musculature in the anterior tip, **e** Lateral view of the anterior region of the body wall musculature in a virtually cropped image stack, revealing the brain supporting musculature, **f** Virtual view from inside of the animal towards the anterior tip posterior to the anterior portion of the brain supporting muscles, **g** Virtually cropped view of an anterior tip with star-shaped muscles, **h** Virtual transverse section through the pharynx with sphincters 1–4, **i** Virtual transverse section at the level of sphincter 5. Abbreviations: amf: anterior point of muscle fusion, bsm: brain supporting muscle, cmds: circular muscle of the digestive system, dllm: dorsolateral longitudinal muscle, dlm: dorsal longitudinal muscle, lca: major caudal lobe, llm: lateral longitudinal muscle, lmds: longitudinal muscle of the digestive system, lr: rostral lobe, np: neuropil, pfg: posterior frontal gland, ph: pharynx, sph1–6: sphincter 1–6, ssm: star-shaped muscle, tmr: transverse muscle ring complex, vllm: ventrolateral longitudinal muscle, vlm: ventral longitudinal muscle

lobes [8]) posterior to it. However, this study reveals a more complex system of several sublobes both in the anterior and posterior region (Fig. 4a, b). A total of four main commissures in the ventral nervous system (two posterior to the pharynx, one approximately half way between the pharynx and the male gonopore, one anterior to the ovary) are recognized. The anterior two commissures, associated with ganglia, connect the two lateral and the median posterior nerve cords with each other (Figs. 1a, c–g, 4a–c, e). The three longitudinal ventro-posterior cords fuse forming a subrectal commissure. Additionally, peripheral nerves are embedded in the epithelial layer of the animal, forming a grid of longitudinal and semicircular to circular nerves being perpendicular to each other, and being related to the central nervous system.

#### Acetylated $\alpha$ -tubulin-IR

**Central nervous system: Brain** The brain of *Lobatocerebrum riegeri* n. sp. consists of a large neuropil surrounded by impressive multi-lobed groups of perikarya from where longitudinal nerves extend laterally, anteriorly and posteriorly (Figs. 4, 5). The central neuropil comprises several commissures, which seem to be connecting the two main ventral cords in a pattern possibly resembling the annelid dorsal and ventral root of the circumesophageal commissure. The dorsal, median and ventro-anterior commissures are constituted as well defined nervous bundles, consisting of more than 40 nerve fibres. The ventroposterior commissures cannot always be resolved as individual structures, but form a thin sheath of nervous fibres (Figs. 3d, f, 4).

At least three pairs of characteristic large lobes (or ganglia) are arranged around the central neuropil, namely the paired anterior rostral lobes anterior to the neuropil and the pairs of posterior major and minor caudal lobes (respectively lca and lci, Figs. 3a–b, 4b, 5b–d). The major caudal lobes (lobus caudalis major according to Rieger [8], lca) are located mid-ventrally between the minor caudal

lobes (lobus caudalis minor according to Rieger [8], lci, Figs. 3a, 4a–b, 5b–d). The minor caudal lobes seem to be subdivided into a lateral and a median sublobe (lcil and lcim, respectively, Fig. 4b). No postcerebral ganglia as described by Rieger [8] have been found, suggesting that either the lateral sub-lobes of the minor caudal lobes or the lateral ganglia, which were found lateral to the central neuropil, have been mistaken for a postcerebral ganglion by Rieger [8]. The rostral lobes (lobus rostralis according to Rieger [8]) appear to be subdivided into one major (lra) and one minor portion (lri) and one lateral sublobe (lrl, Fig. 4a–b).

Although the nervous network of the neuropil is complex and intricate, some major connections could be reconstructed by means of CLSM. Four paired and one unpaired anteriorly directed rostral nerves all originate independently, but adjacent to each other from the anterolateral parts of the neuropil. In addition, several short nerves project out ventrolaterally from the neuropil for 10 to 20 micrometers (lpnp, Figs. 4a–b, 5d). However, no putative specific structure innervated by them could be identified in that region. The four paired and one unpaired rostral nerves anterior to the brain comprise: 1) One pair of ventrolateral anterior nerve cords extending ventro-laterally from the anterior neuropil (avnc, Figs. 3a, d–f, 5d) as an anterior extension of the posterior main ventral cords. Each of the ventrolateral anterior cords splits into two thinner bundles to innervate the tip and the sides of the rostrum (avnc and avlms, respectively, Fig. 4a–b). 2) One pair of dorsolateral nerves splitting up anteriorly (adnc, adlnc, Fig. 4a–b) originating from the lateral neuropil and possibly connected to the nerve stems of the major caudal lobes. 3) One pair of lateral nerve bundles (nlrl, Fig. 4a–d) originating dorsomedially at the dorsal root commissure but bending ventrolaterally between the lateral and anterior rostral lobes, where after they condense into a thick bundle continuing ventrolaterally throughout the rostrum until they fan out in the anterior end. 4) One loose pair of nerve bundles (nlr, Figs. 3d, 4, 5b–c) originating from the anterolateral

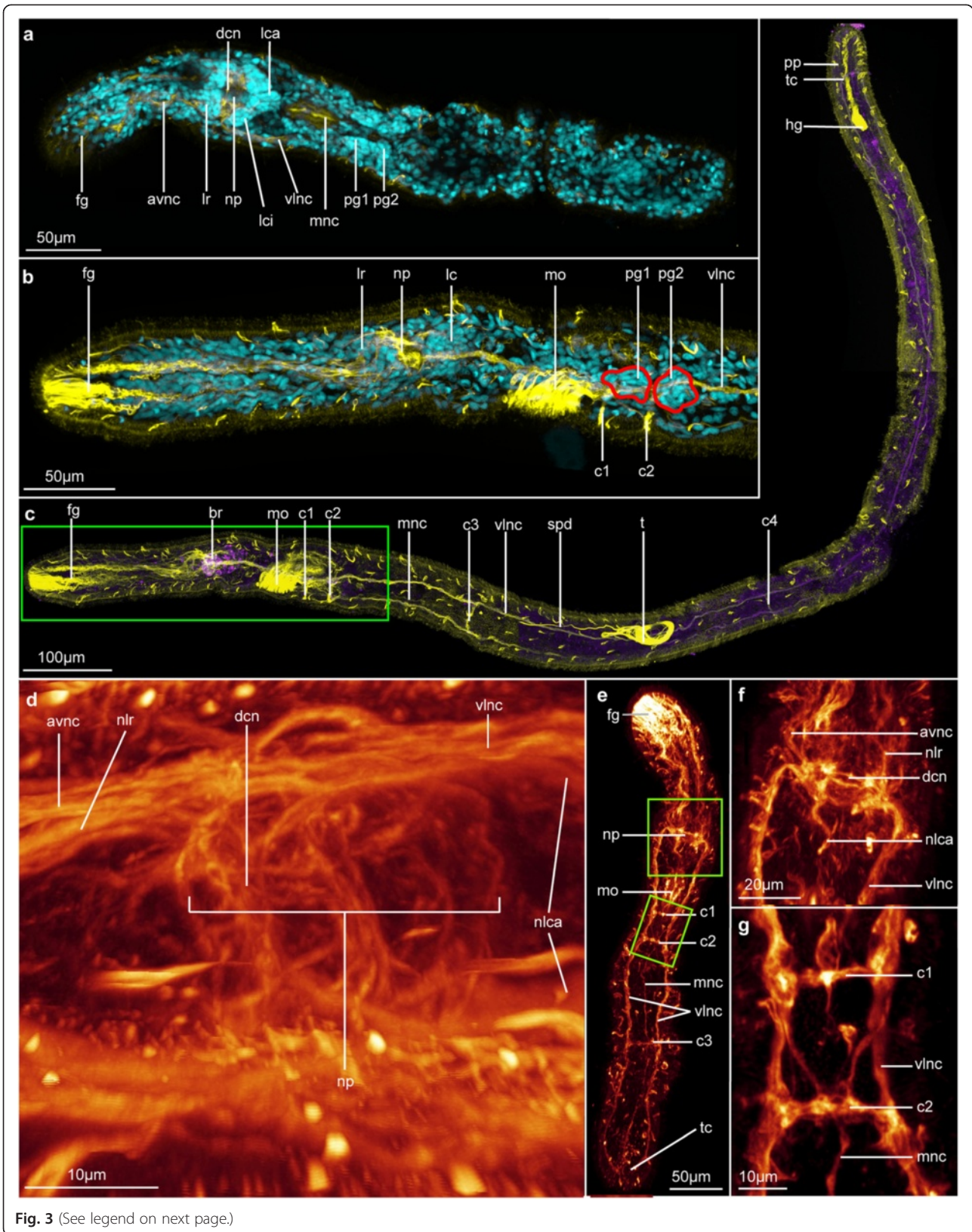


**Fig. 3** (See legend on next page.)

(See figure on previous page.)

**Fig. 3** General and detailed organization of the nervous system of *Lobatocerebrum riegeri* n. sp. as seen with CLSM. DAPI in cyan, FMRF in purple and acetylated  $\alpha$ -tubulin in yellow or "glow". All images are maximum intensity projections of a subset of the original image stack on various locations of the body if not specified below **a** Dorsal view of a juvenile specimen, **b** Lateral view of an adult, pharyngeal ganglia outlines in red, details of the same specimen as **(c)**, **c** Three different substacks of an adult specimen pieced together for an overview-picture. The specimen is twisted and some portions are laterally oriented and others dorso-ventrally oriented, **d** Dorsal view of the details of the brain, **e** Juvenile showing the general organization of the nervous system. Notice the presence of only three trunk commissures, **f** Dorsal view of the details of the brain in a juvenile. Details of the same specimen as **(e)**, **g** Dorsal view of details of the origin of the median nerve cord in a juvenile. Details of the same specimen as **(e)**. Abbreviations: avnc: anterior ventral nerve cord, br: brain, c1–4: commissure 1 - 4, dcn: dorso-anterior commissure of the neuropil, fg: frontal gland, hg: hindgut, lc: caudal lobe, lca: major caudal lobe, lci: minor caudal lobe, lr: rostral lobe, mnc: median nerve cord, mo: mouth opening, nlca: nerve of the major caudal lobe, nlr: nerve of the rostral lobe, np: neuropil, pfg: posterior frontal glands, pg1–2: postpharyngeal ganglia 1 - 2, pp: posterior projection, spd: spermi duct, t: testes, tc: terminal commissure, vlnc: posterior ventro lateral nerve cord

neuropil with minor subbundles (nlri and nlra, respectively, Fig. 4a–d) leading medioventrally through the major and minor rostral lobes, joining anteriorly of these, and continuing into the anterior part of the rostrum, before spreading out. 5) One unpaired median nerve (mrm) originating middorsally from the dorsal commissure (dc) between the two rostral lobes and extending dorsally through the entire rostrum, until it eventually splits at the tip to innervate the anterior edge (Figs. 4a–d, 5b–c). The function of such a strong innervation of the rostrum is unknown. However, some nerves connect directly to specific cilia, which are stiff and longer than the locomotory cilia and therefore assumed to have sensory function. Many nerves, however, do not seem to connect to any specific epidermal structures and no multicellular sensory organ could be found. Posterior to the neuropil, two pairs of thick dorso-posterior nerve stems extend posteriorly into the major (nlca) and minor caudal lobes (nlci, Fig. 4a–d); again branching into the two median and lateral parts of the minor lobes (nlci and nlcil, respectively, Fig. 4a–d). The nerve stem of each major caudal lobe is composed of nerves originating from the dorsal commissure (which is suggested to resemble the dorsal commissure of the dorsal root) as well as lateral nerves of the neuropil, the latter being seemingly continuous with the rostral dorsolateral nerves. If truly continuous, this may indicate that the dorsolateral nerves are sensory nerves transferring sensory inputs from the rostrum to be processed in the major caudal lobes.

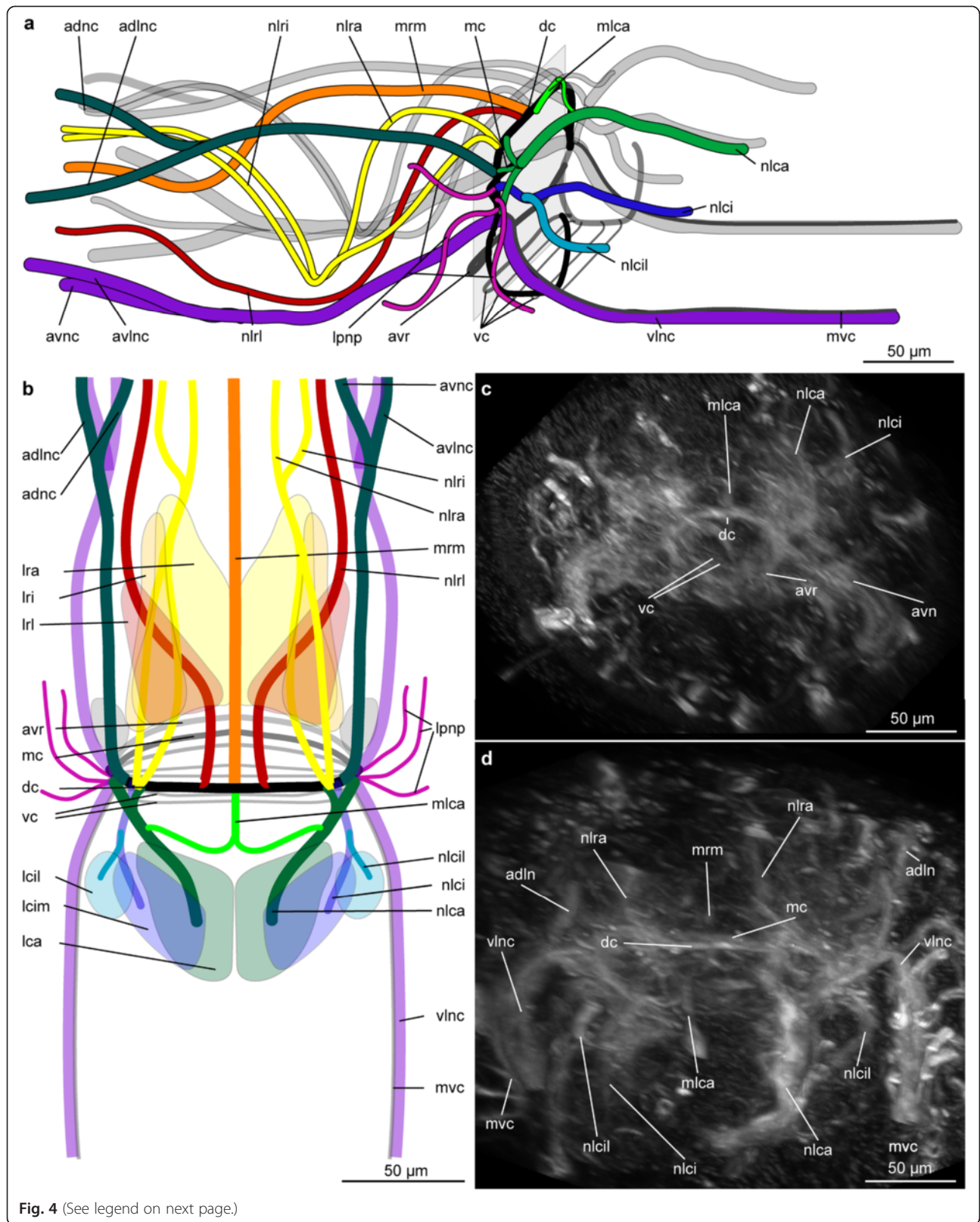
**Central nervous system: Ventral cords and commissures** In all specimens investigated, the posterior parts of the ventrolateral nerve cords emerge from the ventrolateral area of the central neuropil and extend to the terminal commissure anteroventral to the anus (pc, Figs. 3c, e). They are located dorsolateral to the third (lateral) muscle bundle, although this position varies slightly throughout the body, with the longitudinal muscles sometimes being so deeply embedded within the epidermis that they become more externally positioned than the nerve cords (Fig. 1e–h). The ventrolateral nerve cords consist of three to four times more

fibres than the median nerve and measure 3–4  $\mu$ m in diameter. The longitudinal ventromedian nerve is located intraepidermally, between the two most ventral longitudinal muscle bundles (mnc, Fig. 3g). It is formed by contralateral projections of the ventrolateral nerve at the level of the first commissure, which fuse in the ventral midline with their counterpart at the level of the second commissure. Hereafter, the median nerve continues posteriorly to insert at the terminal commissure. Two projections from the terminal commissure extend for 10–15  $\mu$ m dorso-posteriorly (pp, Fig. 3c).

Four trunk commissures are connecting the two ventrolateral nerve cords and the median nerve with each other (c1–4, Figs. 1a, c–h, 3b–c, e, 5a). Each commissure apparently consists of as many nerve fibres as the ventro-lateral cords and measures 3–4  $\mu$ m in diameter. The anteriormost two commissures are located close to each other posterior to the mouth opening, separated by 20–25  $\mu$ m (c1, c2, Figs. 1a and 3e, g). Since few of the perikarya of the commissures were showing immunoreactivity against serotonin or FMRFamide, only the large ganglia of the first and second commissures could be detected by a few serotonergic cells and DAPI-staining, here showing densely grouped nuclei (Fig. 5a, e). These ganglia are situated dorsoposterior to the commissures and each consists of 30–40 cells (pg1–2, Figs. 3a, b and 5e). The third commissure is located between the pharynx and the male gonopore, approximately 30–50  $\mu$ m anterior to the gonopore (c3, Fig. 3c). The fourth commissure (c4, Fig. 3c) is located between the testis and ovary.

Single, presumably sensory, cells are sparsely distributed throughout the epidermis of the entire body, but connect to neither the ventral nerve cords nor the peripheral nerves (ss, Fig. 5f). Normally, they consist of one cell with a single cilium often surrounded by a circle of microvilli (Fig. 5f). There is no correlation between a high abundance of these sensoria and specific organs or body regions.

**Peripheral nervous system** The peripheral nervous system is embedded in the epidermal cell layer and consists of longitudinal and incomplete circular fibres.



(See figure on previous page.)

**Fig. 4** Details of the nerves of the brain of *Lobatocerebrum riegeri* n. sp. as seen with CLSM, acetylated  $\alpha$ -tubulin in grey. **a, b** Schematic drawings based on confocal stacks, **c, d** maximum intensity projections of the original image stack. **a** Brain in dorsolateral view, with the major nerves of the left side colour-coded, the nerves of the right side shaded in grey **b** Dorsal view of the brain with similar colour-coding and indication of the nerves, **c** dorsal view of the central neuropil at the level of the main commissures in the brain; **d** dorsal view of the central neuropil with the major nerve cords as shown in the schematic drawings. Abbreviations: adlnc: anterior dorsolateral nerve cord, adnc: anterior dorsal nerve cord, avc: antero-ventral commissure of the neuropil, avlnc: anterior ventrolateral nerve cord, avnc: anterior ventral nerve cord, dc: dorsal commissure of the neuropil, lca: major caudal lobe, lcil: lateral minor caudal lobe, lcim: median minor caudal lobe, lpnp: lateral projection of the neuropil, lrl: lateral rostral lobe, lra: major rostral lobe, lri: minor rostral lobe, mc: median commissure of the neuropil, mlca: medial nerve innervating the major caudal lobe, mrm: median rostral nerve, nlca: nerve innervating the major caudal lobe, nlci: nerve innervating the median minor caudal lobe, nlcil: nerve innervating the lateral minor caudal lobe, nrl: nerve leading through the lateral rostral lobe, nlra: nerve leading through the major rostral lobe, nlri: nerve leading through the minor rostral lobe, mvc: medioventral nerve cord, vlnc: ventral nerve cord, vc: ventral commissure of the neuropil

These nerves are thinner than the ones of the central nervous system (0.5  $\mu$ m in diameter) and consist of only very few to individual nerve fibres. The longitudinal peripheral nerves (lpn, Figs. 5h–i) trace the longitudinal muscle bundles throughout the body (lm, Fig. 5i). In the most posterior part of the body, though, they could not be detected with acetylated  $\alpha$ -tubulin IR due to the overlaying signal of the central nervous system and the various glands. Their specific origin cannot be assessed, though these thin nerves seem to descend from the central neuropil rather than from the ventrolateral nerve cords.

The incomplete circular nerves (tpn, Fig. 5h) are closely associated with the commissures in the ventral nerve cord, at the level of which they extend from the ventrolateral nerve cords to the dorsal side of the animal. Here, they connect to the longitudinal peripheral nerves exterior to the longitudinal muscle bundles and create a circular connection among these. Additionally and independent of the commissures, one transverse nerve anterior to the pharynx forms an incomplete circle including only lateral and dorsal peripheral longitudinal nerves and three closed rings include all longitudinal peripheral nerves at the level of the seminal receptacles. The latter are set 30–35  $\mu$ m apart (Fig. 1a). Some additional circular peripheral nerve rings are also found scattered throughout the body. However, they could not be related to any specific structures or reveal a consistent pattern in all specimens investigated.

#### Tyrosinated tubulin-IR

Immunoreactivity of the tyrosinated tubulin-antibody did not reveal any additional structures adding to the pattern already seen with acetylated  $\alpha$ -tubulin-IR. On the contrary, the commissure inside the brain as well as the peripheral nerves could not be revealed using this antibody.

#### Serotonin-IR

Serotonin-IR was not only labeling nervous structures, but also glands (uni- and multicellular) and stomach content, where the antibodies most likely got retained

between particles or in vesicles (Fig. 5e). However, strong labeling of some but not all epidermal cells could be found, with the IR being located in the entire cytosol, but not in the nucleus, which made them therefore resemble serotonergic perikarya (spc, Fig. 5e). Since there was no connection to the nervous system, they could also be specialized gland or epidermal cells with so-far unknown function.

Serotonin-IR also labels all three longitudinal nerves of the ventral nervous system, with one or two strands inside the thick bundles. This pattern is also present in all commissures, but serotonin-IR cannot be detected in any of the peripheral nerves. In the ganglionic pairs associated with the two pharyngeal commissures, four to five perikarya show serotonin-IR, but do not display any specific arrangement inside the ganglion: They seem to be randomly spread between the other cells (spg1-2, Fig. 5e). Additional perikarya with serotonin-IR are found scarcely along the ventral nerve cord.

#### FMRFamide-like-IR

FMRFamide-like-IR was not consistent between the two specimens investigated. This is mainly due to the rostral glandular structures, which seem to be lying adjacent to the nervous system in *Lobatocerebrum*, and to differences between the studied individuals. Similar to the serotonin - IR described above, the three ventral nerves of the central nervous system, the posterior projection from the terminal commissure (pp, Fig. 5c), as well as the commissures of the central nervous system are revealed using FMRFamide-like-IR (Figs. 3c and 5a). Interestingly, while several nerve fibres in the lateral nerve cords seem to be FMRFamidergic, only one single fibre in the median nerve cord shows this IR, most likely emerging at the level of the pharyngeal commissures. There are no FMRFamidergic perikarya along the ventral nervous system. Only one FMRFamidergic perikaryon in each of the two subpharyngeal ganglia was detected seemingly contributing to the pharyngeal commissure (fpg1-2, Fig. 5a), though its location does not seem to be truly consistent between all specimens investigated.

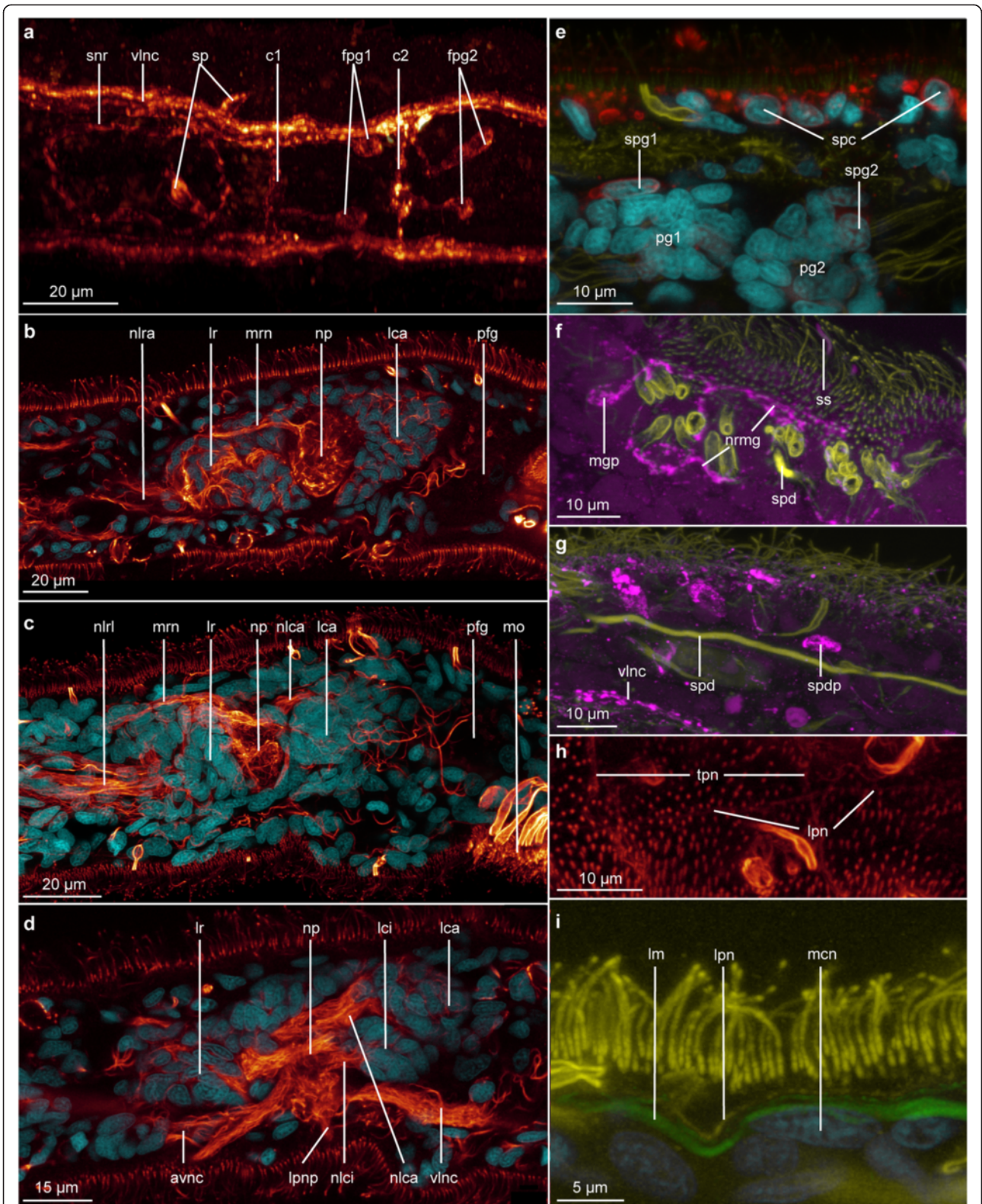


**Fig. 5** (See legend on next page.)

(See figure on previous page.)

**Fig. 5** Details of the nervous system of *Lobatocerebrum riegeri* n. sp. as seen with CLSM. DAPI in cyan, serotonin in red, FMRFamide in purple. The use of “glow” depends on the figure and is indicated for each of them. All images are maximum intensity projections of a subset of the original image stack on various locations of the body if not specified below. Anterior is to the left and posterior to the right **a** Dorsal view of the details of the FMRFamidergic nervous system around the pharynx in “glow”. The background noise has been masked to highlight the nervous system. **b, c** and **d** Single sagittal sections showing details of the brain.  $\alpha$ -tubulin in “glow”, **b–d** Virtual sections through the median plane (**b**) the medio-lateral plane (**c**) and the lateral plane (**d**) of the brain, **e** Coronal substack of the animal showing details of the epidermis and the postpharyngeal ganglia (the outside of the animal is on the upper side of the picture), **f** Dorsal view of a sub-stack of the male gonopore (the outside of the animal is on the upper side of the picture), **g** Dorsal view of a sub-stack of the spermioduct, **h** Dorsal view of a sub-stack of epidermis showing the peripheral nervous system with  $\alpha$ -tubulin in glow, **i** Sub-stack showing a longitudinal section of the epidermis with details on the peripheral nervous system associated to the musculature (the outside of the animal is on the upper side of the picture). Abbreviations: avnc: anterior ventrolateral nerve cord, c1–2: commissure 1 - 2, fpg1–2: FMRFamidergic perikarya of the postpharyngeal ganglia 1 - 2, lca: major caudal lobe, lci: minor caudal lobes, lm: longitudinal muscle, lpn: longitudinal peripheral nerve, lppn: lateral projection of the neuropil, lr: rostral lobe, mcn: nuclei of the myocyte, mo: mouth opening, mop: perikaryon associated with the male gonopore, mrrn: median rostral nerve, nlca: nerve of the major caudal lobe, nlci: nerve of the minor caudal lobe, nlra: nerve of the major rostral lobe, nlrl: nerve of the lateral rostral lobe, np: neuropil, nrmg: nerve ring around the male gonopore, pfg: posterior frontal glands, pg1–2: postpharyngeal ganglia 1 - 2, snr: stomatogastric nerve ring, sp: perikarya of the stomatogastric nerve ring, spc: serotonergic cell, spd: spermioduct, spdp: FMRFamidergic perikarya associated to the spermioduct, spg1: serotonergic perikarya of the postpharyngeal ganglion 1, ss: sensoria, tpn: transverse ring of the peripheral nervous system, vln: ventral longitudinal nerve cord

Possibly as part of the stomatogastric nervous system, two additional pairs of perikarya were revealed dorsal to the mouth and lateral to the pharynx, respectively. Since they are connected ventrally via a thin nerve strand, they seem to constitute the stomatogastric nerve ring described by Rieger [8], snr, Fig. 5a). Surrounding this structure and disguised by the strong IR of the pharyngeal glands, additional perikarya with very weak FMRFamide-like-IR (sp, Fig. 5a) are found. A further differentiation between the perikarya of the stomatogastric nerve ring and the immune-reactive glands is not possible with any antibody employed in this study.

Though no evidence of the peripheral nervous system could be detected with FMRFamide-like - IR, a FMRFamidergic nerve net is found around the male gonopore. It consists of a thin nerve ring around the male gonopore (nrmg, Fig. 5f) and several individual neurites projecting radially into the ring from their perikarya (mgp, Fig. 5f). Though they are found in all specimens, their number and distribution pattern vary strongly. Additionally, four FMRFamidergic perikarya are distributed scarcely along the spermioduct (spdp, Fig. 5f). No nervous system could be found associated with the ovary or the seminal receptacles.

#### Glandular structures

Studied in LM, with acetylated  $\alpha$ -tubulin and DAPI staining in CLSM, and in TEM, Figs. 6, 7. Acetylated  $\alpha$ -tubulin-IR of the glandular cell walls [37] proved useful to identify and describe several types of glandular cells in the epidermis.

#### Epidermal glands

Four types of unicellular epidermal glands were distinguished by acetylated  $\alpha$ -tubulin-IR and CLSM: a) ciliated

glands; b) smooth flask-shaped glands; c) kidney-shaped gland; and d) unicellular adhesive glands.

**Ciliated glands** The ciliated gland cells (cg, Figs. 6a–c, 7b) are the largest of the unicellular epidermal glands (diameter 6.9–8.1  $\mu$ m, length 9.3–11.2  $\mu$ m,  $n = 3$ ,  $r = 1–4$ ,  $m = 5$ ), distally with a ring formed by shortened stiff cilia around their external opening (sc, diameter 0.6–1.5  $\mu$ m,  $n = 3$ ,  $r = 1–4$ ,  $m = 5$ , Fig. 6a, b) and proximally extending into a 30–50  $\mu$ m long ( $n = 3$ ,  $r = 1–4$ ,  $m = 5$ ), thin tail-region lining the basal membrane. The broad distal region of the gland cells containing the nucleus is located intraepidermally, occasionally alongside the longitudinal muscle bundles, since these are sunken into the epidermal layer (Fig. 6a). The gland cell membranes are lined by twelve to twenty pairwise arranged tubulinergic filaments (tst,  $n = 3$ ,  $r = 1–4$ ,  $m = 5$ ). The cell nucleus has approximately the same size and heterochromatin-content as the nuclei of the surrounding epidermal cells (Fig. 6a–b). The gland cells are packed with non-electron-dense to weakly-electron-dense vesicles (gv, Fig. 6c). They are found scattered throughout the entire body, though they are most abundant in the posterior region, mainly from the midgut-hindgut-transition towards the posterior end of the body. Although the cellular tail region of the cell may tangent a nerve cord, no close connection or direct nervous innervation of the glands, nor indications of muscular control, were found with CLSM or TEM.

These cells most likely resemble the ‘mucous gland type 1’ in *L. psammicola* described by Rieger [8, 10], having a similar characteristic ring of shortened cilia around the opening. This is further corroborated by the similar shape and electron density of the vesicles of these glandular cells [8, 10, 11].

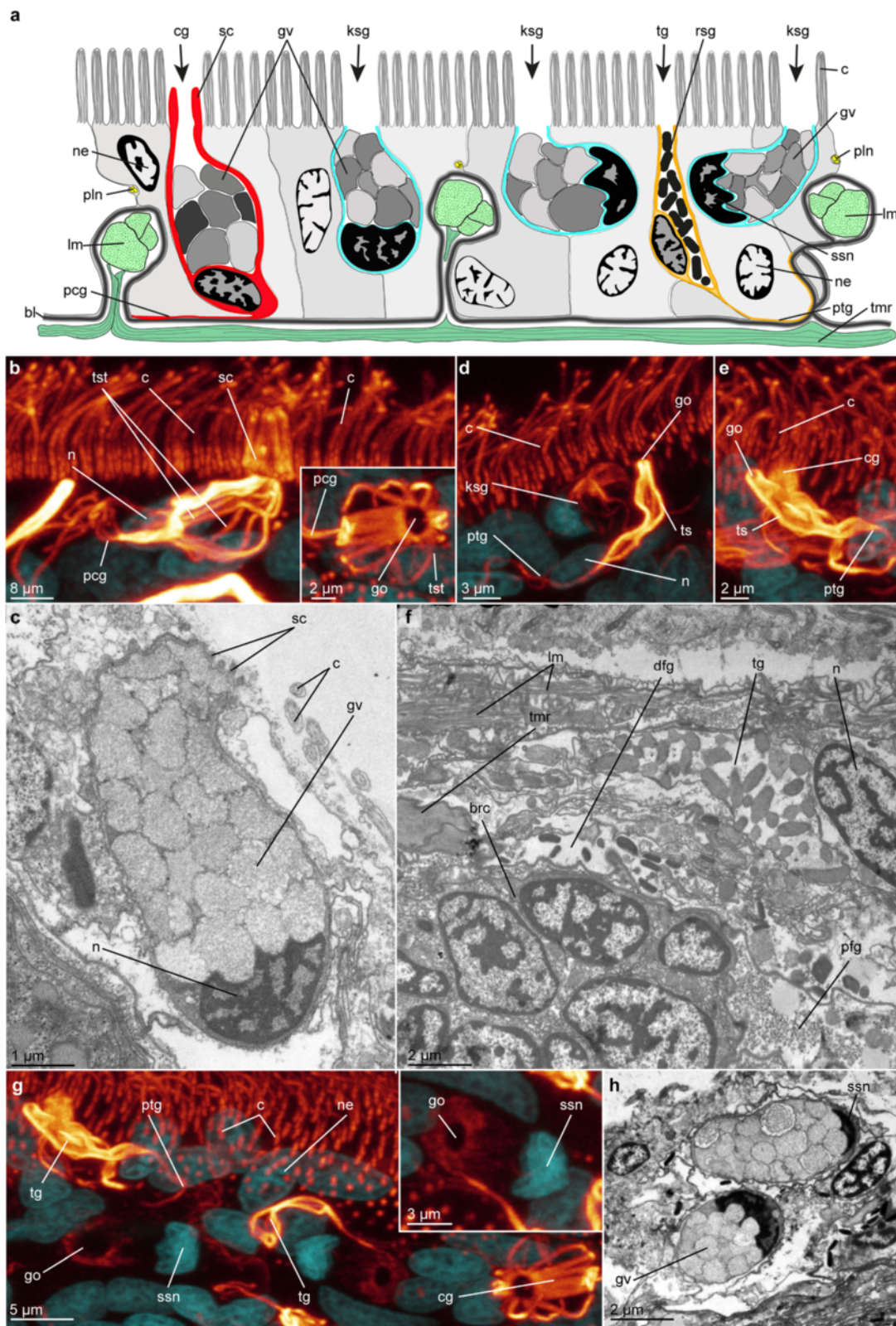


**Fig. 6** (See legend on next page.)

(See figure on previous page.)

**Fig. 6** Epidermal glands in *Lobatocerebrum riegeri* n. sp. as seen with CLSM and TEM. DAPI in cyan, acetylated  $\alpha$ -tubulin in glow. **b, d–e, g** are maximum intensity projections of a subset of the original image stack on various locations of the body, **c, f, h** ultrastructural details of the epidermis. **a** Schematic cross section drawing of the epidermis with all three glandular cell types in their approximate abundance, **b** ciliated gland cell with closed circle of shortened cilia (inset with details of the tubular strands in the cellular membrane), **c** Sagittal section of a ciliated gland cell, **d** Tubular gland cell in the epidermis, **e** Tubular gland cell with long projection in the epidermis, **f** Sagittal section through the epidermis of the rostrum, presenting a tubular epidermal gland adjacent to a duct of the posterior frontal gland and the brain, **g** Kidney-shaped glands in the epidermis (inset with details of the glandular opening), **h** Cross section through a kidney-shaped gland. Abbreviations: afg; anterior frontal gland; bl: basal lamina, bc: brain cell, c: cilium, cg: ciliated gland cell, dfg: duct of the frontal gland, go: glandular opening, gv: glandular vesicle, ksg: kidney-shaped gland cell, lm: longitudinal muscle, n: nucleus, ne: nucleus of epidermal cell, pcg: projection of the ciliated gland cell, pfg: posterior frontal gland, pln: peripheral longitudinal nerve, ptg: projection of the tubular gland cell, rsg: rod-shaped granule, sc: shortened cilium, ssn: sickle-shaped nucleus, tg: tubular gland cell, tmr: transverse muscular ring complex, ts: tubulinergic sheath, tst: tubulinergic strand

**Tubular glands** Tubular gland cells (tg) do not have a ciliary ring around their opening, but a continuous lining of acetylated  $\alpha$ -tubulin IR in the membrane lining the cell (diameter 1.5–3.2  $\mu\text{m}$ , length 7.8–8.9  $\mu\text{m}$ ,  $n = 3$ ,  $r = 1–4$ ,  $m = 5$ , Fig. 6d, e). They are generally characterized by a slender distal neck-area before the cell widens proximally (Fig. 6a, d, e). However, a few cells with wide distal openings have been found. A long, thin tail extends from the basal part of the cell up to 30  $\mu\text{m}$  along the basal lamina, apparently without connecting to any other structure (Fig. 6a). In contrast to the ciliated glands, the smaller sized tubular gland cells mainly occupy the more distal part of the epidermal layer, distal to the muscle bundles (Fig. 6a). These gland cells are filled with electron-dense, rod-shaped granules (0.8–1.5  $\mu\text{m}$  in length, 0.2–0.5  $\mu\text{m}$  in width,  $n = 3$ ,  $r = 1–4$ ,  $m = 5$ ), which are less densely packed than the vesicles of the adhesive glands (Fig. 6e). They are highly abundant throughout the entire body (10–15 cells per 100  $\mu\text{m}$  body length,  $n = 3$ ,  $r = 1–4$ ,  $m = 5$ ), with the densest distribution in the posterior region of the body.

**Kidney-shaped glands** Only one glandular cell type (kidney-shaped gland cell, ksg) can be distinguished by the shape of its nucleus: In contrast to all other epidermal cell nuclei, nuclei of kidney shaped gland cells are strictly sickle-shaped (Fig. 6a, g, h) and their chromatin denser than the also “deformed” nuclei of ciliated glands (Fig. 6c). The cell membrane only contains very few tubulinergic elements; yet, dense acetylated  $\alpha$ -tubulin-IR can be detected around the cell opening (diameter 1.1–1.7  $\mu\text{m}$ ,  $n = 3$ ,  $r = 1–4$ ,  $m = 5$ ) and at its base. The overall appearance of the cell is characteristically kidney-shaped (diameter 3.3–4.7  $\mu\text{m}$ , length 6.9–7.8  $\mu\text{m}$ ,  $n = 3$ ,  $r = 4$ ,  $m = 5$ , Fig. 6e). Kidney-shaped gland cells are mainly found in the distal part of the epidermal layer similar to the tubular gland cells (Fig. 6a). However, the basalmost part of the cell, which contains the nucleus, can also be found close to or even internal to the longitudinal muscle bundles (Fig. 6a, g). These glandular cells are most likely imparting the greenish speckled appearance of the animals in live observations (Additional file 1) due to the refractive index of their content, which consists of non- to weakly-electron

dense and tightly packed vesicles (diameter 0.6–1.2,  $n = 3$ ,  $r = 1–4$ ,  $m = 5$ , Fig. 6h). In contrast to the ciliated gland cells, the vesicles of the kidney-shaped gland cells are less homogenous in the electron-density of their content, and denser in their packing, possibly causing the sickle-shape of the nucleus.

**Unicellular adhesive glands** The unicellular adhesive glands are characterized by a ring of shortened cilia around the opening, which was suggested to facilitate mechanical loosening from the substrate instead of a second enzymatic gland with releasing function [8, 10] and therefore morphologically resembles the ciliated glands though their content and function differ (Fig. 7a, b). Their secretion is granular, but shows a characteristic structure with an inner, electron-dense area in a non-electron-dense oval structure (Fig. 7a, b). Different to the adhesive glands described in *L. psammicola*, the glands of *L. riegeri* n. sp. do not have linear electron-dense structures in the middle of the individual granules, but instead linearly arranged electron-dense dots (Fig. 7a, b). Contrary to the abundance and distribution pattern of the other epidermal glands cells mentioned above, adhesive gland cells are restricted to the ventral surface of the body in lower numbers (1–5 cells per 100  $\mu\text{m}$  ventral body length,  $n = 3$ ,  $r = 1–4$ ,  $m = 5$ ).

#### Frontal glands

The main body of the paired posterior frontal glands (pfg) is found posterior to the brain and anterior to the pharyngeal region (Figs. 5b, c, 7c). This part of the glands is difficult to detect with any of the antibodies described above, but can be found combining the lack of DAPI-signal with overexposed phalloidin-signal to detect cell membranes and nuclei of voluminous cells in a large lobular structure posterior to the brain lobes (Fig. 7c). The glandular nuclei are slightly larger than the ones of the brain (diameter 4.3–5.7  $\mu\text{m} \times 1.4–2.5 \mu\text{m}$ ,  $n = 3$ ,  $r = 1$ ,  $m = 5$ ). While the gland body itself is inconspicuous in CLSM, its long ducts, which are leading ventroanterior of the brain to the tip of the rostrum, are showing distinct acetylated  $\alpha$ -tubulin-IR

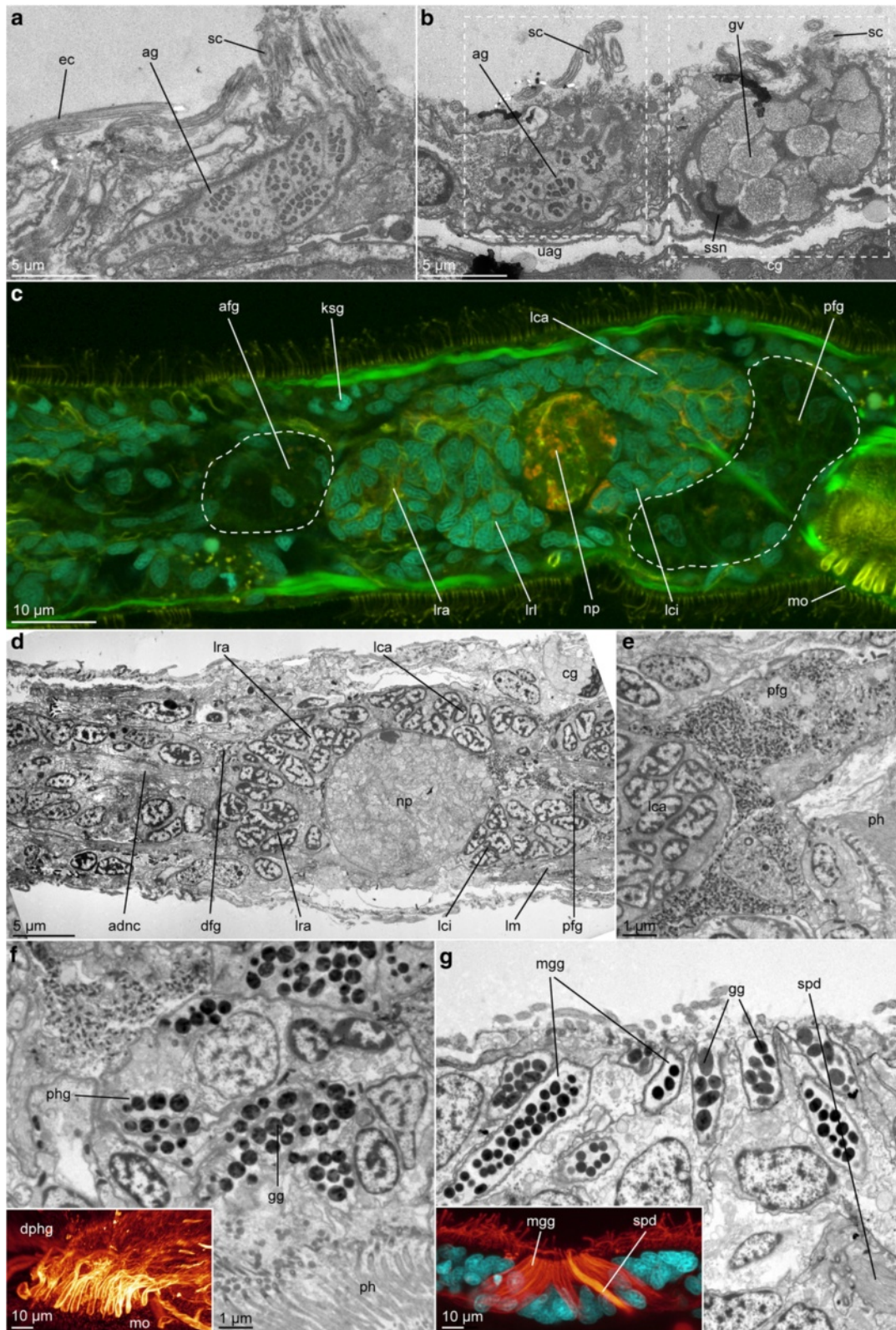


**Fig. 7** (See legend on next page.)

(See figure on previous page.)

**Fig. 7** Specific glandular systems in *Lobatocerebrum riegeri* n. sp. as seen with CLSM and TEM. DAPI in cyan, acetylated  $\alpha$ -tubulin in glow or yellow, actin-filaments in green. **c, g, h** are maximum intensity projections of a subset of the original image stack on various locations of the body, **a, b, d-f** ultrastructural details of glandular structures. **a** Sagittal section through the epidermis and an unicellular adhesive gland, **b** Sagittal section through an unicellular adhesive and a ciliated gland in the epidermis, **c** brain and portions of the anterior and posterior frontal glands (indicated by white dashed line), **d** Sagittal section through the anterior tip of the rostrum with ducts of the posterior frontal glands and nerves, **e** Sagittal section through the mouth opening with glandular cells of the posterior frontal gland and the pharyngeal gland, **f** Sagittal section through the pharyngeal region with distal parts of the pharyngeal glands, **g** Distal regions of the ducts of the pharyngeal glands, **h** Glands around the male gonopore. Abbreviations: afg: anterior frontal gland, ag: adhesive granule, cg: ciliated gland cell, dfg: ducts of the frontal gland, dphg: ducts of the pharyngeal gland, ec: cilia of an epidermis-cell, gg: glandular granules, gv: glandular vesicle, ksg: kidney-shaped gland, lca: major caudal lobe, lci: minor caudal lobe, lrl: lateral rostral lobe, lra: major rostral lobe, mo: mouth opening, mg: male gonopore, mgg: male gonopore gland, np: neuropil, pfg: posterior frontal gland, sc: shortened cilium, spd: spermi duct, ssn: sickle-shaped nucleus, uag: adhesive gland cell

(Fig. 3a–c, e, 7d). Posteriorly the ducts are straight and grouped into two bundles; anteriorly they ramify into a fan of duct openings framing the anterior edge (Figs. 1a, 3b, c, e). Ramifying longitudinal nerves are found accompanying these in the rostrum but possible nervous innervation of the frontal glands could not be resolved. The cellular content of the posterior frontal glands consist of very small (diameter 0.2–0.3  $\mu\text{m}$ ,  $n = 1$ ,  $r = 1$ ,  $m = 10$ ) spherical, electron-dense granules, which seem to increase in diameter towards the anterior tip of the animal and the opening of the duct (Fig. 7d, e). This glandular content can clearly be distinguished by their shape from the content of the epidermal cells described above (big vesicles) and the granules of the anterior frontal glands (rod-shaped granules, Figs. 6a, c, f, h, 7a, b, d–f).

An additional, smaller pair of frontal glands, located anterior to the brain, has been reported by Rieger [10], and is possibly also present in *Lobatocerebrum riegeri* n. sp. (Fig. 7c). As for the posterior frontal glands, their presence could be detected indirectly with CLSM by paired, seemingly empty cavities filled by large cells with elongated nuclei and distinctly tubulinergic ducts. Some of these short ducts opening midventrally did show acetylated alpha-tubulin-IR. However, not all ducts could be traced with certainty to their external ventral openings, since they do not seem to possess the same high density of tubulinergic elements as the ducts of the posterior frontal glands. In the same ventral location of the rostral tip of the animal, TEM showed several tube-like structures with more electron-dense and narrow granules than detected in the tubular glands (Fig. 6f), which are assumed to constitute the secretion of the anterior frontal glands (afg, Fig. 7d).

#### Pharyngeal glands

The major glandular structures of the digestive system are the big, multicellular glands of the pharynx, whose products are secreted in the area of the mouth opening (Fig. 7e). 17–18 elongated ducts (diameter 1.8–3.5  $\mu\text{m}$ , length 70–100  $\mu\text{m}$ ,  $n = 3$ ,  $r = 2$ ,  $m = 5$ , Fig. 7g) of posteriorly located glands surround the mouth opening. They

are arranged in a denser pattern in its posterior third, while they are more loosely set anteriorly. The main glandular body can be detected posterior to the mouth opening, on the ventral side of the body dorsal to the ventral nerve cords. It is seen as an elongated, bag-like structure filled with spherical, electron dense granules (1.2–1.7  $\mu\text{m}$ ,  $n = 2$ ,  $r = 2$ ,  $m = 5$ ) best detected with FMRamide-like-IR or TEM (Fig. 7e–g). These glands are not epidermal, and their cell bodies are found inside both the longitudinal musculature and transverse muscular ring complexes of the body wall.

#### Male gonopore glands

Acetylated tubulin-IR was recovered in cells surrounding the dorsal male gonopore. The openings of 16–20 ( $n = 3$ ,  $r = 2–3$ ,  $m = 5$ ) gland cells constituting the complex (Fig. 7h) are connected to the gland bodies via elongated, thin ducts, which are 1.0–1.5  $\mu\text{m}$  in diameter and are all leading to a sunken-in area (14.8–18.3  $\mu\text{m} \times 6.4–8.2 \mu\text{m}$ ,  $n = 3$ ,  $r = 2–3$ ,  $m = 5$ , Fig. 7h) around the male gonopore. Approximately half of the cells are densely packed around the anterior end, and the other half around the posterior end, with a small gap between the two portions.

#### Reproductive system

*Studied in LM, with acetylated  $\alpha$ -tubulin and DAPI staining in CLSM, Fig. 8.*

In all four adult animals investigated, both male and female reproductive organs or gametes could be found, as well as seminal receptacles to store the mating partner's sperm.

#### Male gonad

The male gonad is located on the dorsolateral side of the animal, posterior to the third commissure. It is an elongated, thin structure, with the gonopore opening on the dorsal surface of the animal (diameter 1.5–2.7  $\mu\text{m}$ ,  $n = 3$ ,  $r = 2–3$ ,  $m = 3$ , Figs. 7g, 8a). A thin channel (diameter 1.4–1.8  $\mu\text{m}$ ,  $n = 3$ ,  $r = 2$ ,  $m = 5$ ) extends posterior to the pore, with a high amount of the long, thin, fibrous sperm stored in the posterior region (Fig. 8a). Where the sperm is produced is unclear; however, the majority of

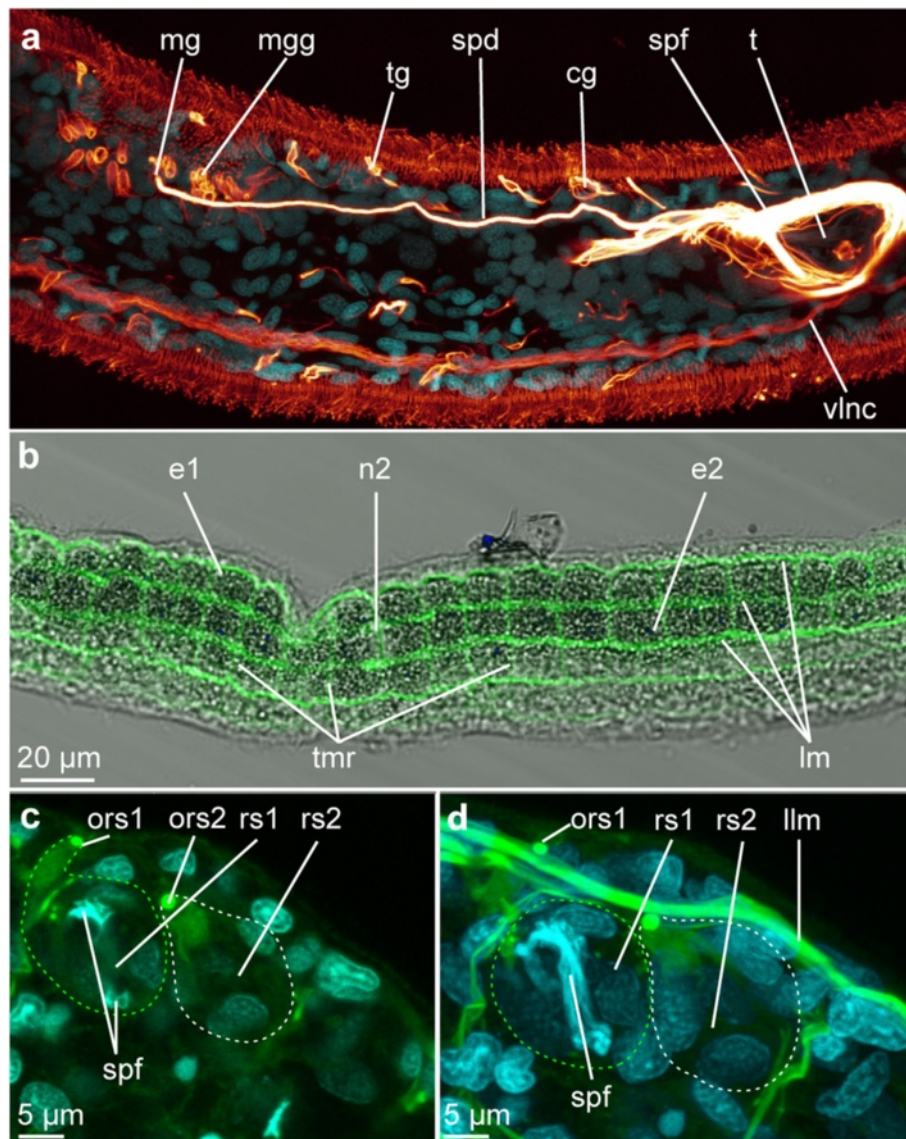


**Fig. 8** Reproductive organs in *Lobatocerebrum riegeri* n. sp. as seen with CLSM and transmitted light. DAPI in cyan, acetylated  $\alpha$ -tubulin in glow, phalloidin in green. All images are maximum intensity projections of a subset of the original image stack. Orientation is anterior to the left and dorsal side up if not indicated otherwise. **a** Testis with spermioduct and glands around the male gonopore, **b** Ovary, **c-d** Seminal receptacles at the level of the tips of the sperm filaments **c** and with bent sperm filaments **d**. The contours of the receptacles are traced with dashed lines to facilitate orientation. Abbreviations: cg: ciliated gland, e1–2: egg 1–2, llm: lateral longitudinal muscle, lm: longitudinal muscle, mg: male gonopore, mgg: male gonopore glands, n2: nucleus of egg 2, ors1–2: opening of the seminal receptacle 1–2, rs1–2: seminal receptacle 1–2, spd: spermioduct, spf: sperm filaments, t: testis, tg: tubular gland, tmr: transverse muscular ring complex, vlnc: ventral longitudinal nerve cord

glands involved in this apparatus are arranged around the gonopore itself, as described above, creating a glandular field ( $16.2\text{--}17.0\ \mu\text{m} \times 3.5\text{--}5.4\ \mu\text{m}$ ,  $n = 3$ ,  $r = 2, 3$ ,  $m = 4$ , Figs. 7a, b, 8a).

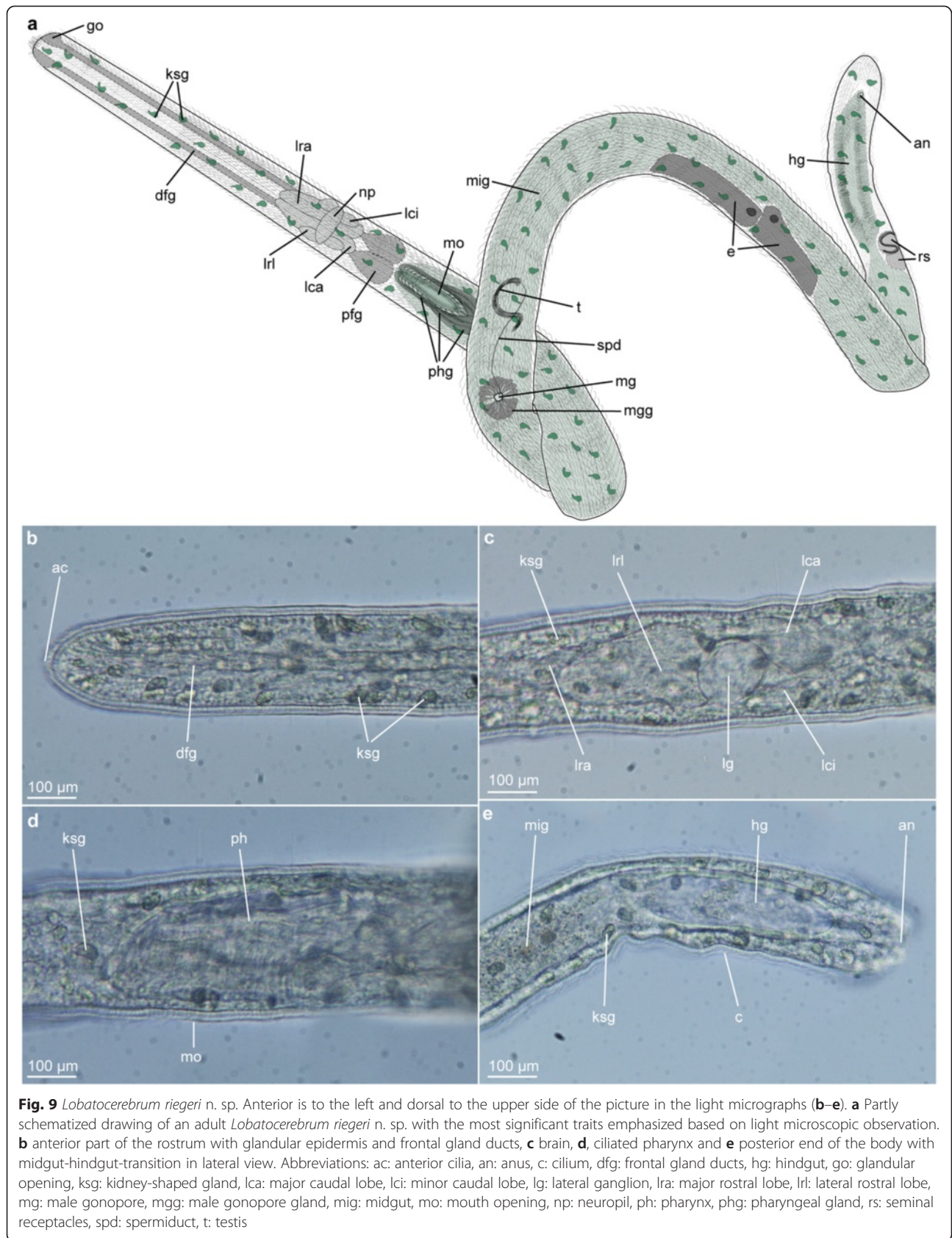
#### Female gonad

Up to four eggs, lined up behind each other and increasing in volume posteriorly (Fig. 8b), are the only structures of the female gonad detected with either immunohistochemistry or live observations. The eggs

are of irregular shape, reflecting the available space in the body. Although the openings of both seminal receptacles and the male gonad have been found, no obvious opening was detected near the eggs, and they may have to be deposited via rupturing of the epidermis.

#### Seminal receptacles

In the posterior part of the body, the adult animals form one to several seminal receptacles (rs, Fig. 8c, d). These receptacles are thin-walled capsules consisting of few



cells without any specific immunoreactivity (Fig. 8c, d). Their diameter is 20–30  $\mu\text{m}$  ( $n = 3$ ,  $r = 1$ ,  $m = 4$ ), and the sperm filaments (spf) can be seen inside, bent and curled up (Fig. 7e). The openings of the receptacles (ors, diameter 0.8–1.7  $\mu\text{m}$ ,  $n = 3$ ,  $m = 3$ ) are on the ventrolateral side of the body (Fig. 8c).

### Motility patterns

*Studied in LM, Additional file 1.*

#### Ciliary locomotion

*Lobatocerebrum riegeri* n. sp. is uniformly ciliated along the entire body and moves mainly by a relatively slow, but steady back and forward ciliary gliding rather than muscular action (Additional file 1). Ciliary mode of locomotion is cost-efficient for minute interstitial animals, yet fast reactions to avoid obstacles are dealt with by contractions of the longitudinal (and to a lesser degree transverse musculature ring complexes) body wall muscles.

#### Muscular locomotion

Behavioral observations of several specimens revealed different movement patterns of the rostrum and the remaining body: while the posterior part of the body was often found curled up and attached to the substrate, the anterior part did exploratory movements, including contraction along the longitudinal body axis and sweeping of the rostrum from side to side (Additional file 1). This coincides with the lack of transverse muscular ring complexes and presence of star-shaped muscles in the rostrum. During these contractions of the longitudinal muscles, the anterior part of the body appears more wrinkled, also indicating that an elongation or contraction of the longitudinal muscles in the anterior region is not affecting the trunk and posterior part of the body. With all the longitudinal muscles being continuous along the entire body, the stabilizing and immobilizing of the median body during longitudinal contractions may be accomplished by counteracting contractions of the transverse muscular ring complexes in the trunk and posterior part of the body.

The animals also regularly curl up or fold their posterior body in sinuous curves, which may facilitate anchoring the body among sand grains in the substrate. The trunk may also show minor contractions and winding movements occasionally providing a forward movement in a snake-like pattern (Additional file 1). This most likely is due to a combination of muscular and ciliary locomotion.

The posteriormost end of the body can also be active and flexible (performing contractions and elongations as well as bending movements), though this motility is limited to a small region anterior to the anus (10–30  $\mu\text{m}$ ,  $n = 3$ ,  $r = 4$ ,  $m = 5$ ). Occasionally, when the posterior part

is curled up or bent, it would act more as an anchor rather than promote forward movement (Additional file 1). *Lobatocerebrum riegeri* n. sp. has never been observed to leave the substrate and swim into the water column.

#### Movements in the digestive system

Although no feeding behavior could be observed, stomach content was moved continuously in both directions, even when the animal was not moving (Additional file 1). This indicates that the weak musculature of the digestive system, maybe together with the body wall musculature, is responsible for movement of the food through the body. The fifth sphincter here probably plays an important role in sealing the digestive tract and prohibiting food getting expelled through the pharynx and mouth opening again, since no movement of food could be observed in the pharynx anterior to this muscular constriction.

### Taxonomy

Phylum Annelida Lamarck, 1809

Family Lobatocerebridae Rieger, 1980

Genus *Lobatocerebrum* Rieger, 1980

Species *Lobatocerebrum riegeri* n. sp.

(Figs. 1, 2, 3, 4, 5, 6, 7, 8, 9, Tables 1, 2, 3, 4, Additional file 1)

*Lobatocerebrum* sp. 2 in [8–11], registered in ZooBank (E3DCE97A-7F7A-4799-827A-DF2EA41AE1A5).

#### Diagnosis

Entirely ciliated *Lobatocerebrum*, unsegmented, hyaline body with glandular epidermis (unicellular, kidney-shaped glands with transparent-green content), 1.08–1.6 mm in length and 0.04–0.06 mm in diameter. Large, lobular brain, with central neuropil displaced 8.22–18.18 U posterior of anterior body edge (relative to total body length). Ventral mouth opening, positioned posterior of the brain, 20.48–34.69U from anterior edge (relative to total body length). Dorsal opening of male gonopore positioned 10–14U posterior to the neuropil (relative to total body length).

#### Type material

Holotype: one 1.57 mm long mature hermaphrodite (testis, ovary with eggs and seminal receptacles present) (ZMUC-POL-2384), beach in front of the Interuniversity Institute for Marine Sciences (IUI) northwest of Eilat, Israel (N 29° 30.211' E 34° 55.068), 9 meters deep, coral sand, collected by the authors 20.02.2014. Paratypes: Two mature and one juvenile specimens (section series, ZMUC-POL-2385, ZMUC-POL-2386, ZMUC-POL-2387), same locality as for holotype, (sampled on 14.02.2014, 16.02.2014 and 18.02.2014); one mature specimen collected by Mike Crezée (section series, ZMUC-POL-2388).

**Table 1** Measurements of the specimen of *Lobatocerebrum riegeri* n. sp. investigated in this study and distances of specific structures and organs to the anterior end of the body

	<i>End of measurement from the anterior tip</i>	<i>Lobatocerebrum riegeri</i> II (CLSM, holotype)	<i>L. riegeri</i> III (CLSM, paratype)	<i>L. riegeri</i> IV (CLSM, paratype)	<i>L. riegeri</i> I (juvenile, CLSM, paratype)	<i>L. riegeri</i> V alive (LM)
Total Length [ $\mu\text{m}$ ]		1571,9	1078	1606	478	1646,6
Total Width [ $\mu\text{m}$ ]		40	79	55	66,5	51,4
Position of neuropile		247	196	204	132	250
Position of the brain						
	Middle of the brain	246	221	204	137,7	266
	Most anterior part	177	179	159	108	215
	Most posterior part	296	251	248	162	304
Position of the mouth						
	Middle of the mouth	322	374	344	182,3	330
	Most anterior part	305	368	293	170	310
	Most posterior part	343	403	375	203	350
Position of the male gonopore		593	476	557		596
Position of the testis						
	Middle of the testis	758	576,5	712		776
	Most anterior part	725	556,5	691		741
	Most posterior part	787	596,5	732		811
Position of the ovary						
	Middle of the ovary	1107	702,5	1053		1150
	Most anterior part	953	597,8	1036		995
	Most posterior part	1248	769,5	1070		1304
Position of the seminal receptacles						
	Middle of the receptacles	1428	960,5	1350		1510
	Most anterior part	1424,9	944,5	1340		1501
	Most posterior part	1432,9	970	1360		1519

The measurements were taken from both live ( $n = 1$ ) and fixed and mounted ( $n = 5$ ) specimens, including one juvenile, as indicated. In the latter, neither the male nor the female gonad could be detected in transmitted light or CLSM-images. Measurements are taken in  $\mu\text{m}$  (in case of body length and width) and as  $\mu\text{m}$  from the anterior end of the respective animal to a specific point as indicated in the first and second column

### Etymology

The species is named in memory of Reinhard M. Rieger, who discovered and described the first representative of Lobatocerebridae.

### Description

Measurements of holotype are given in the text, ranges of all types are given in parentheses; juvenile is not included)

*Lobatocerebrum riegeri* has an elongated, cylindrical, entirely ciliated body, which appears slightly greenish due to the glandular epidermis (Fig. 9a). The total body length is 1.57 mm (varies between 1.08 and 1.6 mm in adults), the body width is 0,04 mm (0.04–0.06 mm, Tables 1, 2). The rostrum is 305  $\mu\text{m}$  (293–368  $\mu\text{m}$ , Fig. 9b); the uniform trunk extends for an additional 1266  $\mu\text{m}$  (710–1336  $\mu\text{m}$ , Table 1). The brain is located dorsally in the rostrum 246  $\mu\text{m}$  (204–266  $\mu\text{m}$ ) from the

anterior tip, extends for 119  $\mu\text{m}$  (30–44  $\mu\text{m}$ ) posteriorly and has an oval, but lobular appearance (two frontal and four posterior lobes embracing the central neuropil visible with LM, Fig. 9c, Tables 1, 2). The mouth opening is 322  $\mu\text{m}$  (330–374  $\mu\text{m}$ ) from the anterior tip; extends for 21 (20–31  $\mu\text{m}$ , Fig. 9d, Tables 1, 2) and the pharynx is heavily ciliated and supplied with several glands. The transitions from the fore- to the mid-gut 480  $\mu\text{m}$  (450–580  $\mu\text{m}$ ) from the anterior tip and from the mid- to the hindgut 820  $\mu\text{m}$  from the anterior tip (800–1300  $\mu\text{m}$ ) are marked by a decrease in diameter, sphincter muscles and change in ciliation pattern (strong in fore- and hindgut, weaker in mid-gut). No protonephridia were detected with the techniques applied (adults and juvenile). The male gonopore 593  $\mu\text{m}$  (476–596  $\mu\text{m}$ ) from the anterior tip and associated gland cells as well as one testis 758  $\mu\text{m}$  (576–758  $\mu\text{m}$ , Fig. 9a, Tables 1, 2) from the anterior tip are all located dorsally. In mature specimens, big, slightly

**Table 2** Comparisons of measurements and distances of specific structures and organs to the anterior tip of different species of Lobatocerebridae

	<i>Lobatocerebrum psammicola</i> live	<i>L. psammicola</i> fixed	<i>Lobatocerebrum</i> sp. 1	<i>Lobatocerebrum</i> sp. 2	<i>Lobatocerebrum riegeri</i>	<i>L. riegeri</i> conclusions/remarks
Total length [mm]	3.0	2.0–2.2	1.1	1.7	1.57 (1.08–1.6 [0.48])	<i>L. riegeri</i> is shorter than <i>L. psammicola</i> and the other reported specimens
Total width [mm]	0.11	0.07–0.08	0.06	0.06	0.04 (0.04–0.06 [0.07])	<i>L. riegeri</i> is thinner than the other species and reported specimens, though not relative to the body length
Relative width	0.036	0.035–0.036	0.055	0.035	0.025 (0.025–0.038 [0.15])	<i>L. riegeri</i> is thinner than the other species and reported specimens, though not relative to the body length
Position of the neuropile [1–100U]	9	7–12	14	12	18.18 (8.22–18.18 [27.61])	→displaced more posteriorly in <i>L. riegeri</i> than in <i>L. psammicola</i> and the other reported specimens
Position of the brain [1–100U]	9	7–12	14	12	15.65 (12.7–20.5 [28.8])	
Position of the mouth [1–100U]	14	10–17	20	20	20.48 (20.48–34.69 [38.14])	→displaced more posteriorly in <i>L. riegeri</i> than in <i>L. psammicola</i> , but in the same range as the other reported species
Position of the male gonopore [1–100U]	38	30–36	No measurements provided	31	37.72 (34.68–44.16)	→ range outside <i>L. sp. 2</i> , but similar to <i>L. psammicola</i>
Position of the testis [1–100U]	47–57	46–56	No measurements provided	35–43	48.21 (44.33–53.48)	→ posterior to <i>L. sp.2</i> , but with the broad range similar to <i>L. psammicola</i>
Position of the ovary [1–100U]	58–63		No measurements provided	48–79	70.42 (65.17–70.42)	→ too broad ranged to be diagnostic
Position of the seminal receptacles [1–100U]	90,5	87–89	No measurements provided	88	90.84 (84.06–90.84)	→ too broad ranged to be diagnostic

The measurements of *Lobatocerebrum psammicola*, *L. sp. 1* and *L. sp. 2* were taken from [8]. *L. riegeri* n. sp. (this study) was obtained from this study and translated in the units used by [8] (in 1–100U for the entire body length). For *L. riegeri* n. sp., all measurements are taken from fixed and mounted specimens in the following order: holotype [range of all adult specimens (juvenile)]. *L. riegeri* n. sp. specimen III was excluded from the range given for body length and width, since it was compressed to a high degree, but was considered for the relative measurements

**Table 3** Compilation of features of the nervous system in representatives of different spiralian groups with previously proposed relationship to *Lobatocerebrum riegeri* n. sp

		ANNELIDA			MOLLUSCA		
		LOBATOCERBRIDAE	SIPUNCULA	ORBINIIDAE	SOLENOGASTRES	CAUDOFOVEATA	GASTROPODA
		<i>Lobatocerebrum riegeri</i> n. sp.	<i>Phascolium strombus</i>	<i>Scoloplos armiger</i>	<i>Dorymenia sarsii</i>	<i>Chaoderma japonicum</i>	<i>Helminthope psammibionta</i>
	Location of the ventral nerve cords	Intraepithelial	Intraepithelial/ subepidermal	Intraepithelial	Subepidermal	Subepidermal	Subepidermal
BRAIN	Lobular structure	+	?	+	-	+	+
	Central neuropile	+	+	+	+	+	+
	Number of brain commissures	4	2	4	1	1	1
NERVE CORDS OF THE CENTRAL NERVOUS SYSTEM	Number of posterior longitudinal nerve cords	1 pair + 1 median cord	1 pair	1 pair	2 pairs (+1 median cord)	2 pairs	2 pairs
	Median posterior nerve cord	+	-	-	+	-	-
	Number of rostral longitudinal nerve cords	2–9	0	0	-	-	2 pairs
GANGLIA AND COMMISSURES ALONG THE VENTRAL NERVE CORD	Total number of ganglia	2 pairs	>2	>2	>2	>2	>2
	Nonganglionated posterior commissures	>2	?	>2	>2	>2	>2
	Presence of a subpharyngeal ganglion	+	+	+	+	+	+
PERIPHERAL NERVOUS SYSTEM		Grid of distinct longitudinal and circular nerves	Nerve plexus	Grid of pairwise arranged longitudinal and several circular nerves per segment	?	?	?
References		This study	[57, 73, 74]	[75, 76]	[40, 41]	[40]	[43]

**Table 3** Compilation of features of the nervous system in representatives of different spiralian groups with previously proposed relationship to *Lobatocerebrum riegeri* n. sp

		NEMERTEA			GNATHOSTOMULIDA			PLATYHELMINTHES	XENACOELOMORPHA
		PALAEONEMERTEA		ANOPLA	BURSOVAGINOIDEA		FILOSPERMOIDEA	CATENULIDA	NEMERTODERMATIDA
		<i>Cephalothrix linearis</i>	<i>Procephalo-thrix linearis</i>	<i>Lineus viridens</i>	<i>Gnathostomula peregrina</i>	<i>Rastrognathia macrostoma</i>	<i>Pterognathia meixneri</i>	<i>Stenostomum leucops</i>	<i>Nemertoderma westbaldi</i>
	Location of the ventral nerve cords	Subepidermal	Subepidermal	Subepidermal	Intraepithelial	Intraepithelial	Intraepithelial	? (mainly subepidermal)	Intraepithelia to subepidermal
BRAIN	Lobular structure	+	+	+	-	? (-)	-	-	-
	Central neuropile	+	+	+	+	? (+)	+	+	- (only commissures formed)
	Number of brain commissures	>2	>2	>2	1	? (1)	1	1	2 rings (dorsally connected)
NERVE CORDS OF THE CENTRAL NERVOUS SYSTEM	Number of posterior longitudinal nerve cords	1 pair	1 pair + 1 dorsal median + 1 ventral median cord	1 pair	1 pair	1 pair	1 pair	1 pair	- (thin fibres, but no cords)
	Median posterior nerve cord	-	+	-	+ (just a short piece)	? (-)	-	-	-
	Number of rostral longitudinal nerve cords	?	4	Approx. 8 pairs	-	?	>3 paired and 2 unpaired	-	-
GANGLIA AND COMMISSURES ALONG THE VENTRAL NERVE CORD	Total number of ganglia	?	?	1 pair	1 pair	? (1 pair)	1 pair	?	?
	Nonganglionated posterior commissures	?	1	?	1	? (1)	1 (2)	?	-
	Presence of a subpharyngeal ganglion	+	+	+	+	? (+)	+	+	-
PERIPHERAL NERVOUS SYSTEM		?	Intraepidermal plexus around the rhynchocoel	Subepidermal plexus, commissural plexus, stomatogastric plexus, proboscidal plexus	5 longitudinal nerves	6 longitudinal nerves	3 dorsal longitudinal nerves	?	?
References		[42, 48]	[42]	[77]	[78]	[17, 79]	[17]	[46, 80]	[81, 82]

Details of the brain, the ventral nervous system, the stomatogastric nervous system and the peripheral nervous system are given in an attempt to reveal common features or possible apomorphies in Lobatocerebridae. Presence of a character is labeled with +, absence with -, numbers and additional informations are given wherever possible. "?" indicates the lack of information in the references mentioned, while reinvestigations from this study (in the case of *L. riegeri* n. sp.) and assumptions based on additional references are included by putting the assessment in brackets (+) or (-). Only species with previously [8-12] or recently [7] suggested relationship to Lobatocerebridae were considered. Insufficient information in one species was supplemented with closely related species, based on the literature acknowledged in the reference-row

**Table 4** Compilation of features of the nervous system in representatives of different annelid groups and *Lobatocerebrum riegeri* n. sp

		ANNELIDA					
		PREVIOUS "PROBLEMATICA", now ANNELIDA					
		LOBATOCEREBRIDAE		DIURODRILIDAE	?	SIPUNCULA	
		<i>Lobatocerebrum riegeri</i> n. sp.	<i>Lobatocerebrum psammicola</i>	<i>Diurodrilus</i> sp.	<i>Jennaria pulchra</i>	<i>Phascolion strombus</i>	<i>Siphonosoma australe</i>
	Location of the ventral nerve cords	Intraepithelial	Intraepithelial	Intraepithelial	Intraepithelial	Intraepithelial	Intraepithelial
BRAIN	Lobular structure	+	+	?	+	?	?
	Central neuropile	+	+	+	+	+	+
	Number of brain commissures	4	?	4	?	2	1
	Dorsal root (dorsal/ventral commissure)	+ (+/+)	?	+ (+/+)	?	?	- (Not differentiated in this species)
	Ventral root (dorsal/ventral commissure)	+ (+/+, individual fibres spread out)	?	+ (+/+)	?	?	- (Not differentiated in this species)
NERVE CORDS OF THE CENTRAL NERVOUS SYSTEM	Number of posterior longitudinal nerve cords	1 pair + 1 median cord	1 pair (+1 median cord?)	2 pairs	1 pair	1 pair	1 pair (fused during development)
	Median posterior nerve cord	+	?	-	-	-	-
	Number of rostral longitudinal nerve cords	2 ventrolateral + < 7 additional, smaller ones	2 (?)	>2	?	0	0
GANGLIA AND COMMISSURES ALONG THE VENTRAL NERVE CORD	Total number of ganglia	2 pairs	2 pairs	1 (fused pair)	?	>2	>2 (during development)
	Nonganglionated posterior commissures	>2	2	>2	1	?	>2 (during development)
	Presence of a subpharyngeal ganglion	+	+	+	?	+	+ (during development)
STOMATOGASTRIC NERVOUS SYSTEM	Stomatogastric nervous system	+ (ring around the pharynx)	+ (ring around the pharynx)	+ (ring around the esophagus)	+ (nerve cells in the pharyngeal epithelium)	+ (ring around the esophagus)	+ (ring around the esophagus, during development)
	Origin of the stomatogastric nervous system	Postpharyngeal ganglion	Postpharyngeal ganglion	prebuccal ganglion	?	brain (?)	brain (?)
PERIPHERAL NERVOUS SYSTEM		Grid of distinct longitudinal and circular nerves	?	1 pair of longitudinal nerves, several branches for innervating organs	Some nerves around the pharynx and gut, otherwise not present or not described	Nerve plexus	?
References		This study	[8–11]	[61]	[9, 83]	[57, 73]	[58]

**Table 4** Compilation of features of the nervous system in representatives of different annelid groups and *Lobatocerebrum riegeri* n. sp

		DINOPHILIDAE	PROTODRILIDAE	PSAMMODRILIDAE	NEREIDIDAE	CAPITELLIDAE	SERPULIDAE	
		<i>Dinophilus gyrocoliatius</i>	<i>Protodrilus</i> sp.	<i>Psammodrillus fauveli</i>	<i>Platynereis</i> sp.	<i>Capitella</i> sp.	<i>Pomatoceros lamarckii</i>	<i>Spirorbis</i> cf. <i>spirorbis</i>
	Location of the ventral nerve cords	Intraepithelial	Intraepithelial	Intraepithelial	Intraepithelial	Intraepithelial	Intraepithelial	Intraepithelial
BRAIN	Lobular structure	-	-	+	+	+	-	+
	Central neuropile	+	+	+	+	+	+	+
	Number of brain commissures	2	4	4	4	4	4	4
	Dorsal root (dorsal/ventral commissure)	?	+	+	+	+	+	+
	Ventral root (dorsal/ventral commissure)	?	+	+	+	+	+	+
NERVE CORDS OF THE CENTRAL NERVOUS SYSTEM	Number of posterior longitudinal nerve cords	3 pairs + median cord	1 pair	1 pair	1 pair	1 pair	1 pair	1 pair
	Median posterior nerve cord	+	-	-	-	+	+	-
	Number of rostral longitudinal nerve cords	0	0 (but innervation of tentacles)	0	0	0	0 (but innervation of tentacles)	0 (but innervation of tentacles)
GANGLIA AND COMMISSURES ALONG THE VENTRAL NERVE CORD	Total number of ganglia	>2	>2	>2	>2	>2	>2	1 (in larvae)
	Nonganglionated posterior commissures	>2	>2	>2	>2	>2	>2	1 (in larvae)
	Presence of a subpharyngeal ganglion	+	+	+	+	+	+	+
STOMATOGASTRIC NERVOUS SYSTEM	Stomatogastric nervous system	+ (ring around the pharynx)	+ (ring around the esophagus)	+ (ring around the esophagus, also tracing the esophagus)	+ (ring around the esophagus)	+ (ring around the esophagus)	+ (fibre along the gut, ring around the esophagus)	-

**Table 4** Compilation of features of the nervous system in representatives of different annelid groups and *Lobatocerebrum riegeri* n. sp

	Origin of the stomatogastric nervous system	Brain (dorso-posterior neuropile)	Brain	Buccal ganglion	Brain	Brain	Brain	-
PERIPHERAL NERVOUS SYSTEM		Regular grid of longitudinal and circular nerves, nerve plexus dorsal to the ventral nervous system	?	?	Grid of distinct longitudinal and circular nerves	Grid of distinct longitudinal and circular nerves	Circular nerves in some segments	Grid of distinct longitudinal and circular nerves
References		[14, 84, 85]	[55, 86]	[87, 88]	[70, 89, 90]	[91]	[92]	[92]

Details of the brain, the ventral nervous system, the stomatogastric nervous system and the peripheral nervous system are given in an attempt to reveal common features or possible apomorphies in Lobatocerebridae. Presence of a character is labeled with +, absence with -, numbers and additional informations are given wherever possible. ? indicates the lack of information in the references mentioned, while reinvestigations from this study (in the case of *L. riegeri* n. sp.) and assumptions based on additional references are included by putting the assessment in brackets (+) or (-). Insufficient information in one species was supplemented with closely related species, based on the literature acknowledged in the reference-row

oval but irregular-shaped eggs can be found in the posterior region of the body 1107  $\mu\text{m}$  (702–1107  $\mu\text{m}$ , Tables 1, 2) from the anterior tip). Seminal receptacles, if present (one to three found in the specimens investigated), can be found in the posterior region of the body 1428  $\mu\text{m}$  (960–1428  $\mu\text{m}$ , Table 1) from the anterior tip, opening laterally. The anus opens dorsally 1500  $\mu\text{m}$  (1000–1500  $\mu\text{m}$ , Fig. 9e) from the anterior tip.

#### Remarks

*Lobatocerebrum riegeri* is smaller (1.08–1.6 mm in adults compared to 2.0–3.0 mm in adults of *L. psammicola*) and thinner (0.04–0.06 mm in adults compared to 0.07–0.11 mm in *L. psammicola*) than the related species [8]. The brain is displaced more posterior (8.22–18.18 U (distance from anterior end to central neuropil relative to total body length) in adults compared to 7–12U in *L. psammicola*) and the mouth opening is displaced further posterior in the body than in the previously described species (12.7–20.5U in adults compared to 10–17U in *L. psammicola*). Further distinguishing *Lobatocerebrum riegeri* from its previously described relative is the fact that it has a different secrete in the unicellular adhesive glands (linearly arranged globular inclusions in the granules in the adhesive glands in *L. riegeri* as compared to linear, rod-shaped inclusions in *L. psammicola*). Additionally, the two localities the different species have been found in (North Carolina, USA for *L. psammicola* and Eilat, Israel for *L. riegeri*) are far apart from each other and therefore the presence of two species seems to be probable. Further studies also involving molecular data are needed to further support this hypothesis, but are unfortunately not available now.

#### Discussion

##### Function and origin of the unique muscular ring complex

The characteristic annelid (and spiralian) muscular arrangement consists of an external circular and internal longitudinal muscle layer [22, 38]. However, the pattern in Lobatocerebridae differs in having externally positioned longitudinal muscles sunken into the epidermis, and within those inner transverse muscles previously mistakenly interpreted as continuous circular muscles [8]. However, each of these ring complexes resembles a discontinuous muscular network, composed by transverse muscle fragments, which together form serially repeated, discontinuous muscular ring complexes interconnecting the longitudinal muscles. Peristaltic body movements normally caused by contraction of circular muscles were never observed in *Lobatocerebrum riegeri*; however, the transverse fragments neither seemed to operate independently, but most likely aid to stabilizing the body wall during contraction of the longitudinal fibers. The lack of ring complex muscles in the rostrum on the other hand

seems to allow for the high flexibility of the long rostral area in *L. riegeri* (Fig. 1b, e–g, Additional file 1). A flexibility which otherwise would have been prevented due to their different interconnecting composition compared to regular spiralian circular muscles, located external of the longitudinal muscles, even along the long rostrum of meiofaunal animals such as the filospiralian Gnathostomulida [17] and catenulid Platyhelminthes ([39], Table 3). Since a similar muscular solution to both granting flexibility of the rostrum and stabilizing the trunk is not found in other annelids (or sipunculids), the muscular ring complex is considered a unique apomorphy of Lobatocerebridae.

##### The paradox of a complex brain in a simple animal

Lobular or compartmentalized, ganglionated brains are commonly found in macroscopic representatives of Spiralia and other metazoan groups (e.g. [18, 40, 41]), but interstitial animals generally do not show such a complex architecture (e.g. [16, 29], Tables 3, 4). However, some interstitial species of nemertean [42], molluscs (especially in several wormlike gastropods such as *Helminthope* [43], *Rhodope* [44], and *Pseudovermis* [45]) and catenulids [46] also show some compartmentalization of the brain having, for example, visual and olfactory centers (Table 3). Another representative with a ganglionated brain is the enigmatic interstitial “worm” *Jennaria pulchra* (Figure 3a in [9]), which is described as representing many plesiomorphies of the trochozoan body plan [47] and possibly being an annelid [9]. Different compartments or lobes of the brain are normally related to processing of different sensory stimuli, yet all conspicuous sensory organs such as eyes, sensory appendages or olfactory nuchal organs are lacking in Lobatocerebridae. Moreover, the indistinct gut content and simple alimentary tract and behavior indicates that *Lobatocerebrum sp.* is an unselective deposit feeder. Though no sensory structures are found adjacent to, or directly connected to specific regions in the brain, it is still striking how the anterior rostrum is strongly innervated with nerves connected to various parts of the brain. Hence, though unlikely, the glandular secretion or the stimuli of the scattered sensory cells may in fact be processed in a much more organized manner and their signaling complexity exceed our expectations. Nonetheless, the complex lobular architecture of the brain in *L. riegeri* seems a functional paradox.

##### Systematic importance of longitudinal nerve configuration

Annelid central nervous systems vary in numbers of main longitudinal nerves, from one ventro-median cord to seven or more ventral nerves (Table 4, [21]). Based upon developmental studies and a broad comparison across Annelida, five ventral cords have been proposed as the ancestral pattern [15], yet this proposed character

evolution was never traced upon a phylogenetic tree. The pattern of five nerves is made up of one pair of ventral, one pair of lateroventral and one median cord. The latter is revealed during neurogenesis in several annelids, and has been found in most interstitial annelids, possibly being an annelid apomorphy. However, it is only found elsewhere in Spiralia in a few exceptional cases (and with somewhat different configuration) (Solenogastres [40], some Nemertea [48], Table 3). According to a parsimonious tracing on the latest Spiralian tree [7] one pair of widely separated ventral cords would be the plesiomorphic state of Spiralia (Table 3 and references therein). Likewise, the basi- or intraepidermal position of the nervous system has also been regarded a plesiomorphic trait in Spiralia [49] as well as in Annelida such as now exemplified by the early branching annelid lineage Oweniidae [50–52] opposed to the derived subepidermal position found in many crown group annelids [53, 54]. However, intraepidermal nerve cords have also been found in Siboglinidae (Worsaae K, Rinskaya-Korsakova, NN, Rouse, GW: Neural reconstruction of bone-eating *Osedax* spp. (Annelida) and evolution of the siboglinid nervous system, submitted) as well as several interstitial annelids [19, 25, 54], showing considerable variance throughout evolution. The intraepidermal position of the paired ventral cords of *Lobatocerebrum* may hereby not be phylogenetically informative, whereas its additional median cord may be an annelid apomorphy. The two widely separated main nerve cords do not resemble a “typical” annelid pattern, but also do not dispute such a relationship, since such a pattern is also found in several other interstitial annelids such as Dinophilidae [15], Protodrilidae [29, 55], and Nerillidae [56].

*Lobatocerebrum* also possess two prominent and several additional long rostral nerves extending from the posteriorly displaced brain to the tip of the animal ([8], this study). This pattern is not found in any other annelids, which normally have the brain located anteriorly [28]. A similar pattern is found in a few examples of distantly related interstitial spiralian among Mollusca, Nemertea, Gnathostomulida, Catenulida (for details see Table 3) but has most likely arisen by convergence.

#### **Lobatocerebrum – an unsegmented annelid?**

The ventral nervous system in annelids most commonly consists of longitudinal nerve cords linked by ganglionated, serially arranged commissures, correlated with other serially repeated structures to form segments [49]. However, a clear outer segmentation as well as regularly distributed segmental paired ganglia are lacking in several groups recently assigned to annelids such as Diurodrilidae, Sipuncula, Echiura Siboglinidae and now also demonstrated for *Lobatocerebrum riegeri*. A similar

layout to that of *L. riegeri* only having two pairs of subpharyngeal ganglia is also found in other spiralian groups (e.g. Gnathostomulida, Catenulida, for more details see Table 3), although the posterior commissures found in *L. riegeri* (ganglionated and non-ganglionated) are often not described or irregularly distributed (Table 3). Besides the low number of ganglia, there is no correlation of the commissural distribution with that of the few observed nephridia in *L. psammicola* [8, 9] nor with any other organ system in *L. riegeri*, which means that *Lobatocerebrum* cannot be regarded as segmented at present. This emphasizes, however, that more detailed studies of the developmental pattern in Lobatocerebridae are needed to check for signs of segmentation during ontogeny as found in Echiura and partly in Sipuncula [57, 59].

#### **A grid-like peripheral nervous system supporting a ventralized central nervous system may be a Spiralian plesiomorphy**

The peripheral nervous system is, especially in spiralian with a ventralized central nervous system, supposed to provide sufficient support and innervation for (sensory) organs in the periphery of the body [49]. Especially sensory cilia and glands are often abundantly distributed in the epidermis of interstitial animals far from the ventral nerve cords and the brain, as can be demonstrated in nearly all spiralian groups [60]. In annelids, the peripheral nervous system is often formed as an irregular grid constituted by longitudinal, oblique and circular nerves [21], relatively similar to those present in *L. riegeri*, though the pattern here appeared more regular and with the longitudinal nerves projecting directly from the neuropil rather than from the nerve cords. Moreover, this is the general pattern for several spiralian, so it cannot be viewed as a diagnostic trait for annelids (see Tables 3 and 4 for details). Supplementing or even replacing this grid, nerve plexi are found around specific organs, most often adjacent to the (male) reproductive organs or the mouth opening in nearly all groups considered for this comparison (see Tables 3 and 4 for details). However, since the grid is generally built from single (or few) fibres, the record of peripheral nervous system architecture especially among interstitial animals is rather incomplete.

#### **Function and origin of the long-necked frontal glands**

The frontal glands in *Lobatocerebrum* are among the diagnostic features of this group; the elongated ducts of the prominent glands can neither be found in other annelid groups (with the exception of Diurodrilidae [61]) nor in the majority of other spiralian groups. However, supposedly similar structures are present in catenulid Platyhelminthes (personal observation) and probably also in a few exceptional nemerteans and gnathostomulids

(W. Sterrer, personal observation). The function of these glands is still unclear, though two options seem most likely: i) the secretion of these glands is used to produce a mucus layer to facilitate ciliary gliding; ii) the secretion is used to bind substances (e.g. pheromones or other chemical compounds) from the environment and thereby enhance the animal's ability to sense the environment and possibly even follow a chemical lead. However, though olfactory organs have been described for many invertebrates [62, 63], with annelids generally having ciliated nuchal organs [64–66], those are rarely glandular or resembling the structure of the frontal glands, why this hypotheses clearly needs further testing.

#### Origin of meiofaunal characteristics of Lobatocerebridae

Lobatocerebridae has been proposed to originate from a macroscopic, presumably annelid (or annelid-like) ancestor by progenesis (somatic arrest during larval or juvenile development due to early maturation [67]) [8, 9, 11]. This idea was based on its acoelomic condition and the presence of characters also present in annelid or spiralian larvae, such as complete ciliation, an intraepithelial nervous system, protonephridia and a rather simple formation of both musculature and ventral nervous system [8, 9, 11]. No single extant macrofaunal lineage possesses juveniles resembling adult Lobatocerebridae; however, the noted features are also common in other meiofaunal representatives of annelids, molluscs, nemerteans and platyhelminths (see Tables 3 and 4, and references herein for details), where progenesis is often seen as the most plausible pathway along which these interstitial animals have derived from a macroscopic ancestor [67]. Conversely, most of these features are also present in the early branching meiofaunal spiralian lineages (Gnathifera, Platyhelminthes, Gastrotricha) and were, according to the latest Spiralian topology, proposed to resemble spiralian plesiomorphies [7]. So when these traits are found in adult meiofauna they may not necessarily reflect an ancestry from a larval or juvenile stage, but could instead represent plesiomorphic states – or as a third alternative, gradual adaptations (reversals) to the constraints of the space-restricted interstitial environment [11, 16, 30, 31].

Meiofaunal spiralians generally have few nerve cords spaced far apart (rather than midventrally fused/condensed), and possess a body wall musculature spread out as a regular grid (rather than having the longitudinal muscles organized into four or fewer bundles, see Tables 3 and 4 and references therein for details). Besides this pattern possibly being the ancestral spiralian condition, there may exist 'universal constraints' on the functionally optimal neuromuscular design when being of microscopic size and with limited cell number, and given the evolutionary toolbox within Spiralia. Hence, the organization of the neuromuscular system may be more directly dependent

on e.g., size, ciliary pattern or acoelomatic condition (e.g. as for the mesodermal blood vascular system and protonephridia [11, 68, 69]) in a way we haven't calculated for. Alternatively (or in addition), the condensation of muscles and nerves into bundles is a pattern often realized during development of annelids and certain spiralians (e.g., [70–72]), and although there is currently no way of testing this statement, the lack of condensation in *Lobatocerebrum* may also be seen as an evolutionary arrest in somatic development (at least of these specific somata) and hereby as a sign of pedomorphic origin rather than gradual adaptation. However, in the recent phylogenomic study placing *Lobatocerebrum* within Annelida [7], the exact position is not well supported, which is why its descent from either macrofaunal or a meiofaunal ancestor cannot be traced with conviction.

#### Conclusion

Although *Lobatocerebrum* was shown to be an annelid in a recent phylogeny [7], previous studies also suggested similarities to other spiralian groups such as Platyhelminthes, Nemertea, Mollusca and Gnathostomulida [8, 10, 11]. Conducting a detailed study of *Lobatocerebrum riegeri* with several complementary microscopical techniques revealed details of the musculature, the nervous system and the glandular system and allowed for a detailed description of *Lobatocerebrum riegeri* next to the previously described *L. psammicola*. Yet, *L. riegeri* is very similar to *L. psammicola*, both representing conservative spiralian patterns and a combination of traits diagnosing it as an annelid. Most features of the neuromuscular system revealed in *L. riegeri* by CLSM and TEM are not in themselves diagnostic to annelids and can either likewise be found in other groups or be unique for Lobatocerebridae. While these features on their own cannot reveal significant information about relationships within and between the spiralian groups, the combination of traits such as a nervous system with a complex brain with several commissures, a prominent median nerve cord and several ganglionated commissures, as well as a glandular, multiciliated epidermis and gliointerstitial system [10] together support an affinity to Annelida.

It is not possible to depict neither from the phylogenetic position nor morphological traits whether Lobatocerebridae originated through pedomorphosis or gradual miniaturization from a macrofaunal ancestor as an adaptation to the interstitial environment - or may even have retained plesiomorphic traits. Nonetheless, the lack of specific resemblance to any juvenile annelid relatives indicates a much more complex evolutionary history than what can be explained by a one-step progenetic evolutionary process. Further studies on the development of organ systems such as the musculature and the nervous system

may prove useful for accessing the origin of Lobatocerebridae. Nonetheless, this study demonstrates that with Lobatocerebridae being annelids [7], Annelida displays an extreme evolutionary plasticity of the neuromuscular system, which is otherwise regarded as highly conservative throughout metazoan evolution.

## Methods

### Sampling

Specimens used for this study were collected in Eilat, Israel, from sand collected from a small (0.5x0.5 m) sand patch between coral blocks at 8.5–9 m depth approximately 100 m southwest of the main pier of the Interuniversity Institute for Marine Sciences (IUI, N 29° 30.211' E 34° 55.068). Animals were extracted and anesthetized using an isotonic magnesium chloride solution: The upper 2–5 cm of sampled sand was mixed with this solution, and the water with floating particles and anesthetized animals decanted through 63 µm meshes with seawater. Revitalized animals were sorted from the petri dish using dissecting compound microscopes. A total of nine specimens was found, examined and afterwards fixed for the techniques described below as well as for molecular analysis.

### Behavioral studies

Animals were observed with a dissecting scope in a petri dish prior to being transferred to an object slide in seawater under cover for examination and imaging in a compound microscope with a mounted camera or a video recorder. For later relaxation, a weak MgCl<sub>2</sub>-solution was added to the slide. Movies were later analyzed in relation to the morphological studies and interpretation.

### Histology, light microscopy (LM) and transmission electron microscopy (TEM)

Specimens were carefully anesthetized with isotonic magnesium chloride and afterwards fixed with 2 % glutaraldehyde in 0.1 M osmolarity-adjusted cacodylate buffer over night at room temperature (RT) and afterwards rinsed and stored in 0.1 M cacodylate buffer. The animals were postfixed in 2 % OsO<sub>4</sub> in 0.05 M K<sub>3</sub>FeCN<sub>6</sub>-solution for 1 h and before embedding in Araldite Epon-812 using standard protocol and polymerization for 20–24 h at 50 °C.

For TEM-analysis, the block was trimmed to the object and sectioned into 40 nm sections using a Leica EM UC7 ultratome (LEICA MICROSYSTEMS, Wetzlar, Germany). Ultrathin section were mounted on Formvar-coated 2x1mm slot grids, contrasted with 2 % uranyl acetate- and 4 % lead citrate-solution and examined using a JEOL JEM 1010-Transmission Electron Microscope (TEM, JEOL Ltd., Tokyo, Japan) in combination with a digital GATAN OneView camera (GATAN, INC.,

Pleasanton, CA, United States). The fixation and preparation caused artifacts such as the slight separation of the epidermis from the internal organs of the animal.

### Immunohistochemistry and CLSM

Specimens were carefully anesthetized with isotonic magnesium chloride and afterwards fixed in 3.7 % paraformaldehyde in phosphate buffered saline (PBS) for 1 to 2 h at RT, followed by several rinses in PBS and storage in PBS with 0.05 % NaN<sub>3</sub>. For the investigation of muscular, nervous, glandular and ciliary system quadruple stainings were applied, including F-actin staining (Alexa Fluor 488-labelled phalloidin, INVITROGEN, Carlsbad, USA), DNA-staining (405 nm fluorescent DAPI) and immunostaining (monoclonal mouse anti-acetylated α-tubulin (SIGMA T6793, St. Louis, USA), polyclonal mouse anti-synapsin 1 (3C11 (anti SYNORF1, DEVELOPMENTAL STUDIES HYBRIDOMA BANK, Iowa, USA) and anti-tyrosinated tubulin (SIGMA T9028), polyclonal rabbit anti-serotonin (5-HT, SIGMA S5545) and anti-FMRamide (IMMUNOSTAR 20091, Hudson, USA)). Prior to adding the primary antibody-mix, the samples were pre-incubated with 0.1 % PBT (PBS + 0.1 % Triton-X, 0.05 % NaN<sub>3</sub>, 0.25 % BSA, and 10 % sucrose) for 2 h. Afterwards, samples were incubated for up to 24 h at RT in the primary antibodies mixed 1:1 (in a final 1:200 concentration (or 1:50 for anti-synapsin 1)). Subsequently, specimens were rinsed in 0.1 % PBT three to six times and incubated with the appropriate secondary antibodies conjugated with fluorochromes (also mixed 1:1 in a final concentration of 1:200; goat anti-mouse labeled with CY5 (JACKSON IMMUNO-RESEARCH, West Grove, USA, 115-175-062), goat anti-rabbit labeled with TRITC (SIGMA T5268)) for up to 24 h at RT. This step was followed by several rinses in 0.1 % PBT and post-incubation for 60 min in Alexa Fluor 488-labeled phalloidin (0.33 M in 0.1 % PBT). Thereafter, specimens were rinsed in PBS (without NaN<sub>3</sub>) and mounted in Fluoromount-G with DAPI (SOUTHERN BIOTECHNOLOGY ASSOCIATES, Inc., Alabama, USA) or Vectashield with DAPI (VECTOR LABORATORIES, Burlingame, USA).

The mounted specimen were scanned using a Olympus Fluoview FV-1000 confocal laser scanning microscope (of K. Worsaae, University of Copenhagen, Denmark), with the acquired z-stacks of scans being either projected into 2D-images or analyzed three-dimensionally using IMARIS 7.1 (BITPLANE SCIENTIFIC SOFTWARE, Zürich, Switzerland). This software package was also used to conduct the measurements presented in the following text ( $n$  = number of specimens analyzed;  $r$  = body region (1 - from the anterior tip to the mouth opening, 2 - from the mouth opening to the male gonopore, 3 - from the male gonopore to the ovary, 4 - from the ovary to the posterior tip of the animal);  $m$  = number of measurements per region).

## Measurements

All measurements on live animals were taken in Adobe Photoshop after the images were acquired using a standardized scale bar, as was the procedure for measurements taken from TEM-pictures. Measurements from CLSM-image stacks were conducted in Imaris 7.1 using the *Measurement-tool* in *Section-mode*. For comparison with the measurements in Rieger [8], distances from the rostral tip to specific organ systems as well as body width and length were calculated in units (U), the entire body length being 100U.

## Photoshop and Illustrator

Contrast and brightness of all two-dimensional projections of confocal data and pictures of TEM-sections were adjusted in Adobe Photoshop CC 2015. Schematic drawing as well as plate-assembly was performed in Adobe Illustrator CC 2015.

## Additional file

### Additional file 1: Motility pattern and details of the adult

*Lobatocerebrum riegeri* n. sp. This movie shows combined clips of alive *Lobatocerebrum riegeri* n. sp. indicating both morphological specificities such as the pharynx and brain and motility patterns. (MP4 116178 kb)

## Abbreviations

ac: anterior cilia; adnc: antero-dorsal nerve cord; adlnc: anterior dorso-lateral nerve cord; afg: anterior frontal gland; ag: adhesive granule; amf: anterior point of muscle fusion; an: anus; anc: anterior nerve cord; avnc: antero-ventral nerve cord; avlnc: anterior ventro-lateral nerve cord; bl: basal lamina; br: brain; brc: brain cell; bsm: brain supporting muscle; c: cilium; c1-4: commissures 1–4; cg: ciliated gland cell; cmdc: circular muscle of the digestive system; dcn: dorso-anterior commissure of the central neuropil; dfc: frontal gland ducts; dllm: dorsolateral longitudinal muscle; dlm: dorsal longitudinal muscle; e1-3: egg 1–3; ec: cili of an epidermis-cell; fpg1-2: FMRFamidegic perikarya of the postpharyngeal ganglia 1 and 2; gd: opening of the frontal glands; go: glandular opening; gv: glandular vesicle; hg: hindgut; ksg: kidney-shaped gland cell; ladnc: lateral branch of the antero-dorsal nerve cord; lavnc: lateral branch of the antero-ventral nerve cord; lca: major caudal lobes; lci: minor caudal lobes; lg: lateral ganglion; llm: lateral longitudinal muscle; lmdc: longitudinal muscle of the digestive system; ln: lateral nerve; lpn: lateral peripheral nerve; lppn: lateral projection of the neuropil; lr: rostral lobe; lra: major rostral lobe; lrl: lateral rostral lobe; mg: male gonopore; mgg: male gonopore gland; mgp: perikaryon associated with the male gonopore; mlca: median nerve and connections from the dorsal commissure to the nerves of the major caudal lobes; mig: midgut; mnc: median nerve cord; mo: mouth opening; mrn: median rostral nerve; ne: epidermal nucleus; nlca: nerve of the major caudal lobe; nlci: nerve of the minor caudal lobe; nlra: nerve of the major rostral lobe; nlri: nerve of the lateral minor rostral lobe; nlm: nerve of the median minor rostral lobe; nlrl: nerve of the lateral rostral lobe; np: neuropil; nrmg: nerve ring around the male gonopore; pcg: projection of the ciliated gland cell; pfg: posterior frontal gland; pgl1-2: postpharyngeal ganglion 1–2; ph: pharynx; phg: pharyngeal gland; pln: peripheral longitudinal nerve; pp: posterior projection; ptg: projection of the tubular gland cell; rs: seminal receptacles; rsg: rod-shaped granules; sc: shortened cilium; snr: stomatogastric nerve ring; sp: perikarya of the stomatogastric nerve ring; spc: serotonergic cell; spd: spermiduct; spf: sperm filaments; sph1-6: sphincter 1–6; ss: sensoria; ssm: star-shaped muscle; ssn: sickle-shaped nucleus; t: testis; tc: terminal commissure; tg: tubular gland; tmr: transverse muscle ring complex; tpn: transverse ring of the peripheral nervous system; ts: tubulineric sheath; tst: tubulineric strands; vcn: ventral commissures of the neuropil; vlm: ventrolateral longitudinal muscle; vln: ventral longitudinal muscle; vlc: ventral longitudinal nerve cord.

## Competing interests

The authors declare that they have no competing interests.

## Authors' contributions

AK, NB and KW drafted the study. All authors (AK, NB, WS and KW) sampled the animals. AK, NB and KW conducted the laboratory experiments. KW and AK drafted the manuscript. All authors (AK, NB, WS and KW) contributed to the manuscript and approved of the final version.

## Acknowledgements

The authors want to express their thanks to ASSEMBLE, who supported the study with the grant LOBATO ("Evolution of two enigmatic invertebrate families with proposed annelid affinity - the Lobatocerebridae and Nerillidae") for a trip to Eilat, Israel to collect the animals this study is mainly based on. The laboratory work as well as salaries of AK and NB was financed by the Villum Foundation (Grant Nr. 102544 to KW). Furthermore, we like to thank Gunde Rieger for continuous support with both material and discussion about Lobatocerebridae. Additionally, we want to thank Willi Salvenmoser and Peter Ladurner for fruitful discussions about the glandular epidermis of *L. riegeri* n. sp. Lis Munk Frederiksen is hereby acknowledged for help with sectioning of embedded material for ultrastructural analysis. We highly appreciated all comments and discussion by Christopher Laumer and Gonzalo Giribet concerning the animal's phylogenetic position. Finally, we want to thank the reviewers and editor for their careful assessment and detailed comments that improved the manuscript.

## Author details

<sup>1</sup>Marine Biological Section, Department of Biology, University of Copenhagen, Universitetsparken 4, 1st floor, 2100 Copenhagen E, Denmark. <sup>2</sup>Bermuda Natural History Museum, Flatts, Bermuda, USA.

Received: 30 July 2015 Accepted: 4 November 2015

Published online: 10 December 2015

## References

- Dunn CW, Hejnol A, Matus DQ, Pang K, Browne WE, Smith SA, et al. Broad phylogenomic sampling improves resolution of the animal tree of life. *Nature*. 2008;452:e06614.
- Giribet G, Sørensen MV, Funch P, Kristensen RM, Sterrer W. Investigations into the phylogenetic position of Micrognathozoa using four molecular loci. *Cladistics*. 2004;20:1–13.
- Bourlat SJ, Nielsen C, Economou AD, Telford MJ. Testing the new animal phylogeny: a phylum level molecular analysis of the animal kingdom. *Mol Phylogenet Evol*. 2008;49(1):23–31. doi:10.1016/j.ympev.2008.07.008.
- Zrzavy J, Mihulka S, Kepka P, Bezdek A, Tietz D. Phylogeny of the Metazoa based on morphological and 18S ribosomal DNA evidence. *Cladistics*. 1998;14:249–85.
- Jenner RA, Littlewood DTJ. Problematica old and new. *Philos Trans of the Royal Soc Series B*. 2008;363:1503–12.
- Haszprunar G, Rieger RM, Schuchert P: Extant "Problematica" within or near the Metazoa. In: The early evolution of metazoa and the significance of problematic taxa. Volume 95. Edited by Simonetta AM, Conway Morris S. Cambridge: Cambridge University Press, New York; 1991:99–105.
- Laumer CE, Bekkouche N, Kerbl A, Goetz F, Neves RC, Sørensen MV, Kristensen RM, Hejnol A, Dunn CW, Giribet G, Worsaae K: Spiralian Phylogeny Informs the Evolution of Microscopic Lineages. *Curr Biol* 2015; 25(15):2000–2006
- Rieger RM. A new group of interstitial worms, Lobatocerebridae nov. fam. (Annelida) and its significance for metazoan phylogeny. *Zoomorphologie*. 1980;95:41–84.
- Rieger RM. Neue Organisationstypen aus der Sandlückenraumfauna: die Lobatocerebriden und *Jennaria pulchra* (New interstitial taxa of vermiform Bilateria). *Verh Dtsch Zool Gesellschaft*. 1991;84:247–59.
- Rieger RM. Fine structure of the body wall, nervous system, and digestive tract in the Lobatocerebridae Rieger and the organization of the gliointerstitial system in Annelida. *J Morphol*. 1981;167:139–65.
- Rieger RM. Comparative ultrastructure and the lobatocerebridae: keys to understand the phylogenetic relationship of Annelida and the acoelomates. In: Westheide W, Hermans CO, editors. *The Ultrastructure of Polychaeta*, 4. Stuttgart, New York: Gustav Fisher Verlag; 1988. p. 373–82.

12. Haszprunar G. The Mollusca: coelomate turbellarians or mesenchymate annelids? In: Taylor JD, editor. Origin and evolutionary radiation of the Mollusca. Oxford: Oxford University Press; 1996. p. 1–28.
13. Kristensen RM. Loricifera, a new phylum with aschelminthes characters from the meiobenthos. *Zool Syst und Evolutions-Forschung*. 1983;21:163–80.
14. Jenner RA, Littlewood DTJ. Invertebrate problematica: kinds, causes, and solutions. In: Telford MJ, Littlewood DTJ, editors. Animal evolution: genomes, fossils, and trees. Oxford: Oxford University Press; 2009. p. 107–26.
15. Müller MCM, Westheide W. Comparative analysis of the nervous systems in presumptive progenetic dinophilid and dorvilleid polychaetes (Annelida) by immunohistochemistry and cLSM. *Acta Zool (Stockholm)*. 2002;83:33–48.
16. Rundell RJ, Leander BS. Masters of miniaturization: convergent evolution among interstitial eukaryotes. *BioEssays: news and reviews in mol, cell and dev biol*. 2010;32:430–7.
17. Sterrer W, Sørensen MV. Gnathostomulida. *Handbook of Zoology*. 2015. p. 135–96.
18. Richter S, Loesel R, Purschke G, Schmidt-Rhaesa A, Scholtz G, Stach T, et al. Invertebrate neurophylogeny: suggested terms and definitions for a neuroanatomical glossary. *Frontiers in Zool*. 2010;7:1–49.
19. Purschke G, Purschke G, Purschke G, Purschke G. On the ground pattern of Annelida. *Org Divers Evol*. 2002;2:181–96.
20. Filippova AV, Tzvetlin AB, Filippova AV, Filippova AV. Muscular system in polychaetes (Annelida). *Hydrobiologia*. 2005;535–536:113–26.
21. Müller MCM. Polychaete nervous systems: ground pattern and variation - cLS microscopy and the importance of novel characteristics in phylogenetic analysis. *Integr Comp Biol*. 2006;46:125–33.
22. Tzvetlin AB, Filippova AV. Muscular system in polychaetes (Annelida). *Hydrobiologia*. 2005;536(535):113–26. Morphology, molecules, evolution and phylogeny in Polychaeta and related taxa.
23. Purschke G, Müller MCM. Evolution of the body wall musculature. *Integr Comp Biol*. 2006;46:497–507.
24. Tzvetlin AB, Zhadan A, Ivanov I, Müller MCM, Purschke G. On the absence of circular muscle elements in the body wall of *Dysonetus pygmaeus* (Chrysopetalidae, "Polychaeta", Annelida). *Acta Zool (Stockholm)*. 2002;83:81–5.
25. Tzvetlin AB, Dahlgren T, Purschke G. Ultrastructure of the body wall, body cavity, nephridia and spermatozoa in four species of the Chrysopetalidae (Annelida, "Polychaeta"). *Zool Anz*. 2002;241:37–55.
26. Harzsch S. Neurophylogeny: Architecture of the nervous system and a fresh view on arthropod phylogeny. *Integr Comp Biol*. 2006;46:162–94.
27. Butler AB, Molnár Z. Development and evolution in nervous systems: development and evolution of ideas. *Trends Neurosci*. 1998;21:177–8.
28. Reichert H. Evolutionary conservation of mechanisms for neural regionalization, proliferation and interconnection in brain development. *Biol Lett*. 2009;5:112–6.
29. Orrhage L, Müller MCM. Morphology of the nervous system of Polychaeta (Annelida). *Hydrobiologia*. 2005;536(535):79–111. (Morphology, molecules, evolution and phylogeny in Polychaeta and related taxa).
30. Boaden PJS. Meiofauna and the origins of the Metazoa. *Zool J Linnean Soc*. 1989;96:217–27.
31. Curini-Galletti M, Artois T, Delogu V, De Smet WH, Fontaneto D, Jondelius U, et al. Patterns of diversity in soft-bodied meiofauna: dispersal ability and body size matter. *PLoS One*. 2012;7:e33801. 13p.
32. Struck TH, Wey-Fabrizius AR, Golombek A, Hering L, Weigert A, Bleidorn C, et al. Platyzoan paraphyly based on phylogenomic data supports a noncoelomate ancestry of spiralia. *Mol Biol Evol*. 2014;31:1833–49.
33. Andrade S, Novo M, Kawauchi G, Worsaae K, Pleijel F, Giribet G, Rouse GW: Articulating the "archiannelids": A phylogenomic approach to annelid relationships with emphasis on meiofaunal taxa. *Molecular Biology and Evolution* 2015, doi:10.1093/molbev/msv157, 16p.
34. Worsaae K, Kristensen RM. Evolution of interstitial Polychaeta (Annelida). *Hydrobiologia*. 2005;535:319–40.
35. Edgecombe GD, Giribet G, Dunn CW, Hejnol A, Kristensen RM, Neves RC, et al. Higher-level metazoan relationships: recent progress and remaining questions. *Org Divers Evol*. 2011;11:151–72.
36. Westheide W. Polychaetes: interstitial families. In: Kernack DM, Barnes RSK, editors. *Synopsis of the British Fauna, Volume 44*. Linnean Society: London; 1990. 152p.
37. Jochová J, Zakeri Z, Lockshin RA. Rearrangement of the tubulin and actin cytoskeleton during programmed cell death in *Drosophila* salivary glands. *Cell Death Differ*. 1997;4:140–9.
38. Filippova AV, Purschke G, Tzvetlin AB, Müller MCM. Musculature in polychaetes: Comparison of *Myrianida prolifera* (Syllidae) and *Sphaerodoropsis* sp. (Sphaerodoridae). *Invertebr Biol*. 2010;129:184–98.
39. Hooge MD. Evolution of body-wall musculature in the Platyhelminthes (Acoelomorpha, Catenulida, Rhabditophora). *J Morphol*. 2001;249: 171–94.
40. Faller S, Rother BH, Todt C, Schmidt-Rhaesa A, Loesel R. Comparative neuroanatomy of Caudofoveata, Solenogastres, Polyplacophora, and Scaphopoda (Mollusca) and its phylogenetic implications. *Zoomorphology*. 2012;131:149–70.
41. Redl E, Scherholz M, Todt C, Wollesen T, Wanninger A. Development of the nervous system in Solenogastres (Mollusca) reveals putative ancestral spiralian features. *Evodevo*. 2014;5:1–17.
42. Beckers P. Nemertean Nervous System - a Comparative Analysis. Germany: Dissertation at the Rheinische Friedrich-Wilhelms-Universität Bonn; 2012. p. 1–121.
43. Brenzinger B, Haszprunar G, Schrödl M. At the limits of a successful body plan - 3D microanatomy, histology and evolution of *Helminthope* (Mollusca: Heterobranchia: Rhodopomorph), the most worm-like gastropod. *Frontiers in Zool*. 2013;10:37.
44. Brenzinger B, Wilson NG, Schrödl M. 3D microanatomy of a gastropod "worm", *Rhodope rousei* n. sp. (Heterobranchia) from southern Australia. *J Molluscan Stud*. 2011;77:375–87.
45. Jörger KM, Stoschek T, Migotto A, Haszprunar G, Neusser TP: 3D microanatomy of the mesopsammic *Pseudovermis salamandrops* Marcus, 1953 from Brazil (Nudibranchia, Gastropoda). *Marine Biodiversity* 2014;44:327–341.
46. Reuter M, Maule AG, Halton DW, Gustafsson MKS, Shaw C. The organization of the nervous system in Plathelminthes. The neuropeptide F-immunoreactive pattern in Catenulida, Macrostromida, Proseriata. *Zoomorphology*. 1995;115:83–97.
47. Zrzavy J. Gastrotricha and metazoan phylogeny. *Zool Scr*. 2003;32:61–81.
48. Beckers P, Loesel R, Bartolomaeus T. The nervous systems of basally branching Nemertea (Palaeonemertea). *PLoS One*. 2013;8:e66137.
49. Bullock TH, Horridge GA. Structure and function in the nervous system of invertebrates. W. H. Freeman: San Francisco, London; 1965.
50. Bubko OV, Minichev YS. The nervous system of Oweniidae. *Zool Zhurnal*. 1972;51:1288–99.
51. Lagutenko YP. Structural organization of the nervous plexus in the oweniids (Polychaeta: Oweniidae). *Zool Zhurnal*. 1985;64:1802–7.
52. Lagutenko YP. Early forms of Evolution of the Basiepidermal nerve Plexus of Bilateria as a Possible Evidence for Primary Diversity of Its Initial State. *J Evol Biochem Physiol*. 2002;38(3):354–63.
53. Clark RB. The Posterior Lobes of *Nephtys* - Observations on 3 New England Species. *Q J Microsc Sci*. 1958;99:505.
54. Golding DW: Polychaeta: nervous system. In *Microscopic Anatomy of Invertebrates*. Volume 7: Annelida. Edited by Harrison FW, Gardiner SL. New York; 1992:153–179.
55. Purschke G: Structure of the prostomial appendages and the central nervous system in the Protodrilida (Polychaeta). *Zoomorphology* 1993;113:1–20 .
56. Goodrich ES: *Nerilla* an archiannelid. *Quarterly Journal of Microscopical Science* 1912, 57(4):397–425
57. Wanninger A, Koop D, Bromham L, Noonan E, Degnan BM. Nervous and muscle system development in *Phascolion strombus* (Sipuncula). *Dev Genes Evol*. 2005;215:509–18.
58. Mainoya JR. Morphological and histochemical observations on the nervous system of two sipunculid species, *Siphonosoma australe* and *S. cumanense*. *Mar Biol*. 1974;27:275–80.
59. Kristof A, Wollesen T, Wanninger A. Segmental mode of neural patterning in *Sipuncula*. *Curr Biol*. 2008;18:1129–32.
60. Rieger RM, Rieger GE. Fine structure of the archiannelid cuticle and remarks on the evolution of the cuticle within Spiralia. *Acta Zool (Stockholm)*. 1976;5:53–68.
61. Worsaae K, Rouse GW. Is *Diurodrilus* an Annelid? *J Morphol*. 2008;269:1426–55.
62. Tolbert LP. Olfactory development in invertebrates. On the scent of central developmental issues. *Ann N Y Acad Sci*. 1998;855:95–103.
63. Krieger J, Breer H. Olfactory reception in invertebrates. *Science*. 1999;286:720–3.
64. Lewbart GA, Riser NW. Nuchal Organs of the Polychaete *Parapionosyllis manca* (Syllidae). *Invertebr Biol*. 1996;115:286–98.

65. Schmidtberg H, Dorresteijn AWC. Ultrastructure of the nuchal organs in the polychaete *Platynereis dumerilii* (Annelida, Nereididae). *Invertebr Biol.* 2010;129:252–65.
66. Purschke G, Hessling R. Analysis of the Central Nervous System and Sense Organs in *Potamodrilus fluviatilis* (Annelida: Potamodrilidae). *Zool Anz.* 2002;241(1):19–35.
67. Gould SJ. Ontogeny and phylogeny. Cambridge: Harvard University Press; 1977.
68. Schmidt-Rhaesa A. The Evolution of organ systems. Cambridge: Oxford University Press; 2007.
69. Rieger RM, Purschke G. The coelom and the origins of the annelid body plan. *Hydrobiologia.* 2005;535(536):127–37.
70. Fischer AH, Henrich T, Arendt D. The normal development of *Platynereis dumerilii* (Nereididae, Annelida). *Frontiers in Zool.* 2010;7:31.
71. Wanninger A. Shaping the things to come: ontogeny of lophotrochozoan neuromuscular systems and the Tetraneuralia concept. *Biol Bull.* 2009;216:293–306.
72. Wanninger A. Morphology is dead - long live morphology! Integrating MorphoEvoDevo and phylogenomics *Frontiers in Ecol and Evolution.* 2015;3:54.
73. Müller CHG, Hylleberg J, Michalik P. Complex epidermal organs of *Phascolion* (Sipuncula): insights into the evolution of bimodal secretory cells in annelids. *Acta Zool.* 2014;96:343–374.
74. Åkesson B. A Study of the Nervous System of the Sipunculoideae with some remarks on the development of the two Species *Phascolion strombi* Montagu and *Golfingia minuta* Keferstein. In: Gleerup CWK, editor. Undersökningar över Öresund, Volume 38. Håkan Ohlssons Boktryckeri: Lund; 1958. 250p.
75. Wilkens V, Purschke G. Pigmented eyes, photoreceptor-like sense organs and central nervous system in the polychaete *Scoloplos armiger* (Orbiniidae, Annelida) and their phylogenetic importance. *J Morphol.* 2009;270:1296–310.
76. Helm C, Krause A, Bleidorn C. Immunohistochemical investigations of the development of *Scoloplos armiger* ("intertidalis clade") indicate a paedomorphic origin of *Proscoplos cygnochaetus* (Annelida, Orbiniidae). *Invertebr Biol.* 2015;134(3):214–30.
77. Beckers P, Faller S, Loesel R. Lophotrochozoan neuroanatomy: An analysis of the brain and nervous system of *Lineus viridis* (Nemertea) using different staining techniques. *Frontiers in Zool.* 2011;8:1–12.
78. Müller MCM, Sterrer W. Musculature and nervous system of *Gnathostomula peregrina* (Gnathostomulida) shown by phalloidin labeling, immunohistochemistry, and cLSM, and their phylogenetic significance. *Zoomorphology.* 2004;123:169–77.
79. Kristensen RM, Nørrevang A. On the Fine Structure of *Rastrognathia macrostoma* gen. et sp.n. placed in Rastrognathiidae fam.n. (Gnathostomulida). *Zool Scripta.* 1977;6:27–41.
80. Ruppert EE, Schreiner SP. Ultrastructure and Potential Significance of Cerebral Light-Refracting Bodies of *Stenostomum virginianum* (Turbellaria, Catenulida). *Zoomorphology.* 1980;96:21–31.
81. Gustafsson MKS, Raikova OI, Reuter M, Jondelius U. The brain of the Nemertodermatida (Platyhelminthes) as revealed by anti-5HT and anti-FMRFamide immunostainings. *Tissue & Cell.* 2000;32(5):358–65.
82. Raikova OI, Reuter M, Gustafsson MKS, Maule AG, Halton DW, Jondelius U. Basiepidermal nervous system in *Nemertoderma westbladi* (Nemertodermatida): GYIRFamide immunoreactivity. *Zoology.* 2004;107:75–86.
83. Rieger RM. *Jennaria pulchra*, nov. gen. nov. spec., eine den psammobionten Anneliden nahestehende Gattung aus dem Küstengrundwasser von North Carolina. *Berichte des naturwissenschaftlich-medizinischen Vereins Innsbruck.* 1991;78:203–15.
84. Fofanova EG, Nezhlin LP, Voronezhskaya EE. Ciliary and nervous structures in juvenile females of the annelid *Dinophilus gyrocolliatus* (O. Schmidt, 1848) (Annelida: Polychaeta). *Russ J Mar Biol.* 2014;40:43–52.
85. Fofanova EG, Voronezhskaya EE. The structure of archiannelid *Dinophilus gyrocolliatus* ventral nerve cords. *Acta Biol Hung.* 2012;63:88–90.
86. Merker G, Harnack MV-V. Zur Feinstruktur des Gehirns und der Sinnesorgane von *Protodrilus rubropharyngaeus* Jaegersten (Archiannelida). *Cell Tissue Res.* 1967;81:221–39.
87. Nørrevang A, Kristensen RM. Description of *Psammodrilus aedificator* sp.n. (Polychaeta), with Notes on the Arctic Interstitial Fauna of Disko Island, W. Greenland. 1982;11:265–79.
88. Worsaae K, Sterrer W. Description of two new interstitial species of Psammodrilidae (Annelida) from Bermuda. *Mar Biol Res.* 2006;2:431–45.
89. Fischer A, Dorresteijn A. The polychaete *Platynereis dumerilii* (Annelida): a laboratory animal with spiralian cleavage, lifelong segment proliferation and a mixed benthic/pelagic life cycle. *BioEssays: news and reviews in molecular, cell and dev biol.* 2004;26:314–25.
90. Denes AS, Jekely G, Steinmetz PRH, Raible F, Snyman H, Prud'homme B, et al. Molecular architecture of annelid nerve cord supports common origin of nervous system centralization in bilateria. *Cell.* 2007;129:277–88.
91. Meyer NP, Seaver EC. Neurogenesis in an annelid: characterization of brain neural precursors in the polychaete *Capitella* sp. I *Dev Biol.* 2009;335:237–52.
92. Brinkmann N, Wanninger A. Neurogenesis suggests independent evolution of opercula in serpulid polychaetes. *BMC Evol Biol.* 2009;9:1–13.

**Submit your next manuscript to BioMed Central and take full advantage of:**

- Convenient online submission
- Thorough peer review
- No space constraints or color figure charges
- Immediate publication on acceptance
- Inclusion in PubMed, CAS, Scopus and Google Scholar
- Research which is freely available for redistribution

Submit your manuscript at  
[www.biomedcentral.com/submit](http://www.biomedcentral.com/submit)



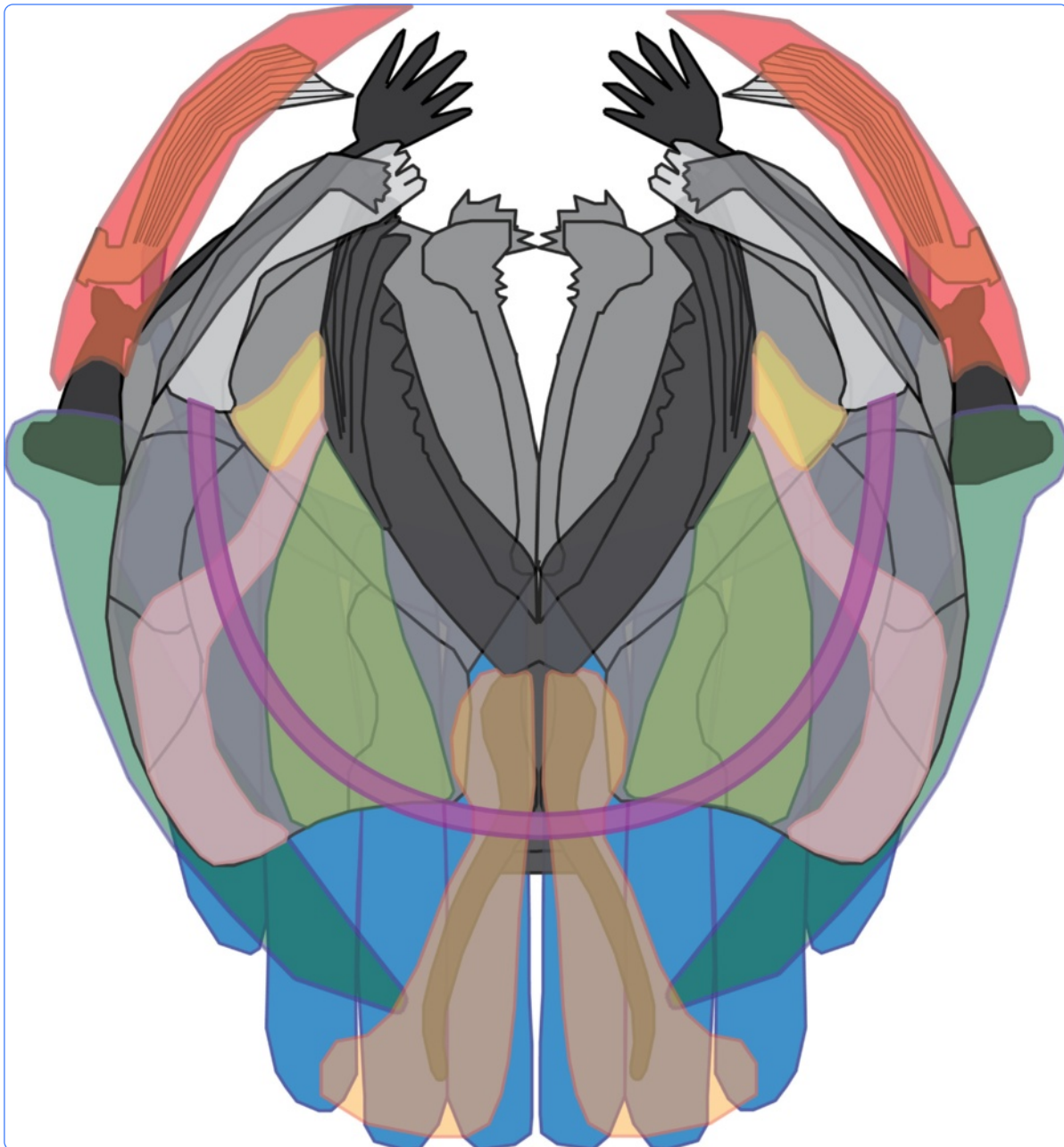
**Manuscript III:**

**Manuscript III: Detailed reconstruction of the musculature in *Limnognathia maerski* (Micrognathozoa) and comparison with other Gnathifera**

Bekkouche N., Kristensen R. M., Hejnol A., Sørensen M. V., and Worsaae, K.

Frontiers in Zoology, Volume 11, issue 71





## Detailed reconstruction of the musculature in *Limnognathia maerski* (Micrognathozoa) and comparison with other Gnathifera

Bekkouche *et al.*



RESEARCH

Open Access

# Detailed reconstruction of the musculature in *Limnognathia maerski* (Micrognathozoa) and comparison with other Gnathifera

Nicolas Bekkouche<sup>1</sup>, Reinhardt M Kristensen<sup>2</sup>, Andreas Hejnal<sup>3</sup>, Martin V Sørensen<sup>4</sup> and Katrine Worsaae<sup>1\*</sup>

## Abstract

**Introduction:** *Limnognathia maerski* is the single species of the recently described taxon, Micrognathozoa. The most conspicuous character of this animal is the complex set of jaws, which resembles an even more intricate version of the trophi of Rotifera and the jaws of Gnathostomulida. Whereas the jaws of *Limnognathia maerski* previously have been subject to close examinations, the related musculature and other organ systems are far less studied. Here we provide a detailed study of the body and jaw musculature of *Limnognathia maerski*, employing confocal laser scanning microscopy of phalloidin stained musculature as well as transmission electron microscopy (TEM).

**Results:** This study reveals a complex body wall musculature, comprising six pairs of main longitudinal muscles and 13 pairs of trunk dorso-ventral muscles. Most longitudinal muscles span the length of the body and some fibers even branch off and continue anteriorly into the head and posteriorly into the abdomen, forming a complex musculature. The musculature of the jaw apparatus shows several pairs of striated muscles largely related to the fibularium and the main jaws. The jaw articulation and function of major and minor muscle pairs are discussed. No circular muscles or intestinal musculature have been found, but some newly discovered muscles may supply the anal opening.

**Conclusions:** The organization in *Limnognathia maerski* of the longitudinal and dorso-ventral muscle bundles in a loose grid is more similar to the organization found in rotifers rather than gnathostomulids. Although the dorso-ventral musculature is probably not homologous to the circular muscles of rotifers, a similar function in body extension is suggested. Additionally, a functional comparison between the jaw musculature of *Limnognathia maerski*, Rotifera and Gnathostomulida, emphasizes the important role of the fibularium in *Limnognathia maerski*, and suggests a closer functional resemblance to the jaw organization in Rotifera.

**Keywords:** CLSM, 3D reconstructions, Jaw apparatus, F-actin, Trophi, Mastax

## Introduction

*Limnognathia maerski* Kristensen & Funch, 2000, is a minute animal living in fresh water ponds and lakes [1-3]. The animal was discovered in 1994 at Disko Island, Greenland, but not described before 2000, and it has subsequently been reported from the Sub Antarctic Crozet Island [1], in a stream from southern Wales, United Kingdom, and in the river Lambourn (Berkshire), United Kingdom (P. E. Schmid and J.M. Schmid-Araya, personal communication). With a unique combination of characters, it is considered the only member of the

recently described Micrognathozoa [2-5], belonging to Gnathifera. However, the phylogenetic relationships within Gnathifera are still debated, and the molecular studies are based on very limited information [5]. So far, the complex jaw apparatus of *L. maerski* has received the main attention in studies, leading to several disputed homology hypotheses for each sclerite of the trophi [1,3,6,7]. However, no detailed studies have addressed the overall morphology of organs systems and further anatomical knowledge on *L. maerski* is warranted in order to compare this unique evolutionary lineage with the other gnathiferan groups, as well as other animals.

*Limnognathia maerski* measures 80-150 µm, possesses a complex set of jaws, a conspicuously arranged ventral ciliation and, so far, only females are known. The

\* Correspondence: kworsaae@bio.ku.dk

<sup>1</sup>Marine Biological Section, Department of Biology, University of Copenhagen, Universitetsparken 4, 2100 Copenhagen Ø, Denmark  
Full list of author information is available at the end of the article

ventrally ciliated head consists of a forehead with ciliary sensory organs and a more posterior part containing the pharyngeal apparatus. The trunk is composed of an accordion-like thorax and a large abdomen with ventral ciliophores and a posterior adhesive pad [3]. In the original description, the overall musculature of *L. maerski* is briefly described. It is composed of several longitudinal and dorso-ventral muscles, minute muscles articulating the dorsal plates and a dense pharyngeal musculature. No circular musculature has been found. However, precise information on the number, configuration and relative size of each set of muscles was not provided. Ultrastructural data provided information on the structure of muscles attachment sites, the absence of myosyncytia and myoepithelia, the cross-striated nature of the pharyngeal musculature, and the mainly obliquely striated longitudinal musculature [3].

Following Sørensen [6], the jaws of *L. maerski* are composed of six main elements: i) The median, ventral-most basal plate with posterior stems and anterior flattened and toothed manus, ii) the large and conspicuous ventral fibularium made of different chambers containing cells, extending dorso-laterally, iii) the latero-ventral ventral jaws (pseudophalangia) that articulate posteriorly with the associated accessory sclerites, iv) the medio-dorsal main jaws, each with a posteriorly projecting cauda, surrounded by the fibularium, v) the dorso-lateral dorsal jaws also confined to the fibularium area, vi) and the pharyngeal lamellae, a pair of lamellate structures positioned antero-laterally to the rest of the jaw apparatus. Additionally, Kristensen and Funch [3], describe the lamella orales as a paired structure similar to the lamellae pharyngea, situated dorso-laterally, inside the fibularium. However, the presence of these structures has not been confirmed in any subsequent studies [1,6].

The animal lives in limnic mosses or in the sediment of relatively calm springs and lakes, and was first recognized for its unusual 'ciliate-like' swimming in the water column. It also uses ciliary motion to glide over surfaces. Occasionally, it performs muscular contractions during lateral bending and longitudinal accordion like contractions for directional change, ventral bending while egg laying and dorsal contraction during vomit behavior [3]. Foraging of *L. maerski* involves fine movements of the jaw apparatus as well as larger movements of the head. While feeding, the ventral jaws are protruded and involved in substrate grasping. During the vomit behavior, the forehead is moved upward and backward, and most of the jaw apparatus is protruded through the mouth opening, while it performs fast snapping movements of the jaw elements and forward and backward movements of the main jaws (see reference [3] and Figure 1B). Accessory sclerites and pseudophalangia may move independent of the rest of the jaw apparatus, allowing the

ventral jaws to move from a rostro-caudal orientation to a dorso-ventral orientation without moving the other jaws elements [3,6,7].

The body wall musculature differs between the putatively closest micrognathozoan relatives: Gnathostomulida and Rotifera. In Gnathostomulida, the overall musculature consists of numerous circular and diagonal muscles and several bundles of longitudinal muscles (six to nine pairs [8-10]) extending the entire body length, where the superimposition of longitudinal, diagonal and circular muscles forms a dense grid like body wall musculature [9,10]. In the majority of rotifers, most of the longitudinal muscles do not extend through the entire body, but are limited to certain body regions, e.g., coronal retractors in the head or muscles in the posterior part of the trunk, being involved in the contraction of the head and foot, respectively [11-13]. Circular muscles are few and usually incomplete transverse, rather than circular (e.g., [11-15]), although some Gnesiotrocha have complete rings [12,16,17]. Most of the diagonal and transverse muscles are usually absent (e.g., [12,18]), and if present they are only few and/or inconspicuous [14,19]. Splanchnic muscles surrounding the gut are not found in Gnathostomulida [9], whereas they present a very thin musculature in Rotifera. This muscular grid is documented for Seisonidae [11] and Monogononta (e.g., [13,19]) but visceral muscles are not found in Bdelloidea [12,14]. Dorso-ventral musculature has not been described for Gnathostomulida [9], and most of the functionally dorso-ventral muscles in Rotifera are supposedly modified incomplete circular muscles [12,19] meaning "true" dorso-ventral muscles, as reported by Kristensen and Funch [3], seem to be unique for Micrognathozoa.

The jaw musculature also differs between Gnathostomulida and Rotifera, due to the organization of their jaws. In gnathostomulids, the jaw apparatus consists of i) a set of main jaws, and in some taxa ii) an unpaired basal plate [20-22]. In rotifers, the jaw apparatus (trophi) includes 7 main elements: the i) unpaired posteriorly directed fulcrum, ii) paired rami, iii) paired unci, and iv) paired manubria. The fulcrum and rami together form the central element, the incus, whilst the unci and manubria form the mallei (e.g., [23-25]). The rotifer incus has been considered homologous with the gnathostomulid main jaws [21,26]. However, it also has been suggested that some parts of the gnathostomulid articularium (antero-lateral parts of the main jaws) are homologous with the rotifer manubria [27]. The gnathostomulid basal plate is considered autapomorphic for the group, and no homologous counterpart has been identified in the rotiferan trophi. The structural differences in the musculature of gnathostomulid and rotiferan jaw apparatuses clearly relate to the differences in the hard parts and the additional number of rotifer jaw elements. Indeed, most of the musculature supplying the

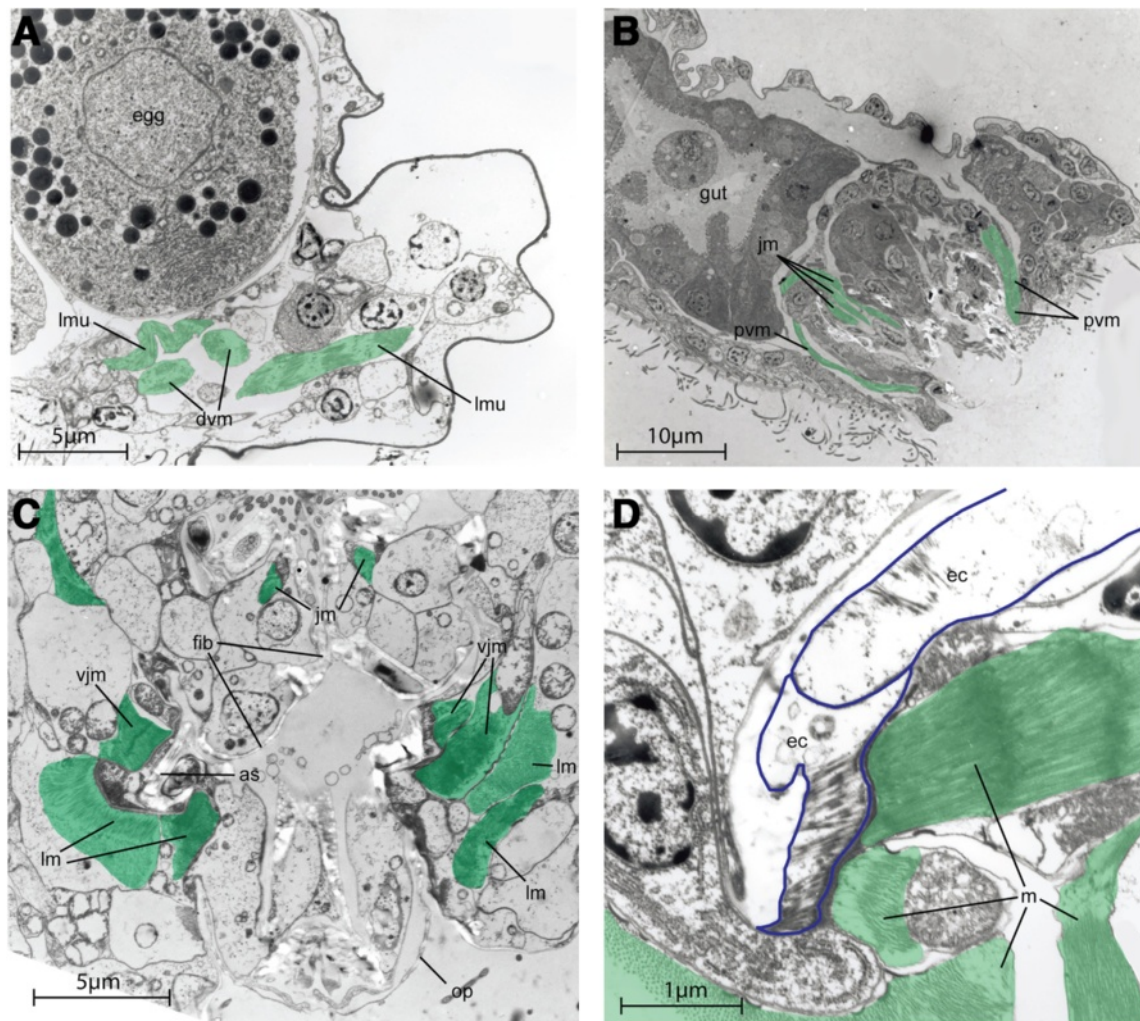


**Figure 1** TEM sections of *Limnognathia maerski*. Muscles highlighted in green. **A**, transversal section of posterior part. Posterior on the right. **B**, sagittal section showing the vomit behaviour. **C**, transversal section of the jaws. The ventral side is on the bottom. **D**, Close up of muscle attachment on a jaw sclerite, showing the non myoepithelial nature of the jaw muscles. Epidermal cells with blue outlines.

rotifer trophi consists of relatively small paired muscles connecting the different jaw elements (sclerites), while, in Gnathostomulida, the main jaws are mainly moved together by large muscles attached to the pharynx wall. The movement between jaw elements in Gnathostomulida is consequently achieved by U-shaped muscles (bent transversal muscles) and laterally attached transversal muscles.

Recently, several CLSM studies of phalloidin-stained musculature have been carried out on a great number of microscopic animals, revealing comprehensive information on their overall musculature [9,11,28-30] and also, in the case of gnathiferans, on the musculature of the rotifer mastax [31,32] or gnathostomulid pharynx [26]. Combined with TEM, many details can be inferred on the relative position of muscles and their ultrastructure, but also connections to the other

part of the body. In order to compare the general muscular organization as well as jaw musculature of *L. maerski* with other animals, we here describe its musculature employing F-actin staining and confocal laser microscopy (CLSM) as well as transmission electron microscopy (TEM).

## Results

The overall musculature is organised into seven main pairs of longitudinal muscles extending from head to abdomen and 13 oblique dorso-ventral muscles localised in the thoracic and the abdominal part (Figures 2, 3, and 4). No circular muscles are present. The musculature furthermore comprises the dense pharyngeal muscle and the fine anterior forehead muscle. Cross striated muscles are found in the body wall musculature (Figure 1A) as well as in the jaw musculature (Figures 1B,C,D and 5C,D).

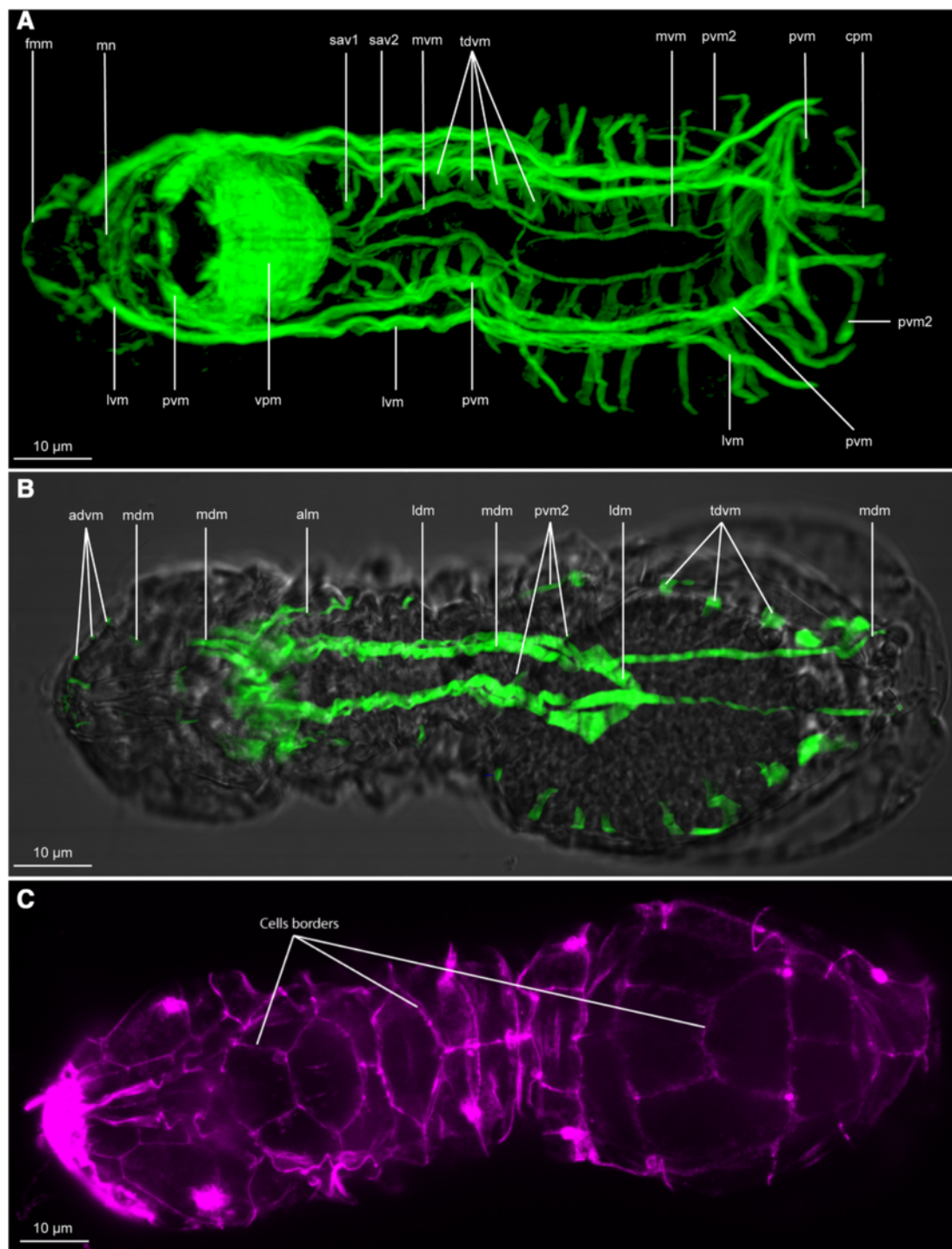


**Figure 2** CLSM of phalloidin stained muscle system and light microscopy of *Limnognathia maerski*. Anterior end is positioned left on all pictures. **A**: Ventral view, Z-stack of the ventral portion, showing only the muscle system. **B**: Single section showing CLSM of the dorsal muscle system and the contour of the specimen, visualized with transmitted light. **C**: Synapsin2 staining of *L. maerski*, maximum intensity projection of a dorsal substack. Lines show the border of the dorsal cells to which the dorso-ventral muscles attach (illustrated in Figure 4B). advm, anterior dorso-ventral muscles; alm, anterior lateral muscle; cpm, ciliated adhesive pad muscle; fmm, front margin muscle; ldm, lateral dorsal muscle; lvm, lateral ventral muscle; mdm, median-dorsal muscle; mvm, medio-ventral muscle; mn, muscle network; pvm, paramedian ventral muscle; pvm2, posterior lateral muscle; sav1,2, small anterior ventral longitudinal muscles; tdvm, trunk dorso-ventral muscles; vpm, ventral pharyngeal muscles.

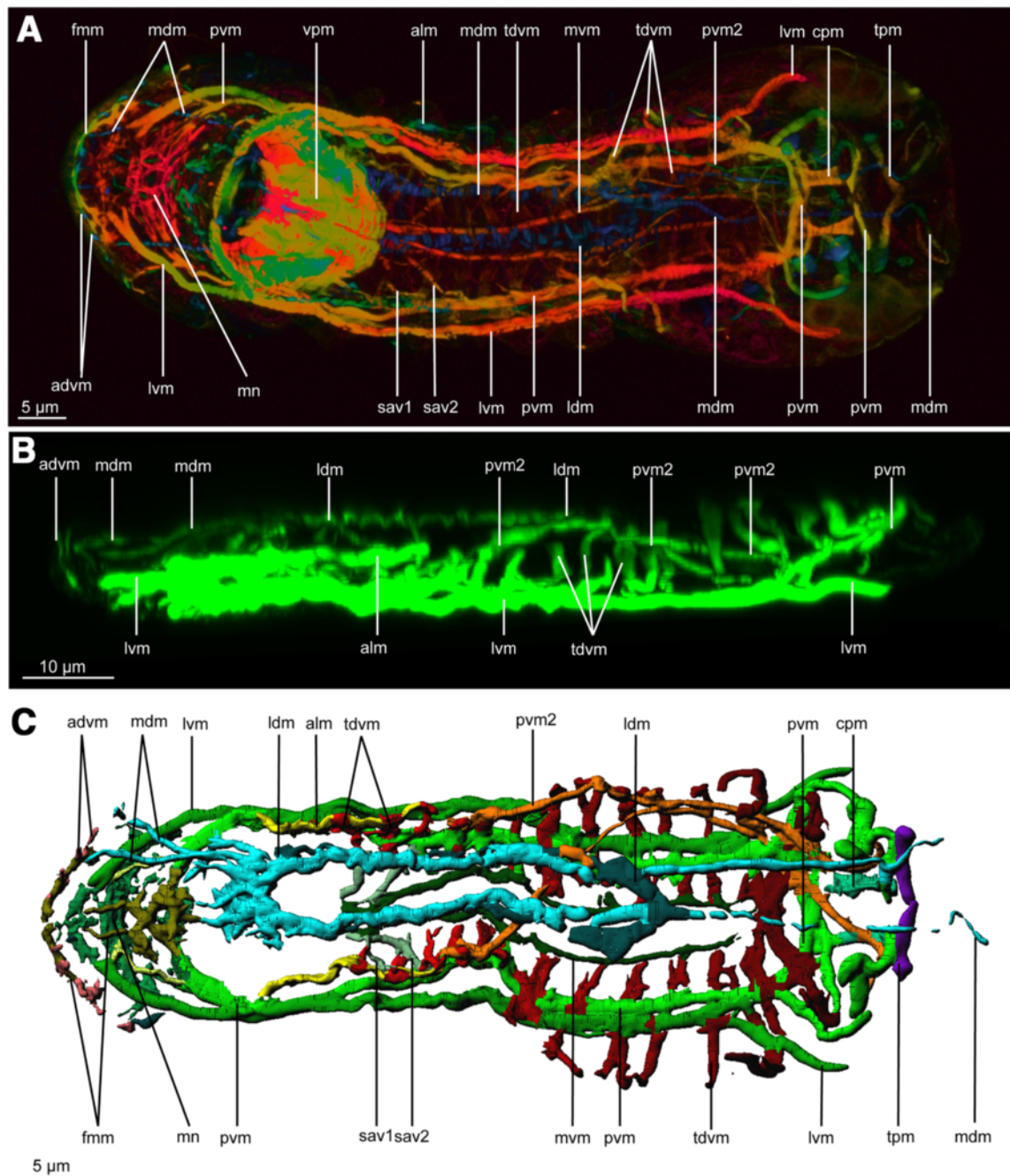


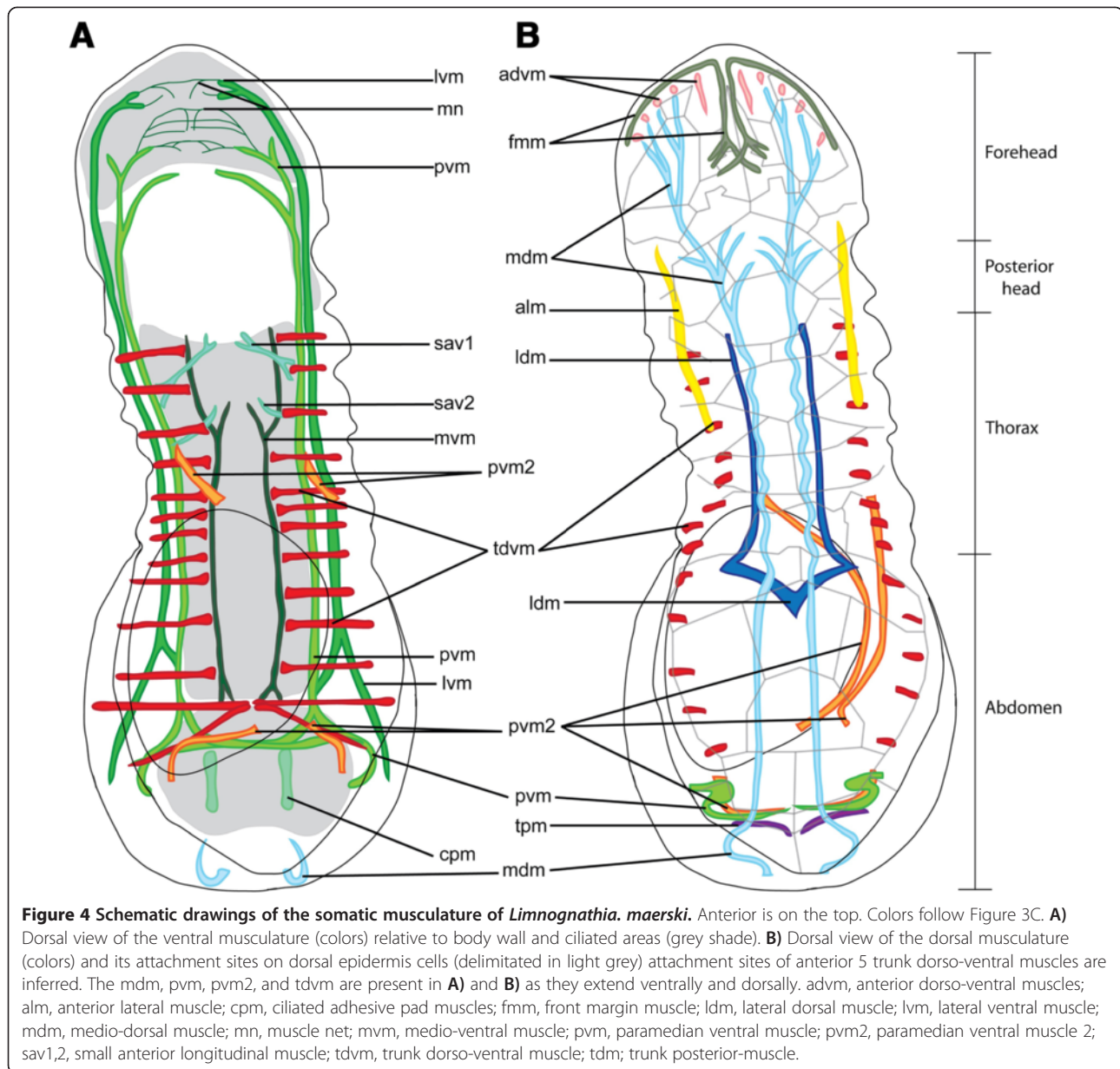
**Figure 3** CLSM of phalloidin stained muscle system of *Limnognathia maerski*. Anterior end is positioned left on all pictures. **A**, Ventral view of the maximum depth intensity projection. **B**, lateral view reconstruction of a dorso-ventral Z-stack. Same specimen as Figure 2A,B. **C**, Dorsal view of the isosurface reconstruction of the muscular system. Same specimen as Figure 2A,B. advm, anterior dorso-ventral muscles; alm, anterior lateral muscle; cpm, ciliated pad muscle; fmm, front margin muscles; ldm, lateral dorsal muscle; lvm, Lateral ventral muscle; mdm, medio-dorsal muscle; mn, muscle network; mvm, medio-ventral muscle; pvm, paramedian ventral muscle; pvm2, posterior lateral muscle; sav1,2, small anterior ventral longitudinal muscles; tdvm, trunk dorso-ventral muscles; tpm, transversal posterior muscle; vpm, ventral pharyngeal muscles.

### Longitudinal musculature

The longitudinal musculature of the trunk consists of seven pairs of main muscles (*three ventral, two lateral, two dorsal*) as well as two short anterior pairs of muscles and two short posterior pairs of muscles.

### Ventral muscles

The three ventral main muscles extend the body length aiding the body contraction and extension (Figures 2A, 3 and 4). The longitudinal ventral muscles are implicated in longitudinal contractions and ventral bending.



The paired medio-ventral muscles (mvm, Figures 2A, 3A,C, 4 and 5A,B) consist of two muscle fibres that form bundles originating directly posterior to the ventral pharyngeal muscle and extend along the ventral wall of the gut (mvm: Figure 5A). At its posterior extremity, each medio-ventral muscle separates into two very short muscle fibers that each extends four micrometers before inserting into the epidermis that is anterior of the adhesive ciliated pad (mvm: Figure 4).

Medially, two pairs of small anterior ventral longitudinal muscles (sav1, sav2, Figures 2A, 3A,C and 4) supply the anterior part of the thorax, each originating from the mid-line directly posterior to the ventral pharyngeal muscle. The anteriormost muscle pair (sav1) is bifurcated at both

ends: the anterior bifurcation inserts medially just behind the pharynx, while the posterior bifurcation originates in a more lateral region close to the paramedian ventral muscle (sav1: Figure 4). The posteriormost muscle pair (sav2) inserts medially at the level of mvm and extends laterally toward (and originates close to) the paramedian ventral muscle (described below, sav2: Figure 4).

Latero-anterior to the pharynx are three muscles that come together to form the paramedian ventral muscle (pvm, Figures 2A, 3A,B,C, 4 and 5A,B); consequently, the paramedian ventral muscle is trifurcated at its anterior insertion but extends posteriorly as a single muscle bundle. The paramedian ventral muscle follows the course of the trunk and abdomen, where it eventually

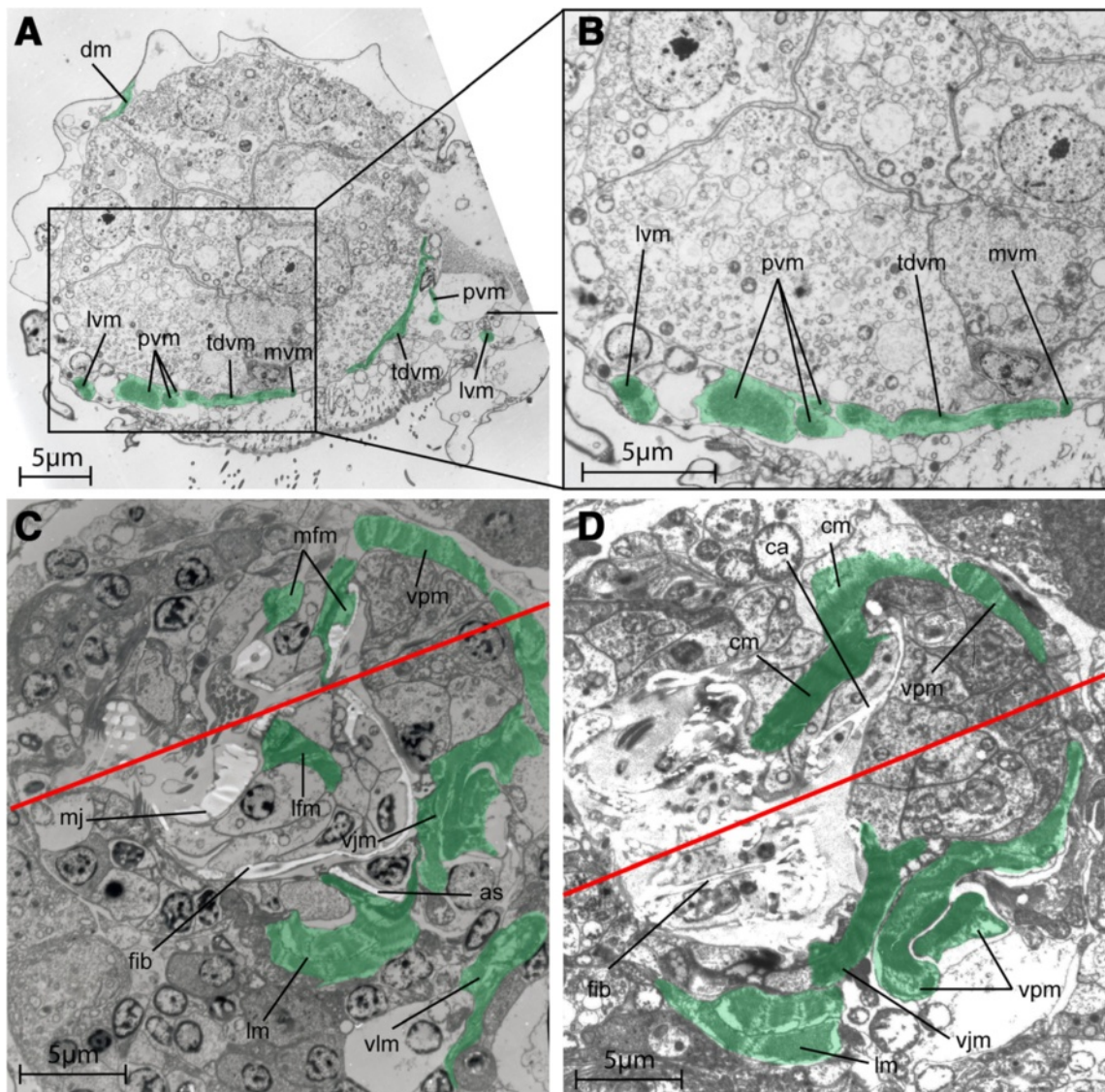


**Figure 5** TEM sections of *Limnognathia maerski*. Muscles highlighted in green. **A**, transversal section of the trunk. Dorsal side on top. **B**, close up of figure A, showing the ventral musculature. **C**, **D**, coronal section the jaws. The red line shows the symmetry axis of the jaws. The front is on the left. The section in C is more ventral than the section in D. as, accessory sclerite; dm, dorsal muscle; ca, cauda; cm, cauda muscle; fib, fibularium; lfm, lateral fibularium main jaw muscle; lm, pharyngeal lamella muscle; lvm, lateral ventral muscle; mfm, median fibularium main jaw muscle; mj, main jaws; mvm, medio-ventral muscle; pvm, paramedian ventral muscle; tdvm, trunk dorso-ventral muscle; vjm, ventral jaw muscle; vlm, ventral lateral muscle; vpm, ventral pharyngeal muscle.

bifurcates into two separate bundles. The ipsilateral muscle bundle extends dorsally where it joins the paramedian ventral muscle 2 on the same side of the abdomen, while the contralateral muscle extends to the opposite side of the body and joins the contralateral last dorso-ventral muscle. Thus, each of the last dorso-ventral muscle bundles consists of three separate muscles: a dorso-ventral muscle, an ipsilateral branch of the paramedian ventral muscle and a contralateral branch of the paramedian ventral muscle from the opposite side of the body. (pvm: Figures 2A, 3A, 4 and 5). The paramedian longitudinal muscle follows the

outline of the ventral ciliated area and contractions may change the direction during swimming or crawling (pvm: Figure 4).

Each of the two lateral ventral muscles (lvm; Figures 2A, 3A,B,C and 5A,B) inserts anterior of the mouth where they each bifurcate into two smaller branches. Posteriorly, each lateral ventral muscle extends along the trunk and abdomen as a single bundle that eventually bifurcates again. The inner branch joins the paramedian ventral muscle, while the lateral branch inserts in the region of the large posterior gland.

A pair of ciliated adhesive pad muscles (cpm: Figures 2A, 3A,C and 4), which are present as short longitudinal bands, extend from an anterior zone of the ciliated pad (just posterior of the paramedian ventral muscle midline) to a posterior zone of the ciliated pad (cpm: Figure 4). The adhesive ciliated pad muscle is probably involved in the adhesive ciliated pad area contractions. Contraction of the adhesive ciliated pad muscles could contract this area and allow the animal to release from the substratum.

#### **Lateral muscles**

Two pairs of lateral muscles are present in the trunk. The pair of anterior lateral muscles (alm: Figures 2A, 3B, C and 4B) originates anterior of the mouth, probably bifurcating from the paramedian longitudinal muscle, and continues two thirds into the abdomen, appearing to attach to the lateral epidermal cells. They are positioned at a mid dorso-ventral level. The paired paramedian ventral muscles 2 (pvm2: Figures 2A,B and 3A,B,C) originate ventrally to the paramedian ventral muscles, separating at the mid-thoracic level. Each muscle reaches the dorsal side along the anterior part of the abdomen (pvm2: Figure 2B), extends ventrally at the level of the adhesive ciliated pad and returns at an antero-dorsal position, joining the very posterior dorsal epidermal cells and the paramedian ventral muscle. From this point, both paramedian ventral muscle 2 muscles join close to the midline at their posteriormost point, at the level of the last dorsal plate. If an egg is present at the level of the abdomen, one of the posterior lateral muscles is pushed by the egg to the contralateral side to return to the ipsilateral side at the level of the adhesive ciliated pad (pvm2: Figures 2A, 3A,C and 4). This muscle extends along the dorsal side of the gut, being probably implicated in dorsal bending of the animal.

#### **Dorsal muscles**

Two dorsal pairs of muscles extend through the trunk. The two pairs are close to the midline and extend as two contiguous muscles (Figures 2B, 3A,C and 4).

The medio-dorsal muscle (mdm: Figures 2B, 3A,B,C and 4, dm: Figure 5) is an elongate band that extends from the head to the abdomen and is composed of several thinner muscles that branch off in the forehead and posterior head regions. Anteriorly, the medio-dorsal muscle branches twice (with additional subbranches) that insert close to the frontal margin where the anterior dorso-ventral muscles insert (adv: Figures 2B, 3A-C and 4). In the posterior head region, the medio-dorsal muscle supplies several short muscle branches just dorsal of the pharynx (mdm: Figures 2B, 3C and 4). At the very posterior part of the animal, the medio-dorsal muscle lines the body wall, to insert at the ventro-

posterior extremity of the abdomen (mdm: Figures 2B, 3A,C and 4B).

The lateral dorsal muscles (ldm: Figure 2B, 3A,B, and 4, dm: 5) originate as a pair of muscles that both insert at the midline in the trunk region (mdm: Figure 4). Each muscle extends antero-laterally for about 10 micrometers before curving back medially and continuing anteriorly as a strictly longitudinal muscle band that inserts dorsal to the pharynx (Figures 2B, 3A,C and 4B).

#### **Transversal posterior muscles**

Additionally, at the very posterior region, a complex of transversal and dorso-ventral muscles is present (Figures 3C and 4). It is partially formed by the longitudinal muscle extending posteriorly, from the ventral to the dorsal side. Posterior of these muscles, two pairs of dorsal small transversal muscles line each side of the body. It is difficult to determine with certitude if these two pairs are the continuity of the posterior lateral muscle. However, the anteriormost pair of lateral muscles seems to be a continuity of the paramedian ventral muscle (pvm: Figures 2A, 3A,C and 4) while the transversal posterior muscle pair seems to be another set of muscles (tpm: Figures 3A,C and 4). Both pairs of transversal posterior muscles are very dorsal and according their anatomical position could be implicated in a possible anus opening. Along with the posterior longitudinal and dorso-ventral musculature, the complex posterior musculature is probably involved in the oviposition, substrate adherence and, eventually, defecation.

#### **Dorso-ventral musculature**

The dorso-ventral musculature consists mostly of two sets of muscles: the anterior dorso-ventral muscles and the trunk dorso-ventral muscles (Figure 3C and 4). The posteriormost dorso-ventral complex is the continuation of the paramedian muscle and the paramedian ventral muscle 2 when they fold in the posterior region, and is not serially homologous to the trunk dorso-ventral muscles.

#### **Anterior muscles**

Five pairs of anterior dorso-ventral muscles (adv: Figures 2B, 3A,B,C and 4) supply the front margin. They appear to support the frontal ciliated sensory region. On each side, the medianmost dorso-ventral head muscle inserts dorsally, at the anterior head margin, close to the mid-line (Figure 2B).

#### **Trunk muscles**

Thirteen pairs of oblique trunk dorso-ventral muscles (tdvm: Figures 2A,B, 3A-C; 4; 5A,B) supply the thorax and the abdomen. Each trunk dorso-ventral muscle inserts close to the midline on either side of the medio-

ventral muscle, extends laterally dorsal to the paramedian ventral muscle and the lateral ventral muscle, and then curves dorsally to insert on epidermal cells (tdvm: Figures 2A; 4; 5A,B). They join the epidermal cells dorsally, extending along the body sides. They line the gut cells very closely, probably functioning as body-wall musculature as well as gut musculature (tdvm: Figure 5A,B). Five pairs supply the thoracic region and eight supply the abdomen region (tdvm: Figures 2A,B; 3A-C; 4). The penultimate and the last pair of dorso-ventral muscles insert ventrally at the midline where the medio-ventral muscle inserts as well, forming a very muscular zone five micrometres anterior of the adhesive pad. A few micrometres posteriorly, the two paramedian muscles cross transversally, forming with the two last dorso-ventral trunk muscles a triangular set of ventral muscles at the anterior area of the adhesive ciliated pad (tdvm: Figures 2A; 3C; 4).

#### Forehead musculature

The head musculature is a continuity of the longitudinal body musculature as well as a few specific muscles.

On the frontal margin, the paired frontal margin muscles (fmm: Figures 2A; 3A,C; 4) follow the coronal plan supplying the anterior ciliated region. The median extremity of each muscle is dorsal and bends posteriorly to continue dorsally as two longitudinal median head muscles. At the distal extremities, the front margin muscles are more ventral and supply the frontal ciliated zone. The five pairs of anterior dorso-ventral muscles also supply the frontal ciliated area. The anterior dorso-ventral muscles extend dorsally and quite close to the frontal margin muscle, thus appearing to be in contact with it. In front of the pharynx, dorsally, a cross like complex of small muscles consists of the front margin muscles continuing as a longitudinal median head muscle and trifurcates as two lateral small bundles and one median bundle. The bundles of the front margin muscles of each side join the midline with other contralateral front margin muscle (fmm: Figures 3C; 4).

Ventro-anteriorly, in front of the mouth opening the continuity of the lateral ventral muscle and the paramedian ventral muscle form a thin muscle network (mn: Figure 2A; 3A,C; 4), probably implicated in some anterior glands or changes of the shape of the head.

#### Pharynx musculature

The pharynx musculature includes the major ventral pharyngeal muscle and several paired and unpaired muscles articulating the jaws. Jaw muscles have a non-epidermal origin, with each muscle being connected to an epidermal cell associated to a sclerite (Figure 1D). Thus, the musculature of the jaws is probably of

mesodermal origin. The function of the musculature is interpreted according to previous studies on feeding behaviour and live observations.

Ventral of the trophi, lining the fibularium, several longitudinal fibres form a large ventral pharyngeal muscle plate (vpm, Figures 2A; 3A; 5C,D; 6A-C) and continues anteriorly as two small lateral muscle fibres. This ventral pharyngeal muscle plate is formed by 8-10 longitudinal cross striated muscle fibres (Figures 1B; 5C, D; 6A,C). The longest median muscle filament presents 8 z-bands (Figure 6A-C). However, even though the ventral pharyngeal muscle plate mostly underlies the fibularium, the ventral pharyngeal muscle is shifted more posteriorly compared to the fibularium. The plate is rounded at the lateral and posterior edges, hereby enveloping the trophi (including the fibularium) laterally and caudally (vpm: Figure 5C,D).

Dorsal to the fibularium, two pairs of muscles extend between the fibularium and the main jaws: one pair of lateral fibularium/main jaw muscles (lfm: Figures 5C; 6D-F), and one pair of median fibularium/main jaw muscles (mfm: Figures 5C; 6D-F). Both of them attach to the fibula caudalis of the fibularium. The lateral fibularium/main jaw muscle originates at the fibula caudalis (of the camera dorsalis 1), and supplies the anterior part of the main jaws. The median fibularium/main jaw muscle originates posterior of the fibula caudalis (of the camera dorsalis 1 and 2), and supplies a less anterior part of the main jaws than the lateral fibularium/main jaw muscle.

One pair of strong caudal muscles lines each cauda of the main jaws (cm: Figures 5D; 6D-F). They are thicker in their posterior parts where they follow the paired caudae of the main jaw. The contraction of this muscle moves the main jaws together.

Two short anterior fibularium/main jaw muscles (afm: Figure 6G-I) attach to the anterior part of the fibula lateralis at the camera lateralis, and link in this way the fibularium with the anterior parts of the main jaws.

Altogether, the anterior fibularium main jaw muscle, the lateral fibularium main jaw muscles, the median fibularium/main jaw muscles and the caudal muscle, are probably responsible for the opening of the main jaws and their previously described backward/forward movements (Kristensen and Funch [3]).

An unpaired very thin striated U-shaped dorsal jaw muscle (djm: Figure 6G-I) attaches at each extremity to the posterior ends of each dorsal jaw.

Lateral to the fibularium, one pair of strong cross striated ventral jaw muscles (vjm: Figures 5C,D; 6G-I) inserts at the posterior part of the accessory sclerite. They extend posterior of the trophi, attaching the sides of the fibularium and inserting posteriorly at the pharynx epithelium.

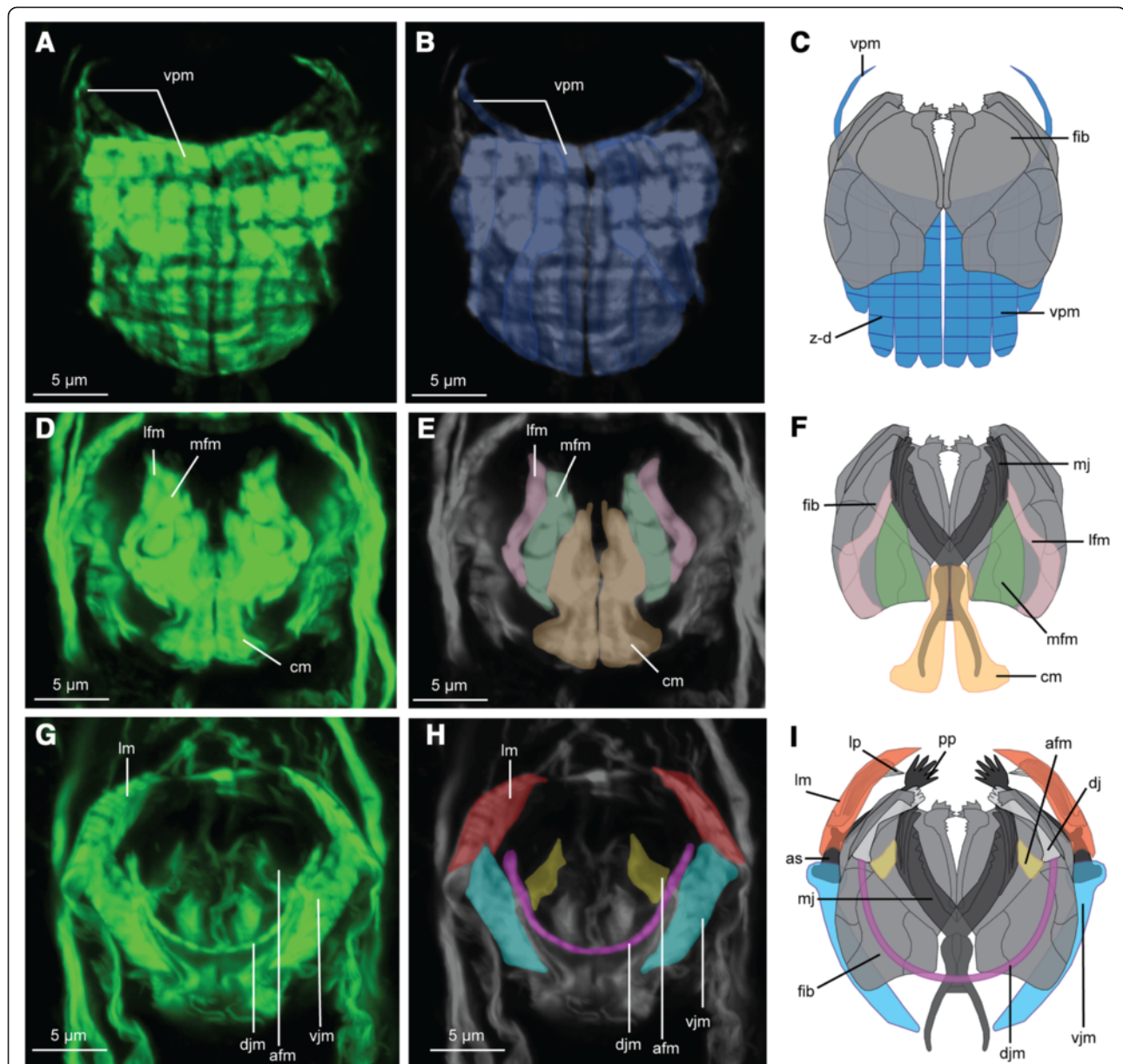


**Figure 6** Musculature and reconstruction of the jaw apparatus of *Limnognathia maerski* in dorsal view. Anterior is on the top for all the pictures. **A, B, C:** ventral part of the jaw system. **D, E, F:** median part of the jaw system. **G, H, I:** dorsal part of the jaw system. **A, D, G:** CLSM of phalloidin stained muscle system, dorsal view of a projection of a sub sample of the Z-stack. **B, E, H:** enlightenment of the different muscle systems of the jaws. **C, F, I:** schematic drawing of the dorsal view of the myoanatomy of the jaw system linked to the cuticular elements in greys. Jaw drawing after Sørensen [6]. as: accessory sclerite; afm: anterior fibularium-main jaw muscle; cm: caudal muscle; dj: dorsal jaws; djm: dorsal jaw muscle; fib: fibularium; lm: pharyngeal lamella muscle; lp: pharyngeal lamella; pp: pseudo-phalangium; vjm: ventral jaw muscle; vpm: ventral pharyngeal muscles; z-b: Z-bands of the cross striated muscles of the ventral pharyngeal muscle.

Anterior to the other parts of the trophi, two strong pharyngeal lamellae muscles (lm: Figures 5C,D; 6G-I) supply the accessory sclerites and the pharyngeal lamellae. The two pharyngeal lamellae muscles are very large and in the continuity of the paramedian ventral muscle and anterior lateral muscle. They enlarge dorso-ventrally at the terminal part. This observation confirms the supposed

function of the pharyngeal lamellae (initially lamella oralis) as a supporting structure. This dorso-ventrally enlarged muscle could function in opening and closing the pharyngeal lamellae as a fan, affecting the volume of the pharynx. The ventral jaw muscle is probably functioning together with the pharyngeal lamellae muscle as an antagonist. Indeed, both muscles are connected to the accessory

sclerite. When the pharyngeal lamellae muscles are contracted and the ventral jaw muscles relaxed, the pharyngeal lamellae will open and increase the volume of the pharynx cavity, also probably opening the mouth and allowing ventral jaws extrusion.

#### Anti-Synapsin1 immunoreactivity

Anti-Synapsin 1 immunoreactivity (IR) was tested in ongoing studies of the nervous system (Bekkouche et al. unpublished) and surprisingly yielded a very distinct IR at the borders of the dorsal epidermis cells. This immunoreactivity, which is presented as spots along the borders, resembles the distribution pattern of the unique zip-junctions in *Limnognathia* (equivalents of adherens junctions) (Figure 2C). However this IR interpretation warrants further confirmation. Most importantly, the very distinct cell border signal has been proved useful in the present study for co-localizing the attachment sites of the dorso-ventral muscles. Thereafter it was possible, even in specimens not stained against Synapsin1, to retrieve the borders of the dorsal cells of the epidermis by increasing the brightness of the phalloidin stain (data not shown). The attachment of the last eight trunk dorso-ventral muscles to the dorsal epidermal cells could then be inferred in several specimens (Figure 4B). Furthermore, the synapsin 1 staining clearly shows that *Limnognathia maerski* has cell borders in the epidermis (as opposed to being syncytial) and therefore does not belong to Syndermata (Rotifera and Acanthocephala).

## Discussion

### Notes on the longitudinal musculature

In *L. maerski* most of the longitudinal musculature extends the entire body length, or at least the entire trunk, yet some muscles are restricted to certain areas, e.g., the adhesive ciliated pad (cpm: Figures 2A; 3A,C; 4A), the thorax (ldm: Figures 3A,C; 4B), the anterior part of the thorax (sav1,2: Figures 2A; 3A,C; 4A), etc. This repartition of the musculature supports functionally the separation of *L. maerski* into a head, a thorax and an abdomen. Similarly, in rotifers, many longitudinal muscles extend a subpart of the body, aiding the retraction of the foot or the corona [11,12]. Contrarily, most of the longitudinal muscles of Gnathostomulida extend the entire body length [9,10].

### Is the dorso-ventral musculature of *L. maerski* comparable to circular musculature?

The trunk dorso-ventral musculature of *L. maerski* (tdvm: Figures 2A,B; 3A,B,C; 4; 5A,B) superficially resembles the repeated incomplete circular muscles found in many rotifers. However, as described by Leasi and Ricci [12]: “the muscular system of rotifers generally consists of somatic and splanchnic (visceral) fibers.

Somatic musculature is composed of two layers: an external layer made of separate circular rings and an internal layer of longitudinal muscles”. *Limnognathia maerski* lacks splanchnic fibers and the somatic musculature is only composed of longitudinal muscles. However, internal of these are found the dorso-ventral muscles. These are serially repeated along the lateral outline of the gut (tdvm: Figure 5A,B). The median position of the trunk dorso-ventral muscles, relative to the two pairs of lateral and paramedian ventral longitudinal muscles, does not conform to the somatic circular muscles found in rotifers, and homology of these muscles is unlikely. However, they can be functionally compared to those of rotifers: with lack of both outer and inner circular musculature, these dorso-ventral muscles may act both as a splanchnic musculature, aiding the movement of the food throughout the digestive system, as well as somatic dorso-ventral musculature, elongating the body during contraction. In rotifers, the incomplete circular muscles act as antagonists of the longitudinal musculature. When these somatic circular muscles contract, the pressure of the body fluids is redistributed and prompts the extension of the body [12]. The same function is assumed in *L. maerski* for the trunk dorso-ventral muscles. It is interesting to note the medio-ventral longitudinal muscles as they seem to extend at the same level as the ventralmost part of the trunk dorso-ventral muscles (tdvm and mvm: Figures 2A; 3A; 4; 5A,B). This suggests that the medio-ventral longitudinal muscles may specifically work as antagonists of the trunk dorso-ventral muscles in the same way as for rotifers.

Giribet et al. [5] propose, among other hypotheses, a relationship between Micrognathozoa and Cyclophora. In Cyclophora, inner dorso-ventral muscles are also present in the Pandora larva and the dwarf male life stages [33-35]. In the dwarf male, several sets of dorso-ventral muscles are present along the entire body length, while in the Pandora larva, only three pairs of dorso-ventral anterior muscles are present in addition to the incomplete circular muscles repeated through the entire body length. It is, though, difficult to establish any functional comparison with *L. maerski* since there is no gut present in these two cyclophoran stages.

Similar to *L. maerski*, dorso-ventral muscles are found internal of the longitudinal muscles in kinorhynchs [36]. Moreover, in the gastrotrich *Draculiciteria*, two sets of dorso-ventral muscles are found: one inside and one outside the longitudinal musculature, each supposed to be derived from splanchnic and somatic circular muscles, respectively [37]. The organization found in kinorhynchs can be compared to the attachment of the trunk dorso-ventral muscles to the epidermal cells containing the dorsal plates in *L. maerski*, even though the two conditions obviously are analogous. Additionally, in both

**Table 1 Previously proposed homologies of *Limnognathia maerski* jaw parts and Rotifera jaw parts**

Jaw elements in <i>Limnognathia maerski</i>	Proposed homologies with rotifer trophi according to the authors		
	Kristensen and Funch [3]	De Smet [1]	Sørensen [6]
Basal plates		Basal platelet (epipharynx)	Autapomorphy
Fibularium	Ramus	Manubrium + uncus	Autapomorphy
Ventral jaws	Uncus	Pseudomalleus (epipharynx)	Uncus
Accessory sclerites	Manubrium	Pseudomanubrium (epipharynx)	Manubrium
Main jaws dentarium	Ramus	Ramus	Ramus
Main jaws articularium	Fulcrum	Fulcrum	Fulcrum
Lamellae pharyngea	Epipharynx	Oral lamellae (epipharynx)	Epipharynx
Dorsal jaws	Autapomorphy	Pleural rod	Autapomorphy

kinorhynchs and *Draculiciteria*, as well as in rotifers, the contraction of the dorso-ventral musculature is supposed to be involved in the body extension [36,37].

This comparison between small sized pseudocoelomate or acoelomate animals, leads to the supposition that dorso-ventral muscles play a similar role as circular muscles, aiding the fluid circulation in the body and in *L. maerski*, possibly also changing the shape of the relatively large cells of the endodermis. Thus, the dorso-ventral muscle contractions possibly aid the movement of food particles in the gut, the vomit behavior, and the yet non-observed defecation.

#### Functional considerations of the pharynx musculature Considerations on the jaw musculature of *L. maerski*

Six paired main elements are described in the jaws of *L. maerski*: i) The median basal plates ii) the large ventral fibularia, extending dorso-laterally, iii) the lateral-most ventral jaws, iv) the medio-dorsal main jaws, with posteriorly projecting caudae, v) the dorso-lateral dorsal jaws confined to the fibularium area, vi) and the antero-lateral pharyngeal lamellae [6]. For comparison we refer to the Table 1 that summarizes the various jaw homology hypotheses proposed in the literature between the Rotifera and *L. maerski*. A general consensus appears to exist for the homologies between the articularium and cauda of Gnathostomulida, the ramus and fulcrum of Rotifera and the main jaws and caudae of *L. maerski* [1,3,6,38].

No separate musculature associated to the basal plate in *L. maerski* has been found. Moreover, detailed examination of the ventral view of the SEM images of the jaws of *L. maerski* does not show any clear separation between the basal plates and the fibularium [1,6], suggesting that the basal plate could be an integrated part of the fibularium.

The dorsal jaw muscle apparently only connects the two dorsal jaws and is not attached to the pharyngeal wall. In Sørensen [6], the dorsal jaws are described as caudally attached to the internal side of the fibularia, possibly by a flexible ligament on each side, positioning

the jaws in a 90° angle to the main jaws. A contraction of the dorsal jaw muscles would then pull apart the tips of the dorsal jaws, turning the jaws about 45° from their resting position.

The fibularium, as the most conspicuous jaw structure, is involved in the attachment of three out of eight jaw muscles systems, suggesting that the fibularium acts primarily as a supporting structure for the jaws and the pharynx, rather than an element directly implicated in the mastication. This assumption is consistent with the strong ventral pharyngeal muscle underlying the fibularium.

#### Comparison of the pharyngeal musculature of *L. maerski* with those of other animals

The ventral jaws and accessory sclerites of *L. maerski* make up as a functional unit that has been considered homologous with either the rotifer mallei [3,6] or the rotifer epipharynx [1] (see also Table 1). The ventral jaws can be moved independently and extruded through the mouth opening during foraging while the rest of the jaws are not. In rotifers, the different sclerites are more closely connected through ligaments, and the mallei cannot be fully protruded without also protruding parts of the incus as well (e.g., in *Bryceella stylata* [31] and *Dicranophorus forcipatus* [39]). In *L. maerski* no ligamentous connections exist between the ventral jaws and either the fibularium or main jaws, which allow the ventral jaws to move more independently from the other main elements of the jaw apparatus.

The ventral jaw muscle of *L. maerski* (vjm: Figure 5C, D; 6G-I) can be compared to the musculus circumglandulis of Rotifera. This muscle connects the rami with other parts of the mallei [31,39,40]. Its ventral position, connection with the ramus and conspicuous shape, resembles the ventral pharyngeal muscle (conspicuous muscle made of several bundle) or the ventral jaw muscle (connection and position) in *L. maerski*. However, in rotifers this muscle is assumed to perform the spreading of the rami and eventually also the

compression of the salivary glands [31], and such functions are not likely for the ventral jaw muscles in *L. maerski*. Hence, no equivalent of the ventral jaw muscle of *L. maerski* is found in Rotifera.

Underlying the fibularium, the conspicuous plate of the ventral pharyngeal muscle is present (vpm, Figures 2A; 3A; 5C,D; 6A-C). Composed of several longitudinal parallel muscles fibers, this structure is found neither in gnathostomulids nor rotifers. In Gnathostomulida though, a pharyngeal capsule is found, but it is formed by circular muscles enveloping the pharynx [27], which is structurally different from *L. maerski*. However, a strikingly similar ventral set of longitudinal muscles, encompassing two fanlike muscles forming a similar bowl, is found in the microscopic worm *Diurodrilus* (*Spiralia incertae sedis*) [30]. In *Diurodrilus*, this pharyngeal bowl also lines the pharynx ventrally, whereas its posterior part extends further dorsally compared to what is apparent in *L. maerski*. In *L. maerski*, the configuration of the muscle plate indicates that it is implicated in the extrusion and sinking movements of the fibularium and possibly causes changes in the volume of the pharyngeal cavity.

Functionally, this muscle could also be similar to the mastax receptor retractor found in the rotifer *Pleurotrocha petromyzon* as well as other rotifers with virgate mastax [40], aiding the total movement of the mastax by changing the shape of the pharynx cavity. However, the rotifer mastax receptor retractors are located dorsal to the jaw, which makes an actual homology with the micrognathozoan ventral pharyngeal muscle unlikely. We assume a similar function of the ventral pharyngeal muscle in *L. maerski*, which when contracting seems to move the entire jaws system, during the so-called vomit behavior. Morphologically, the similarity of the plate-bowl-shaped ventral pharyngeal muscle of *L. maerski* and *Diurodrilus* is striking [30] and not found in Rotifera and Gnathostomulida.

The main jaws represent the central element of the micrognathozoan jaw apparatus, and there is a consensus about homologizing the main jaws with the rotifer incus [1,3,6] (see also Table 1). Two different sets of main jaw muscles connect the main jaws with other sclerites or with the pharyngeal wall. The first set, related to the fibularium, is a “lateral connection” created by the anterior fibularium main jaw muscle, the lateral fibularium main jaw muscle and the median fibularium main jaw muscle. The second one, independent of the fibularium, is a “posterior connection” created by the caudal muscle. In *L. maerski*, the “lateral connection” is the most prominent in the main jaws and it is operated by 3 sets of muscles (anterior fibularium main jaw muscle, lateral fibularium main jaw muscle, median fibularium main jaw muscle, respectively afm, lfm, mfm:

Figure 6D-I). In Gnathostomulida, the lateral connection is also dominant, realized by the diductor muscles [9,26] which do not connect to a lateral sclerite but to the dorsal wall of the pharynx. In *L. maerski*, the fibularium has the function of attaching the muscles involved in the lateral connection. Among rotifers, sparse examples of lateral connections can be found. The only muscle having this arrangement is the musculus ramo-manubricus found in *Filinia longiseta* [41] and *Trichocerca rattus* [33], both having very peculiar trophi (respectively malleoramate and asymmetrical virgate). In Rotifera, though, the posterior connection is well documented in the abundant work of the series of confocal and TEM studies by the Ahlrichs Group [31,32,39-41], who refers to this muscle as the musculus fulcro ramicus. Furthermore, Riemann and Ahlrichs, emphasize the wide repartition of this muscle within Rotifera, suggesting the homology of this muscle across the taxon [39]. Then, the cauda muscle of *L. maerski* (cm: Figure 6D-F) could also be homologous to the musculus fulcro ramicus of Rotifera. A difference between those two muscles is that the cauda muscle seems to embed, or at least extend closely the cauda, while the musculus fulcro ramicus is more diagonal in its orientation. Additionally, the cauda muscle goes more posterior and seems to insert in the pharyngeal wall, while the musculus fulcro-ramicus is posteriorly restricted to the fulcrum.

Only muscles functionally implicated in the opening of the main jaws (not in the closing) have been found in *L. maerski*. As proposed for Rotifera and Gnathostomulida, we assume that the kinetic energy release of the cuticular parts provokes a passive closing of the pincer like sclerites in *L. maerski* [26,27,39].

## Conclusions

Due to its simplicity, the longitudinal musculature of *L. maerski* is only roughly comparable to the musculature of other groups. However, the dorso-ventral musculature shows a functional similarity to the semi-circular muscles of the closely related Rotifera and other meiofaunal animals.

With regards to the pharyngeal musculature, only one specific homology between the cauda muscle of *L. maerski* and the musculus fulcro ramicus of rotifers can be hypothesized. However, the functional and morphological comparisons of the jaw musculature among gnathiferans aid the understanding of how such small complex systems can be moved. Two different “strategies” can be observed in the jaw apparatus of Rotifera versus Gnathostomulida: in rotifers, sclerites are moved by muscles connected to other jaw parts whereas in gnathostomulids the less complex jaws are moved by muscles connected directly to the pharyngeal wall. It is not surprising considering the complexity of the jaws of

*L. maerski* that the jaw musculature and function are more comparable to that of Rotifera. However, the independence of the ventral jaw of *L. maerski* relative to the rest of the trophi is an interesting difference between *L. maerski* and Rotifera. Additionally, the striking similarity between the ventral pharyngeal muscle of Micrognathozoa and the pharyngeal bowl-shaped muscle of *Diurodrilus* is interesting in relation to the debated close relationship between the jaw-less *Diurodrilus* and Micrognathozoa [3,30].

Several functional analogies and common patterns could be shown between *L. maerski* and other Gnathifera or small sized animals, but the systematic value of the musculature of *L. maerski* still appears quite limited. However, further studies are needed in Gnathifera. De Smet [1] emphasizes the poor knowledge of the epipharynx of Rotifera. For example, Riemann and Ahlrichs [39], in their study on *Dicranophorus forcipatus* cannot assign any clear function to the hypopharyngeal elements. Furthermore, no complete detailed studies of the musculature and function of trophi of the Seisonidae, Bdelloidea (both Rotifera) and Filospermoidea (Gnathostomulida) have been done so far. Nevertheless, a systematic comparison will still be challenging since the trophi of Bdelloidea and Seisonidea are very modified, and the jaws of Filospermoidea have a relatively simple pincer-like structure, such as in *Haplognathia*.

## Material and methods

### Collection of specimens

Specimens used for TEM were part of the original material that were collected at the type locality in the Isunngua Spring on Disko Island, West Greenland, 69°43'N 51° 56'W, and used for the description of Micrognathozoa [3]. Specimens for CLSM were collected in July-August 2010 and 2013 at the same locality.

### Transmission electron microscopy

Specimens were fixed in trialdehyde 8% (after Kalt and Tandler [42] and Lake, [43], without acrolein) and postfixed in 1% osmium-tetroxide with 0.1M sodium cacodylate buffer for 1 hour (h) at 20°C. Specimens were then dehydrated through an ethanol series, transferred to propylene oxide, and embedded in epoxy resin type TAAB 812°. Ultrathin serial sections were stained with uranyl acetate and lead citrate [44]. TEM examinations were performed with a JEOL JEM 100SX transmission electron microscope.

### Cytochemistry and CLSM

Specimens of *L. maerski* were fixed for 2 h at room temperature (or overnight at 4°C) in 2% paraformaldehyde in 0.15M phosphate buffered saline (PBS), pH 7.4, rinsed and stored in PBS plus 0.05% NaN<sub>3</sub>. Entire specimens were preincubated two hours in PTA (PBS with 0.5% Triton-X, 0.05% NaN<sub>3</sub>, 0.25% bovine serum

albumin (BSA) and 5% sucrose) and afterwards incubated for 2h at room temperature in 0.34 μM Alexa fluor 488 phalloidin (Invitrogen, A12379) in PTA and finally mounted in Vectashield® (Vector Laboratories, Burlingame, CA) containing DAPI. For immunostaining against synapsin1, specimens were preincubated two hours in PTA and incubated for 12h at room temperature with antibodies anti synapsin1 raised in Rabbit (ENZO life Sciences, ADI-VAS-SV061-E). Then the specimens were rinsed in PBS, pre-incubated 2h in PTA and incubated 12h at room temperature with the secondary antibody anti-rabbit, conjugated with the fluorophore FITC (SIGMA, prod. num. f0382). Finally the specimens were rinsed in PBS and mounted in Vectashield®. Preparations were analyzed with an Olympus Fluoview FV1000 CLSM or a Leica TCS SP5 CLSM. The specificity of the antibodies was tested by examining specimens where each of the primary and secondary antibodies were omitted.

### Image treatment

Z-stacks or parts of them of CLSM files were projected into 2D-images (MIP images = maximum intensity pixel images) and 3D iso-surface reconstructed in Imaris v7 (Bitplane AG, Zürich, Switzerland). Depth coded Z-stack images of F-actin staining are also presented (Leica imaging software), where the depth-gradient follows the area of the spectral light with the uppermost structures appearing red, and the more distant one blue. Free hand drawings and plate setups were done with Adobe Illustrator CS6 and Image modification done with Adobe Photoshop CS6.

### Competing interests

The authors declare that they have no competing interests.

### Authors' contributions

AH, KW, MVS, NB, RMK collected the animals. RMK made the transmission electron micrographs. AH, KW, NB stained the specimens for phalloidin and scanned specimens for CLSM. KW, MVS, NB, RMK, coordinated and participated in the analysis. KW and NB conceptualized, drafted the manuscript and designed the study. RMK, MVS, AH revised the manuscript. All authors read and approved the final manuscript.

### Acknowledgements

The Arctic Station of Qeqertarsuaq, University of Copenhagen provided an excellent working platform with cooling container and we are greatly indebted to the crew of the station as well as R/V Porsild. The fieldwork on Greenland was supported by the Carlsberg Foundation (Grant no. 2009\_01\_0053), (Grant no. 2012\_01\_0123), (Grant no. 2010\_01\_0802) and the Villum foundation (Grant no. 102544). The lab cost and the salary of the first author was supported by the Carlsberg foundation (Grant no. 2010\_01\_0802) and the Villum foundation (Grant no. 102544). We especially thank Prof. Rick Hochberg for his constructive critical reading and detailed comments on the manuscript.

### Author details

<sup>1</sup>Marine Biological Section, Department of Biology, University of Copenhagen, Universitetsparken 4, 2100 Copenhagen Ø, Denmark. <sup>2</sup>Natural History Museum of Denmark, Universitetsparken 15, 2100 Copenhagen Ø, Denmark. <sup>3</sup>Sars International Centre for Marine Molecular Biology, University of Bergen, Thormøhlensgate 55, Bergen N-5008, Norway. <sup>4</sup>Natural History Museum of Denmark, Øster Voldgade 5-7, 1350 Copenhagen K, Denmark.

Received: 25 June 2014 Accepted: 22 September 2014  
Published online: 01 October 2014

## References

1. De Smet WH: A new record of *Limnognathia maerski* Kristensen & Funch, 2000 (Micrognathozoa) from the subantarctic Crozet Islands, with redescription of the trophi. *J Zool* 2002, **258**:381–393.
2. Kristensen RM: An introduction to Loricifera, Cyclophora, and Micrognathozoa. *Integr Comp Biol* 2002, **42**:641–651.
3. Kristensen RM, Funch P: Micrognathozoa: a new class with complicated jaws like those of Rotifera and Gnathostomulida. *J Zool* 2000, **246**:1–49.
4. Funch P, Kristensen RM: Coda: The Micrognathozoa—a new class or phylum of freshwater meiofauna? In *Freshwater meiofauna: Biology and ecology*. Edited by Rundle SD, Robertson AL, Schmid-Araya JM. Leiden, The Netherlands: Backhuys Publishers; 2002.
5. Giribet G, Sørensen MV, Funch P, Kristensen RM, Sterrer W: Investigations into the phylogenetic position of Micrognathozoa using four molecular loci. *Cladistics* 2004, **20**:1–3.
6. Sørensen MV: Further structures in the jaw apparatus of *Limnognathia maerski* (Micrognathozoa), with notes on the phylogeny of the gnathifera. *J Morphol* 2003, **255**:131–145.
7. Sørensen MV, Kristensen RM: Micrognathozoa. In *Handbook of Zoology, Gastrotricha, Cycloneuralia and Gnathifera*. Edited by Schmidt-Rhaesa A. Berlin, Boston: Walter De Gruyter GmbH; 2014. In press.
8. Lammert V: Gnathostomulida. In *Microscopic Anatomy of Invertebrates, Volume 4 Aschelminthes*. Edited by Harrison FW, Ruppert EE. New York, Chichester, Brisbane, Toronto, Singapore: John Wiley & Sons edition; 1991.
9. Müller MCM, Sterrer W: Musculature and nervous system of *Gnathostomula peregrina* (Gnathostomulida) shown by phalloidin labeling, immunohistochemistry, and cLSM, and their phylogenetic significance. *Zoomorphology* 2004, **123**:169–177.
10. Tyler S, Hooge MD: Musculature of *Gnathostomula armata* Riedl 1971 and its ecological significance. *Mar Ecol-P S Z N I* 2001, **22**:71–83.
11. Leasi F, Neves RC, Worsaae K, Sørensen MV: Musculature of *Seison nebaliae* Grube, 1861 and *Paraseison annulatus* (Claus, 1876) revealed with CLSM: a comparative study of the gnathiferan key taxon Seisonacea (Rotifera). *Zoomorphology* 2012, **131**:185–195.
12. Leasi F, Ricci C: Musculature of two bdelloid rotifers, *Adineta ricciae* and *Macrotrachela quadricornifera*: organization in a functional and evolutionary perspective. *J Zoo Syst Evol Res* 2010, **48**:33–39.
13. Sørensen MV: Musculature in three species of Proales (Monogononta, Rotifera) stained with phalloidin-labeled fluorescent dye. *Zoomorphology* 2005, **124**:47–55.
14. Hochberg R, Litvaitis MK: Functional morphology of the muscles in *Philodina* sp. (Rotifera : Bdelloidea). *Hydrobiologia* 2000, **432**:57–64.
15. Wilts EF, Ahlrichs WH, Arbizu PM: The somatic musculature of *Bryceella stylata* (Milne, 1886) (Rotifera: Proalidae) as revealed by confocal laser scanning microscopy with additional new data on its trophi and overall morphology. *Zool Anz* 2009, **248**:161–175.
16. Hochberg R, Lilley G: Neuromuscular organization of the freshwater colonial rotifer, *Sinantherina socialis*, and its implications for understanding the evolution of coloniality in Rotifera. *Zoomorphology* 2010, **129**:153–162.
17. Santo N, Fontaneto D, Fascio U, Melone G, Caprioli M: External morphology and muscle arrangement of *Brachionus urceolaris*, *Floscularia ringens*, *Hexarthra mira* and *Notommata glyphura* (Rotifera, Monogononta). *Hydrobiologia* 2005, **546**:223–229.
18. Riemann O, Wilts EF, Ahlrichs WH, Kieneke A: Body musculature of *Beauchampiella eudactyloa* (Gosse, 1886) (Rotifera: Euchlanidae) with additional new data on its trophi and overall morphology. *Acta Zool-Stockholm* 2009, **90**:265–274.
19. Kotikova EA, Raikova OI, Flyatchinskaya LP, Reuter M, Gustafsson MKS: Rotifer muscles as revealed by phalloidin-TRITC staining and confocal scanning laser microscopy. *Acta Zool-Stockholm* 2001, **82**:1–9.
20. Sørensen MV: An SEM study of the jaws of *Haplognathia rosea* and *Rastrognaithia macrotoma* (Gnathostomulida), with a preliminary comparison with the rotiferan trophi. *Acta Zool-Stockholm* 2000, **81**:9–16.
21. Sørensen MV, Sterrer W: New characters in the gnathostomulid mouth parts revealed by scanning electron microscopy. *J Morphol* 2002, **253**:310–334.
22. Sterrer W: Systematics and Evolution within Gnathostomulida. *Syst Zool* 1972, **21**:151–173.
23. Clément P, Wurdak E: Rotifera. In *Microscopic Anatomy of Invertebrates, Volume 4, Aschelminthes*. Edited by Harrison FW, Ruppert EE. New York, Chichester, Brisbane, Toronto, Singapore: John Wiley & Sons edition; 1991.
24. Sørensen MV: On the evolution and morphology of the rotiferan trophi, with a cladistic analysis of Rotifera. *J Zoo Syst Evol Res* 2002, **40**:129–154.
25. Wallace RL, Snell TL, Nogrady T: Rotifera: Volume 1. Biology, Ecology and Systematics. In *Guides to the Identification of Microinvertebrates of the Continental Waters of the World*. Edited by Dumont HJ. Leiden: Kenobi Productions, Ghent and Backhuys Publishing; 2006.
26. Sørensen MV, Tyler S, Hooge MD, Funch P: Organization of pharyngeal hard parts and musculature in *Gnathostomula armata* (Gnathostomulida: Gnathostomulidae). *Can J Zool* 2003, **81**:1463–1470.
27. Herlyn H, Ehlers U: Ultrastructure and function of the pharynx of *Gnathostomula paradoxa* (Gnathostomulida). *Zoomorphology* 1997, **117**:135–145.
28. Leasi F, Todaro MA: The muscular system of *Musellifer delamarei* (Renaud-Mornant, 1968) and other chaetonotids with implications for the phylogeny and systematization of the Paucitubulatina (Gastrotricha). *Biol J Linn Soc* 2008, **94**:379–398.
29. Neves RC, Bailly X, Leasi F, Reichert H, Sørensen MV, Kristensen RM: A complete three-dimensional reconstruction of the myoanatomy of Loricifera: comparative morphology of an adult and a Higgins larva stage. *Front Zool* 2013, **10**:19.
30. Worsaae K, Rouse GW: Is *Diurodrilus* an Annelid? *J Morphol* 2008, **269**:1426–1455.
31. Wilts EF, Wulfken D, Ahlrichs WH: Combining confocal laser scanning and transmission electron microscopy for revealing the mastax musculature in *Bryceella stylata* (Milne, 1886) (Rotifera: Monogononta). *Zool Anz* 2010, **248**:285–298.
32. Wilts EF, Wulfken D, Ahlrichs WH, Arbizu PM: The musculature of *Squatinella rostrum* (Milne, 1886) (Rotifera: Lepadellidae) as revealed by confocal laser scanning microscopy with additional new data on its trophi and overall morphology. *Acta Zool-Stockholm* 2012, **93**:14–27.
33. Clément P: Movements in rotifers: correlations of ultrastructure and behavior. *Hydrobiologia* 1987, **147**:339–359.
34. Neves RC, Cunha MR, Funch P, Kristensen RM, Wanninger A: Comparative myoanatomy of cyclophoran life cycle stages. *J Morphol* 2010, **271**:596–611.
35. Neves RC, Kristensen RM, Wanninger A: Three-dimensional reconstruction of the musculature of various life cycle stages of the cyclophoran *Symbion americanus*. *J Morphol* 2009, **271**:257–270.
36. Neuhaus B, Higgins RP: Ultrastructure, biology, and phylogenetic relationships of Kinorhyncha. *Integr Comp Biol* 2002, **42**:619–632.
37. Hochberg R, Litvaitis MK: The musculature of *Draculiciteria tessalata* (Chaetonotida, Paucitubulatina): implications for the evolution of dorsoventral muscles in Gastrotricha. *Hydrobiologia* 2001, **452**:155–161.
38. Sørensen MV: Phylogeny and jaw evolution in Gnathostomulida, with a cladistic analysis of the genera. *Zool Scr* 2002, **31**:461–480.
39. Riemann O, Ahlrichs WH: Ultrastructure and function of the mastax in *Dicranophorus forcipatus* (Rotifera : Monogononta). *J Morphol* 2008, **269**:698–712.
40. Wulfken D, Wilts EF, Martinez-Arbizu P, Ahlrichs WH: Comparative analysis of the mastax musculature of the rotifer species *Pleurotrocha petromyzon* (Notommatidae) and *Proales tillyensis* (Proalidae) with notes on the virgate mastax type. *Zool Anz* 2010, **249**:181–194.
41. Wulfken D, Ahlrichs WH: The ultrastructure of the mastax of *Filinia longiseta* (Flosculariaceae, Rotifera): Informational value of the trophi structure and mastax musculature. *Zool Anz* 2012, **251**:270–278.
42. Kalt MR, Tandler B: Study of Fixation of Early Amphibian Embryos for Electron Microscopy. *J Ultra Mol Struct R* 1971, **36**:633–645.
43. Lake PS: Trialdehyde fixation of crustacean tissue for electron microscopy. *Crustaceana* 1973, **24**:244–246.
44. Reynolds ES: The use of lead citrate at high pH as an electron-opaque stain in electron microscopy. *J Cell Biol* 1963, **17**:208–212.

doi:10.1186/s12983-014-0071-z

Cite this article as: Bekkouche et al.: Detailed reconstruction of the musculature in *Limnognathia maerski* (Micrognathozoa) and comparison with other Gnathifera. *Frontiers in Zoology* 2014 **11**:71.

**Manuscript IV:**

**Nervous system and ciliary structures of Micrognathozoa  
(Gnathifera) – evolutionary insight from an early branch in  
Spiralia**

Bekkouche N., and Worsaae, K.

Submitted to Royal Society Open Science



ROYAL SOCIETY  
OPEN SCIENCE

**Nervous system and ciliary structures of Micrognathozoa  
(Gnathifera) – evolutionary insight from an early branch in  
Spiralia.**

Journal:	<i>Royal Society Open Science</i>
Manuscript ID	Draft
Article Type:	Research
Date Submitted by the Author:	n/a
Complete List of Authors:	Bekkouche, Nicolas; University of Copenhagen, Biology Worsaae, Katrine; University of Copenhagen, Biology;
Subject:	structural biology < BIOLOGY, neuroscience < BIOLOGY, evolution < BIOLOGY
Keywords:	Limnognathia maerski, meiofauna, neuromorphology, retrocerebral organ, acetylated $\alpha$ -tubulin, serotonin
Subject Category:	Biology (whole organism)

SCHOLARONE™  
Manuscripts

1  
2  
3  
4  
5  
6  
7  
8  
9  
10  
11  
12  
13  
14  
15  
16  
17  
18  
19  
20  
21  
22  
23  
24  
25  
26  
27  
28  
29  
30  
31  
32  
33  
34  
35  
36  
37  
38  
39  
40  
41  
42  
43  
44  
45  
46  
47  
48  
49  
50  
51  
52  
53  
54  
55  
56  
57  
58  
59  
60

1 Nervous system and ciliary structures of  
2 Micrognathozoa (Gnathifera) –  
3 evolutionary insight from an early branch  
4 in Spiralia

5 Nicolas Bekkouche, Katrine Worsaae

6 Marine Biological Section, Department of Biology, University of Copenhagen,  
7 Universitetsparken 4, 2100 Copenhagen, Denmark.

8 Corresponding author: kworsaae@bio.ku.dk

9 The manuscript is formatted for submission to Proceedings Royal society Open  
10 Science

## 17 **Abstract**

18 Recent studies show that Gnathifera, comprising Rotifera, Gnathostomulida and Micrognathozoa,  
19 constitute the sister group to the remaining Spiralia (containing, e.g., flatworms, segmented  
20 worms and mollusks). Therefore, a better understanding of Gnathifera is central for unravelling  
21 the evolution of the highly diverse Spiralia. Here we describe the previously unstudied nervous  
22 system and ciliary structures of Micrognathozoa using immunohistochemistry and confocal laser  
23 scanning microscopy. The nervous system is simple with a large brain, paired subesophageal  
24 ganglia, two trunk commissures, two pairs of ventral longitudinal nerves, and peripheral nerves.  
25 The paired ventro-lateral nerve cords are confirmed to be a symplesiomorphy of Gnathifera  
26 (possibly even Spiralia), whereas the paired medio-ventral nerves are not previously reported in  
27 Gnathifera. A pharyngeal ganglion is described for Micrognathozoa; a complex structure with two  
28 apical tufts of ciliary receptors, now shown to be shared by all Gnathifera. The ventral pattern of  
29 external ciliophores is redescribed and nephridia with multiciliated collecting tubes similar to  
30 those of Rotifera are confirmed. A range of new details from a simple nervous system and  
31 complex set of ciliary structures in a microscopic metazoan is hereby unraveled. The many  
32 resemblances with Rotifera corroborate their close relationship and shed more light on the  
33 evolution of Gnathifera.

## 34 **Keywords**

35 *Limnognathia maerski*, meiofauna, neuro-morphology, retrocerebral organ, acetylated  $\alpha$ -tubulin,  
36 serotonin.

## 37 **Introduction**

38 *Limnognathia maerski* Kristensen and Funch, 2000 (Micrognathozoa) [1] is a recently described  
39 species belonging to the bilaterian clade "Gnathifera". Recent phylogenomic studies show that  
40 Gnathifera is likely the sister group of all other Spiralia, and therefore is of crucial importance to  
41 understand animal evolution [2, 3]. However, studies on the different organ systems of Gnathifera  
42 are still warranted. Indeed, this clade is constituted of small, sometimes rare animals, collection of  
43 which is difficult and time-consuming, namely Gnathostomulida, Rotifera (= Syndermata, including  
44 Acanthocephala) and Micrognathozoa. The deep interrelationships between these three lineages

1  
2  
3  
4  
5  
6  
7  
8  
9  
10  
11  
12  
13  
14  
15  
16  
17  
18  
19  
20  
21  
22  
23  
24  
25  
26  
27  
28  
29  
30  
31  
32  
33  
34  
35  
36  
37  
38  
39  
40  
41  
42  
43  
44  
45  
46  
47  
48  
49  
50  
51  
52  
53  
54  
55  
56  
57  
58  
59  
60

45 is now resolved with both phylogenomics [3] and morphology [1, 4, 5] supporting a sister group  
46 relationship between Micrognathozoa and Rotifera, and Gnathostomulida being sister group to  
47 this clade. Although rotifers are relatively well studied in many aspects, most of their internal  
48 morphology still needs further investigation, as is the case for the internal organization in  
49 Gnathostomulida and Micrognathozoa.

50 Several confocal laser scanning microscopy (CLSM) have been conducted on gnathiferans, but  
51 most of them have focused on the musculature, e.g., in rotifers [6-8], one genus of  
52 Gnathostomulida [9, 10] and Micrognathozoa [11]. On the other hand, CLSM studies on the  
53 nervous system of Gnathifera are quite scarce (e.g., for rotifers [12-15] and for gnathostomulids,  
54 [10, 16]), and no studies have yet been carried out on Micrognathozoa. According to previous  
55 studies, the nervous system of Gnathostomulida consists of an anterior brain, a buccal ganglion,  
56 an anterior and a posterior commissure, and a variable number of longitudinal nerves extending  
57 along parts or the entire body length (three paired and two unpaired in *Gnathostomula paradoxa*  
58 Ax, 1956 [10, 17], six pairs in *Rastrognathia macrostoma* Kristensen & Nørrevang, 1977 [18], and  
59 three paired and two unpaired pairs in *Pterognathia meixneri* Sterrer, 1969 [19, 20]. Most studied  
60 rotifers show the presence of a brain, a mastax ganglion, a pair of ventro-lateral nerve cords as  
61 well as various head and peripheral nerves innervating the muscles and the sensory organs.  
62 However extensive studies of the nervous system of rotifers are rare and most recent publications  
63 focused on specific immunoreactivity [e.g. 12-14].

64 Micrognathozoa were first collected from a cold freshwater spring in 1994 in Greenland [1], and  
65 thereafter reported from sub-antarctic islands [21], and the United Kingdom [11]. But specimens  
66 from the United Kingdom are extremely rare, and the sub-antarctic islands as well as Greenland  
67 are remote localities, making the study of fresh material difficult. These ventrally ciliated  
68 meiofaunal animals, measuring up to 150µm in length comprising a head, thorax and abdomen,  
69 have very complex jaws, and only females are known so far. The complexity of the jaws (sclerites)  
70 has attracted most of the attention, and together with the original description, the sclerite  
71 arrangement has been described in details [1, 21, 22], but recently, the musculature of  
72 Micrognathozoa was finally resolved [11].

1  
2  
3  
4 73 The nervous system was superficially addressed in the original description [1], and therein  
5  
6 74 described as comprising a bilobed brain connected to a pair of ventro-lateral nerve cords with two  
7  
8 75 paired ganglia (in the thorax and in the posterior-most part of the abdomen). Furthermore, the  
9  
10 76 presence of a buccal ganglion is suspected but not confirmed [23]. The ventral ciliation was  
11  
12 77 described as consisting of a dense head ciliation, four pairs of head ciliophores, 18 pairs of  
13  
14 78 ciliophores arranged in two midventral longitudinal rows, and a posterior adhesive ciliary pad.  
15  
16 79 Moreover, two pairs of protonephridia were originally described in the thorax [1] with later  
17  
18 80 discussion on the possible opening of their canal cells into a common collecting tubule [23] and  
19  
20 81 the location of the nephridiopore remaining unknown.

21  
22 82 The nervous system and ciliary patterns of *L. maerski* (Micrognathozoa) are here described in  
23  
24 83 detail, using confocal laser scanning microscopy and immunohistochemistry, in order to  
25  
26 84 understand the structure and evolution of these different organ systems within Gnathifera, the  
27  
28 85 earliest branching clade in Spiralia.

## 29 **Material and method**

### 30 31 32 87 **Collection of specimens**

33  
34  
35 88 Mosses were collected at the type locality in the Isunngua Spring on Disko Island, West Greenland,  
36  
37 89 69°43'N 51°56'W 31 July 2013. The mosses were squeezed into a 32µm mesh and the extract  
38  
39 90 thereafter sorted in dissecting scope, picking up the animals alive with a pipette or an Irwin loop.

### 40 41 42 91 **Immunohistochemistry and CLSM**

43  
44  
45 92 Specimens were anesthetized with 1% magnesium chloride solution added drop by drop until no  
46  
47 93 movements were visible and fixed in 3.7% paraformaldehyde in phosphate buffered saline (PBS)  
48  
49 94 for one to two hours at room temperature (RT), followed by six rinses in PBS and storage in PBS  
50  
51 95 with 0.05% NaN<sub>3</sub>. For the investigation of the muscular, nervous, glandular and ciliary system,  
52  
53 96 triple or quadruple staining were applied, including F-actin staining (Alexa Fluor 488-labelled  
54  
55 97 phalloidin, INVITROGEN, Carlsbad, USA), DNA-staining (405nm fluorescent DAPI) and antibodies  
56  
57 98 against neurotransmitters and tubulin (monoclonal mouse anti-acetylated  $\alpha$ -tubulin (SIGMA  
58  
59 99 T6793, St. Louis, USA), polyclonal rabbit anti-serotonin (5-HT, SIGMA S5545) and anti-FMRF-amide  
60

1  
2  
3  
4 100 (IMMUNOSTAR 20091, Hudson, USA)). Prior to adding the primary antibody-mix, the samples  
5  
6 101 were pre-incubated with 1% PTA (PBS + 0.1% Triton-X, 0.05% NaN<sub>3</sub>, 0.25% BSA, and 5% sucrose)  
7  
8 102 for one hour. Samples were incubated over night at RT in primary antibodies (mixed 1:1 with  
9  
10 103 glycerol) in a final 1:400 concentration. Subsequently, specimens were rinsed in PBS six times and  
11  
12 104 incubated with the secondary antibodies conjugated with fluorochromes overnight (mixed 1:1  
13  
14 105 with glycerol) in a final concentration of 1:400; goat anti-mouse labeled with CY5 (JACKSON  
15  
16 106 IMMUNO-RESEARCH, West Grove, USA, 115-175-062), goat anti-mouse labeled with FITC  
17  
18 107 (JACKSON IMMUNO-RESEARCH, West Grove, USA, 115-175-062), and goat anti-rabbit labeled with  
19  
20 108 TRITC (SIGMA T5268) over night at RT. Afterwards they were rinsed in PBS five times and  
21  
22 109 preincubated for 60 minutes in Alexa Fluor 488-labeled phalloidin (0.33M in 1% PBT). Thereafter,  
23  
24 110 specimens were rinsed in PBS (without NaN<sub>3</sub>) and mounted in Fluoromount-G with DAPI  
25  
26 111 (SOUTHERN BIOTECHNOLOGY ASSOCIATES, Inc., Alabama, USA) or Vectashield with DAPI (VECTOR  
27  
28 112 LABORATORIES, Burlingame, USA). The specificity of the antibodies was tested by omitting each of  
29  
30 113 the primary and secondary antibodies.

31  
32 114 The mounted specimens were scanned using an Olympus Fluoview FV-1000 confocal laser  
33  
34 115 scanning microscope (of K. Worsaae, University of Copenhagen, Denmark), with the acquired z-  
35  
36 116 stacks of scans being either projected into 2D-images or analyzed three-dimensionally using  
37  
38 117 IMARIS 7.1 (BITPLANE SCIENTIFIC SOFTWARE, Zürich, Switzerland). This software package was also  
39  
40 118 used to conduct the measurements presented in the following text. Schematic drawings and plate  
41  
42 119 setup were done with Adobe Illustrator CS6 and image adjustments conducted in Adobe  
43  
44 120 Photoshop CS6.

## 45 46 121 **Results**

### 47 122 **Nervous system**

48  
49 123 The nervous system consists of a large brain occupying most of the forehead, with a dorsal  
50  
51 124 neuropil, two pairs of major longitudinal nerves connected by paired subpharyngeal ganglia, an  
52  
53 125 anterior and a posterior commissure, a peripheral nervous system related to the sensory cilia  
54  
55 126 (sensoria), as well as a pharyngeal ganglion (figures 1 and 2).  
56  
57  
58  
59  
60

1  
2  
3  
4 127 The nervous system has been investigated with antibodies directed against acetylated  $\alpha$ -tubulin,  
5  
6 128 serotonin and FMRF-amide. The quality and strength of the signal of the immunoreactivity (IR)  
7  
8 129 varied substantially between the different specimens examined, even among freshly collected  
9  
10 130 materiel, with simultaneously fixed and stained specimens. Moreover, in some specimens, for  
11  
12 131 acetylated  $\alpha$ -tubulin-like immunoreactivity (LIR) and serotonin-LIR, the signal of the ciliation masks  
13  
14 132 the longitudinal nerves. However, although the acetylated  $\alpha$ -tubulin-like-immunoreactive (LI-  
15  
16 133 reactive) signal revealed more or less details in different specimens, it always supports the same  
17  
18 134 pattern. Not all specimens showed clear serotonin-LIR in the nerves, ganglia and brain. In most  
19  
20 135 specimens, FMRF-amide-LIR only shows a clear pattern in the pharyngeal ganglion and the rest of  
21  
22 136 the signal appears to be unspecific signal.

### 23 137 **Longitudinal nerves**

24  
25 138 Two pairs of nerves originate from each ventro-lateral side of the brain neuropil, and the two  
26  
27 139 nerves of each side fuse lateral to the pharynx to form the paired circumesophageal connective  
28  
29 140 (cc, figures 1A,F and 2A,F), extending postero-ventrally to the subpharyngeal ganglia (spg, figures  
30  
31 141 1A,F and 2A described below). The ventro-lateral nerve cords (vlnc, figures 1A-C,F,H and 2A,H)  
32  
33 142 originate from the subpharyngeal ganglia extending throughout the trunk until they connect in the  
34  
35 143 terminal commissure in the posterior abdomen (pc, figures 1A,B,G and 2E). Posterior to the  
36  
37 144 pharynx, the nerves are interconnected by the anterior commissure (ac, figure A1,F) of the paired  
38  
39 145 subpharyngeal ganglia, the ganglia also supplying the ventro-lateral nerve cords, the  
40  
41 146 circumesophageal connective, and the ventro-median nerve (vmn, figures 1A-C,F and 2A,H). The  
42  
43 147 presence of one to two pairs of perikarya supplying the ventro-lateral nerve cords is suspected,  
44  
45 148 but could not be confirmed with certainty. The ventro-lateral nerve cords are 1,5 $\mu$ m thick and  
46  
47 149 extend along most of the body length, surrounding the adhesive ciliary pad area until the posterior  
48  
49 150 commissure at the posterior margin of the adhesive ciliary pad, where no associated ganglia  
50  
51 151 (clusters of perikarya) could be detected with neither DAPI staining nor the applied  
52  
53 152 neurotransmitters. Co-localization with phalloidin staining shows that the ventro-lateral nerve  
54  
55 153 cords lie adjacent to the paired paramedian ventral muscles (pvm and vlnc, figure 2H, and see  
56  
57 154 [11]) and to the lateral margin of the trunk locomotory ciliation. Thus, it is likely that the ventro-  
58  
59 155 lateral nerve cords innervate either one or both of these systems.  
60

1  
2  
3  
4 156 A pair of longitudinal ventro-median nerves (vmn, figures 1A-C,F and 2A,H) extends from the sub-  
5  
6 157 pharyngeal ganglia. They are each about 1 $\mu$ m wide, extend mid-ventrally along the thorax and the  
7  
8 158 anterior part of the abdomen; laterally lining the ventral ciliation, and reaching the anterior edge  
9  
10 159 of the adhesive ciliary pad. Co-localization with phalloidin staining shows that the ventro-median  
11  
12 160 nerve is adjacent to the medio-ventral muscle (mvm and vmn, figure 2H, and see [11]). We  
13  
14 161 therefore assume that the ventro-median nerves possibly innervate the thoracic median  
15  
16 162 ciliophores (tmc, figure 3A,C,E), the abdominal ciliophores (abc, figure 3A,C,E), and the median  
17  
18 163 longitudinal muscle.

19  
20 164 All the nerves described above show acetylated  $\alpha$ -tubulin-LIR. Serotonin-LIR is found in the ventro-  
21  
22 165 lateral nerve cords and the median longitudinal nerves as well as in the perikarya of the brain and  
23  
24 166 pharyngeal ganglion (described below). None of the longitudinal nerves show FMRF-amide-LIR.

### 25 26 167 **Peripheral nerves and sensoria**

27  
28 168 Along the lateral sides of the thorax and the abdomen, several pairs of cells show acetylated  $\alpha$ -  
29  
30 169 tubulin-LIR, each bearing one sensory cilium (=sensorium) (ss, figures 1A,D,E, 2A and 3B). We  
31  
32 170 assume that as for Rotifera [24], each sensorium is a ciliated nerve cell projecting axons towards  
33  
34 171 the central nervous system; the axons and possibly interneurons constituting the peripheral  
35  
36 172 nervous system (pns, figures 1A,D and 2A). Following the nomenclature of Kristensen and Funch  
37  
38 173 [1] the sensoria are present as three pairs of lateralia (la3-5, figure 3A; la1-2 could not be found),  
39  
40 174 three pairs of dorsalia (do1-3 figure 3A) and two pairs of caudalia (dorsal and ventral, cd1-2, figure  
41  
42 175 3A). Perikarya (scb, figure 1A,D) of five previously described additional sensoria could not be  
43  
44 176 identified with acetylated  $\alpha$ -tubulin-LIR. On each lateral side, he recovered lateralia 3-5 as well as  
45  
46 177 dorsalia 1-3 seem to project axons into one longitudinal dorso-lateral and one lateral neurite  
47  
48 178 bundle, respectively, which meet up in the thorax and together join the circumesophageal  
49  
50 179 connectives, anterior of the subpharyngeal ganglia. An additional branch of these peripheral  
51  
52 180 nerves is found between lateralia 5 and the ventro-lateral nerve cord. Axons of the caudalia  
53  
54 181 possibly connect to the posterior commissure, yet, this could not be ascertained due to the strong  
55  
56 182 acetylated  $\alpha$ -tubulin-LIR of the posterior glands.

### 57 58 59 60 183 **Brain**

1  
2  
3  
4 184 The compact, undivided brain occupies most of the head (br, figures 1A,E, 2A,B,G and 4H,I). It was  
5  
6 185 visualized with DAPI, acetylated  $\alpha$ -tubulin-LIR, serotonin-LIR and FMRF-amide-LIR.

7  
8  
9 186 *DAPI*

10  
11 187 The brain (br, figures 1A,E, 2A,B,G and 4H,I) consists of very densely packed small perikarya with  
12  
13 188 small nuclei (nuclei diameter 1.5 to 2.5 $\mu$ m, almost indistinguishable from each other) surrounding  
14  
15 189 the neuropil. In the center of the brain, slightly dorsally, is an area free of nuclei (measuring 6-7 $\mu$ m  
16  
17 190 longitudinally and 10-13 $\mu$ m laterally) corresponding to the space occupied by the neuropil. Two  
18  
19 191 auxiliary ganglia (ag, figures 1A and 2A,G) are present postero-lateral to the brain, each consisting  
20  
21 192 of approximately 10 densely packed, small nuclei.

22  
23 193 *Acetylated  $\alpha$ -tubulin-LIR*

24  
25 194 Fine details of the acetylated  $\alpha$ -tubulin-LIR were difficult to interpret due to the very diffuse IR,  
26  
27 195 however, few structures could be described: A triangular neuropil is present centrally in the brain  
28  
29 196 (np, figures 1A and 2A,B,F), which seems to comprise two very faint and diffuse anterior and  
30  
31 197 posterior commissures. Each of them supplies a paired nerve extending ventro-posteriorly, the  
32  
33 198 lateralmost nerve supplies the auxiliary ganglion of the brain (ag, figure 1A), where after they fuse  
34  
35 199 into a circumesophageal connective (cc, figures 1A,B,F and 2A,F) lateral to the pharynx. Ventro-  
36  
37 200 posterior of the brain, a pair of short nerves of the mouth ciliation (nmc, figures 1A, and 3D)  
38  
39 201 innervates the paired ciliated tufts at the anterior edge of the mouth (mc, figures 1A, 2A,B and  
40  
41 202 3A,B,D, see below).

42  
43 203 *Serotonin-LIR*

44  
45 204 Six pairs of serotonin-LI-reactive perikarya (sb1-6, figure 4G-I) are present around the serotonin-  
46  
47 205 LI-reactive anterior and posterior commissures of the brain neuropil (sacb and spcb, figure 4G-I):  
48  
49 206 one lateral pair (sb1, figure 4G-I) projects neurites into the anterior commissure, and a pair of  
50  
51 207 para-median perikarya (sb2, figure 4G,H) sends neurites into the posterior commissure. Both  
52  
53 208 commissures are connected by an unpaired serotonin-LI-reactive median and a paired serotonin-  
54  
55 209 LI-reactive lateral connective (slcb and smcb, figure 4G-I). Two pairs of serotonin-LI-reactive nerves  
56  
57 210 extend from the posterior commissure: one short pair of serotonin-LI-reactive brain posterior  
58  
59  
60

1  
2  
3  
4 211 projections ending blindly (sbpp, figure 4G) and one pair of serotonin-LI-reactive  
5  
6 212 circumesophageal connectives (scc, figure 4G); the latter corresponding to the inner-branch of the  
7  
8 213 acetylated  $\alpha$ -tubulin-LI-reactive circumesophageal connective (cc, figures 1A and 2A,F). A cluster  
9  
10 214 of two serotonin-LI-reactive perikarya (sb3-4, figure 4G-I) is present on each side, postero-lateral  
11  
12 215 to the posterior commissure, which sends a pair of anterior projections to join the lateral  
13  
14 216 connective of the brain. Finally, two pairs of perikarya (one large posterior (sb5, figures 4G,H) and  
15  
16 217 one small anterior (sb6, figures 3G,H) supply a pair of serotonergic anterior projections (sbap,  
17  
18 218 figure 3G-I) extending to the anterior margin of the animal.

#### 19 219 *FMRF-amide-LIR*

20  
21  
22 220 The brain shows a characteristic FMRF-amide-LIR pattern in the neuropil (figure 1E), however, due  
23  
24 221 to the background signal of the anti-FMRF-amide staining, only one anterior pair of dorso-lateral  
25  
26 222 FMRF-amide-LI-reactive brain perikarya could be identified (fbp, figure 1E), which is connected to  
27  
28 223 the neuropil by an FMRF-amide-LI-reactive nerve.

#### 29 30 224 **Subpharyngeal ganglia**

31  
32  
33 225 One pair of ventral subpharyngeal ganglia (spg, figures 1A,F and 2A) is present postero-laterally to  
34  
35 226 the pharynx, supplying the circumesophageal connectives, the ventro-lateral nerve cords, the  
36  
37 227 ventro-median nerves, and the anterior commissure. It consists of approximately six to eight  
38  
39 228 nuclei and is only visible with DAPI (no IR with the tested antibodies could be seen).

#### 40 41 229 **Pharyngeal ganglion**

42  
43  
44 230 The pharyngeal ganglion is an unpaired cluster of nerve cells, surrounded by the fibularium  
45  
46 231 sclerite, and situated dorso-posteriorly in the pharynx (pg, figures 1A-C,E, 2A,B,G and 4A-F),  
47  
48 232 probably innervating the jaw elements. It shows positive IR for all antibodies tested (directed  
49  
50 233 against acetylated  $\alpha$ -tubulin, serotonin and FMRF-amide), revealing a consistent number and  
51  
52 234 location of nuclei (stained with DAPI) in all examined specimens. A dense, filamentous acetylated  
53  
54 235  $\alpha$ -tubulin-LI-reactive net of nerve fibers infiltrates the entire structure and allows the delimitation  
55  
56 236 of the ganglion (atpg, figures 1C,2F and 4A,C), together with the densely packed nuclei. Of the  
57  
58 237 approximately 60 cells identified with DAPI-staining, three paired serotonin-LI-reactive perikarya

1  
2  
3  
4 238 are clustered medio-posteriorly in two longitudinal rows, followed by one unpaired serotonergic-  
5  
6 239 LI-reactive perikaryon (s1-4, figure 4A,B) and four pairs of FMRF-amide-LI-reactive perikarya are  
7  
8 240 found at the lateral and posterior margins of the pharyngeal ganglion (fp1-4, figure 4A,D,F) as well  
9  
10 241 as one antero-dorsal pair of perikarya (fp5, figure 4A,E) and a pair of anterior FMRF-amide-LI-  
11  
12 242 reactive positive spots lacking associated nuclei (fs, figures 4A,F).

13  
14 243 How the pharyngeal ganglion is related to the central nervous system could not be resolved, since  
15  
16 244 no nerves extending out of the pharyngeal ganglion could be identified. One pair of tufts of  
17  
18 245 presumably pharyngeal sensory cilia (described below) originate directly from the pharyngeal  
19  
20 246 ganglion (phc, figures 1A,B,F, 2A,B, 3A,B,D,F and 4A,C). One pair of strongly acetylated  $\alpha$ -tubulin-  
21  
22 247 LI-reactive structures are found postero-laterally to the pharyngeal ganglion, they do not seem to  
23  
24 248 consist of cilia, and their function are unknown (apo, figures 1B, 2F and 4C).

## 25 26 249 **Ciliation**

27  
28  
29 250 The ciliation can be separated into five different systems: the external ventral locomotory ciliation,  
30  
31 251 mouth ciliation, sensory cilia, as well as the internally ciliated nephridia and oviducts.

### 32 33 252 **Locomotory ciliation**

#### 34 35 36 253 *Head ciliation*

37  
38  
39 254 On the head, the ventral ciliation can be divided into a semicircular anterior ciliated field in front  
40  
41 255 of the mouth opening (acf, figures 2A,B and 3A,D,G) separated by a transverse head groove (hgr,  
42  
43 256 figures 2A,B and 3A,G) from a horseshoe shaped posterior ciliated field (pcf, figures 2A,B and  
44  
45 257 3A,G) surrounding the mouth.

#### 46 47 258 *Ciliophores*

48  
49 259 Acetylated  $\alpha$ -tubulin-LIR, as well as phalloidin staining proved useful to reconstruct the ventral  
50  
51 260 ciliary pattern of *Limnognathia maerski*. The packed cilia of each ciliophore could be differentiated  
52  
53 261 in optical sections with acetylated  $\alpha$ -tubulin-LIR, supported by phalloidin staining, which weakly  
54  
55 262 marks the ventral cell walls. This showed that instead of one longitudinal row of paired ciliophores

1  
2  
3  
4 263 as described in Kristensen and Funch [1], the trunk ciliation consists of a more complex pattern at  
5  
6 264 the anterior part of the thorax.

7  
8  
9 265 At the posterior part of the head and the anterior part of the thorax, the organization of the  
10  
11 266 ciliophores is the most complicated. All four pairs of head ciliophores described in the original  
12  
13 267 description of *L. maerski*, which were supposed to be lining the oral plate, could not be found.  
14  
15 268 However, one pair of head ciliophores (hc, figure 3A,C,E,G) could be found, followed by two pairs  
16  
17 269 of laterally adjacent ciliophores. These three pairs of ciliophores are likely to correspond to some  
18  
19 270 of the head ciliophores described by Kristensen and Funch [1]. Three unpaired, transversely  
20  
21 271 elongated ciliophores (mac, figure 3A,C,E) and two pairs of antero-lateral ciliophores (alc, figure  
22  
23 272 3A,C) are found posterior to the oral plate. More posteriorly, on the thorax, two paired  
24  
25 273 longitudinal rows of ciliophores are present: one row of four lateral ciliophores (tlc, figure 3A,C,E)  
26  
27 274 and one row of five median ciliophores (tmc, figure 2A,C,E). The row of thoracic lateral ciliophores  
28  
29 275 is in tight contact with the thoracic median row of ciliophores, giving a mosaic appearance,  
30  
31 276 probably explaining the previous indiscernibility of each row. The cells of the median row are  
32  
33 277 larger and are adjacent to the midline. The thoracic lateral ciliophores are smaller and each of  
34  
35 278 them is in contact with two thoracic median ciliophores. At the posterior part of the thorax and  
36  
37 279 the anterior part of the abdomen, only two longitudinal rows exist, each consisting of six  
38  
39 280 abdominal ciliophores (abc, figure 2A,C,E), corresponding to the observations of the original  
40  
41 281 description [1]. On the midline between each median quartet of ciliophores, one small nonciliated  
42  
43 282 epidermal medio-ventral cell (mvc, figure 2C,D) is present.

#### 44 283 *Adhesive ciliary pad*

45  
46 284 The ciliary adhesive pad (acp, figures 1A,G, 2A,B and 3A-C) consists of five pairs of multiciliated  
47  
48 285 cells: two lateral, two median and one posterior, as described in the original description [1].

#### 49 286 **Mouth ciliation**

50  
51 287 In accordance with the original description [1], a mouth ciliation is found most likely involved in  
52  
53 288 food uptake. However, it only covers the anterior edge of the mouth cavity, comprising paired  
54  
55 289 laterally elongated tufts of >10 approximately 7µm long cilia (mc, figures 1A, 2A,B and 3A,B,D).

1  
2  
3  
4 290 The present CLSM study revealed a conspicuous previously undescribed pharyngeal ciliary tuft in  
5  
6 291 the mouth cavity (phc, figures 1A,B,F, 2A,B, 3A,B,D,F and 4A,C). It extends between the main jaws  
7  
8 292 (mj, figure 3F) and its ciliary roots originate from the pharyngeal ganglion, suggesting that the cilia  
9  
10 293 have sensory function. The cilia are 6-7 $\mu$ m long and curved (phc, figures 2B, 3A,B,D,F and 4C), and  
11  
12 294 each of the paired tufts consists of >10 cilia, as also seen in the TEM micrographs shown in  
13  
14 295 Kristensen and Funch, 2000 ([1], figure 23) and Sørensen and Kristensen, 2015 ([25], fig. 3.12.B)

### 15 16 296 **Nephridia**

17  
18 297 Three pairs of acetylated  $\alpha$ -tubulin-LI-reactive ventro-lateral longitudinal ciliary structures are  
19  
20 298 found along the thorax and anterior abdomen. The present CLSM data in combination with the  
21  
22 299 TEM data of Sørensen and Kristensen (2015) allow us to reconstruct these structures as an  
23  
24 300 anterior and a posterior pair of protonephridia with an intermediate collecting tube, in accordance  
25  
26 301 with Sørensen and Kristensen [23] but opposing the interpretation of three pairs of nephridia  
27  
28 302 given by Sørensen et al. [26] (fig. 16.13 and 16.15). The present study offers the following more  
29  
30 303 detailed description:

31  
32 304 The anterior pair of nephridia originates in the anteriormost thorax, each nephridium comprising  
33  
34 305 two adjacent protonephridial units with two monociliated terminal cells each; all four cilia (8-  
35  
36 306 10 $\mu$ m long) joining in one common canal cell (nph1, figures 1B, 2A, 3B,E and fig. 3.15 in Sørensen  
37  
38 307 and Kristensen [23]). The posterior pair of nephridia (nph2, figures 1B, 2A and 3B,E) contains only  
39  
40 308 one unit (contrary to the double units proposed by Sørensen and Kristensen [23], but see fig  
41  
42 309 3.15B) with two monociliated terminal cells (cilia 7-10 $\mu$ m long), possibly originating in the anterior  
43  
44 310 abdomen and extending anteriorly into to the posterior thorax, where it meets the collecting  
45  
46 311 tubule. The intermediate collecting tubule (ct, figures 1B, 2A and 3B,E) consists of more than five  
47  
48 312 tightly packed cilia, but the exact number could not be determined. It extends through the second  
49  
50 313 third of the thorax and is 11-13 $\mu$ m long. The consistent longer length of the cilia of the collecting  
51  
52 314 tubule and higher cilia density, similar to what is shown in Sørensen and Kristensen [23], are  
53  
54 315 elements allowing us to differentiate these collecting tubules from the actual protonephridia. No  
55  
56 316 associated nephridiopore or additional structure could be found.

### 57 58 59 60 317 **Oviducts**

1  
2  
3  
4 318 One pair of acetylated  $\alpha$ -tubulin-LI-reactive L-shaped ducts here interpreted as oviducts (od,  
5  
6 319 figures 2A and 3B) is present in the posterior part of the abdomen, but does not consist of cilia.  
7  
8 320 They originate lateral to the midline, posterior to the oocyte, extend 6-7 $\mu$ m postero-medially,  
9  
10 321 terminating in an ovipore (ovp, figure 3A,B,C) in the center of the adhesive ciliary pad. Non ciliated  
11  
12 322 oviducts are also reported in Rotifera [27-29], whereas nothing similar has been found in  
13  
14 323 Gnathostomulida [30, 31].

15  
16 324 Anterior of the oviduct, a pair of putatively associated 10 $\mu$ m long dorsal accessory cilia (aco, figure  
17  
18 325 2A,E) is present. Each cilium is adjacent to the oocyte; oriented obliquely, extending from a dorso-  
19  
20 326 median to a ventro-lateral position. Their function is unknown.

## 21 22 327 **Glands**

23  
24  
25 328 A tripartite glandular complex consisting of a central gland (mhg, figure 2A,C,D) and a pair of  
26  
27 329 lateral, elongated glands (lhg, figure 2A,C,D) are found in the dorsal head region of *Limnognathia*  
28  
29 330 *maerski* (hg, figure 2B). All glands show acetylated  $\alpha$ -tubulin-LIR in the cell wall and appear to  
30  
31 331 open dorso-apically on the head. The median gland extends dorso-posteriorly to the level of the  
32  
33 332 pharynx and possesses numerous and densely packed nuclei (mhg, figure 2C). The two lateral  
34  
35 333 glands consist of an elongated longitudinal canal anteriorly (embedding few elongated nuclei (lhg,  
36  
37 334 figure 2C), which extends posterior of the median gland until the dorso-lateral sides of the pharynx  
38  
39 335 (Fig. 2D).

40  
41 336 One pair of large glandular cells is found ventro-laterally in the posterior-most abdomen (pgl,  
42  
43 337 figures 1A, 2A,E and 3B); their full configuration was detected through background signal of non-  
44  
45 338 specific fluorescence as well as specific acetylated  $\alpha$ -tubulin-LIR. Each cell is 15 to 20 $\mu$ m long,  
46  
47 339 ellipsoid shaped, broadest at its base and narrowing into a neck region, with a 2 $\mu$ m wide opening;  
48  
49 340 the elongated nucleus is positioned at the external side of the cell (npg, figure 2E). The cell wall of  
50  
51 341 the neck region contains numerous, distinct acetylated  $\alpha$ -tubulin-LIR, longitudinally striated  
52  
53 342 components; their signal becoming less obvious towards the expanded cellular base. FMRF-amide-  
54  
55 343 LIR and serotonin-LIR is visible in the cell opening (opg, figure 2A,E). Their position corresponds to  
56  
57 344 the "paired openings of unknown function" of Sørensen and Kristensen [23] visible with SEM,  
58  
59 345 which therefore are not nephridiopores as previously suggested.

1  
2  
3  
4 346 **Discussion**

5  
6  
7 347 **Evolution of ventral cords and associated commissures in Gnathifera**

8  
9  
10 348 The presence of two ventro-lateral nerve cords in *Limnognathia maerski* was confirmed [1, 23]  
11 349 and their precise configuration explained, unraveling an anterior (with associated subpharyngeal  
12 350 ganglia) and a posterior commissure, as well as two ventro-median nerves branching off from the  
13 351 main ventrolateral cords at the subpharyngeal ganglia; these paired ventro-median nerves are not  
14 352 previously reported in Gnathifera.

15  
16  
17  
18  
19 353 In Rotifera, only one pair of longitudinal ventro-lateral nerves has been consistently found with  
20 354 FMRF-amide-LIR, catecholamine-LIR, serotonin-LIR and SCPb-LIR in representatives of both  
21 355 Bdelloidea and Monogononta [12-15, 27, 32, 33]. TEM-investigations by Ahlrichs ([34] , fig. 5A)  
22 356 also suggest the presence of at least two longitudinal nerves in the neck region of the early  
23 357 branching Seisonidea. However, antibody-staining only shows a subset of the nervous system and  
24 358 acetylated  $\alpha$ -tubulin-LIR has not been tested in these studies. Yet, in a total reconstruction of the  
25 359 nervous system of Monogononta based on light microscopy by Remane [35] (figure 5B), no  
26 360 ventro-median nerves were found even though more delicate nerves were described, such as the  
27 361 peripheral nerves. These have been shown to branch off dorso-laterally from the subpharyngeal  
28 362 ganglia and innervate the sensory organs and dorso-ventral muscles [36], similar to what is here  
29 363 described for *L. maerski*. Though no anterior commissure and ganglia resembling those of *L.*  
30 364 *maerski* are generally found in Rotifera, similarities can exceptionally be found in the FMRF-amide-  
31 365 LI-reactive and SCPb-LI-reactive perikarya and trunk commissure in *Notommata copeus* Ehrenberg,  
32 366 1934 [37] (Monogononta) [13], the FMRF-amide-LI-reactive trunk commissure in *Euchlanis*  
33 367 *dilatata* (Ehrenberg, 1932) [14, 38], or the so called geniculate ganglion of Monogononta [35]  
34 368 (figure 5B).

35  
36  
37  
38  
39  
40  
41  
42  
43  
44  
45  
46  
47  
48  
49 369 In Gnathostomulida, confocal and TEM studies show a more variable number of one to three pairs  
50 370 of longitudinal nerves (plus one dorsal and one median unpaired nerve in *Gnathostomula*  
51 371 *peregrina* Kirsteuer, 1969 [39] (figure 5C)), of which the paired ventro-lateral nerves form an  
52 372 anterior as well as a posterior commissure in *G. peregrina* [10]. Similar to *L. maerski*, their  
53 373 circumesophageal connectives also originate as two distinct bundles of neurites in *G. peregrina*

1  
2  
3  
4 374 [10] (figure 5A,C), further supporting the homology of two ventro-lateral cords in Gnathifera. This  
5  
6 375 character is likely to be shared between most Spiralia [40] suggesting that the ventro-lateral nerve  
7  
8 376 cord of Gnathifera is possibly a symplesiomorphy of this group. However with Gnathostomulida  
9  
10 377 being sister group to the remaining Gnathifera [3] and the only sporadic finding of an anterior  
11  
12 378 commissure and/or subpharyngeal ganglia in both Gnathostomulida and Rotifera, the homology of  
13  
14 379 these specific substructures of the ventral cords remains to be tested. The reported ventro-  
15  
16 380 median nerve in *G. peregrina* is unpaired but two separate medio-ventral strands originating in the  
17  
18 381 anterior trunk are observed in new ongoing studies of other gnathostomulids (Gąsiorowski,  
19  
20 382 Bekkouche and Worsaae unpublished), warranting further analyses of their possible homology to  
21  
22 383 the medio-ventral nerves of *L. maerski*.

#### 23 384 **Finding of a synapomorphic pharyngeal ganglion with ciliary receptors in Gnathifera**

25  
26 385 The present study confirms the presence of a formerly suspected pharyngeal ganglion in  
27  
28 386 *Limnognathia maerski* [23] with numerous nucleated cells, an observation refuting the suggestion  
29  
30 387 of Gorelick [41], proposing that “Micrognathozoan jaws may also be enervated by anucleate  
31  
32 388 neurons”. In Rotifera, a “mastax ganglion” is suspected but not yet confirmed in Seisonidae [27],  
33  
34 389 and data is scarce on Bdelloidea since only the presence of catecholaminergic nerves related to  
35  
36 390 the mastax suggests its presence in *Rotatoria tardigrada* Ehrenberg, 1832 [32, 38]. However, for  
37  
38 391 Monogononta, this ganglion has shown IR for serotonin, catecholamines and FMRF-amide [13, 14,  
39  
40 392 32, 42]. Yet, IR, nerves, and perikarya repartition are extremely variable and no detailed  
41  
42 393 comparison with *L. maerski* is possible. In Gnathostomulida, Herlyn and Ehlers [43] reject the  
43  
44 394 presence of a buccal ganglion after failing at finding any correspondent structures in  
45  
46 395 *Gnathostomula paradoxa*. However, other researches do not support this conclusion and the so-  
47  
48 396 called buccal ganglion, has been described in Filospemoidea with TEM [20] and in  
49  
50 397 Bursovaginoidea with TEM and CLSM [10, 16, 18, 20]. CLSM studies [10, 16] further show the  
51  
52 398 presence of FMRF-amide-LI-reactive perikarya in the buccal ganglion of *Gnathostomula peregrina*.  
53  
54 399 Although connections between the central nervous system and the pharyngeal ganglion of *L.*  
55  
56 400 *maerski* have not been found, studies of Gnathostomulida [16, 20] and Rotifera [32], indicate that  
57  
58 401 a pair of nerves originates dorso-laterally from the posterior of the brain, supplying the  
59  
60 402 buccal/mastax ganglion (mgc, Fig, 5B). The present study, as well as the literature, indicates that

1  
2  
3  
4 403 homologs to the pharyngeal ganglion of *L. maerski* are found in most Gnathifera (figure 5), thus  
5  
6 404 this character might be a synapomorphy of this group.  
7

8  
9 405 The here discovered pharyngeal cilia extending between the main jaws in *Limnognathia maerski*  
10  
11 406 can actually be recovered in previously published transmission electron micrographs such as figs.  
12  
13 407 23 and 25 in [1]. Intriguingly, sensory cilia with similar position, innervation and configuration are  
14  
15 408 also found in rotifers such as the Bdelloidea (*Philodina roseola* Ehrenberg, 1832 [24, 38] and  
16  
17 409 *Philodina acuticornis odiosa* Milne, 1916 [44, 45]), or Monogononta (*Asplanchna brightwellii*  
18  
19 410 Gosse, 1850 [24, 46]). These cilia likewise protrude between the basal parts of the rami  
20  
21 411 (assumedly homologous to the main jaws of *L. maerski*) and are also anchored at the mastax  
22  
23 412 ganglion (assumedly homologous to the ganglion in *L. maerski*). Additionally, in *Asplanchna*  
24  
25 413 *brightwellii* the proximal part of the ciliated sensory receptors is well separated into two bundles  
26  
27 414 resembling the paired configuration in *L. maerski* [24]; all supporting their homology and their  
28  
29 415 organization into densely ciliated tufts as a putative synapomorphy of Micrognathozoa and  
30  
31 416 Rotifera. Though so far, data on the early branching rotifer Seisonidae are lacking. In  
32  
33 417 Gnathostomulida, pharyngeal ciliation has never been described, however, scarce cilia are visible  
34  
35 418 in the pharynx of *Gnathostomula paradoxa* ([43] fig. 3), and ongoing investigations indicate the  
36  
37 419 existence of possible homologous short paired ciliary receptors, between the jaws connected to  
38  
39 420 the buccal ganglion in *Gnathostomula paradoxa*, *Austrognathia microconulifera* Farris, 1977 [47]  
40  
41 421 and *Haplognathia* spp. (Gąsiorowski, Bekkouche and Worsaae unpublished). The putative  
42  
43 422 common presence of paired ciliary receptors on the pharyngeal ganglia across Gnathifera thereby  
44  
45 423 further supports the homology of the pharyngeal ganglion (as well as its possibly common sensory  
46  
47 424 function) in Gnathifera.

#### 425 **Increased resolution of ciliary patterns revealed with high quality CLSM**

48  
49 426 Acetylated  $\alpha$ -tubulin-LIR as well as phalloidin and DAPI show a more complex pattern of ventral  
50  
51 427 ciliophores than previously described in *Limnognathia maerski* [1]. These results show the  
52  
53 428 relevance of CLSM to resolve spatial patterns in microscopic animals since the collapse of cilia  
54  
55 429 makes difficult the identification of independent cells with light microscopy or scanning electron  
56  
57 430 microscopy. Similar complex anterior ciliary arrangements have been found in the gastrotrichs  
58  
59 431 *Diuronotus aspetos* Todaro, Balsamo & Kristensen, 2005 [48] (Bekkouche and Worsaae,  
60

1  
2  
3  
4 432 unpublished), *Diplodasys rothei* Kieneke, Narkus, Hochberg & Schmidt-Rhaesa, 2013 [49] or the  
5  
6 433 microscopic annelids *Diurodrilus* spp. [50]. Interestingly *L. maerski* and *Diurodrilus* have been  
7  
8 434 comprehensively compared [1, 50], and even though phylogenomics recently confirmed that  
9  
10 435 *Diurodrilus* is a distantly related genus of annelids [2, 51], this is another similar character between  
11  
12 436 these two animals. However, though these overall similarity in patterns may reflect homoplasy,  
13  
14 437 the detailed patterns has been shown to be of systematic significance within, e.g., *Diurodrilus* and  
15  
16 438 Gastrotricha [50, 52, 53] and may also potentially be useful for discriminating Micrognathozoa  
17  
18 439 from Greenland versus Antarctica, which was not possible according to jaw morphology [21].

## 19 440 **Nephridial system of Micrognathozoa shows more similarity with Rotifera than** 20 21 441 **Gnathostomulida**

22  
23  
24 442 The protonephridial system of *Limnognathia maerski* resembles the one of Rotifera, although only  
25  
26 443 few studies have reconstructed the excretory system of Rotifera in details. However, Ahlrichs  
27  
28 444 provided the complete reconstruction of the protonephridial system of *Paraseison annulatus*  
29  
30 445 (Claus, 1876) [54] (Seisonidae) [34] and *Proales reinhardti* (Ehrenberg, 1934) [37] (Monogononta)  
31  
32 446 [55] from ultrathin section and TEM. Both rotifers possess a terminal syncytium with several  
33  
34 447 multiciliated terminal organs and a capillary canal (resembling the canal cell in *L. maerski*).  
35  
36 448 Furthermore, the terminal syncytium connects to a multiciliated canal region, which shows  
37  
38 449 resemblance to the collecting tubules of *L. maerski*. The main difference in this configuration being  
39  
40 450 the monociliated nature of the terminal organs of *L. maerski* versus the multiciliated organs found  
41  
42 451 in most rotifers [34, 36, 55, 56]. The protonephridial system of Gnathostomulida has been  
43  
44 452 described in detail for *Haplognathia rosea* (Sterrer, 1969) [19] (Filospermoidea) and  
45  
46 453 *Gnathostomula paradoxa* by Lammert [20]. They consist of serially independent organs, each  
47  
48 454 comprising a monociliated terminal cell, a canal cell and a nephridiopore cell; an arrangement  
49  
50 455 found in other animals [57, 58]. Therefore, it can be assumed that the monociliated terminal cells  
51  
52 456 of *L. maerski* is a pleisiomorphic condition shared with Gnathostomulida, whereas the  
53  
54 457 multiciliated collecting tubule supplying the different canal cells is a synapomorphy of *L. maerski*  
55  
56 458 and Rotifera.

## 57 459 **Do Micrognathozoa possess a retrocerebral organ?**

1  
2  
3  
4 460 The tripartite anterior gland of *Limnognathia maerski*, consisting of one unpaired median and a  
5  
6 461 pair of medio-lateral glands opening dorso-apically is very similar in position and size to the  
7  
8 462 retrocerebral organ found in most Rotifera, where they are assumed to play a role in the  
9  
10 463 lubrication of the cilia [24, 27, 36]. If the two organs are homologous, the median gland of *L.*  
11  
12 464 *maerski* would correspond to the retrocerebral sac, while the lateral glands would correspond to  
13  
14 465 the subcerebral glands more similar to what is found in Bdelloidea [36] (where the retrocerebral  
15  
16 466 sac likewise opens medially and the two subcerebral glands open medio-laterally); hereby  
17  
18 467 indicating that this may be the plesiomorphic condition in Rotifera, and that the retrocerebral  
19  
20 468 organ might be a synapomorphy of Micrognathozoa and Rotifera.

## 21 **Conclusion**

22  
23  
24 470 This study shows a striking simplicity of the micrognathozoan nervous system, in opposition to the  
25  
26 471 complexity in muscular [11] - and ciliary systems (present study), but it also illustrates the need of  
27  
28 472 CLSM studies together with TEM investigations on meiofaunal animals. Indeed, previous TEM  
29  
30 473 results on Micrognathozoa could not lead to the observation of the second ventro-median pair of  
31  
32 474 longitudinal nerves or the exact details of the ventral ciliation. On the other hand, some  
33  
34 475 conclusions of this paper could not have been possible without previous TEM studies as the  
35  
36 476 identification of the protonephridial unit versus the collecting tubule.

37  
38 477 Indeed, many characters described in this study seem to be autapomorphies of Micrognathozoa,  
39  
40 478 such as the presence of a paired ventro-median nerve, or the specific arrangement of ciliophores.  
41  
42 479 On the other hand, some characters constitute putative synapomorphies of Micrognathozoa and  
43  
44 480 Rotifera, such as the peripheral nervous system innervating the sensory structures, the presence  
45  
46 481 of dense tufts of pharyngeal sensory cilia, the organization of the protonephridia and the potential  
47  
48 482 presence of a retrocerebral organ. Furthermore, resolving the morphology of the nervous system  
49  
50 483 of Micrognathozoa allowed us to hypothesize that a ciliated pharyngeal ganglion is a  
51  
52 484 synapomorphy of all Gnathifera and that the presence of two ventro-lateral nerve cords is a  
53  
54 485 symplesiomorphy of Gnathifera, and more generally of Spiralia [40].

55  
56 486 Although this study informs on the inner anatomy of Micrognathozoa, many details still warrants  
57  
58 487 further ultrastructural studies such as the protonephridia and the oviducts, or the connection of  
59  
60

1  
2  
3  
4 488 the pharyngeal ganglion to the brain. Additionally, many Gnathifera lack detailed descriptions with  
5  
6 489 CLSM such as the rotifer group Seisonidae, where only the musculature has been described [7],  
7  
8 490 and the gnathostomulid groups Filospemoidea and Conophoralia. In the context of the latest  
9  
10 491 phylogenomic results [2, 3] where Gnathifera has a key phylogenetic position within protostomes  
11  
12 492 we hope that these issues will soon be addressed.

### 13 **Acknowledgements**

14  
15  
16 494 The Arctic Station of Qeqertarsuaq, University of Copenhagen provided an excellent working  
17  
18 495 platform with cooling container and we are thankful to the crew of the station as well as R/V  
19  
20 496 Porsild. We also thank Ludwik Gąsiorowski for data on Gnathostomulida, and Alexandra Kerbl for  
21  
22 497 her help with proofreading the manuscript.

### 23 **Funding statement**

24  
25  
26 499 The fieldwork on Greenland, the lab cost and the salary of the first author were supported by the  
27  
28 500 Villum foundation (Grant no. 102544).

### 29 **Competing interests**

30  
31  
32 502 We have no competing interests.

### 33 **Authors' contributions**

34  
35  
36 503  
37  
38 504 NB and KW conceptualized and designed the study, collected the animals, analyzed the data, and  
39  
40 505 wrote the manuscript. NB gathered most of the immunohistochemical data and made the  
41  
42 506 illustrations.

### 43 **References**

- 44  
45  
46 508 1. Kristensen RM, Funch P. 2000. Micrognathozoa: a new class with complicated jaws like those of  
47  
48 509 Rotifera and Gnathostomulida. *Journal of Morphology*;246(1):1-49. (doi: 10.1002/1097-  
49  
50 510 4687(200010)246:1<1::AID-JMOR1>3.0.CO;2-D).
- 51  
52 511 2. Struck TH, Wey-Fabrizius AR, Golombek A, Hering L, Weigert A, Bleidorn C, et al. 2014. Platyzoan  
53  
54 512 paraphyly based on phylogenomic data supports a non-coelomate ancestry of spiralia. *Molecular Biology*  
55  
56 513 *and Evolution*;31(7):1833-1849. (10.1093/molbev/msu143).
- 57  
58 514 3. Laumer CE, Bekkouche N, Kerb A, Goetz F, Neves RC, Sorensen MV, et al. 2015. Spiralian Phylogeny  
59  
60 515 Informs the Evolution of Microscopic Lineages. *Current Biology*;25(15):2000-2006.  
516 (doi:10.1016/j.cub.2015.06.068).

- 1  
2  
3  
4 517 4. Ahlrichs WH. 1997. Epidermal ultrastructure of *Seison nebaliae* and *Seison annulatus*, and a  
518 comparison of epidermal structures within the Gnathifera. *Zoomorphology (Berlin)*;117(1):41-48. (doi:  
519 10.1007/s004350050028).
- 520 5. Wulfken D, Ahlrichs WH. 2012. The ultrastructure of the mastax of *Filinia longiseta*  
521 (Flosculariaceae, Rotifera): Informational value of the trophi structure and mastax musculature.  
522 *Zoologischer Anzeiger*;251(4):270-278. (doi: 10.1016/j.jcz.2012.02.001).
- 523 6. Leasi F, Ricci C. 2010. Musculature of two bdelloid rotifers, *Adineta ricciae* and *Macrotrachela*  
524 *quadricornifera*: organization in a functional and evolutionary perspective. *Journal of Zoological Systematics*  
525 *and Evolutionary Research*;48(1):33-39. (doi: 10.1111/j.1439-0469.2009.00538.x).
- 526 7. Leasi F, Neves RC, Worsaae K, Sørensen MV. 2012. Musculature of *Seison nebaliae* Grube, 1861 and  
527 *Paraseison annulatus* (Claus, 1876) revealed with CLSM: a comparative study of the gnathiferan key taxon  
528 Seisonacea (Rotifera). *Zoomorphology*;131(3):185-195. (doi: 10.1007/s00435-012-0155-2).
- 529 8. Wilts EF, Ahlrichs WH, Arbizu PM. 2009. The somatic musculature of *Bryceella stylata* (Milne, 1886)  
530 (Rotifera: Proalidae) as revealed by confocal laser scanning microscopy with additional new data on its  
531 trophi and overall morphology. *Zoologischer Anzeiger*;248(3):161-175. (doi: 10.1016/j.jcz.2009.08.001).
- 532 9. Tyler S, Hooge MD. 2001. Musculature of *Gnathostomula armata* Riedl 1971 and its ecological  
533 significance. *Marine Ecology-Pubblicazioni Della Stazione Zoologica Di Napoli I*;22(1-2):71-83. (doi:  
534 10.1046/j.1439-0485.2001.00737.x).
- 535 10. Müller MCM, Sterrer W. 2004. Musculature and nervous system of *Gnathostomula peregrina*  
536 (Gnathostomulida) shown by phalloidin labeling, immunohistochemistry, and cLSM, and their phylogenetic  
537 significance. *Zoomorphology*;123(3):169-177. (doi: 10.1007/s00435-004-0099-2).
- 538 11. Bekkouche N, Kristensen RM, Hejnol A, Sorensen MV, Worsaae K. 2014. Detailed reconstruction of  
539 the musculature in *Limnognathia maerski* (Micrognathozoa) and comparison with other Gnathifera.  
540 *Frontiers in Zoology*;11(71). (doi: 10.1186/s12983-014-0071-z).
- 541 12. Hochberg R. 2006. On the serotonergic nervous system of two planktonic rotifers, *Conochilus*  
542 *coenobasis* and *C. dossuarius* (Monogononta, Flosculariaceae, Conochilidae). *Zoologischer*  
543 *Anzeiger*;245(1):53-62. (doi: 10.1016/j.jcz.2006.04.001).
- 544 13. Hochberg R. 2007. Topology of the nervous system of *Notommata copeus* (Rotifera: Monogononta)  
545 revealed with anti-FMRamide, -SCPb, and -serotonin (5-HT) immunohistochemistry. *Invertebrate*  
546 *Biology*;126(3):247-256. (doi: 10.1111/j.1744-7410.2007.00094.x).
- 547 14. Kotikova EA, Raikova OI, Reuter M, Gustafsson MKS. 2005. Rotifer nervous system visualized by  
548 FMRamide and 5-HT immunocytochemistry and confocal laser scanning microscopy.  
549 *Hydrobiologia*;546:239-248. (doi: 10.1007/1-4020-4408-9\_24).
- 550 15. Hochberg A, Hochberg R. 2015. Serotonin immunoreactivity in the nervous system of the free-  
551 swimming larvae and sessile adult females of *Stephanoceros fimbriatus* (Rotifera: Gnesiotrocha).  
552 *Invertebrate Biology*;134(4):261-270. (doi: 10.1111/ivb.12102).
- 553 16. Schmidt-Rhaesa A. 2016. Gnathostomulida. In: Schmidt-Rhaesa A, Harzsh S, Purscke G, editors.  
554 *Structure and Evolution of Invertebrate Nervous Systems*. New York: Oxford University Press. p. 118-121.
- 555 17. Ax P. 1956. *Die Gnathostomulida, eine rätselhafte Wurmgruppe aus dem Meeressand*. Mainz,;  
556 Verlag der Akademie der Wissenschaften und der Literatur; in Kommission bei F. Steiner. 32 p.
- 557 18. Kristensen RM, Nørrevang A. 1977. On the fine structure of *Rastrognathia macrostoma* gen. et sp.n  
558 placed in Rastrognathiidae fam.n. (Gnathostomulida). *Zoologica Scripta*;6(1):27-41. (doi: 10.1111/j.1463-  
559 6409.1977.tb00757.x).
- 560 19. Sterrer W. 1969. Beiträge zur Kenntnis der Gnathostomulida I. Anatomie und Morphologie des  
561 Genus *Pterognathia* Sterrer. *Arkiv för Zoologi*;22(1):1-125.
- 562 20. Lammert V. 1986. Vergleichende Ultrastruktur-Untersuchungen an Gnathostomuliden und die  
563 phylogenetische Bewertung ihrer Merkmale: Göttingen. 219 p.

- 1  
2  
3  
4 564 21. De Smet WH. 2002. A new record of *Limnognathia maerski* Kristensen & Funch, 2000  
5 565 (Micrognathozoa) from the subantarctic Crozet Islands, with redescription of the trophi. *Journal of*  
6 566 *Zoology*;258:381-393. (doi: 10.1017/S095283690200153x).
- 7 567 22. Sørensen MV. 2003. Further structures in the jaw apparatus of *Limnognathia maerski*  
8 568 (Micrognathozoa), with notes on the phylogeny of the gnathifera. *Journal of Morphology*;255(2):131-145.  
9 569 (doi: 10.1002/Jmor.10038).
- 10 570 23. Sørensen MV, Kristensen MK. 2015. 3. Micrognathozoa. In: Schmidt-Rhaesa A, editor. *Handbook of*  
11 571 *Zoology, Gastrotricha and Gnathifera*. 3: De Gruyer.
- 12 572 24. Clément P, Wurdak E. 1991. Rotifera. In: Harrison FW, Ruppert EE, editors. *Microscopic Anatomy of*  
13 573 *Invertebrates, Volume 4, Aschelminthes*. John Wiley & Sons ed. New York, Chichester, Brisbane, Toronto,  
14 574 Singapore. p. 219-297.
- 15 575 25. Sørensen MV, Tyler S, Hooge MD, Funch P. 2003. Organization of pharyngeal hard parts and  
16 576 musculature in *Gnathostomula armata* (Gnathostomulida : Gnathostomulidae). *Canadian Journal of*  
17 577 *Zoology-Revue Canadienne De Zoologie*;81(9):1463-1470. (doi: 10.1139/Z03-135).
- 18 578 26. Sørensen MV, Worsaae K, Kristensen MK. 2016. The Gnathifera. In: Brusca RC, Moore W, Shuster  
19 579 SM, editors. *Invertebrates*. 3 ed. Massachusetts, USA: Sinauer Associates, Inc. p. 613-634.
- 20 580 27. Ricci C, Melone G, Sotgia C. 1993. Old and new data on Seisonidea (Rotifera). *Hydrobiologia*;255-  
21 581 256:495-511. (doi: 10.1007/BF00025879).
- 22 582 28. Amsellem J, Ricci C. 1982. Fine structure of the female genital apparatus of *Philodina* (Rotifera,  
23 583 Bdelloidea). *Zoomorphology (Berlin)*;100(2):89-105. (doi: 10.1007/BF00310356).
- 24 584 29. Bentfeld ME. 1971. Studies of oogenesis in the rotifer, *Asplanchna*. I. Fine structure of the female  
25 585 reproductive system. *Z Zellforsch Mikrosk Anat*;115(2):165-183. (doi: 10.1007/BF00391123).
- 26 586 30. Sterrer WS, M. V. 2015. 2. Phylum Gnathostomulida. In: Schmidt-Rhaesa A, editor. *Handbook of*  
27 587 *Zoology, Gastrotricha and Gnathifera*. 3: De Gruyer. p. 135-196.
- 28 588 31. Riedl RJ. 1969. Gnathostomulida from America. *Science*;163(3866):445-452. (doi:  
29 589 10.1126/science.163.3866.445).
- 30 590 32. Kotikova EA. 1995. Localization and neuroanatomy of catecholaminergic neurons in some rotifer  
31 591 species. *Hydrobiologia*;313-314:123-127. (doi: 10.1007/BF00025940).
- 32 592 33. Leasi F, Pennati R, Ricci C. 2009. First description of the serotonergic nervous system in a bdelloid  
33 593 rotifer: *Macrotrachela quadricornifera* Milne 1886 (Philodinidae). *Zoologischer Anzeiger*;248(1):47-55. (doi:  
34 594 10.1016/j.jcz.2008.10.002).
- 35 595 34. Ahlrichs W. 1993. Ultrastructure of the protonephridia of *Seison annulatus* (Rotifera).  
36 596 *Zoomorphology (Berlin)*;113(4):245-251. (doi: 10.1007/BF00403315).
- 37 597 35. Remane A. 1933. Aschelminthes. Rotatoria. *Bronn's Klassen un Ordnungen des Tier-Reichs, Bd 4,*  
38 598 *Abt 2, 1.* leipzig: Akademische Verlagsgesellschaft. p. 1-557.
- 39 599 36. Fontaneto D, De Smet W. 2015. 4. Rotifera. In: Schmidt-Rhaesa A, editor. *Handbook of Zoology,*  
40 600 *Gastrotricha and Gnathifera*. 3: De Gruyer.
- 41 601 37. Ehrenberg CG. 1834. Organisation in der Richtung des kleinsten Raumes. *Physiologische*  
42 602 *Abhandlungen*:1-192.
- 43 603 38. Ehrenberg CG. 1832. *Über die Entwicklung und Lebensdauer der Infusionsthier; nebst ferneren*  
44 604 *Beiträgen zu einer Vergleichung ihrer organischen Systeme*. 194 p.
- 45 605 39. Kristeuer E. 1969. *On some species of Gnathostomulida from Bimini, Bahamas*. 21 p.
- 46 606 40. Hejnol A, Lowe CJ. 2015. Embracing the comparative approach: how robust phylogenies and  
47 607 broader developmental sampling impacts the understanding of nervous system evolution. *Royal Society*  
48 608 *Philosophical Transactions Biological Sciences*;370(1684):20150045. (doi: 10.1098/rstb.2015.0045).
- 49 609 41. Gorelick R. 2014. Do Micrognathozoa have micro-genomes? *Biological Journal of the Linnean*  
50 610 *Society*;112(3):640-644. (doi: 10.1111/bij.12284).
- 51 611 42. Kotikova EA. 1998. Catecholaminergic neurons in the brain of rotifers. *Hydrobiologia*;387-388:135-  
52 612 140. (doi: 10.1023/A:1017007426591).

- 1  
2  
3  
4 613 43. Herlyn H, Ehlers U. 1997. Ultrastructure and function of the pharynx of *Gnathostomula paradoxa*  
5 614 (Gnathostomulida). *Zoomorphology*;117(3):135-145. (doi: 10.1007/s004350050038).  
6 615 44. Koehler JK, Hayes TL. 1969. The rotifer jaw: a scanning and transmission electron microscope study.  
7 616 I. The trophi of *Philodina acuticornis odiosa*. *Journal of Ultrastructure Research*;27(5):402-418.  
8 617 45. Milne W. 1916. On the bdelloid Rotifera of South Africa. Part I. *Journal of the Quekett Microscopical*  
9 618 *Club*:39-84.  
10 619 46. Gosse PH. 1850. Description of *Asplanchna priodonta*, an animal of the Class Rotifera. *Annals and*  
11 620 *Magazine of Natural History*:1-18.  
12 621 47. Farris RA. 1977. Three new species of Gnathostomulida from the west Atlantic. *Internationale*  
13 622 *Revue der Gesamten Hydrobiologie*;62(6):765-796. (doi: 10.1002/iroh.1977.3510620603).  
14 623 48. Todaro MA, Balsamo M, Kristensen RM. 2005. A new genus of marine chaetonotids (Gastrotricha),  
15 624 with a description of two new species from Greenland and Denmark. *Journal of the Marine Biological*  
16 625 *Association of the United Kingdom*;85(6):1391-1400. (doi: 10.1017/S0025315405012579).  
17 626 49. Kieneke A, Narkus S, Hochberg R, Schmidt-Rhaesa A. 2013. *Diplodasys rothei* n. sp. (Gastrotricha,  
18 627 Macrotrichida), a new marine gastrotrich species from the Bahamas. *Meiofauna Marina*;20:49-61.  
19 628 50. Worsaae K, Rouse GW. 2008. Is *Diurodrilus* an Annelid? *Journal of Morphology*;269(12):1426-1455.  
20 629 (doi: 10.1002/Jmor.10686).  
21 630 51. Struck TH, Golombek A, Weigert A, Franke FA, Westheide W, Purschke G, et al. 2015. The evolution  
22 631 of annelids reveals two adaptive routes to the interstitial realm. *Current Biology*;25(15):1993-1999. (doi:  
23 632 10.1016/j.cub.2015.06.007).  
24 633 52. Hyman LH. 1951. *Acanthocephala, Aschelminthes, and Entoprocta : the pseudocoelomate Bilateria*.  
25 634 New York: Mac Graw-Hill. VII, 572 p.  
26 635 53. Villora-Moreno S. 1996. Ecology and distribution of the Diurodrilidae (Polychaeta), with  
27 636 redescription of *Diurodrilus benazzii*. *Cahiers de Biologie Marine*;37(1):99-108.  
28 637 54. Claus C. 1876. Über die Organisation und systematische Stellung der Gattung *Seison* Grube.  
29 638 *zoologisch-botanischen Gesellschaft in Wien*:76-90.  
30 639 55. Ahlrichs WH. 1993. On the protonephridial system of the brackish-water rotifer *Proales reinhardtii*  
31 640 (Rotifera, Monogononta). *Microfauna Marina*;8:39-53.  
32 641 56. Riemann O, Ahlrichs WH. 2010. The evolution of the protonephridial terminal organ across Rotifera  
33 642 with particular emphasis on *Dicranophorus forcipatus*, *Encentrum mucronatum* and *Erignatha clastopis*  
34 643 (Rotifera: Dicranophoridae). *Acta Zoologica*;91(2):199-211.  
35 644 57. Lammert V. 1985. The fine structure of protonephridia in Gnathostomulida and their comparison  
36 645 within Bilateria. *Zoomorphology (Berlin)*;105(5):308-316. (doi: 10.1007/BF00312062).  
37 646 58. Schmidt-Rhaesa A. 2007. *The evolution of organ systems*. Oxford & New York: Oxford University  
38 647 Press. i-x, 1-385 p.

42  
43 648 **List of abbreviations (for reviewers only)**

- 44  
45  
46 649 **abc**, abdominal ciliophores;  
47  
48 650 **ac**, anterior commissure;  
49  
50 651 **acf**, anterior ciliated field;  
51  
52 652 **aco**, accessory cilia of the oviduct;  
53  
54 653 **acp**, adhesive ciliary pad;  
55  
56 654 **ag**, auxiliary ganglion;  
57  
58  
59  
60

1  
2  
3  
4  
5  
6  
7  
8  
9  
10  
11  
12  
13  
14  
15  
16  
17  
18  
19  
20  
21  
22  
23  
24  
25  
26  
27  
28  
29  
30  
31  
32  
33  
34  
35  
36  
37  
38  
39  
40  
41  
42  
43  
44  
45  
46  
47  
48  
49  
50  
51  
52  
53  
54  
55  
56  
57  
58  
59  
60

- 655 **alc**, anterior lateral ciliophores;
- 656 **apo**, acetylated  $\alpha$ -tubulin-LI-reactive pharyngeal organ;
- 657 **atpg**, acetylated  $\alpha$ -tubulin-LI-reactive pharyngeal ganglion;
- 658 **bg**, buccal ganglion;
- 659 **br**, brain;
- 660 **cc**, circumesophageal connective;
- 661 **cd1,2**, caudalia 1 and 2;
- 662 **cg**, caudal ganglion;
- 663 **ct**, collecting tubule;
- 664 **dln**, dorso-lateral nerve;
- 665 **dmn**, dorso-median nerve;
- 666 **do1-3**, dorsalia 1 to 3;
- 667 **eg**, epipharyngeal ganglion;
- 668 **egg**, egg;
- 669 **fbp**, FMRF-amide-LI-reactive brain perikarya;
- 670 **fib**, fibularium;
- 671 **fp1-5**, FMRF-amide-LI-reactive perikarya of the pharyngeal ganglion;
- 672 **fs**, FMRF-amide-LI-reactive spot of the pharyngeal ganglion;
- 673 **gg**, geniculate ganglion;
- 674 **gl**, gut lumen;
- 675 **gut**, gut;
- 676 **hc**, head ciliophores;
- 677 **hgr**, head groove;
- 678 **hg**, head gland;
- 679 **jw**, jaw;

- 1  
2  
3  
4 680 **la3-5**, lateralia 3 to 5;  
5  
6 681 **lhg**, lateral head gland;  
7  
8 682 **lm**, longitudinal muscles;  
9  
10 683 **ln**, lateral nerve;  
11  
12 684 **mac**, median anterior ciliophores;  
13  
14 685 **mc**, mouth ciliation;  
15  
16 686 **mg**, mastax ganglion;  
17  
18 687 **mgc**, mastax ganglion connective;  
19  
20 688 **mhg**, median head gland;  
21  
22 689 **mj**, main jaw;  
23  
24 690 **mo**, mouth opening;  
25  
26 691 **mvc**, medio-ventral aciliated cells;  
27  
28 692 **mvm**, median ventral muscle;  
29  
30 693 **mvn**, main ventral nerve;  
31  
32 694 **nmc**, nerve of the mouth ciliation;  
33  
34 695 **np**, neuropil;  
35  
36 696 **npg**, nuclei of the posterior gland;  
37  
38 697 **nph1-2**, nephridia 1 and 2;  
39  
40 698 **ns**, nervous system;  
41  
42 699 **od**, oviduct;  
43  
44 700 **op**, oral plate;  
45  
46 701 **opg**, opening of the posterior gland;  
47  
48 702 **ovp**, ovipore;  
49  
50 703 **pc**, posterior commissure;  
51  
52 704 **pcf**, posterior ciliated field;  
53  
54  
55  
56  
57  
58  
59  
60

1  
2  
3  
4  
5  
6  
7  
8  
9  
10  
11  
12  
13  
14  
15  
16  
17  
18  
19  
20  
21  
22  
23  
24  
25  
26  
27  
28  
29  
30  
31  
32  
33  
34  
35  
36  
37  
38  
39  
40  
41  
42  
43  
44  
45  
46  
47  
48  
49  
50  
51  
52  
53  
54  
55  
56  
57  
58  
59  
60

- 705 **pg**, pharyngeal ganglion;
- 706 **pgl**, posterior gland;
- 707 **phc**, pharyngeal cilia;
- 708 **pns**, peripheral nervous system;
- 709 **pvm**, paramedian ventral muscle;
- 710 **s1-4**, serotonin-LI-reactive perikarya of the pharyngeal ganglion;
- 711 **sbr**, serotonin-LI-reactive brain;
- 712 **sacb**, serotonin-LI-reactive anterior commissure of the brain;
- 713 **sbap**, serotonin-LI-reactive brain antero-lateral nerve projection;
- 714 **sb1-6**, serotonin-LI-reactive perikarya of the brain;
- 715 **sbpp**, serotonin-LI-reactive brain posterior projection;
- 716 **scb**, sensorium cell body;
- 717 **scc**, serotonin-LI-reactive circumesophageal connective;
- 718 **slcb**, serotonin-LI-reactive lateral connective of the commissure of the brain;
- 719 **smcb**, serotonin-LI-reactive median connective of the commissure of the brain;
- 720 **spcb**, serotonin-LI-reactive posterior commissure of the brain;
- 721 **spg**, subpharyngeal ganglion;
- 722 **ss**, sensorium;
- 723 **tlc**, trunk lateral ciliophores;
- 724 **tmc**, trunk median ciliophores;
- 725 **uvmn**, unpaired ventro-median nerve;
- 726 **vg**, vesicular ganglion;
- 727 **vlc**, ventral locomotory ciliophores;
- 728 **vlnc**, ventro-lateral nerve cord;
- 729 **vmn**, ventro-median nerve;

1  
2  
3  
4 730 **vn**; ventral nerve;

5  
6 731 **vs**, visceral nerve;

7  
8 732 **Figure captions**

9  
10  
11 733 **Figure 1: General nervous system of *Limnognathia maerski*. A)** Schematic drawing of the nervous  
12 734 system of *L. maerski*. Structures recognized with DAPI in blue, acetylated  $\alpha$ -tubulin-LI-reactive  
13 735 nervous system in orange/yellow, and locomotory ciliation in light grey. **B-G)** CLSM maximum  
14 736 intensity projection. Acetylated  $\alpha$ -tubulin-LIR color in glow, serotonin-LIR in red, FMRF-amide-LIR  
15 737 in purple and DAPI in cyan. **B)** General overview of the nervous system. Note that some  
16 738 deformation occurred during scanning, resulting in an artefactual elongation of the pharyngeal  
17 739 ganglion **C)** General overview of the serotonin-LI-reactive nervous system **D)** Details of sensoria  
18 740 and peripheral nervous system **E)** Overview of the FMRF-amide-LI-reactive brain and pharyngeal  
19 741 ganglion **F)** Details of the anterior commissure and subpharyngeal ganglion **G)** Details of the  
20 742 posterior commissure. Anterior end of specimens pointing left on all figures. **ac**, anterior  
21 743 commissure; **acp**, adhesive ciliary pad; **ag**, auxiliary ganglion; **apo**, acetylated  $\alpha$ -tubulin-LI-reactive  
22 744 pharyngeal organ; **br**, brain; **cc**, circumesophageal connective; **ct**, collecting tubule; **egg**, egg; **fbp**,  
23 745 FMRF-amide-LI-reactive brain perikarya; **jw**, jaw; **mc**, mouth ciliation; **nmc**, nerve of the mouth  
24 746 ciliation; **np**, neuropil; **nph1-2**, nephridia 1 and 2; **pc**, posterior commissure; **pg**, pharyngeal  
25 747 ganglion **pgl**, posterior gland; **phc**, pharyngeal cilia; **pns**, peripheral nervous system; **sbr**, serotonin-  
26 748 LI-reactive brain; **scb**, sensorium cell body; **spg**, subpharyngeal ganglion; **ss**, sensorium; **vlc**, ventral  
27 749 locomotory ciliophores; **vlnc**, ventro-lateral nerve cord; **vmn**, ventro-median nerve.

28  
29  
30  
31  
32  
33  
34  
35  
36  
37  
38  
39  
40  
41  
42 750 **Figure 2: Profile and details of the nervous system in *Limnognathia maerski*. A)** Schematic  
43 751 drawing of a lateral view of *L. maerski*. Glandular system in blue, nervous system in orange/yellow  
44 752 and ciliation in green. **B-H)** CLSM maximum intensity projections. Acetylated  $\alpha$ -tubulin-LIR in glow,  
45 753 DAPI in cyan, serotonin-LIR in green, and phalloidin in red. **B)** Virtual mid-sagittal section on the  
46 754 midline of the animal. **C-D)** Maximum intensity projection of substacks. **C)** Details of the anterior  
47 755 of the glands of the head. **D)** Details of the posterior of the glands of the head. **E)** Details of the  
48 756 posterior glands. **F)** Details of the acetylated  $\alpha$ -tubulin-LI-reactive brain. **G)** Details of the auxiliary  
49 757 ganglion. **H)** Details of the relative position of the longitudinal nerves and musculature. Anterior  
50 758 end of specimens pointing left on all figures. **acf**, anterior ciliated field; **aco**, accessory cilia of the  
51  
52  
53  
54  
55  
56  
57  
58  
59  
60

1  
2  
3  
4 759 oviduct; **acp**, adhesive ciliary pad; **ag**, auxiliary ganglion; **apo**, acetylated  $\alpha$ -tubulin-LIR-reactive  
5  
6 760 pharyngeal organ; **atpg**, acetylated  $\alpha$ -tubulin-LIR-reactive pharyngeal ganglion; **br**, brain; **cc**,  
7  
8 761 circumesophageal connective; **ct**, collecting tubule; **egg**, egg; **gl**, gut lumen; **gut**, gut; **hg**, head  
9  
10 762 gland; **hgr**, head groove; **jw**, jaw; **lhg**, lateral head gland; **mc**, mouth ciliation; **mhg**, median head  
11  
12 763 gland; **mo**, mouth opening; **mvm**, median ventral muscle; **np**, neuropil; **npg**, nuclei of the posterior  
13  
14 764 gland; **nph1,2**, nephridia 1 and 2; **od**, oviduct; **op**, oral plate; **opg**, opening of the posterior gland;  
15  
16 765 **pc**, posterior commissure; **pcf**, posterior ciliated field; **pg**, pharyngeal ganglion; **pgl**, posterior  
17  
18 766 gland; **phc**, pharyngeal cilia; **pns**, peripheral nervous system; **pvm**, paramedian ventral muscle;  
19  
20 767 **spg**, subpharyngeal ganglion; **ss**, sensorium; **vlc**, ventral locomotory ciliophores; **vlnc**, ventro-  
21  
22 768 lateral nerve cord; **vmn**, ventro-median nerve.

23  
24 769 **Figure 3: Ciliation of *Limnognathia maerski*. A)** Schematic drawing of the ventral locomotory  
25  
26 770 ciliation of *L. maerski*. Ciliation in various colors, nervous system in grey. **B-C)** CLSM maximum  
27  
28 771 intensity projections. **B)** Maximum depth intensity projection of the acetylated  $\alpha$ -tubulin-LIR **C)**  
29  
30 772 Ventral locomotory cell borders as seen with phalloidin in green **D)** Details of the head ciliation as  
31  
32 773 seen with acetylated  $\alpha$ -tubulin-LIR **E)** Details of the trunk ciliation as seen with acetylated  $\alpha$ -  
33  
34 774 tubulin-LIR in glow and DAPI in cyan **F)** Details of the relative position of the pharyngeal cilia as  
35  
36 775 seen with acetylated  $\alpha$ -tubulin-LIR in glow and transmitted light in grey **G)** Details of the head  
37  
38 776 ciliated areas as seen with serotonin-LIR. Anterior end of specimen pointing left for **A)**, and to the  
39  
40 777 top for **B-G)**. **abc**, abdominal ciliophores; **acf**, anterior ciliated field; **acp**, adhesive ciliary pad; **alc**,  
41  
42 778 anterior lateral ciliophores **ct**, collecting tubule; **cd1,2**, caudalia 1 and 2; **do1-3**, dorsalia 1 to 3; **fib**,  
43  
44 779 fibularium; **hc**, head ciliophores; **hgr**, head groove; **jw**, jaw; **la3-5**, lateralia 3 to 5; **lm**, longitudinal  
45  
46 780 muscles; **mac**, median anterior ciliophores; **mc**, mouth ciliation; **mj**, main jaw; **mo**, mouth opening;  
47  
48 781 **mvc**, medio-ventral aciliated cells; **nmc**, nerves of the mouth ciliation; **nph1,2**, nephridia 1 and 2;  
49  
50 782 **ns**, nervous system; **od**, oviduct; **op**, oral plate; **ovp**, ovipore; **pcf**, posterior ciliated field; **pgl**,  
51  
52 783 posterior gland; **phc**, pharyngeal cilia; **ss**, sensorium; **tlc**, trunk lateral ciliophores; **tmc**, trunk  
53  
54 784 median ciliophores; **vlc**, ventral locomotory ciliophores.

55  
56 785 **Figure 4: Details of the pharyngeal ganglion and the serotonergic brain of *Limnognathia maerski*.**  
57  
58 786 **A,G)** Schematic drawings with acetylated  $\alpha$ -tubulin-LIR in yellow, FMRF-amide-LIR in purple, DAPI  
59  
60 787 in blue and serotonin-LIR in green. **B-F** and **H,I)** CLSM maximum intensity projection with

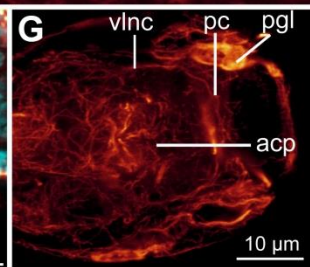
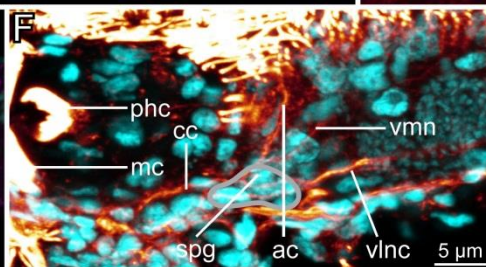
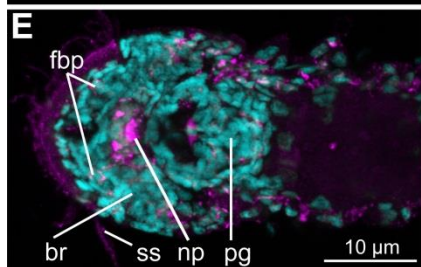
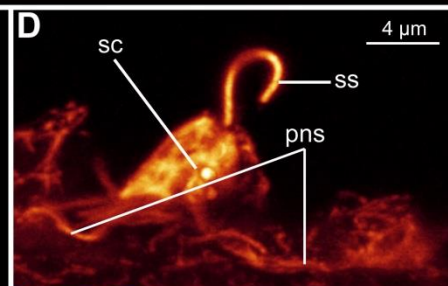
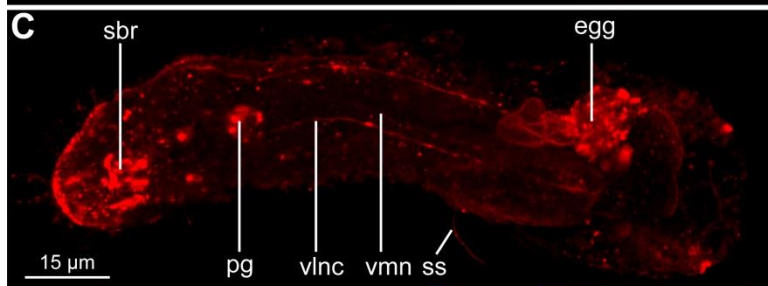
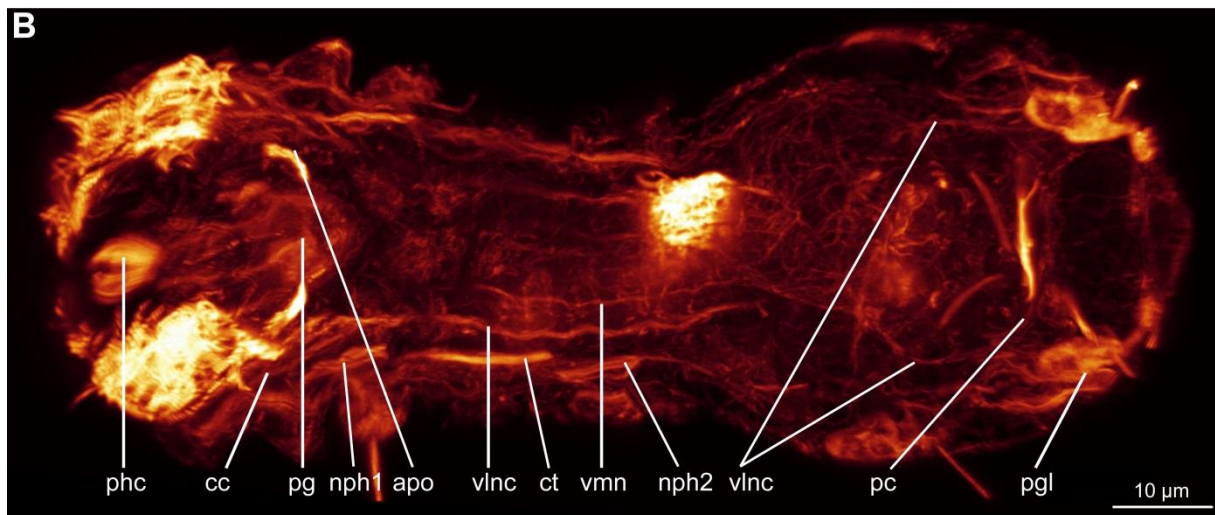
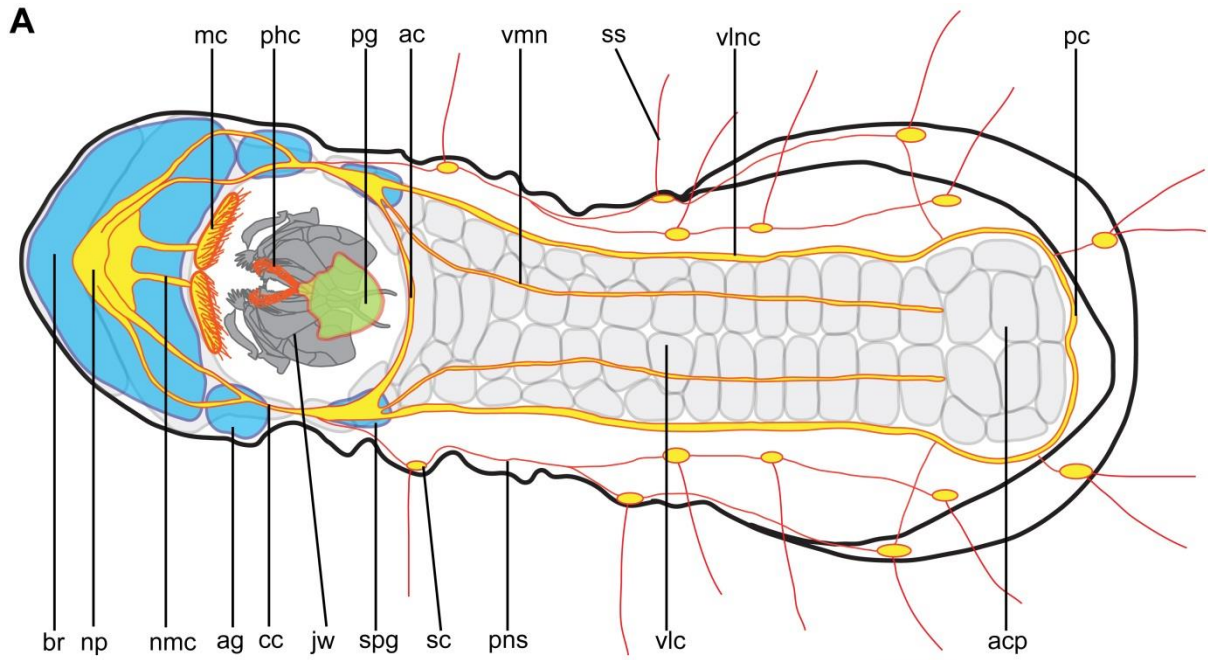
1  
2  
3  
4 788 acetylated  $\alpha$ -tubulin-LIR in yellow, FRMF-amide-LIR in purple, DAPI in cyan, and serotonin-LIR in  
5  
6 789 green in **B**) and in glow in **H**) and **I**). **A**) Schematic drawing of the pharyngeal ganglion **B**) Details of  
7  
8 790 the serotonergic-LIR of the pharyngeal ganglion. **C**) Overview of the acetylated  $\alpha$ -tubulin-LIR of the  
9  
10 791 pharyngeal ganglion **D, E, F**) Successive substacks of the ventral, median and dorsal sections of the  
11  
12 792 pharyngeal ganglion as seen with FMRF-amide-LIR **G**) Schematic drawing of the serotonergic brain  
13  
14 793 **H**) Details of the serotonin-LI-reactive brain **I**) Overview of the serotonin-LI-reactive brain. Anterior  
15  
16 794 end of specimens pointing to the top on all figures. **apo**, acetylated  $\alpha$ -tubulin-LI-reactive  
17  
18 795 pharyngeal organ; **atpg**, acetylated  $\alpha$ -tubulin-LI-reactive pharyngeal ganglion; **br**, brain; **fp1-5**,  
19  
20 796 FMRF-amide-LI-reactive perikarya of the pharyngeal ganglion; **fs**, FMRF-amide-LI-reactive spot of  
21  
22 797 the pharyngeal ganglion; **phc**, pharyngeal cilia; **s1-4**, serotonin-LI-reactive perikarya of the  
23  
24 798 pharyngeal ganglion; **sacb**, serotonin-LI-reactive anterior commissure of the brain; **sb1-6**,  
25  
26 799 serotonin-LI-reactive perikarya of the brain; **sbap**, serotonin-LI-reactive brain antero-lateral nerve  
27  
28 800 projection; **sbpp**, serotonin-LI-reactive brain posterior projection; **scc**, serotonin-LI-reactive  
29  
30 801 circumesophageal connective; **slcb**, serotonin-LI-reactive lateral connective of the commissure of  
31  
32 802 the brain; **smcb**, serotonin-LI-reactive median connective of the commissure of the brain; **spcb**,  
33  
34 803 serotonin-LI-reactive posterior commissure of the brain.

35  
36  
37  
38  
39  
40  
41  
42  
43  
44  
45  
46  
47  
48  
49  
50  
51  
52  
53  
54  
55  
56  
57  
58  
59  
60

804 **Figure 5: Comparison of the nervous system of Gnathifera.** Schematic drawing of the dorsal view  
805 of the nervous system of three Gnathifera. Different colors represent parts of the nervous system  
806 that may be homologous between the different animals, but see the text for a full discussion. Grey  
807 structures are parts of the nervous system that cannot be homologized. Anterior end pointing left  
808 on all figures. **A**) Micrognathozoa: *Limnognathia maerski*, **B**) Rotifera, Monogononta, modified  
809 from Remane 1933 [35], **C**) Gnathostomulida: *Gnathostomula peregrina*, modified from Müller  
810 and Sterrer, 2004 [10]. **ac**, anterior commissure; **ag**, auxiliary ganglion; **br**, brain; **bg**, buccal  
811 ganglion; **cc**, circumesophageal connective; **cg**, caudal ganglion; **dln**, dorso-lateral nerve; **dmn**,  
812 dorso-median nerve; **eg**, epipharyngeal ganglion; **gg**, geniculate ganglion; **ln**, lateral nerve; **mg**,  
813 mastax ganglion; **mgc**, mastax ganglion connective; **mvn**, main ventral nerve; **pc**, posterior  
814 commissure; **pg**, pharyngeal ganglion, **pns**, peripheral nervous system; **spg**, subpharyngeal  
815 ganglion; **uvmn**, unpaired ventro-median nerve; **vg**, vesicular ganglion; **vlnc**, ventro-lateral nerve  
816 cord; **vmn**, ventro-median nerve; **vn**, ventral nerve; **vs**, visceral nerve.

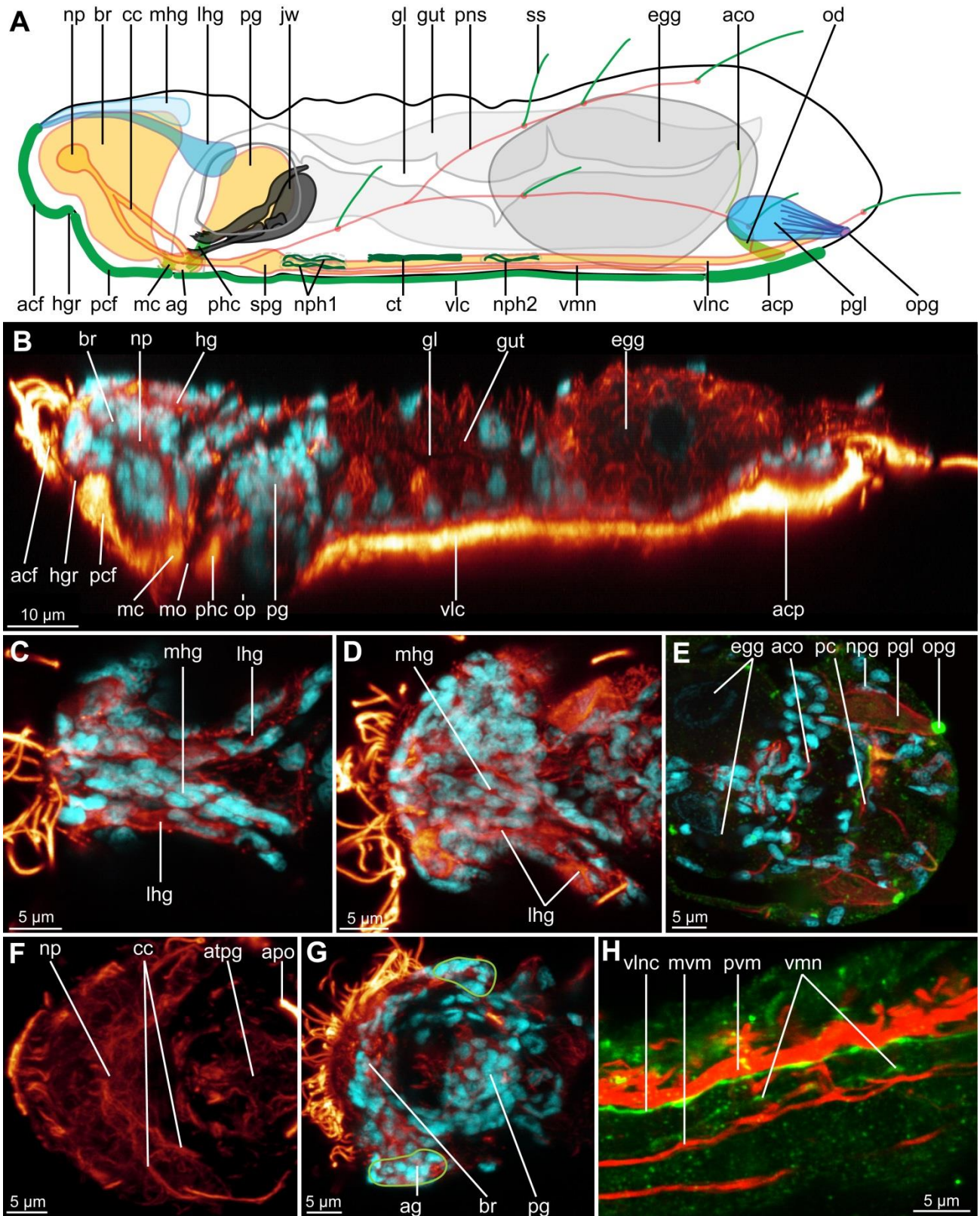
**Figure 1: General nervous system of *Limnognathia maerski*.** **A)** Schematic drawing of the nervous system of *L. maerski*. Structures recognized with DAPI in blue, acetylated  $\alpha$ -tubulin-LI-reactive nervous system in orange/yellow, and locomotory ciliation in light grey. **B-G)** CLSM maximum intensity projection. Acetylated  $\alpha$ -tubulin-LIR color in glow, serotonin-LIR in red, FMRF-amide-LIR in purple and DAPI in cyan. **B)** General overview of the nervous system. Note that some deformation occurred during scanning, resulting in an artefactual elongation of the pharyngeal ganglion **C)** General overview of the serotonin-LI-reactive nervous system **D)** Details of sensoria and peripheral nervous system **E)** Overview of the FMRF-amide-LI-reactive brain and pharyngeal ganglion **F)** Details of the anterior commissure and subpharyngeal ganglion **G)** Details of the posterior commissure. Anterior end of specimens pointing left on all figures. **ac**, anterior commissure; **acp**, adhesive ciliary pad; **ag**, auxiliary ganglion; **apo**, acetylated  $\alpha$ -tubulin-LI-reactive pharyngeal organ; **br**, brain; **cc**, circumesophageal connective; **ct**, collecting tubule; **egg**, egg; **fbp**, FMRF-amide-LI-reactive brain perikarya; **jw**, jaw; **mc**, mouth ciliation; **nmc**, nerve of the mouth ciliation; **np**, neuropil; **nph1-2**, nephridia 1 and 2; **pc**, posterior commissure; **pg**, pharyngeal ganglion **pgl**, posterior gland; **phc**, pharyngeal cilia; **pns**, peripheral nervous system; **sbr**, serotonin-LI-reactive brain; **scb**, sensorium cell body; **spg**, subpharyngeal ganglion; **ss**, sensorium; **vlc**, ventral locomotory ciliophores; **vlnc**, ventro-lateral nerve cord; **vmn**, ventro-median nerve.

Figure 1



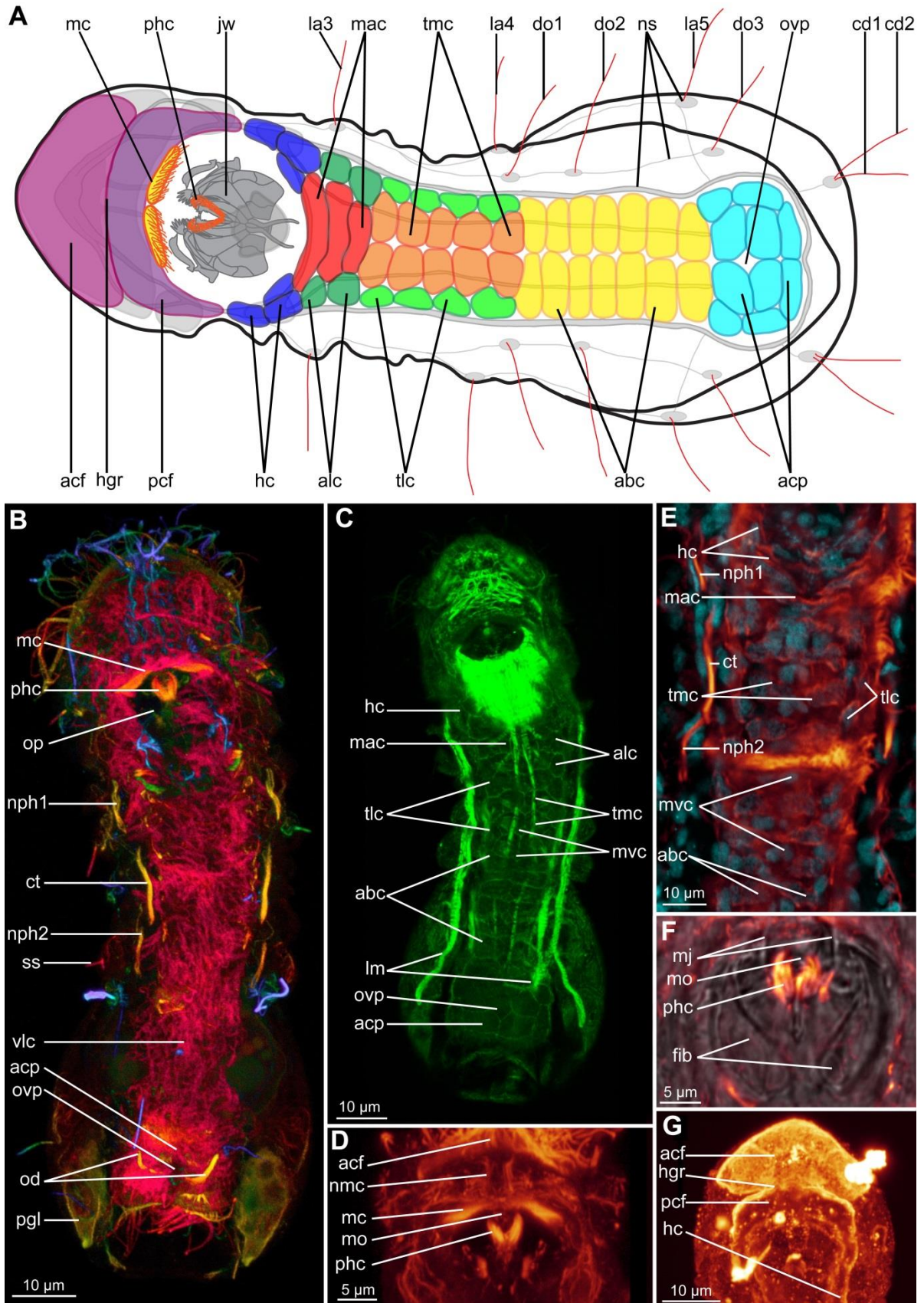
**Figure 2: Profile and details of the nervous system in *Limnognathia maerski*.** **A)** Schematic drawing of a lateral view of *L. maerski*. Glandular system in blue, nervous system in orange/yellow and ciliation in green. **B-H)** CLSM maximum intensity projections. Acetylated  $\alpha$ -tubulin-LIR in glow, DAPI in cyan, serotonin-LIR in green, and phalloidin in red. **B)** Virtual mid-sagittal section on the midline of the animal. **C-D)** Maximum intensity projection of substacks. **C)** Details of the anterior of the glands of the head. **D)** Details of the posterior of the glands of the head. **E)** Details of the posterior glands. **F)** Details of the acetylated  $\alpha$ -tubulin-LI-reactive brain. **G)** Details of the auxiliary ganglion. **H)** Details of the relative position of the longitudinal nerves and musculature. Anterior end of specimens pointing left on all figures. **acf**, anterior ciliated field; **aco**, accessory cilia of the oviduct; **acp**, adhesive ciliary pad; **ag**, auxiliary ganglion; **apo**, acetylated  $\alpha$ -tubulin-LI-reactive pharyngeal organ; **atpg**, acetylated  $\alpha$ -tubulin-LI-reactive pharyngeal ganglion; **br**, brain; **cc**, circumesophageal connective; **ct**, collecting tubule; **egg**, egg; **gl**, gut lumen; **gut**, gut; **hg**, head gland; **hgr**, head groove; **jw**, jaw; **lhg**, lateral head gland; **mc**, mouth ciliation; **mhg**, median head gland; **mo**, mouth opening; **mvm**, median ventral muscle; **np**, neuropil; **npg**, nuclei of the posterior gland; **nph1,2**, nephridia 1 and 2; **od**, oviduct; **op**, oral plate; **opg**, opening of the posterior gland; **pc**, posterior commissure; **pcf**, posterior ciliated field; **pg**, pharyngeal ganglion; **pgl**, posterior gland; **phc**, pharyngeal cilia; **pns**, peripheral nervous system; **pvm**, paramedian ventral muscle; **spg**, subpharyngeal ganglion; **ss**, sensorium; **vlc**, ventral locomotory ciliophores; **vlnc**, ventro-lateral nerve cord; **vmn**, ventro-median nerve.

**Figure 2**



**Figure 3: Ciliation of *Limnognathia maerski*.** **A)** Schematic drawing of the ventral locomotory ciliation of *L. maerski*. Ciliation in various colors, nervous system in grey. **B-C)** CLSM maximum intensity projections. **B)** Maximum depth intensity projection of the acetylated  $\alpha$ -tubulin-LIR **C)** Ventral locomotory cell borders as seen with phalloidin in green **D)** Details of the head ciliation as seen with acetylated  $\alpha$ -tubulin-LIR **E)** Details of the trunk ciliation as seen with acetylated  $\alpha$ -tubulin-LIR in glow and DAPI in cyan **F)** Details of the relative position of the pharyngeal cilia as seen with acetylated  $\alpha$ -tubulin-LIR in glow and transmitted light in grey **G)** Details of the head ciliated areas as seen with serotonin-LIR. Anterior end of specimen pointing left for **A)**, and to the top for **B-G)**. **abc**, abdominal ciliophores; **acf**, anterior ciliated field; **acp**, adhesive ciliary pad; **alc**, anterior lateral ciliophores **ct**, collecting tubule; **cd1,2**, caudalia 1 and 2; **do1-3**, dorsalia 1 to 3; **fib**, fibularium; **hc**, head ciliophores; **hgr**, head groove; **jw**, jaw; **la3-5**, lateralialia 3 to 5; **lm**, longitudinal muscles; **mac**, median anterior ciliophores; **mc**, mouth ciliation; **mj**, main jaw; **mo**, mouth opening; **mvc**, medio-ventral aciliated cells; **nmc**, nerves of the mouth ciliation; **nph1,2**, nephridia 1 and 2; **ns**, nervous system; **od**, oviduct; **op**, oral plate; **ovp**, ovipore; **pcf**, posterior ciliated field; **pgl**, posterior gland; **phc**, pharyngeal cilia; **ss**, sensorium; **tlc**, trunk lateral ciliophores; **tmc**, trunk median ciliophores; **vlc**, ventral locomotory ciliophores.

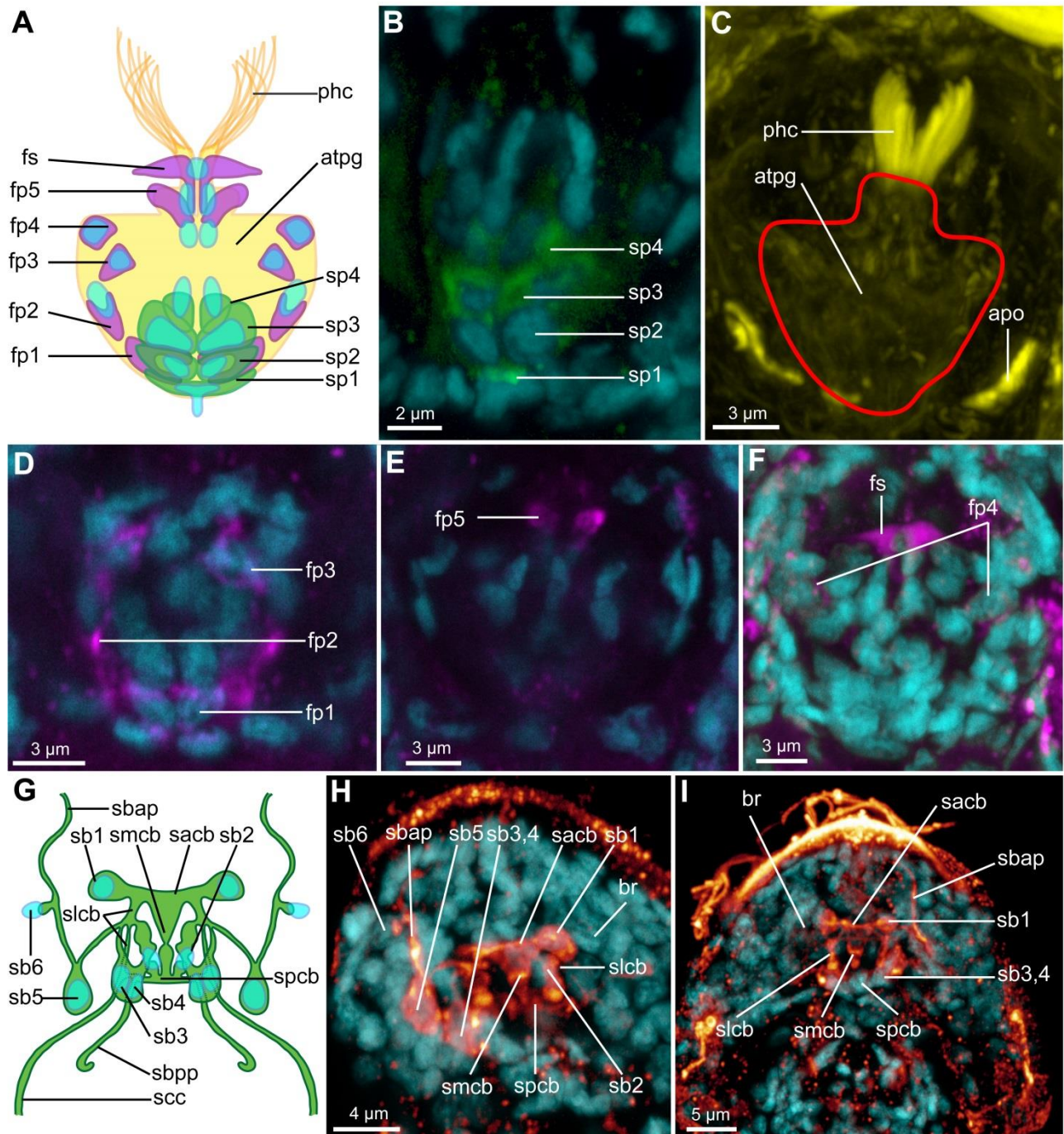
**Figure 3**



**Figure 4: Details of the pharyngeal ganglion and the serotonergic brain of *Limnognathia maerski*.**

**A,G)** Schematic drawings with acetylated  $\alpha$ -tubulin-LIR in yellow, FMRF-amide-LIR in purple, DAPI in blue and serotonin-LIR in green. **B-F and H,I)** CLSM maximum intensity projection with acetylated  $\alpha$ -tubulin-LIR in yellow, FMRF-amide-LIR in purple, DAPI in cyan, and serotonin-LIR in green in **B)** and in glow in **H)** and **I)**. **A)** Schematic drawing of the pharyngeal ganglion **B)** Details of the serotonergic-LIR of the pharyngeal ganglion. **C)** Overview of the acetylated  $\alpha$ -tubulin-LIR of the pharyngeal ganglion **D, E, F)** Successive substacks of the ventral, median and dorsal sections of the pharyngeal ganglion as seen with FMRF-amide-LIR **G)** Schematic drawing of the serotonergic brain **H)** Details of the serotonin-LI-reactive brain **I)** Overview of the serotonin-LI-reactive brain. Anterior end of specimens pointing to the top on all figures. **apo**, acetylated  $\alpha$ -tubulin-LI-reactive pharyngeal organ; **atpg**, acetylated  $\alpha$ -tubulin-LI-reactive pharyngeal ganglion; **br**, brain; **fp1-5**, FMRF-amide-LI-reactive perikarya of the pharyngeal ganglion; **fs**, FMRF-amide-LI-reactive spot of the pharyngeal ganglion; **phc**, pharyngeal cilia; **s1-4**, serotonin-LI-reactive perikarya of the pharyngeal ganglion; **sacb**, serotonin-LI-reactive anterior commissure of the brain; **sb1-6**, serotonin-LI-reactive perikarya of the brain; **sbap**, serotonin-LI-reactive brain antero-lateral nerve projection; **sbpp**, serotonin-LI-reactive brain posterior projection; **scc**, serotonin-LI-reactive circumesophageal connective; **slcb**, serotonin-LI-reactive lateral connective of the commissure of the brain; **smcb**, serotonin-LI-reactive median connective of the commissure of the brain; **spcb**, serotonin-LI-reactive posterior commissure of the brain.

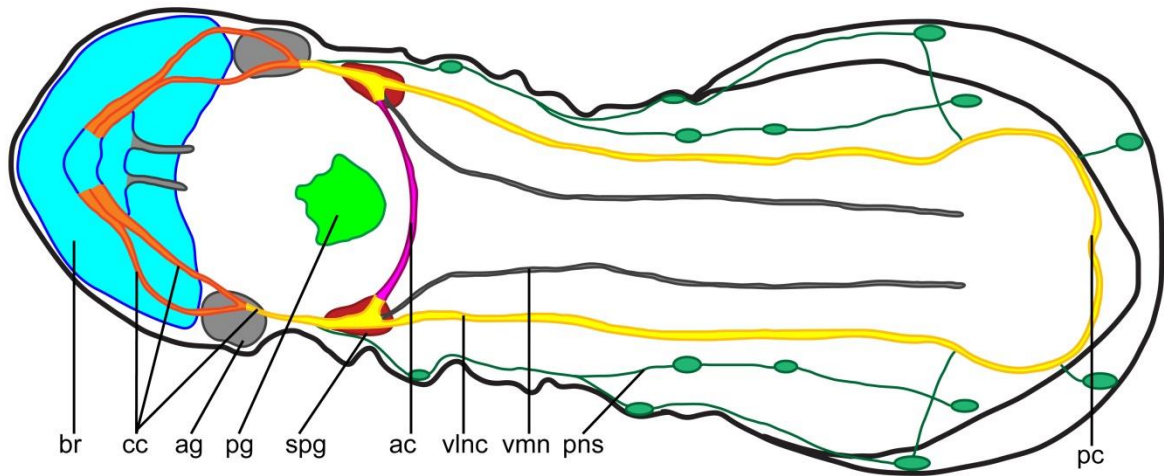
**Figure 4**



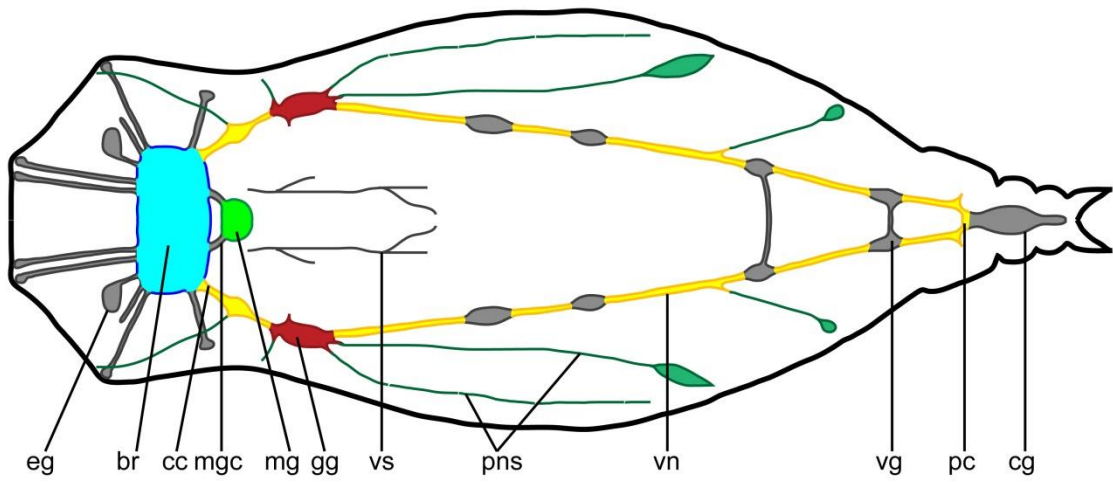
**Figure 5: Comparison of the nervous system of Gnathifera.** Schematic drawing of the dorsal view of the nervous system of three Gnathifera. Different colors represent parts of the nervous system that may be homologous between the different animals, but see the text for a full discussion. Grey structures are parts of the nervous system that cannot be homologized. Anterior end pointing left on all figures. **A)** Micrognathozoa: *Limnognathia maerski*, **B)** Rotifera, Monogononta, modified from Remane 1933 [35], **C)** Gnathostomulida: *Gnathostomula peregrina*, modified from Müller and Sterrer, 2004 [10]. **ac**, anterior commissure; **ag**, auxiliary ganglion; **br**, brain; **bg**, buccal ganglion; **cc**, circumesophageal connective; **cg**, caudal ganglion; **dln**, dorso-lateral nerve; **dmn**, dorso-median nerve; **eg**, epipharyngeal ganglion; **gg**, geniculate ganglion; **ln**, lateral nerve; **mg**, mastax ganglion; **mgc**, mastax ganglion connective; **mvn**, main ventral nerve; **pc**, posterior commissure; **pg**, pharyngeal ganglion, **pns**, peripheral nervous system; **spg**, subpharyngeal ganglion; **uvmn**, unpaired ventro-median nerve; **vg**, vesicular ganglion; **vlnc**, ventro-lateral nerve cord; **vmn**, ventro-median nerve; **vn**, ventral nerve; **vs**, visceral nerve.

Figure 5

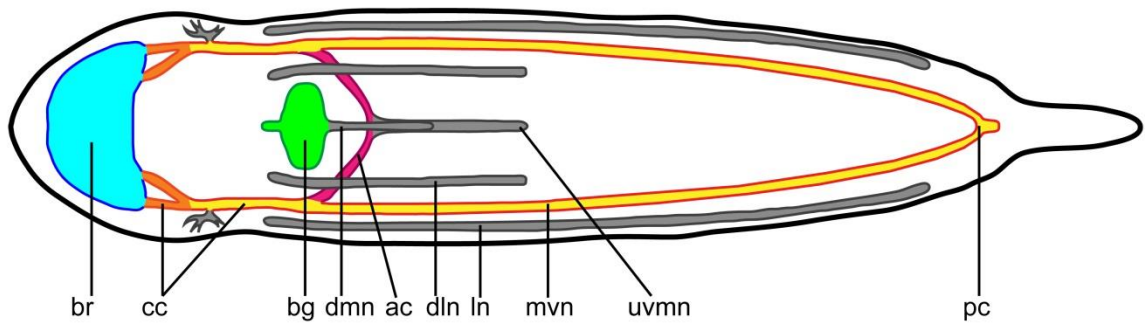
**A:** Micrognathozoa



**B:** Rotifera



**C:** Gnathostomulida





**Manuscript V:**

**Neuromuscular study of early branching *Diuronotus aspetos* (Paucitubulatina) gives insight on the evolution of organs system within Gastrotricha**

Bekkouche N., and Worsaae, K.

Submitted to Zoological Letters



## Zoological Letters

### Neuromuscular study of early branching *Diuronotus aspetos* (Paucitubulatina) gives insight on the evolution of organs systems within Gastrotricha

--Manuscript Draft--

<b>Manuscript Number:</b>			
<b>Full Title:</b>	Neuromuscular study of early branching <i>Diuronotus aspetos</i> (Paucitubulatina) gives insight on the evolution of organs systems within Gastrotricha		
<b>Article Type:</b>	Research article		
<b>Funding Information:</b>	<table border="1" style="width: 100%;"> <tr> <td style="width: 60%;">Villum fundation (102544)</td> <td>Dr Katrine Worsaae</td> </tr> </table>	Villum fundation (102544)	Dr Katrine Worsaae
Villum fundation (102544)	Dr Katrine Worsaae		
<b>Abstract:</b>	<p><b>Background:</b> <i>Diuronotus</i> is one of the latest described genera of Paucitubulatina, constituting one of the three major clades in Gastrotricha. Morphology suggests that <i>Diuronotus</i> is an early branch of Paucitubulatina, making it a key taxon to understand the evolution of this morphologically understudied group. Here we test its phylogenetic position employing molecular data and Bayesian inference, and provide detailed description of the muscular, nervous, and ciliary systems of <i>Diuronotus aspetos</i>, using immunohistochemistry and confocal laser scanning microscopy.</p> <p><b>Results:</b> We confirm its proposed position within Muselliferidae, and find this family sister group to Xenotrichulidae. The muscular system revealed with F-actin staining shows a simple, though singular, organization of the trunk musculature with a reduction to three pairs of longitudinal muscles and addition of up to five paired longitudinal rows of dorso-ventral muscles versus the six longitudinal and two dorso-ventral pairs, found in most Paucitubulatina. The pharynx is for the first time described in details with acetylated <math>\alpha</math>-tubulin immunoreactivity, including different nerves, two pairs of sensory cilia, paired anterior glands, and a unique canal system of unknown function. The central nervous system revealed with acetylated <math>\alpha</math>-tubulin, serotonin and FMRF-amide-like immunoreactivity is in overall similar to other Gastrotricha, but additionally exposes an anterior nerve ring, several anterior longitudinal nerves, and four ventral commissures (pharyngeal, trunk, pre-anal, and terminal). High-resolution imaging made it possible to trace innervations of ciliary structures and muscles, revealing new functional information of specific nerves. Two pairs of protonephridia are documented, while other Paucitubulatina have one. Moreover, the precise arrangement of multiciliated cells is unraveled, yielding a pattern of possibly systematic importance.</p> <p><b>Conclusion:</b> several neural structures resemble those found in Xenotrichula (Xenotrichulidae), and may turn out to represent paucitubulatinan or even gastrotrich apomorphies. However, in order to trace the character evolution, detailed morphological studies on additional Paucitubulatina as well as a robust gastrotrich phylogeny are necessary. Yet, the present study offers new inputs on the evolution of organ systems and so far neglected characters in Gastrotricha.</p> <p><b>Keywords</b></p>		
<b>Corresponding Author:</b>	Katrine Worsaae, PhD University of Copenhagen Copenhagen, DENMARK		
<b>Corresponding Author Secondary Information:</b>			
<b>Corresponding Author's Institution:</b>	University of Copenhagen		
<b>Corresponding Author's Secondary Institution:</b>			
<b>First Author:</b>	Nicolas Bekkouche		
<b>First Author Secondary Information:</b>			
<b>Order of Authors:</b>	Nicolas Bekkouche Katrine Worsaae, PhD		
<b>Order of Authors Secondary Information:</b>			

[Click here to view linked References](#)

1  
2 1 Neuromuscular study of early branching *Diuronotus*  
3  
4  
5  
6  
7 2 *aspetos* (Paucitubulatina) gives insight on the  
8  
9  
10  
11 3 evolution of organs system within Gastrotricha  
12  
13  
14  
15

16 4 Nicolas Bekkouche<sup>1</sup> and Katrine Worsaae<sup>1</sup>  
17  
18

19  
20 5 Marine Biological Section, Department of Biology, University of Copenhagen, Universitetsparken 4,  
21  
22 6 2100 Copenhagen Ø, Denmark  
23  
24

25  
26 7 Corresponding author: [kworsaae@bio.ku.dk](mailto:kworsaae@bio.ku.dk), +4541230073  
27  
28

29 8  
30  
31

32  
33 9  
34  
35

36 10  
37  
38

39  
40 11  
41  
42

43 12  
44  
45

46  
47 13  
48  
49

50 14  
51  
52

53  
54 15  
55  
56

57 16  
58  
59  
60  
61  
62  
63  
64  
65

# Abstract

**Background:** *Diuronotus* is one of the latest described genera of Paucitubulatina, constituting one of the three major clades in Gastrotricha. Morphology suggests that *Diuronotus* is an early branch of Paucitubulatina, making it a key taxon to understand the evolution of this morphologically understudied group. Here we test its phylogenetic position employing molecular data and Bayesian inference, and provide detailed description of the muscular, nervous, and ciliary systems of *Diuronotus aspetos*, using immunohistochemistry and confocal laser scanning microscopy.

**Results:** We confirm its proposed position within Muselliferidae, and find this family sister group to Xenotrichulidae. The muscular system revealed with F-actin staining shows a simple, though singular, organization of the trunk musculature with a reduction to three pairs of longitudinal muscles and addition of up to five paired longitudinal rows of dorso-ventral muscles versus the six longitudinal and two dorso-ventral pairs, found in most Paucitubulatina. The pharynx is for the first time described in details with acetylated  $\alpha$ -tubulin immunoreactivity, including different nerves, two pairs of sensory cilia, paired anterior glands, and a unique canal system of unknown function. The central nervous system revealed with acetylated  $\alpha$ -tubulin, serotonin and FMRF-amide-like immunoreactivity is in overall similar to other Gastrotricha, but additionally exposes an anterior nerve ring, several anterior longitudinal nerves, and four ventral commissures (pharyngeal, trunk, pre-anal, and terminal). High-resolution imaging made it possible to trace innervations of ciliary structures and muscles, revealing new functional information of specific nerves. Two pairs of protonephridia are documented, while other Paucitubulatina have one. Moreover, the precise arrangement of multiciliated cells is unraveled, yielding a pattern of possibly systematic importance.

139 **Conclusion:** several neural structures resemble those found in *Xenotrichula* (Xenotrichulidae), and  
2  
3  
40 may turn out to represent paucitubulatinan or even gastrotrich apomorphies. However, in order  
5  
641 to trace the character evolution, detailed morphological studies on additional Paucitubulatina as  
7  
8  
942 well as a robust gastrotrich phylogeny are necessary. Yet, the present study offers new inputs on  
10  
11  
1243 the evolution of organ systems and so far neglected characters in Gastrotricha.

## 15 Keywords

17  
18  
19  
2045 Neurobiology, meiofauna, Chaetonotida, DNA, phalloidin, *Musellifer*.

## 2446 Background

27  
28  
2947 Gastrotricha are small, often sub-millimetric, interstitial worms, ubiquitously found in most  
30  
31  
3248 aquatic environments with a long debated phylogenetic position [1-3]. They were first considered  
33  
3449 closely related to various meiofaunal, protostome groups such as rotifers (Trochelminthes [4]),  
35  
36  
3750 kinorhynchs (Nematorhyncha [5]) or Gnathostomulida (Neotrichozoa [6, 7]). Later, molecular  
38  
3951 phylogenies placed them within Spiralia with uncertain affinities; within the debated group  
40  
41  
4252 Platyzoa, comprising Gastrotricha, Platyhelminthes and Gnathifera [1, 8, 9]. Recent phylogenomic  
43  
44  
4553 studies propose a sister group relationship between Platyhelminthes and Gastrotricha [3, 10].  
46  
4754 However, the controversy over the phylogenetic position of Gastrotricha masks other problems  
48  
49  
5055 existing within the group. Indeed, compared to the diversity and omnipresence of these animals,  
51  
5256 relatively few phylogenetic and detailed morphological studies have been conducted on this group  
53  
54  
5557 and the evolution of, e.g., nervous system, muscular system and nephridia is unresolved [11-13].  
56  
5758 Also, the diversity is still largely unexplored, exemplified by the recent erection of the family  
58  
59  
60  
61  
62  
63  
64  
65

159 Hummondasyidae (Macrodasysida) in 2014 [14] as well as the genera *Thaidasys* in 2015 [15] and  
2  
3  
40 *Bifidochaetus* in 2016 [16].

5  
6  
761 *Diuronotus* [17] is another recently described gastrotrich genus (2005), comprising two described  
8  
9  
1062 species: *Diuronotus aspetos* Todaro, Balsamo, and Kristensen, 2005 [17] (Fig. 1) and, *Diuronotus*  
11  
1263 *rupperti* Todaro, Balsamo, and Kristensen, 2005 [17], and one undescribed species *Diuronotus* sp.  
13  
14  
1564 [18-20], transferred from *Halichaetonotus* [17]. They are all found in marine interstitial  
16  
1765 environments of the North Atlantic; *D. aspetos* from Greenland [17] and Germany [2, 21], *D.*  
18  
19  
2066 *rupperti* from Denmark [17] and *Diuronotus* sp. from North Carolina, USA [18]. *Diuronotus* was  
21  
22  
2367 placed in Muselliferidae (Paucitubulatina, Chaetonitida) next to *Musellifer* [22] with which it  
24  
2568 shares the presence of a ciliated so-called ‘muzzle’ (or snout) and specific ultrastructural traits of  
26  
27  
2869 scales and sperm [23].

29  
30  
3170 Gastrotricha are divided into two main taxa: the supposedly monophyletic Macrodasysida and the  
32  
33  
3471 possibly paraphyletic Chaetonotida, divided further into the Multitubulatina, (consisting of one  
35  
3672 genus, *Neodasys*, and possessing multiple adhesive glands) and the diverse Paucitubulatina  
37  
38  
3973 (possessing generally only two adhesive tubes) [24]. Muselliferidae, belonging to Paucitubulatina,  
40  
41  
4274 is the possible sister group to all remaining Paucitubulatina according to morphological [22, 25]  
43  
4475 and molecular [26, 27] studies. However, Paps and Riutorts (2012) [28] find an alternative  
45  
46  
4776 topology with Xenotrichulidae positioned as sister group of the remaining Paucitubulatina, and  
48  
49  
5077 Muselliferidae being the sister group to Chaetonotidae. Kieneke et al. (2008) [29] find  
51  
5278 Proichthyidiidae as sister group to the remaining Paucitubulatina, and Muselliferidae forming a  
53  
54  
5579 clade together with Xenotrichulidae sister group to other Paucitubulatina. Nonetheless, these  
56  
5780 different topologies overall suggest a key position of Muselliferidae within Gastrotricha,  
58  
59  
60  
61  
62  
63  
64  
65

181 emphasizing the importance of this family for understanding of the evolution of Gastrotricha.  
2  
3  
482 Indeed, some features of Muselliferidae, namely the marine habitat and the well-developed  
5  
683 hermaphroditism are supposed to be plesiomorphic character traits of Chaetonotida. Yet, detailed  
7  
8  
984 morphological studies on this family are still lacking, most likely due to the paucity of these  
10  
11  
1285 animals and their late discovery [26, 30].  
13  
14

1586 Recently, a series of papers employing confocal laser scanning microscopy (CLSM) described the  
16  
1787 detailed muscular arrangement of several Paucitubulatina, namely *Musellifer* [22], Xenotrichulidae  
18  
19  
2088 [22, 31], Chaetonotidae [22, 32], and Dasydytidae [11, 33], and notably, the helicoidal  
21  
22  
2389 musculature, proposed to be a gastrotrich synapomorphy [34]. These recent works were used to  
24  
2590 infer the plesiomorphic arrangement of the musculature of Gastrotricha as constituted by two  
26  
27  
2891 ventro-lateral longitudinal muscles surrounded by outer circular muscles, and longitudinal  
29  
30  
3192 splanchnic muscles surrounded by helicoidal and intestinal circular muscles [2]. In Paucitubulatina,  
32  
3393 the longitudinal muscles appear to be more numerous, and the outer circular muscles, if present,  
34  
35  
3694 are incomplete and consist of dorso-ventral muscles [2]. These dorso-ventral or semi-circular  
37  
3895 muscles are found in marine chaetonotids [22], but are often missing or highly reduced in  
39  
40  
4196 freshwater chaetonotids [11, 22, 33] emphasizing the importance of studying the marine  
42  
4397 *Diuronotus* in order to resolve their evolution and contribute to the broader understanding of  
44  
45  
4698 muscular evolution within Gastrotricha.  
47  
48

4999 To date, only one confocal study on *Xenotrichula* describes the nervous system of a member of  
50  
51  
52100 Paucitubulatina in detail [12], while it has been extensively described for Multitubulatina  
53  
54  
55101 (*Neodasys*) [13] and in several Macrodasyida with combined immunohistochemistry and CLSM  
56  
57102 (e.g., [35, 36]), or transmission electron microscopy (TEM) [37]. One of the conclusions of the  
58  
59  
60  
61  
62  
63  
64  
65

103 *Xenotrichula* study [13] is the low structural variation of the nervous system within Gastrotricha,  
2  
3  
104 always comprising a bilobed brain with a ventral commissure, a pair of anteriorly projecting  
4  
5  
105 longitudinal nerves, a pair of ventro-lateral nerve cords along the trunk, and a terminal  
6  
7  
8  
106 commissure. These features were also interpreted as ancestral conditions of Gastrotricha in  
9  
10  
11  
107 Kieneke and Schmidt-Rhaesa (2015) [2, 12]. Yet, only one Paucitubulatina, *Xenotrichula*, was  
12  
13  
108 considered for this state reconstruction. Moreover, substantial variation exists, such as the  
14  
15  
16  
109 presence of an additional ventral nerve in *Oregodasys cirratus* Rothe & Schmidt-Rhaesa, 2010 [38]  
17  
18  
19  
110 and dorsal nerves in *Xenodasys riedli* (Schöpfer-Sterrerr, 1969) [39, 40], or additional trunk  
20  
21  
22  
111 commissures in *Dactylopodola* and *Oregodasys cirratus*. These studies underline the unexplored  
23  
24  
112 diversity of gastrotrich nervous systems, which may especially concern the diverse group of  
25  
26  
27  
113 Paucitubulatina, with only one study on the nervous system so far [13] and a total lack of data on  
28  
29  
114 Muselliferidae.  
30  
31  
32

33  
34  
35  
115 Several studies have described the ultrastructure and repartition of protonephridia in  
36  
37  
38  
116 Gastrotricha, with a few of them addressing species of Paucitubulatina [41, 42]. Members of  
39  
40  
41  
117 Paucitubulatina are suggested to always possess one pair of trunk protonephridia [41], although  
42  
43  
44  
118 again, data on Muselliferidae are lacking. Each nephridium was found to encompass two  
45  
46  
47  
119 monociliated terminal cells with coaxial cilia, a long canal cell, and a nephridopore cell [2].  
48  
49  
50

51  
52  
53  
120 In order to enhance our understanding of the evolution of major organ systems within  
54  
55  
56  
121 Gastrotricha we acquired new morphological data on *Diuronotus aspetos*, using CLSM techniques  
57  
58  
59  
122 and immunohistochemistry to describe its arrangement of the musculature, nervous system, and  
60  
61  
62  
123 ciliation in detail. To assess the previously proposed relationship of *D. aspetos* within  
63  
64  
65  
124 Muselliferidae, we analysed the phylogenetic position within Chaetonotida, using molecular data.  
66

125 In this phylogenetic context, the morphology of *Diuronotus* and possible homologies are  
2  
3  
126 compared and discussed relative to other Chaetonotida, and Gastrotricha in general.  
4  
5

## 6 7 **Material and methods** 8

### 9 10 11 12 **Collecting** 13

14  
15  
16 For *Diuronotus aspetos*, the samples were taken with a mini van Veen grab from shallow water (3-  
17  
18 6 m water depth) of Flakkerhuk (69°38.63'N 51°51.13'W), Disko Island, West Greenland. All  
19  
20 specimens were collected during the Arctic summer in August 2013. Sediment was well-sorted  
21  
22 sand of fine to medium grain size. The specimens have been extracted with MgCl<sub>2</sub> narcotization  
23  
24 and decantation.  
25  
26  
27

28  
29  
30 For DNA, specimens of *Xenotrichula* sp. have been sampled in Ystad, Sweden (55°26.28'N  
31  
32 13°55.44'E) in subterranean environment on a beach with fine to medium sized sand, and  
33  
34 extracted with MgCl<sub>2</sub> narcotization and decantation. Marine *Aspidiophorus* sp. were sampled from  
35  
36 cultures of *Dinophilus gyrociliatus* from Copenhagen University, where they are contaminants and  
37  
38 unfortunately of unknown origin.  
39  
40  
41

### 42 43 44 **Sequence acquisition** 45

46  
47  
48 Total genomic DNA was obtained from whole specimens using the Qiagen DNeasy Blood & Tissue  
49  
50 Kit (Qiagen Inc., Valencia, CA, USA) following the manufacturer's protocol, except for performing  
51  
52 the DNA elution in 160 µL of AE buffer in order to increase the final DNA concentration.  
53  
54

55  
56 Polymerase chain reactions (PCR) using Sanger based markers were prepared to a final volume of  
57  
58 25 µL with 12.5 µL of GoTaq® Green Master Mix (Promega Corporation, Madison, WI, USA), 1 µL of  
59  
60

145 each primer (10  $\mu$ M concentration), 10-8.5  $\mu$ L of Milli-Q water (adjusted to amount of DNA  
2  
3  
146 template), and 0.5-2  $\mu$ L of DNA template. Reaction mixtures were heated in a Bio-Rad G1000  
4  
5  
147 Thermal Cycler at 94°C for 3 minutes, followed by 35-40 cycles (primer specific) of 94°C for 30 s,  
6  
7  
8  
148 specific primer pair annealing temperatures for 30 s, and an extension at 68°C for 45 s (unless  
9  
10  
11  
149 indicated otherwise), and a final extension-phase of 5 min at 72°C. The COI primer set  
12  
13  
150 dgLCO1490/dgHCO2198 [43] was run with two cycling steps, both variable in temperature. COI  
14  
15  
16  
151 annealing temperatures were 45°C for 45 s and 51°C for 45s, respectively with extensions of 30s.  
17  
18  
19  
152 Overlapping fragments of the small 18S rDNA (ca. 1800 bp) were obtained using paired primers  
20  
21  
22  
153 corresponding to fragment 1 and 3 of the 18S rDNA [44]: (1) 18S1f/18S5R (ca. 900 bp) and (3)  
23  
24  
154 18Sa2.0/18S9r (ca. 800 bp) both overlapping. Both primer sets (1) and (3) had annealing  
25  
26  
155 temperatures set to 49°C. The 28S primer set used was 28SD3/28SG758 [45, 46] with an annealing  
27  
28  
29  
156 temperature of 53°C.  
30  
31  
32

357 All newly generated sequences were deposited in the GenBank<sup>®</sup> database with the following  
34  
35  
158 accession numbers NB#####, NB#####, NB#####, NB#####, and NB##### (Table 1).  
36  
37  
38

## 159 Phylogenetic analysis

39  
40  
41  
42

160 Sequences were cleaned on BioEdit [47], and a consensus has been realized from the reverse and  
43  
44  
45  
161 forward sequences. Sequences were blasted on NCBI [48]. In parallel, COI, 18S and 28S of  
46  
47  
48  
162 *Diuronotus aspetos* were found from its transcriptome [3], using Blastall from NCBI. Sangers and  
49  
50  
51  
163 transcriptome acquired COI, 18S and 28S genes were aligned and compared, showing low quality  
52  
53  
164 and short length of Sangers sequences. Consequently, COI and 28S of the transcriptome were  
54  
55  
165 kept, while a consensus of 18S from the transcriptome and the Sangers sequencing was done  
56  
57  
58  
166 having an identical overlapping segment. This hybrid approach was possible since specimens used  
59  
60  
61  
62  
63  
64  
65

167 for the transcriptome and the Sanger sequences came from the same sample. Sequences of  
2  
3  
168 *Aspidiophorus* sp. and *Xenotrichula* sp. were added to the dataset. Sequences of other gastrotrichs  
4  
5  
169 acquired from GenBank, based on the tree of K anneby et al. 2012 [49] were added, selecting  
6  
7  
8  
170 sequences from each genus (except *Bifidochaetus* [16]) for which sequences were not available at  
9  
10  
11  
171 the time of the analysis), and representing the shortest and deepest branches possible. Sequences  
12  
13  
14  
172 from K anneby et al. [26] for *Musellifer*, K anneby and Todaro [50] for Neogosseidae, and Todaro et  
15  
16  
173 al. [51] for the macrodasyidans outgroups have additionally been collected from GenBank.  
17  
18  
19  
174 Subsequently, the sequences were aligned gene per gene with Muscle in Seaview [47], checked by  
20  
21  
22  
175 hand, and the three genes were concatenated with Sequence Matrix [52]. Finally, this dataset was  
23  
24  
176 analyzed with Bayesian inference in MrBayes 3.2.6 [53] under the model GTR+I+ . The gamma  
25  
26  
27  
177 shape parameter, the substitution rates, the proportion of invariable sites, and the character state  
28  
29  
30  
178 frequencies were all unlinked. The dataset was partitioned according to each gene and by codon  
31  
32  
33  
179 position for COI and analyzed with 4 MCMC chains for each run, for 30 million generations. Chains  
34  
35  
180 were sampled every 1000<sup>th</sup> generations and the burn-in was set to 25%. Convergence of the two  
36  
37  
38  
181 runs as well as analysis quality was ascertained by checking the log likelihood graphs, the average  
39  
40  
182 standard deviation of split frequencies, and the model fit with Tracer [54].  
41  
42

### 183 Immunohistochemistry and CLSM 43 44 45 46

184 Specimens were anesthetized with isotonic magnesium chloride and fixed in 3.7%  
47  
48  
49  
185 paraformaldehyde in phosphate buffered saline (PBS) for one to two hours at room temperature  
50  
51  
52  
186 (RT), followed by six rinses in PBS and storage in PBS with 0.05% NaN<sub>3</sub>. Triple or quadruple  
53  
54  
55  
187 stainings were applied for the investigation of muscular, nervous, glandular and ciliary systems,  
56  
57  
188 including F-actin staining (Alexa Fluor 488-labelled phalloidin, INVITROGEN, Carlsbad, USA), DNA-  
58  
59  
60  
61  
62  
63  
64  
65

189 staining (405nm fluorescent DAPI) and antibodies against neurotransmitters and tubulinergic  
2  
3  
190 elements (monoclonal mouse anti-acetylated  $\alpha$ -tubulin (SIGMA T6793, St. Louis, USA), polyclonal  
4  
5  
191 chicken anti acetylated  $\alpha$ -tubulin (SAB3500023-100UG), polyclonal rabbit anti-serotonin (5-HT,  
6  
7  
8  
192 SIGMA S5545) and anti-FMRF-amide (IMMUNOSTAR 20091, Hudson, USA)). Prior to adding the  
9  
10  
11  
193 primary antibody-mix, the samples were pre-incubated with 1% PTA (PBS + 1% Triton-X, 0.05%  
12  
13  
14  
194 NaN<sub>3</sub>, 0.25% BSA, and 5% sucrose) for one hour. Samples were incubated over night at RT in  
15  
16  
195 primary antibodies mixed 1:1 with glycerol (in a final 1:400 concentration). Subsequently,  
17  
18  
196 specimens were rinsed in PBS six times and incubated with the secondary antibodies conjugated  
19  
20  
21  
197 with fluorochromes over night at RT (mixed 1:1 with glycerol; 1:400 goat anti-mouse labeled with  
22  
23  
24  
198 CY5 (JACKSON IMMUNO-RESEARCH, West Grove, USA, 115-175-062), 1:400 goat anti-mouse  
25  
26  
199 labeled with TRITC (JACKSON IMMUNO-RESEARCH, West Grove, USA, 115-175-062), 1:400 goat  
27  
28  
200 anti-rabbit labeled with TRITC (SIGMA T5268), and 1:200 goat anti-chicken labeled with Dylight  
29  
30  
31  
201 (JACKSON IMMUNO-RESEARCH, West Grove, USA, 103-495-1550)). They were rinsed in PBS five  
32  
33  
34  
202 times and one time in 1% PTA and pre-incubated for 60 minutes in Alexa Fluor 488-labeled  
35  
36  
203 phalloidin (0.33M in 1% PTA). Thereafter, specimens were rinsed in PBS (without NaN<sub>3</sub>) and  
37  
38  
39  
204 mounted in Fluoromount-G with DAPI (SOUTHERN BIOTECHNOLOGY ASSOCIATES, Inc., Alabama,  
40  
41  
42  
205 USA) or Vectashield with DAPI (VECTOR LABORATORIES, Burlingame, USA). The specificity of the  
43  
44  
206 antibodies was tested by examining specimens, where either the primary or secondary antibodies  
45  
46  
47  
207 were omitted. Chicken anti acetylated  $\alpha$ -tubulin staining did not give satisfying results and is  
48  
49  
50  
208 therefore not shown in this study (Sigma SAB3500023-100UG).  
51  
52

53  
209 The mounted specimens were scanned using an Olympus Fluoview FV-1000 confocal laser  
54  
55  
210 scanning microscope (of K. Worsaae, University of Copenhagen, Denmark), with the acquired z-  
56  
57  
58  
211 stacks of scans being either projected into 2D-images or analyzed three-dimensionally using  
59  
60  
61  
62  
63  
64  
65

12 IMARIS 7.1 (BITPLANE SCIENTIFIC SOFTWARE, Zürich, Switzerland). This software package was also  
2  
3  
4 used to conduct the measurements presented in the following text according to the conventions  
5  
6 introduced by Hummon et al. 1992 [55], i.e. position in the body is given in units (U) as a relative  
7  
8 measurements to total body length, measured from anterior to posterior. Schematic hand  
9  
10 drawings and plate setup were done with Adobe Illustrator CS6 and image adjustments conducted  
11  
12 in Adobe Photoshop CS6.  
13  
14  
15  
16  
17  
18

19

20

21

22

23

24

25

26

27

28

29

30

31

32

33

34

35

36

37

38

39

40

41

42

43

44

45

46

47

48

49

50

51

52

53

54

55

56

57

58

59

60

61

62

63

64

65

## **Results**

### **Phylogeny**

The tree (Fig. 1) shows a fully supported sister group relationship (100% posterior probability (PP)) between the monophyletic Muselliferidae (100% PP) and Xenotrichulidae (100% PP), herein together called “group A”. Within Muselliferidae the genus *Musellifer* (100% PP) (represented only by *Musellifer delamarei* (Renaud-Mornant, 1968) [56] and *Musellifer reichardt* Kånneby, Atherton & Hochberg, 2014) [26]) is found to be sister group to *Diuronotus aspetos*. Group A is found next to “group B”, together constituting the Paucitubulatina (100% PP), with group B showing a monophyletic Dasydytidae (100% PP) and Neogosseidae (100% PP) nested within “Chaetonotidae”, the latter hereby becoming paraphyletic. Supports are high in all nodes of the tree, except for some of the numerous inner nodes of group B.

### **Musculature**

231 The body wall musculature consists of several pairs of longitudinal muscles, numerous dorso-  
2  
3  
232 ventral muscles, a thin helicoidal musculature, semi-circular and complete circular muscles, as well  
4  
5  
233 as pharyngeal musculature. The pharyngeal musculature is especially dense and has an  
6  
7  
8  
234 organization typical of chaetonotid gastrotrichs, as described below in more detail (Figs. 2 and 3).

### 235 **Radial muscles**

236 The pharynx, sensu stricto, is formed by three rows of very dense radial pharyngeal muscles (rpm,  
17  
18  
237 Figs. 2D,E,M and 3C,D), and extend to U26 (units are calculated as length from anterior end,  
19  
20  
238 relative to total length, see material and methods). The radial muscles are cross-striated and each  
22  
23  
239 of them presents three to six Z-discs, which are less numerous anteriorly. The myoepithelial nuclei  
24  
25  
240 of the pharynx have a distinctive folded and elongated shape (mn, Fig. 2M). The pattern and  
27  
28  
241 repartition of these nuclei seems to be specific and corresponding nuclei could be found in the  
29  
30  
242 same position in different specimens.

### 243 **Helicoidal muscles**

244 Helicoidal muscles (hm, Figs. 2N and 3A,B,D,E) are very thin (0.5-1.2 $\mu$ m) and limited to the anterior  
38  
39  
40  
245 half of the specimen. It is difficult to confirm the presence of the helicoidal muscles most around  
42  
43  
246 the pharynx due to the strong signal of other pharyngeal muscles (dashed lines in Fig. 3C-D). In few  
44  
45  
247 locations along the midline of the pharynx very faint diagonal fibers were observed, suggesting  
47  
48  
248 that the helicoidal musculature is actually present along the entire pharyngeal region. Distinct  
49  
50  
249 helicoidal muscles are found extending from the midgut/pharynx junction at U26 until U42,  
52  
53  
250 enveloping the dorsal longitudinal muscle but not the ventral and ventro-lateral longitudinal  
54  
55  
251 muscles.

252 **Longitudinal musculature**

2  
3  
4  
253 Three longitudinal muscles span the entire body length: a pair of ventral longitudinal muscles (vlm,  
5  
6  
754 Figs. 2 and 3), a pair of ventro-lateral longitudinal muscles (vllm, Figs. 2 and 3), and a pair of dorsal  
8  
9  
1055 longitudinal muscles (dlm, Figs. 2 and 3). The ventral longitudinal muscle bundle splits several  
11  
12  
256 times in a pattern described below for the different body regions.

15  
1657 Pharyngeal region

17  
18  
19  
258 Several longitudinal muscles are present along the pharynx. Some are limited to the pharyngeal  
20  
21  
2259 region, while others are the continuity of the body longitudinal muscles mentioned above. Two  
23  
24  
260 sets of muscles are strictly limited to the pharyngeal region: a pair of lateral and a pair of dorsal  
25  
26  
2761 muscles. The lateral pharyngeal longitudinal muscle (lplm, Figs. 2D,E and 3C,D) extends adjacent to  
28  
29  
3062 the pharynx along its entire length. The pharyngeal dorsal longitudinal muscles (pdlm, Figs.  
31  
32  
3363 2D,E,M,O and 3B-D) extend close to the pharyngeal midline along its total length, ventral to the  
34  
35  
3664 dorsal longitudinal muscles. Moreover, several somatic and splanchnic longitudinal muscles supply  
36  
37  
3865 the pharyngeal region.

39  
40  
4166 The paired ventral longitudinal muscle (vlm, Figs. 2 and 3) originating in the head, splits along the  
42  
43  
4467 pharynx into a complex pattern (see Fig. 3B). One of its branches extends more laterally and splits  
45  
46  
4768 into several sub-branches, supplying the lateral sides of the head.

48  
49  
5069 The paired ventro-lateral longitudinal muscle (vllm, Figs. 2 and 3) lines the pharynx until reaching  
51  
52  
5370 the head, where it bifurcates at U7, one branch extending ventro-laterally and the other dorso-  
54  
55  
5671 laterally. Each of them subsequently splits into several minor branches, supplying the lateral sides  
57  
58  
5972 of the head. These muscles together with the antero-lateral branch of the ventral longitudinal  
60  
61  
62  
63  
64  
65

273 muscle (vlm), and the head diagonal muscle (hdm, see below) all supply the antero-lateral part of  
2  
3  
274 the head, and besides anchoring the longitudinal muscles for overall body contraction, they may  
4  
5  
275 function separately in contraction of the head (Figs. 2J and 3A,C).  
6  
7

8  
9  
10  
11  
12  
13  
14  
15  
16  
17  
18  
19  
20  
21  
22  
23  
24  
25  
26  
27  
28  
29  
30  
31  
32  
33  
34  
35  
36  
37  
38  
39  
40  
41  
42  
43  
44  
45  
46  
47  
48  
49  
50  
51  
52  
53  
54  
55  
56  
57  
58  
59  
60  
61  
62  
63  
64  
65

276 The paired dorsal longitudinal muscle (pdlm) spans the anterior-most extremity of the pharynx.

### Trunk region

277  
278 Three main longitudinal muscles, i.e. ventral, lateral and dorsal, are supplying the trunk. The paths  
18  
19  
20  
21  
22  
23  
24  
25  
26  
27  
28  
29  
30  
31  
32  
33  
34  
35  
36  
37  
38  
39  
40  
41  
42  
43  
44  
45  
46  
47  
48  
49  
50  
51  
52  
53  
54  
55  
56  
57  
58  
59  
60  
61  
62  
63  
64  
65

279 of the lateral and dorsal longitudinal muscles are relatively straight throughout the body.  
280 However, just posterior to the pharynx, the dorsal longitudinal muscle lines the intestine (Figs. 2F  
281 and 3C,D,E), while it runs closer to the dorsal body wall more posteriorly (Figs. 2G,H and 3F,G). The  
282 ventral longitudinal muscle splits into three muscle bundles at the anterior trunk. Two of these  
283 branches run in parallel mid-ventrally along the trunk (lvlm, mvlm, Figs. 2A,C,F-H,P and 3A,B,F-H),  
284 whereas the third branch extends dorso-laterally and supplies the dorso-lateral sides of the body  
285 until meeting the median-most branch at U86 (dvlm, Figs. 2A,G,L and 3A,B,F).

### Posterior region

286  
287 The median branch of the longitudinal ventral muscle splits posteriorly into two bundles at U86.  
288 One very short (8 $\mu$ m) portion supplies medially the posterior part of the adhesive gland of the  
289 posterior tube, while another longer branch extends into the primary tube, supplying it for  
290 approximately two thirds of its length to U97 (Fig. 3A). Additionally, the lateral branches of the  
291 ventral and lateral longitudinal muscles also extend along the primary tube. The dorsal  
292 longitudinal muscle supplies the anterior third of the secondary tube.

### **Diagonal muscles**

294 The head diagonal muscle (hdm, Figs. 2J,P and 3A,B,C) forms a V-shape with two medially joined  
2  
3  
295 branches. The median part of the muscle is situated in the midline of the body in the posterior  
4  
5  
296 region of the head while the two extremities extend to the antero-lateral region of the head.  
6  
7

8  
9  
297 At the dorso-posterior pharynx, a pair of pharyngeal dorsal diagonal muscles decussate (pddm,  
10  
11  
12  
298 Figs. 2P and 3B,D), ventral to the pharyngeal dorsal longitudinal muscle and the dorsal longitudinal  
13  
14  
299 muscle. Though their orientation is similar to the helicoidal muscles, their exclusively dorsal  
15  
16  
300 extension and their greater width differ significantly from the helicoidal muscles.  
17  
18

19  
20  
301 Three diagonal muscles are found in the furca, extending from one side to the contralateral one.  
21  
22

23  
302 The two anterior muscles (tmd, Figs. 2A,B,H,I,K and 3A,B,G,H) extend from the midline at U86,  
24  
25  
303 halfway to the primary and the secondary tube, respectively. The posterior diagonal muscle (pdm,  
26  
27  
304 Figs. 2I,K, and 3A,B,H) extends from U89 laterally into the first third of the secondary tube.  
28  
29  
30  
31

### 305 **Circular muscles**

32  
33  
34  
35

306 Pharyngeal circular muscles (pcm 2E,M,O,P and 3A,B,C,D) are present around the pharynx. These  
36  
37  
307 muscles are numerous (ca. 110 in one specimen), positioned proximal to each other, and 1-  
38  
39  
40  
308 1.50 $\mu$ m thick with increasing diameter towards the posterior region.  
41  
42  
43

309 Two sphincters are present at each extremity of the pharynx: one anterior pharyngeal sphincter  
44  
45  
310 (aps, Figs. 2B,O,P and 3A,B) located just posterior to the mouth, and one posterior pharyngeal  
46  
47  
48  
311 sphincter (pps, Figs. 2M,O,P and 3A,B) marking the transition between the intestine and the  
49  
50  
51  
312 pharynx. The anterior sphincter is smaller, being 1 $\mu$ m thick and has a diameter of 17 $\mu$ m, while the  
52  
53  
54  
313 posterior sphincter is more prominent with 8 $\mu$ m thickness and a diameter of 23 $\mu$ m.  
55  
56  
57  
58  
59  
60  
61  
62  
63  
64  
65

314 Supplementary circular muscles of the adhesive glands (cmag, Figs. 2H,I,K and 3A,B,G,H) are  
2  
3  
315 present in the tubes, forming a muscular layer around the large adhesive glands (ag, Fig. 2K). They  
4  
5  
316 thereby supply two cavities - one for each tube. The muscular layer surrounding the primary tube  
6  
7  
8  
317 is smaller than the one surrounding the secondary tube, and both structures are connected. This  
9  
10  
11  
318 suggests that both tubes are supplied by a single set of glands controlled by muscles. Three  
12  
13  
14  
319 adjacent nuclei are found within the layer of circular muscles at the base of the gland (agn, Fig.  
15  
16  
320 2K), near the anus, around U88.

### 321 **Semi-circular muscles**

322 Ventrally opened semicircular muscles (scm, Figs. 2L and 3A,B,F,G) are present in the posterior  
23  
24  
25  
323 part of the specimen, but do not extend into the tubes. They originate ventrally, from each side of  
26  
27  
28  
324 the body, and extend to the dorsal side. From there, they project to the contralateral side,  
29  
30  
31  
325 external to the longitudinal musculature. They are more numerous in the posterior region,  
32  
33  
326 anterior to the furca, where they are separated by 2-5  $\mu\text{m}$ . Semicircular muscles are less numerous  
34  
35  
36  
327 and spaced further apart (5-8  $\mu\text{m}$ ) in the anterior region of the ovary. They seem to only supply  
37  
38  
39  
328 the ovary region: their contraction probably reducing the body diameter and may be involved in  
40  
41  
329 the movement/release of eggs.

### 430 **Dorso-ventral muscles**

431 Numerous thin muscles (1-2  $\mu\text{m}$  in diameter) traverse the entire trunk dorso-ventrally (dvm, Figs.  
44  
45  
46  
47  
48  
331 2A-C,E-H,K,L,N and 3A,B,E-G). These dorso-ventral muscles are spaced approximately 5  $\mu\text{m}$  apart  
49  
50  
51  
332 in the region between U18 and U95. In this region, two pairs are found laterally in transverse  
52  
53  
333 sections of the pharyngeal region (one external and one more internal pair, dvm, Figs. 2D,E and  
54  
55  
334 3A,B). This number increases more posteriorly in the trunk, where up to five pairs of dorso-ventral  
56  
57  
58  
335

336 muscles can be detected (dvm, Figs. 2G,K,L, and 3A,B,F). The dorso-ventral muscles extend dorso-  
2  
3  
337 ventrally between the different longitudinal muscles and the ciliary bands in various combinations.  
5  
338 However, they are never found external to the ventro-lateral longitudinal muscles or between the  
7  
8  
339 pair of dorsal longitudinal muscles.

## 340 **Nervous system**

341 The nervous system of *Diuronotus aspetos* is described from acetylated  $\alpha$ -tubulin-like  
17  
18  
342 immunoreactivity (LIR, Figs. 4, 5, 6), serotonin-LIR (Fig. 7) and FMRF-amide-LIR (Fig. 8) (all different  
20  
21  
343 LIR of the head region are summarized in Fig. 9). Similar to previously investigated Gastrotricha,  
22  
23  
344 the nervous system consists of paired nerve cords, which originate from a bilobed dorsal brain and  
25  
26  
345 extend posteriorly. In the following section, previously described and undescribed structures are  
27  
28  
346 detailed, such as: i) multiple pairs of longitudinal nerve projections in the head (danp, dlpn, hln,  
30  
31  
347 Figs. 6A,B,E,J and 9A,B), ii) paired anterior ventro-median nerves (avmn, Fig. 6A,D and 9B), iii)  
32  
33  
348 dorsal nerves posterior to the brain (hdpn, Figs. 6A,H and 9A), iv) paired ventro-lateral nerve cords  
35  
36  
349 (vlnc, Figs. 6B-D,F,G,K and 9B), v) paired posterior nerves, projecting into the adhesive tubes (nppt,  
38  
39  
350 Fig. 6K), vi) bilobed, dorsal brain with three commissures (a main neuropil and an anterior and  
40  
41  
351 dorsal commissure, together forming a nerve ring encircling the pharynx) (np and anr, Figs. 6A-  
43  
44  
352 C,E,H-J and 9A,B), vii) two pairs of ganglia along the nerve cord: one anterior and one terminal  
45  
46  
353 (pgg and ang, Figs. 6B,F,K and 9B), viii) four ventral trunk commissures (spc, tvc, pac and pco, Figs.  
48  
49  
354 6B,D,G,K and 9B), ix) a pharyngeal nervous system, consisting of three longitudinal nerves (one per  
51  
52  
355 pharyngeal row of radial muscles) and supplementary minor nerves (Figs. 4 and 5). Additionally,  
53  
54  
356 the serotonin-LIR and FMRF-amide-LIR gave very detailed results, allowing us to collect precise  
56  
57  
357 data on the number, position and connection of perikarya (Figs. 7, 8 and 9).

158 **Acetylated  $\alpha$ -tubulin-like immunoreactivity (acetylated  $\alpha$ -tubulin-LIR)**

2  
3  
4  
359 Acetylated  $\alpha$ -tubulin-LIR provides information on most neurites, cilia as well as other portions of  
5  
6  
360 cytoskeletons of the cells. However, not all minor neurites of the nervous system are traced and  
8  
9  
361 the description focuses on the central nervous system and sensory structures.

11  
12  
13 **Stomatogastric nervous system**

14  
15  
16  
363 The stomatogastric nervous system, confined to the pharynx, consists mainly of three main  
18  
19  
364 longitudinal nerves: a dorsal (dpn, Figs. 4A,D-H,J-N and 5A,B,E) and two ventro-lateral nerves (vpn,  
20  
21  
365 Figs. 4B,F-H,L-N and 5E), extending basally along the midline of each row of radial muscles (Fig. 4).

22  
23  
24  
366 The nerves are closely related to three structures: kinocilia, anterior pharyngeal glands and a  
25  
26  
367 pharyngeal canal system. The dorsal pharyngeal nerve (dpn, Figs. 4A,D-H,K-O and 5A,B,E)  
28  
29  
368 originates at the mouth, where it supplies a buccal nerve ring (bnr, Figs. 4A,B and 5A), encircling  
30  
31  
369 the mouth (probably innervating the anterior sphincter (aps, Figs. 2B,O,P and 3A,B) opening and  
33  
34  
370 closing the mouth). At U4, two anterior diagonal pharyngeal nerves (adpn Figs. 4A and 5A)  
36  
37  
371 originate from the dorsal nerve, extend antero-laterally to the anterior edges of the pharynx and  
38  
39  
372 medially join back the dorsal nerve. At U3, one pharyngeal dorso-ventral nerve (pdvn, Figs. 4A,B  
41  
42  
373 and 5A) originates from each of the anterior diagonal nerve, and supply ventrally a pharyngeal  
43  
44  
374 gland longitudinal nerve (plgn, Figs. 4B and 5C) innervating an anterior pharyngeal gland (apg, Figs.  
46  
47  
375 4A,C,I and 5C) (which opens into the mouth). On the right side of the specimen, a dorso-anterior  
48  
49  
376 pharyngeal canal nerve (dpcn, Figs. 4A,D,J and 5A) extends posteriorly from the anterior diagonal  
50  
51  
377 nerve, possibly supplying the asymmetric dorsal pharyngeal canal (dpc, Figs. 4A,F,G,L,M and 5E).  
54  
55  
378 At U9 a pharyngeal nerve ring (pnr, Figs. 4A,B,E,K and 5B,D) supplying the ventral and dorsal  
56  
57  
379 nerves is present. A pair of paramedian dorsal pharyngeal nerves (dnpn, Figs. 4A,F,L and 5E)

380 originates from the dorsal nerve at U19 and extends in a parallel fashion on each side, to fuse  
2  
3  
381 again with the dorsal nerve at U26 (Figs. 4A,G,M and 5E). The dorsal nerve extends more  
5  
382 posteriorly where it innervates a two-celled pharyngeal posterior cluster (ppc, Figs. 4A and 5I) at  
7  
8  
383 the posterior margin of the pharynx. Two nerves extend the terminal part of the ventro-lateral  
10  
11  
384 pharyngeal sections: the lateral gland longitudinal nerve (plgn, Figs. 4A and 5C), and a median  
12  
13  
385 kinocilium longitudinal nerve (plkn, Figs. 4B,C and 5G), with the latter supplying a mouth and a  
15  
16  
386 pharyngeal kinocilia, respectively, at U1 and U6 (mk and pk, Figs. 4B-D,J,I and 5C,G). The gland and  
17  
18  
387 kinocilium nerves originate at U7 from an elongated ventro-lateral pharyngeal ganglion (vlpg, Figs.  
20  
21  
388 4 and 5H,F), consisting of three nuclei and extending from U7 to U12 (probably integrating the  
23  
24  
389 signal collected by the two kinocilia and responsible for the putative terminal gland secrete  
25  
26  
390 release). The ganglion seems to be furthermore related to the ventro-lateral pharyngeal canal  
28  
29  
391 (vlpc, Figs. 4A,B,E-G,K-N and 5F,I) described below. The ventral pharyngeal nerves (vpn, Figs.  
30  
31  
392 4B,F,G,L,M and 5D) (supplied by perikarya at U15 and U19) extend from the ganglion, until U28.  
33  
34  
35  
393 Due to the unknown nature of the canal system and its main acetylated  $\alpha$ -tubulin-LIR (as well as a  
36  
37  
394 weak FMRF-amide-LIR), it is described in this nervous system section. It consists of radially  
39  
40  
395 flattened cavities, sometimes asymmetrical, extending longitudinally within the pharynx (Figs.  
42  
43  
396 4A,B,E,F,K,L and 5D,E). Six pharyngeal canals extend the pharynx: i) the unpaired right ventro-  
44  
45  
397 anterior pharyngeal canal (avrc, Figs. 4B,E,F,K,L and 5D) extending from U6 to U26; ii-iii) The paired  
47  
48  
398 ventro-lateral pharyngeal canals (vlpc, Figs. 4A,B,E-H,K-N and 5F,I), extending from U7 (at the level  
49  
50  
399 of the pharyngeal ganglia (vlpg, Figs. 4A and 5H,F)) to U30, and merging dorso-posteriorly; iv-v) the  
52  
53  
400 paired ventro-posterior pharyngeal canals extending from U23 for the left one (lpvc, Figs.  
54  
55  
401 4B,G,H,M,N and 5D) and from U26 for the right one (rpvc, Figs. 4B,G,H,M,N and 5D) to U28; vi) the  
57  
58  
402 dorsal pharyngeal canal (dpc, Figs. 4A,F,G,L,M and 5E) extending along the right side from U6 to  
60  
61  
62  
63  
64  
65

403 U15, then reaching the midline and bifurcating in two symmetrical branches, following the  
2  
3  
404 paramedian dorsal nerves of the pharynx between U19 and U27. Few nuclei are embedded in the  
5  
6  
405 pharyngeal canal system (Fig. 4A,B,G).  
7  
8

#### 406 Central nervous system

10  
11  
12

407 The neuropil (np, Figs. 6A,C,E,H,J and 9A) is 14µm thick and its center is positioned at U15. One  
14  
15  
408 3µm broad nerve extends antero-medially from the neuropil and branches laterally to form a  
17  
18  
409 dorsal and a ventral commissure at U12 and U9, respectively, together constituting an anterior  
19  
20  
410 nerve ring (anr, Figs. 5D, 6A-C,I,J and 9A,B). At the dorsal section of the anterior nerve ring (anr,  
22  
23  
411 Fig. 9), the acetylated α-tubulin-LIR is relatively weak, and the commissure consists of two  
24  
25  
412 transverse (anterior FMRF-amide-like-immunoreactive (LI-reactive) and posterior serotonin-LI-  
27  
28  
413 reactive) nerves, which eventually fuse dorso-laterally, forming the lateral sections of the anterior  
29  
30  
414 nerve ring. One anterior and one posterior indistinct longitudinal nerves (cpn, Figs. 6B,I and 9B)  
31  
32  
33  
415 extend from the ventral portion of the anterior nerve ring, innervating two median ciliary patches  
35  
36  
416 (described below). The neuropil supplies ventrally a pair of anterior ventro-median nerves (avmn,  
37  
38  
417 Figs. 6B,D, and 9B) extending between the anterior nerve ring and the post-pharyngeal ganglion  
40  
41  
418 posteriorly (pgg, Figs. 6B,F and 9B). It extends parallel to the pharyngeal median ciliated cell  
42  
43  
419 (pmcc, Fig. 10B,G), probably innervating it. Two pairs of dorso-median anterior nerves projections  
45  
46  
420 (danp, Figs. 6A,J and 9A) and two pairs of dorso-lateral anterior nerve projections (dlnp, Figs. 6A,J  
48  
49  
421 and 9A) extend from the anterior nerve ring and the lateral sides of the neuropil, respectively,  
50  
51  
422 projecting anteriorly. One pair of head lateral nerves (hln, Figs. 6A,B,E,J and 9A,B) extends from  
53  
54  
423 the lateral sides of the neuropil and bifurcates, posteriorly supplying a cell with a large and diffuse  
55  
56  
424 nucleus (possibly a gland cell (lgcb, Figs. 6A,E and 9A)), and anteriorly forming a nerve projection.  
58  
59  
60  
61  
62  
63  
64  
65

425 Each of these anterior nerve projections probably innervates head sensory organs. Dorso-laterally,  
2  
3  
426 the posterior sides of the neuropil supply the ventro-lateral nerve cord (vlnc, Figs. 6B,C,D,F,G,J,K  
5  
6  
427 and 9B) of *D. aspetos*, which extends along the entire length of the specimen adjacent to the  
7  
8  
428 lateral longitudinal ciliary bands and the ventro-lateral longitudinal muscle, probably innervating  
10  
11  
429 these two structures. Two head dorso-posterior nerve (hdpn, Figs. 5E, 6A,H and 9A), extending  
12  
13  
430 along the pharynx, eventually supply the post-pharyngeal ganglion. They may innervate the  
15  
16  
431 anterior portion of the dorsal longitudinal muscle. A pair of head diagonal nerves (hdn, Figs. 6A,H  
17  
18  
432 and 9A) originates dorso-laterally of the neuropil, decussate dorsal to the pharynx at U22, and  
20  
21  
433 each extend ventro-laterally to a single perikaryon at U23. Comparison across specimens suggests  
23  
24  
434 that the position of these diagonal nerves corresponds to the position of the pharyngeal dorsal  
25  
26  
435 diagonal muscle (pddm, Figs. 2P and 3B,D), which it probably innervates. At U27 and U29, two thin  
28  
29  
436 nerves originate from the anterior ventro-median nerve, and form together at U28 a sub-  
30  
31  
437 pharyngeal commissure (spc, Figs. 6B,D and 9B). At U50, anterior to the testis, a thin trunk ventral  
33  
34  
438 commissure (tvc, Fig. 6G) is present. At U84, an anal ganglion (ang, Fig. 6K) of six to eight cells  
35  
36  
439 supplies a pre-anal commissure (pac, Fig. 6K). Posterior to the anus, at U87, the two ventro-lateral  
37  
38  
440 nerve cords form the posterior commissure (pco, Fig. 6C,K), from which two nerve projections of  
41  
42  
441 the primary tube (nppt, Fig. 6C,K) extend.  
43  
44

#### 442 **Serotonin-like immunoreactivity (serotonin-LIR)**

47  
48

443 The nervous system shown by serotonin-LIR consists of a dorsal neuropil, the anterior nerve ring,  
50  
51  
444 anterior and posterior projections, the two ventro-lateral nerve cords, one posterior commissure  
53  
54  
445 as well as several perikarya.  
55  
56  
57  
58  
59  
60  
61  
62  
63  
64  
65

446 Three main commissures (an anterior (sacn), a median (smcn) and a posterior (spcn)) in the brain  
2  
3  
447 neuropil show serotonin-LIR (Fig. 7A,D, E) as well as an isolated patch postero-medial to the  
5  
448 neuropil (spp, Fig. 7A,D,E). Three longitudinal nerves showing serotonin-LIR are found in the brain:  
7  
8  
449 i) the median-most brain nerve (smbn, Fig. 7A,D), ii) the paramedian brain nerve (spbn, Fig. 7A,D),  
10  
11  
450 and iii) the lateral brain nerve (slbn, Fig. 7A,D). Four very thin lateral nerves of the posterior  
12  
13  
451 commissure of the neuropil (slpn, Fig. 7A,D) form complex connections with the other nerves of  
15  
16  
452 the brain as well as to the dorso-medial perikaryon (sdmp, Fig. 7A,C,D,E). A postero-lateral nerve  
17  
18  
453 node (spln, Fig. 7A,D,E) is present postero-laterally to the neuropil, being formed by the merging  
20  
21  
454 of several nerves, and supplies the ventro-lateral nerve cord (slnc, Fig. 7B,C,F). One dorso-lateral  
23  
24  
455 perikaryon (sdlp, Fig. 7A,C,D,E) supplies the postero-lateral nerve node, with a short nerve. The  
25  
26  
456 median-most brain nerve extends anteriorly from the posterior of the neuropil until U6 (Fig. 7A).  
28  
29  
457 The lateral brain nerve is short and extends from the postero-lateral nerve node, being supplied by  
30  
31  
458 some of the commissures of the neuropil (Fig. 7A). The paramedian brain nerve originates from  
33  
34  
459 the postero-lateral nerve node and supplies the serotonin-like-LI-reactive anterior nerve ring (sanr,  
36  
37  
460 Fig. 7A-D), subsequently extending more posteriorly as an anterior nerve projection until U4 (Fig.  
38  
39  
461 7A,D). The anterior nerve ring consists dorsally of two and ventrally of one serotonin-LI-reactive  
41  
42  
462 nerves (sanr, Fig. 7A,B). The ventro-lateral nerve cord, consisting of two serotonergic-LI-reactive  
43  
44  
463 neurites, extends ventrally to supply a serotonin-LI-reactive para-pharyngeal cluster (sppc, Figs.  
46  
47  
464 7B-E and 9B) consisting of three perikarya, and extends to the posterior end forming the posterior  
48  
49  
465 commissure. Additionally, single serotonin-LI-reactive perikarya of the post-pharyngeal ganglion  
51  
52  
466 and of the anal ganglion are present respectively at U33 and U93 (spog, and spag, Fig. 7B,C,F) as  
54  
55  
467 well as nerve projections of the primary tube (snpt, Fig. 7C,F).

#### 468 **FMRF-amide-like immunoreactivity (FMRF-amide-LIR)**

60  
61  
62  
63  
64  
65

469 The FMRF-amide-LI-reactive nervous system consists of the brain neuropil, the anterior nerve ring,  
2  
3  
470 the anterior ventro-median nerve, the ventro-lateral nerve cord, the sub-pharyngeal commissure  
4  
5  
471 and the posterior commissure. Different parts of the nervous system show varying  
6  
7  
8  
472 immunoreactivity intensities, as illustrated in Fig. 8.

10  
11  
12  
473 The neuropil (fnp, Fig. 8A,C,D,F,G) consists of four connectives: two anterior and two posterior,  
13  
14  
1574 supplied by several posterior and lateral perikarya. Antero-laterally to the neuropil, one pair of  
16  
17  
475 perikarya supplies a very short dorso-lateral anterior nerve projections (fpp, Fig. 8A,D,F,G)  
18  
19  
2076 (corresponding to the base of the acetylated  $\alpha$ -tubulin-LI-reactive projections (dlnp; Figs. 6A,J and  
21  
22  
2377 9A)). Additionally, three lateral perikarya of the brain (flpb, Fig. 8A,F,G) and a pair of dorso-  
24  
25  
478 posterior clusters of the brain (fdpc, Figs. 8A,F,G and 9A) with three perikarya, are present.

26  
27  
2879 Comparisons between differently stained specimens, and use of DAPI, enabled us to infer that the  
29  
30  
480 postero-median cell of the FMRF-amide-LI-reactive dorso-posterior cluster corresponds to the  
31  
32  
3381 serotonin-LI-reactive dorso-posterior perikarya (sdmp, Fig.7; fdpc, Figs. 8A and 9A). Anteriorly, the  
34  
35  
482 neuropil supplies the anterior ventro-median nerve (fvmn, Figs. 8B,I and 9B), also supplied by two  
36  
37  
383 ventro-lateral perikarya of the brain (fvpb, Fig. 8A,E,I) and a ventral perikaryon of the anterior  
39  
40  
484 nerve ring (fvpr, Fig. 8B,I). The nerve ring (fanr, Fig. 8A-D,G,H,J) is supplied by one anterior and one  
41  
42  
485 posterior unpaired dorso-median perikarya (fpar, Fig. 8A,D,F,H). Ventro-posterior to the neuropil,  
43  
44  
486 a pair of tricellular clusters also supply the ventro-median nerve (fvnc, Fig. 8N,I), which extends  
45  
46  
47  
487 further posterior until the two FMRF-amide-LI-reactive perikarya of the post-pharyngeal ganglion  
48  
49  
50  
5188 (fppg, Fig. 8B,C,K). The paired ventro-lateral nerve cords (flnc, Fig. 8B,C,I,K,L) is supplied by the  
52  
53  
5489 postero-lateral part of the neuropil and by three anterior perikarya (fapn, Fig. 8B,C,E,I) (two  
54  
55  
56  
490 anterior and one posterior, separated by 8 $\mu$ m). The FMRF-amide-LI-reactive sub-pharyngeal  
57  
58  
591 commissure (fspc, Fig. 8B,I), ventro-lateral nerve cord, posterior commissure (fpco, Fig. 8C,L), and  
60  
61  
62  
63  
64  
65

492 nerve projections of the primary tube (fnpt, Fig. 8C,L) follow the description of the acetylated  $\alpha$ -  
2  
3  
493 tubulin-LIR.  
4  
5  
6

## 494 Ciliation 7 8 9

10  
1495 The locomotory ciliation consists of a dense ventro-anterior ciliated area and two thin ciliated  
12  
13  
1496 bands, which are extending to the posterior part of the specimen at U87 (Fig. 10C). This general  
15  
16  
1497 pattern supports the original description of Todaro et al. [17], although numerous details can be  
17  
18  
1498 added. CLSM allowed the identification of individual multiciliated cells and determination of their  
20  
21  
1499 precise pattern.  
22  
23  
24

2500 Dorsally, the muzzle is covered by two transverse rows of multiciliated cells. The anterior row  
26  
27  
2501 consists of three pairs of relatively small head dorso-anterior ciliated cells ( $3\mu\text{m}$ , hacc, Fig.  
28  
29  
302 10A,E,F), while the posterior row is constituted by a pair of larger head postero-lateral dorsal  
31  
32  
303 ciliated cells (hpcc, Fig. CA,E) and a head dorso-median ciliated cell (hmcc, Fig. CA,E) of similar size  
34  
35  
304 ( $6\mu\text{m}$ ). The pattern of the head lateral ciliated cells (hlcc, Fig. 10A,F) could not be resolved in  
36  
37  
305 details due to the dorso-ventral mounting of the specimen. However, at least four cells at the  
38  
39  
40  
41  
42  
43  
44  
45  
46  
47  
48  
49  
50  
51  
506 dorso-lateral level are present, and probably the same number at the ventro-lateral level.  
52  
53

507 The ventral head bears 20 multiciliated cells organized in four paired longitudinal rows and one  
54  
55  
508 median row, containing 2,2,3,2,2,2,3,2,2 cells (Fig. 10B). Posterior to the head, ventral to the  
56  
57  
58  
59  
60  
61  
62  
63  
64  
65  
66  
67  
68  
69  
70  
71  
72  
73  
74  
75  
76  
77  
78  
79  
80  
81  
82  
83  
84  
85  
86  
87  
88  
89  
90  
91  
92  
93  
94  
95  
96  
97  
98  
99  
100  
101  
102  
103  
104  
105  
106  
107  
108  
109  
110  
111  
112  
113  
114  
115  
116  
117  
118  
119  
120  
121  
122  
123  
124  
125  
126  
127  
128  
129  
130  
131  
132  
133  
134  
135  
136  
137  
138  
139  
140  
141  
142  
143  
144  
145  
146  
147  
148  
149  
150  
151  
152  
153  
154  
155  
156  
157  
158  
159  
160  
161  
162  
163  
164  
165  
166  
167  
168  
169  
170  
171  
172  
173  
174  
175  
176  
177  
178  
179  
180  
181  
182  
183  
184  
185  
186  
187  
188  
189  
190  
191  
192  
193  
194  
195  
196  
197  
198  
199  
200  
201  
202  
203  
204  
205  
206  
207  
208  
209  
210  
211  
212  
213  
214  
215  
216  
217  
218  
219  
220  
221  
222  
223  
224  
225  
226  
227  
228  
229  
230  
231  
232  
233  
234  
235  
236  
237  
238  
239  
240  
241  
242  
243  
244  
245  
246  
247  
248  
249  
250  
251  
252  
253  
254  
255  
256  
257  
258  
259  
260  
261  
262  
263  
264  
265  
266  
267  
268  
269  
270  
271  
272  
273  
274  
275  
276  
277  
278  
279  
280  
281  
282  
283  
284  
285  
286  
287  
288  
289  
290  
291  
292  
293  
294  
295  
296  
297  
298  
299  
300  
301  
302  
303  
304  
305  
306  
307  
308  
309  
310  
311  
312  
313  
314  
315  
316  
317  
318  
319  
320  
321  
322  
323  
324  
325  
326  
327  
328  
329  
330  
331  
332  
333  
334  
335  
336  
337  
338  
339  
340  
341  
342  
343  
344  
345  
346  
347  
348  
349  
350  
351  
352  
353  
354  
355  
356  
357  
358  
359  
360  
361  
362  
363  
364  
365  
366  
367  
368  
369  
370  
371  
372  
373  
374  
375  
376  
377  
378  
379  
380  
381  
382  
383  
384  
385  
386  
387  
388  
389  
390  
391  
392  
393  
394  
395  
396  
397  
398  
399  
400  
401  
402  
403  
404  
405  
406  
407  
408  
409  
410  
411  
412  
413  
414  
415  
416  
417  
418  
419  
420  
421  
422  
423  
424  
425  
426  
427  
428  
429  
430  
431  
432  
433  
434  
435  
436  
437  
438  
439  
440  
441  
442  
443  
444  
445  
446  
447  
448  
449  
450  
451  
452  
453  
454  
455  
456  
457  
458  
459  
460  
461  
462  
463  
464  
465  
466  
467  
468  
469  
470  
471  
472  
473  
474  
475  
476  
477  
478  
479  
480  
481  
482  
483  
484  
485  
486  
487  
488  
489  
490  
491  
492  
493  
494  
495  
496  
497  
498  
499  
500  
501  
502  
503  
504  
505  
506  
507  
508  
509  
510  
511  
512  
513  
514  
515  
516  
517  
518  
519  
520  
521  
522  
523  
524  
525  
526  
527  
528  
529  
530  
531  
532  
533  
534  
535  
536  
537  
538  
539  
540  
541  
542  
543  
544  
545  
546  
547  
548  
549  
550  
551  
552  
553  
554  
555  
556  
557  
558  
559  
560  
561  
562  
563  
564  
565  
566  
567  
568  
569  
570  
571  
572  
573  
574  
575  
576  
577  
578  
579  
580  
581  
582  
583  
584  
585  
586  
587  
588  
589  
590  
591  
592  
593  
594  
595  
596  
597  
598  
599  
600  
601  
602  
603  
604  
605  
606  
607  
608  
609  
610  
611  
612  
613  
614  
615  
616  
617  
618  
619  
620  
621  
622  
623  
624  
625  
626  
627  
628  
629  
630  
631  
632  
633  
634  
635  
636  
637  
638  
639  
640  
641  
642  
643  
644  
645  
646  
647  
648  
649  
650  
651  
652  
653  
654  
655  
656  
657  
658  
659  
660  
661  
662  
663  
664  
665  
666  
667  
668  
669  
670  
671  
672  
673  
674  
675  
676  
677  
678  
679  
680  
681  
682  
683  
684  
685  
686  
687  
688  
689  
690  
691  
692  
693  
694  
695  
696  
697  
698  
699  
700  
701  
702  
703  
704  
705  
706  
707  
708  
709  
710  
711  
712  
713  
714  
715  
716  
717  
718  
719  
720  
721  
722  
723  
724  
725  
726  
727  
728  
729  
730  
731  
732  
733  
734  
735  
736  
737  
738  
739  
740  
741  
742  
743  
744  
745  
746  
747  
748  
749  
750  
751  
752  
753  
754  
755  
756  
757  
758  
759  
760  
761  
762  
763  
764  
765  
766  
767  
768  
769  
770  
771  
772  
773  
774  
775  
776  
777  
778  
779  
780  
781  
782  
783  
784  
785  
786  
787  
788  
789  
790  
791  
792  
793  
794  
795  
796  
797  
798  
799  
800  
801  
802  
803  
804  
805  
806  
807  
808  
809  
810  
811  
812  
813  
814  
815  
816  
817  
818  
819  
820  
821  
822  
823  
824  
825  
826  
827  
828  
829  
830  
831  
832  
833  
834  
835  
836  
837  
838  
839  
840  
841  
842  
843  
844  
845  
846  
847  
848  
849  
850  
851  
852  
853  
854  
855  
856  
857  
858  
859  
860  
861  
862  
863  
864  
865  
866  
867  
868  
869  
870  
871  
872  
873  
874  
875  
876  
877  
878  
879  
880  
881  
882  
883  
884  
885  
886  
887  
888  
889  
890  
891  
892  
893  
894  
895  
896  
897  
898  
899  
900  
901  
902  
903  
904  
905  
906  
907  
908  
909  
910  
911  
912  
913  
914  
915  
916  
917  
918  
919  
920  
921  
922  
923  
924  
925  
926  
927  
928  
929  
930  
931  
932  
933  
934  
935  
936  
937  
938  
939  
940  
941  
942  
943  
944  
945  
946  
947  
948  
949  
950  
951  
952  
953  
954  
955  
956  
957  
958  
959  
960  
961  
962  
963  
964  
965  
966  
967  
968  
969  
970  
971  
972  
973  
974  
975  
976  
977  
978  
979  
980  
981  
982  
983  
984  
985  
986  
987  
988  
989  
990  
991  
992  
993  
994  
995  
996  
997  
998  
999  
1000

512 pharynx, only one paired lateral row of cells is present, which extends until the posterior trunk, as  
2  
3  
513 described originally [17].  
4  
5  
6

514 The two ventro-median ciliary patches at U7 and U11 (acp,pcp, Fig. 10B,H,I, position of patches  
8  
9  
515 measured from the center) are innervated by two short diffuse 5µm wide longitudinal nerves (cpn,  
10  
11  
516 Figs. 6B,I and 7B), joining perpendicularly the anterior nerve ring. Each patch also shows an  
12  
13  
14  
517 acetylated α-tubulin-LI-reactive positive ring around the ciliated area. The divergent morphology  
16  
17  
518 of these anucleate multiciliated cells and their close relation to the nervous system suggest that  
18  
19  
519 they could be sensory structures.  
20  
21  
22

520 Several sensoria are scattered along the body (ss, Fig. 10D,J), and two pairs of pharyngeal sensory  
23  
24  
25  
521 cilia (mk and pk, Figs. 3A-D,I,J, 4C,G and 10I) are located in the pharyngeal region (see the nervous  
26  
27  
28  
522 system section for further details).  
29  
30  
31

523 Two pairs of nephridia are found along the body (Fig. 10D): the anterior pair is situated ventro-  
32  
33  
34  
524 laterally and the posterior pair is located dorso-laterally, relatively close to the midline. The  
35  
36  
37  
525 anterior pair of protonephridia (apn, Fig. 10D,J) is situated anterior to the testis at U42 and the  
38  
39  
526 cilia are 20µm long. The posterior pair of protonephridia (ppn, Fig. 10D,K) is situated at U74 with  
40  
41  
42  
527 15µm long cilia. Each nephridium seems to possess two straight coaxial cilia (c, c', Fig. 10J,K),  
43  
44  
45  
528 thereby resembling the general paucitubulatinian protonephridia with two adjacent monociliated  
46  
47  
48  
529 terminal cells, projecting into a non-ciliated canal cell and ending with a nephridiopore epidermal  
49  
50  
530 cell [2, 41]. The canal cell and the nephridiopore cell have not been stained, why we lack  
51  
52  
531 information on the orientation and opening of protonephridia in *D. aspetos*.  
53  
54  
55  
56

## 532 Discussion

53  
54  
55  
56  
57  
58  
59  
60  
61  
62  
63  
64  
65

## 533 Phylogeny

534 The present phylogenetic analysis confirm that *Diuronotus aspetos* belongs to the monophyletic  
535 family Muselliferidae as proposed previously based on morphology [22, 23, 26]. We furthermore  
536 find Xenotrichulidae sister group to Muselliferidae (100% support), opposed to its position next to  
537 Group B (“Chaetonotidae” + Dasytydae + Neogosseidae) in Kånneby et al. [26] (69% PP).  
538 Moreover, the placement of *D. aspetos* considerably reduces the internal branch length of  
539 Muselliferidae, diminishing the possibility of long-branch attraction, with e.g. *Neodasys* ([49] and  
540 present study) or *Dactylopodola* [26], and the support of group B is now maximum. Two other  
541 interesting points can be noted: Furthermore the sister group relationship between Neogosseidae  
542 and Dasydytidae is recovered [50], and the sister group relationship of marine *Aspidiophorus* to  
543 the remaining members of the Group B is found again, similarly to Kånneby et al. 2012 [49], but  
544 not Kånneby and Todaro 2015 [50].

## 545 Musculature

546 The overall musculature of *Diuronotus aspetos* is relatively simple, consisting of only three pairs of  
547 longitudinal muscles in the trunk as well as a unique arrangement of multiple dorso-ventral  
548 muscles. The three pairs of longitudinal muscles in *D. aspetos* is, despite its generally larger size,  
549 less than what is found in most Paucitubulatina, having at least five pairs of longitudinal muscles  
550 that are often distributed as three pairs of splanchnic and three pairs of somatic muscles  
551 (*Musellifer*, *Draculiciteria*, *Heteroxenotrichula*, *Xenotrichula*, *Chaetonotus*, *Aspidiophorus*, and  
552 *Polymerurus*) [22, 31, 32]. The previously proposed hypothetical ancestral state of musculature in  
553 Paucitubulatina [2] shows a split of the dorsal longitudinal muscle (musculus dorsalis) into two  
554 branches, not present in *D. aspetos* that instead has a branch of the ventral longitudinal muscle

555 running dorsally. The more complex branching pattern of the ventral longitudinal muscle might be  
2  
3  
556 an adaptation to the large size of *D. aspetos*, compensating for the low number of longitudinal  
4  
5  
557 muscle.  
6  
7

8  
9  
558 The helicoidal musculature encircles the dorsal longitudinal muscles but not the ventral  
10  
11  
12  
559 longitudinal muscles or the ventro-lateral longitudinal muscles. The relative position of the dorsal  
13  
14  
560 longitudinal muscle indicates a homology to the dorsal splanchnic muscle of other Paucitubulatina.  
15  
16  
17  
561 However, its more dorsal position indicate that it support the body wall rather than the digestive  
18  
19  
20  
562 tract (see Kieneke and Schmidt-Rhaesa (2015) [2] for further discussion and limitations of this  
21  
22  
563 notion), perhaps furthermore compensating for the missing dorso-dermal muscle branch in *D.*  
23  
24  
25  
564 *aspetos* (see[2]). The ventro-lateral longitudinal muscle of *D. aspetos* can be homologized with the  
26  
27  
28  
565 somatic ventro-lateral muscle (or musculus lateralis) of other Gastrotricha, and the ventral  
29  
30  
31  
566 longitudinal muscle resembles those found in the paucitubulatinan *Muselifer delamerei*,  
32  
33  
34  
567 *Xenotrichula intermedia* Remane, 1934 [57] and *Heteroxenotrichula squamosa* Wilke, 1954 [58]  
35  
36  
568 [22].  
37  
38

39  
40  
41  
570 The unique semi-circular muscles of *D. aspetos* may aid the oviposition together with the dorso-  
42  
43  
44  
571 ventral muscles, hereby functionally replacing the dorso-dermal longitudinal muscle split  
45  
46  
47  
572 enveloping the egg in other Paucitubulatina [22]. They likely act as the posterior complete circular  
48  
49  
50  
573 muscles found in the region of the sexual organs of *Neodasys cf. uchidai* Remane, 1961 [59, 60].  
51  
52  
574 Functionally similar circular muscles are also found in the meiofauna gnathiferan *Gnathostomula*  
53  
54  
575 *armata* Riedl, 1971 [61] and *Gnathostomula peregrina* Kirsteuer, 1969 [62] (Gnathostomulida),  
55  
56  
57  
58  
59  
60  
61  
62  
63  
64  
65 here arranged in dense pattern around the posterior male organs [63, 64].

576 The evolution of the dorso-ventral muscles of Chaetonotida as deriving from the circular  
2  
3  
577 musculature has been one of the central debates in previous studies [22, 31]. In Macrodasysida and  
5  
578 Multitubulatina, the circular musculature consists of splanchnic and somatic elements, the former  
7  
8  
579 encircling the intestine and the latter, which derives from splanchnic elements, encircles the  
10  
11  
580 ventro-lateral longitudinal muscle on both sides [2, 22, 59]. In Paucitubulatina, the trunk circular  
12  
13  
581 muscles are either absent, incomplete or derived as dorso-ventral muscles as in Xenotrichulidae  
15  
16  
582 and *Musellifer* with dorso-ventral orientation [2, 22, 31, 65]. Compared to these arrangements,  
18  
19  
583 the configuration is unique in *D. aspetos* with more than two sets of dorso-ventral muscles in the  
20  
21  
584 transverse axis. The median-most dorso-ventral muscles can possibly be homologized with the  
23  
24  
585 visceral circular muscles in other gastrotrichs, however, the lateral sets of dorso-ventral muscles  
25  
26  
586 present various arrangements relative to the longitudinal muscles throughout the body length,  
28  
29  
587 making homologies difficult to assess. Furthermore, dorso-ventral muscles do not seem to be  
30  
31  
588 present lateral to the ventro-lateral longitudinal muscle, which would be an arrangement  
33  
34  
589 expected from a derived somatic semi-circular muscle such as found in other Paucitubulatina [20,  
36  
37  
590 22]. Consequently, solely the inner-most dorso-ventral muscles of *D. aspetos* can be homologized  
38  
39  
591 with semi-circular muscles of other Paucitubulatina.

41  
42  
592 The head diagonal muscle of *D. aspetos* may be homologous to the head semi-circular muscle  
44  
45  
593 found in *Musellifer delamerei* and *Dactylopodola baltica* (Remane, 1926) [22, 66, 67] showing the  
47  
48  
594 same anterior position and shape though a different orientation. The posterior diagonal muscle  
49  
50  
595 and the diagonal muscle of the tubes resemble a muscle found in the posterior region of  
52  
53  
596 *Heteroxenotrichula squamosa* (figure 3A, [22]), but no similar muscle exist in *Musellifer delamerei*,  
55  
56  
597 *Xenotrichula intermedia* or *X. punctata* Wilke, 1954 [22, 58]. The so called cross-over muscles  
57  
58  
598 found in Macrodasysida with a bilobed caudal end has a similar function, being involved in the  
60  
61  
62  
63  
64  
65

599 movement of the posterior tubes, yet with the lack of presence in other Paucitubulatina and  
600 different morphology in *D. aspetos* it is most likely of convergent origin [2, 66, 68].

## 601 Nervous system

602 To date, *Xenotrichula intermedia* and *Xenotrichula velox* Remane, 1927 [69] are the only other  
603 Paucitubulatina for which the nervous system has been studied with CLSM [13], therefore the  
604 present study adds valuable information. On the other hand, the nervous system of *Neodasys*  
605 (Multitubulatina was described in details with CLSM ) [12, 39], as well as several Macrodasysida [15,  
606 35, 36, 38, 39, 70, 71]. Furthermore *Cephalodasys maximus* Remane, 1926 [67] and *Turbanella*  
607 *cornuta* Remane, 1925 [72] have been described in detail with TEM [37, 73]. This offers a broad,  
608 but not comprehensive, bibliographic material to compare the nervous system of *D. aspetos* with  
609 other Gastrotricha.

## 610 Stomatogastric nervous system

611 Similar to other Chaetonotida [12, 13, 18], one dorso-median and two ventro-lateral longitudinal  
612 nerves constitute the overall pharyngeal nervous system of *Diuronotus aspetos*. However, the  
613 present study finds several additional structures previously undescribed for chaetonotids such as:  
614 i) five additional symmetric and one asymmetric longitudinal nerves branching off from the main  
615 nerves, ii) two previously undescribed commissures (anterior-most buccal nerve ring, middle  
616 pharyngeal nerve ring), and iii) a pair of ventro-lateral pharyngeal ganglia (innervating anterior  
617 sensory structures).

618 However, only the pharyngeal nervous system of *Cephalodasys maximus* has been  
619 comprehensively described [37] and little is known about the pharyngeal nervous system of

620 Chaetonotida (but see [12, 13]). Nonetheless, ultrastructural studies by Teuchert (1877) [73] and  
2  
3  
621 Ruppert (1982) [18] provide various details of the pharynx in several gastrotrichs, including some  
5  
622 details on *Diuronotus* sp.  
7

8  
9  
1023 In Macrodasysida the inverted organization of the pharynx generally offers one ventro-median and  
11  
12  
624 two dorso-lateral nerves as well as one additional dorso-median nerve [18]. In *Turbanella cornuta*,  
13  
14  
625 an additional asymmetric “thick” ventro-lateral nerve is also present in the pharynx [73], which  
16  
17  
626 resembles the one short asymmetric dorso-lateral longitudinal nerve found in *D. aspetos* to a  
18  
19  
627 certain degree. *Cephalodasys maximus* presents a pair of ventro-lateral asymmetric nerves (one  
21  
22  
628 short, one long) in the pharynx, but they originate more posteriorly from the pharyngeal nerve  
23  
24  
629 ring [37]. The different origin contradicts a homology with the asymmetric nerve of *D. aspetos* but  
26  
27  
630 show that asymmetry in the pharynx of gastrotrichs might be a frequent phenomenon since these  
29  
30  
631 three gastrotrichs are morphologically and phylogenetically diverse (e.g. [15, 29]).  
31  
32

33  
632 The present study show the presence of two pairs of pharyngeal kinocilia (versus one from TEM  
35  
36  
633 observations by Ruppert [18] in *D. aspetos*, absent in other Paucitubulatina, including *Musellifer*  
37  
38  
634 [18]. Macrodasysida and *Neodasys* possess multiple triplets of pharyngeal cilia [18], which suggests  
40  
41  
635 that they have been dramatically reduced in number in Paucitubulatina, and a single short pair  
42  
43  
636 may have either re-appeared in *Diuronotus* or alternatively be overlooked in previous studies on  
44  
45  
637 several Paucitubulatina. Ruppert [18] also discusses the presence of discrete glands opening in the  
48  
49  
638 mouth of *Chaetonotus* and *Musellifer*, possibly homologous to the anterior pharyngeal glands here  
50  
51  
639 described for *D. aspetos*.  
53  
54

55  
640 Herein is further revealed a presently undescribed pharyngeal canal system within the  
56  
57  
641 musculature, occasionally lined by nerves. However, a single transverse TEM micrograph of  
59  
60  
61  
62  
63  
64  
65

642 *Diuronotus* sp. by Ruppert (fig. 14, [18]) - proposedly from the level of the ventro-lateral  
2  
3  
643 pharyngeal ganglion - reveals a dorso-lateral as well as three ventro-lateral electron-lucent areas,  
4  
5  
644 which most likely resemble the canal system. The system may be unique to *Diuronotus* or  
6  
7  
8  
645 Muselliferidae, and its function is unknown.

## 646 **Central nervous system**

647 The overall morphology of the nervous system of *Diuronotus aspetos* is similar to other  
11  
12  
13  
14  
15  
1648 gastrotrichs [2] consisting of a “dumbbell-shaped” dorsal brain with a dorsal neuropil and a pair of  
17  
18  
19  
20  
2149 ventro-lateral nerves. However, additional nerves and specific perikarya are found in *D. aspetos*.

## 650 Longitudinal nerves

651 Anterior to the brain neuropil of *Diuronotus aspetos*, four pairs of dorsal nerve projections are  
23  
24  
25  
26  
27  
28  
29  
30  
31  
32  
33  
34  
35  
36  
37  
38  
39  
40  
41  
42  
43  
44  
45  
46  
47  
48  
49  
50  
51  
52  
53  
54  
55  
56  
57  
58  
59  
60  
61  
62  
63  
64  
65

652 found (acetylated  $\alpha$ -tubulin-LI-reactive, in addition to several minor neurites left undescribed),  
653 most likely related to the anterior sensoria. Similar nerve projections are described in *Neodasys*  
654 *chaetonotoideus* Remane, 1927 [12, 74], *Cephalodasys maximus* [37] and *Thaidasys tongiorgii*  
655 Todaro, Dal Zotto & Leasi, 2015 [15] but due to the scarcity of these descriptions, a closer  
656 homology cannot yet be stated. Another two pairs of nerves project antero-ventrally from the  
657 brain (serotonin-LI-reactive) in *D. aspetos*, one of which may be homologous to the commonly  
658 found single pair of serotonin-LI-reactive ventral projections in other gastrotrichs (e.g. *Neodasys*  
659 *chaetonotoideus*, *Dactylopodola* or *Oregodasys cirratus* [12, 36, 38]. A similar positioned pair of  
660 FMRF-amide-LI-reactive projections is present in *Lepidodasys worsaae* Hochberg and Atherton,  
661 2011 [70] and *Xenotrichula* [13, 70], and in *Oregodasys cirratus* these are expressing both FMRF-  
662 amide-LIR and serotonin-LIR [38], suggesting that the neurotransmitters of these nerves can vary,  
663 and that these nerves are a general character of Gastrotricha (cf. nervous system drawing in [2]).

664 Another striking character found in *D. aspetos* is the paired anterior ventro-median nerve in the  
2  
3  
665 anterior trunk. Short, paired anterior ventro-median nerves are also found in *Thaidasys tongiorgii*,  
5  
666 *Turbanella* cf. *hyalina* Schultze, 1853 [75], and extending the entire body length in *Oregodasys*  
7  
8  
667 *cirratus* [15, 38, 39]. However, the exact connection to other nerves and their extension differs  
10  
11  
668 from those of *D. aspetos*. Moreover, studies of the closely related *Neodasys chaetonotoideus* and  
12  
13  
669 *Xenotrichula* [12, 13] did not find similar paired anterior ventro-median nerves and we therefore  
15  
16  
670 consider the ventro-median nerves in *D. aspetos* a convergence related to the different ciliation of  
17  
18  
671 this species.  
19  
20  
21  
22

672 The paired short dorso-lateral nerves in *D. aspetos* (hdpn, Figs. 6A,H and 9A) are similar in position  
23  
24  
673 and extension to the paired dorsal nerves described in the distantly related *C. maximus* [37] as  
25  
26  
27  
674 well as the dorsal pharyngeal fibers found in the closely related *Xenotrichula* [13], of which the  
28  
29  
30  
675 latter at least seems to be homologous to the dorsal nerves of *D. aspetos*.  
31  
32

### 676 Ganglia and perikarya

33  
34  
35  
36  
37

677 Several immunoreactive perikarya can be compared to other gastrotrichs, mostly *Neodasys* and  
38  
39  
678 *Xenotrichula*. However, immunoreactivity of the perikarya is quite variable, and only a fraction of  
40  
41  
42  
679 the brain cells are immunoreactive.  
43  
44  
45

680 Only five pairs of serotonin-LI-reactive perikarya are found in the brain of *Diuronotus aspetos*,  
46  
47  
48  
681 situated postero-laterally to the neuropil. They comprise two dorsal pairs of perikarya, supplying  
49  
50  
51  
682 the neuropil, and a ventral pair of para-pharyngeal clusters (spgg, Figs. 7B-E and 9B) with three  
52  
53  
683 perikarya each, supplying the ventro-lateral nerve cords. The closely related *Xenotrichula* does not  
54  
55  
56  
684 possess a serotonin-LI-reactive equivalent to the ventral clusters, but possesses four dorsal pairs  
57  
58  
685 of serotonin-LI-reactive perikarya [13], two of which are likely homologous to the two dorsal pairs  
59  
60  
61  
62  
63  
64  
65

686 found in *D. aspetos*. *Neodasys chaetonotoideus* possesses three dorso-lateral serotonin-LI-reactive  
2  
3  
687 perikarya, which have similar positions and connection to the neuropil than the dorsal serotonin-  
5  
688 LI-reactive perikarya of *D. aspetos*. Moreover, *N. chaetonotoideus* possesses a similar paired  
7  
8  
689 cluster of para-pharyngeal serotonin-LI-reactive perikarya, associated to the ventro-lateral nerve  
10  
11  
690 cords. This suggests that *N. chaetonotoideus* and *D. aspetos* might share some plesiomorphic traits  
12  
13  
691 of their serotonin-LI-reactive nervous system, whereas *Xenotrichula* represents a derived  
15  
16  
692 condition. In the so far investigated Macrodasysida, the serotonin-LI-reactive brain is generally  
17  
18  
693 simpler than in Chaetonotida, comprising only one dorsal commissure and one pair of dorso-  
20  
21  
694 lateral perikarya [15, 38, 71] (sometimes two [76]), although additional serotonin-LI-reactive  
23  
24  
695 perikarya can be found in *Dactylopodola* [36], and *Paradasys subterraneus* Remane, 1934 [57].  
25  
26

27  
696 The FMRF-amide-LI-reactive perikarya of the brain of *D. aspetos* are numerous (at least 16 paired  
29  
30  
697 and two unpaired of various intensity of the immunoreactivity) and surround the brain neuropil  
31  
32  
698 dorsally, ventrally and laterally. Due to the high number and variation of FMRF-amide-LIR of the  
34  
35  
699 brain in Gastrotricha, we limit our comparison of *D. aspetos* to the closely related *Xenotrichula*  
36  
37  
700 [13]. Homologies of the perikarya depend on whether the anterior dorsal and ventral FMRF-  
39  
40  
701 amide-LI-reactive commissures in *Xenotrichula* are homologous to the anterior nerve ring of *D.*  
42  
43  
702 *aspetos*. If so, the two dorso-median FMRF-amide-LI-reactive perikarya found connected to the  
44  
45  
703 anterior dorsal commissure in *Xenotrichula*, may be homologous to the two dorso-median found  
47  
48  
704 in *D. aspetos*. The additional two described paired lateral and ventral FMRF-amide-LI-reactive  
49  
50  
705 perikarya in *Xenotrichula* are difficult to homologize with those of *D. aspetos*. However, one pair of  
52  
53  
706 undescribed ventral FMRF-amide-LI-reactive perikarya is found laterally on the ventral  
54  
55  
707 commissure of *Xenotrichula* (fig. 4H, [13]) and is possibly homologous to the ventral perikarya of  
57  
58  
708 the FMRF-amide-LI-reactive nerve ring in *D. aspetos*. Finally, one of the cells of the FMRF-amide-LI-  
60  
61  
62  
63  
64  
65

709 reactive dorso-posterior cluster of the brain of *D. aspetos* may be homologous to the single pair of  
2  
3  
710 perikarya found in *Xenotrichula* in the same position.  
4  
5  
6

711 In a position similar to the post-pharyngeal ganglion of *D. aspetos*, two pairs of FMRF-amide-LI-  
8  
9  
712 reactive (no serotonin-LIR) perikarya are described supplying the ventro-lateral nerve cord in  
10  
11  
713 *Xenotrichula* [13]. Between these two pairs, two short transverse FMRF-amide-LI-reactive neurites  
12  
13  
14  
714 almost constitute a commissure similar to the one of *D. aspetos*, suggesting that the posterior-  
15  
16  
715 most pair of perikarya in *Xenotrichula* is homologous to the ganglia found in *D. aspetos*.  
17  
18  
19  
20

716 An anal pair of serotonin-LI-reactive perikarya contained in the anal ganglion is found in *D. aspetos*  
21  
22  
717 as well as a posterior commissure, similar to what is described for *Xenotrichula* and *Neodasys*  
23  
24  
25  
718 *chaetonotoideus* [12, 13]. Yet, no equivalent is found in any Macrotrichida. Herein observations  
26  
27  
28  
719 show that the anal ganglion consists of several cells, contrary to other Chaetonotida [77].  
29  
30  
720 Moreover, we describe an additional pre-anal commissure, originating at the anal ganglion, only  
31  
32  
33  
721 revealed by acetylated  $\alpha$ -tubulin-LIR and hitherto not found in other gastrotrichs.  
34  
35  
36

## 722 Brain commissures

37  
38  
39  
40

723 *Diuronotus aspetos* does show a commissure situated directly ventrally to the main brain neuropil  
41  
42  
724 contrary to most Gastrotricha documented, including Chaetonotida (e.g. [12, 13, 15, 39]). This  
43  
44  
45  
725 character was central in previous discussions on a possible close relationship between  
46  
47  
48  
726 Cycloneuralia and Gastrotricha (e.g. [36, 39, 78, 79]), rejected today (e.g. [3, 80]) since, recent  
49  
50  
727 interpretations of the brain of Gastrotricha show that it is not truly circular [80]. In *D. aspetos*, the  
51  
52  
53  
728 anterior nerve ring is associated to the brain and its ventral portion resembles the ventral brain  
54  
55  
729 commissure of other Gastrotricha, although being more anterior. Furthermore, *Xenotrichula*  
56  
57  
58  
730 possesses one ventral FMRF-amide-LI-reactive commissure anterior of the brain [13]. If the FMRF-  
59  
60  
61  
62  
63  
64  
65

731 amide-LI-reactive anterior commissure of the brain and ventral commissure of *Xenotrichula* are  
2  
3  
732 continuous, it can be speculated that *Xenotrichula* also possesses an anterior nerve ring.  
4  
5  
6

## 733 **Ventral ciliation**

7  
8  
9

10  
134 The main difference from the original description is that the head ventral ciliation forms two  
12  
13  
735 medially separated ciliated areas in *Diuronotus aspetos*. Furthermore, a more detailed pattern has  
14  
15  
16  
736 been deduced, showing the relevance of CLSM for determining ciliary arrangement [81-83] (but  
17  
18  
737 also Kerbl et al., in prep; Bekkouche and Worsaae, in prep, respectively on Dinophilidae (Annelida)  
19  
20  
21  
738 and Micrognathozoa). This also opens the way to a new kind of characters in interstitial animals,  
22  
23  
24  
739 which could have a systematics value: the pattern of the multi-ciliated cells. Indeed, preliminary  
25  
26  
740 results showing variation in the pattern of the ventral multi-ciliated cells of Thaumastodermatidae  
27  
28  
29  
741 support this idea (Bekkouche and Worsaae unpublished). Unfortunately, though the description of  
30  
31  
742 the general pattern of the ventral ciliation is common in Chaetonotida, details are rare. In few  
32  
33  
34  
743 cases, more details were given, for instance for Neogosseidae (with exact description of the ciliary  
35  
36  
37  
744 bands [84]). A few studies described ciliary patches in the head of some Chaetonotidae (e.g. [85,  
38  
39  
745 86]), but no exact information about the cells themselves is given, why it is unknown if each patch  
40  
41  
42  
746 or band is constituted by one or several cells. This limitation of light and electron microscopy can  
43  
44  
45  
747 be overcome by employment of CLSM, but due to the lack of similar studies, we cannot yet  
46  
47  
748 comment on the evolution of the fine detailed ciliation pattern of Gastrotricha.  
48  
49

50  
749 Interestingly, some Paucitubulatina show unpaired ciliary patches on the ventral midline of the  
51  
52  
53  
750 head, e.g. *Halichaetonotus atlanticus*, Kisielewski, 1988 [85], *Arenotus strixinoi* Kisielewski, 1987  
54  
55  
56  
751 [86] or *Kijanebalola devestiva* Todaro, Perissinotto & Bownes, 2013 [84], but details are lacking to  
57  
58  
752 draw hypothesize any homology with the ventro-median ciliary patches of *D. aspetos*.  
59  
60  
61  
62  
63  
64  
65

## 753 **Protonephridial system**

754 Until the present study, all three previously studied Paucitubulatina were known to possess only  
755 one pair of protonephridia (*Xenotrichula carolinensis stylensis* Mock, 1979 [87], *Chaetonotus*  
756 *maximus* Ehrenberg, 1831 [41, 88] and *Polymerurus nodicaudus* (Voigt, 1901) [42, 89]. In this  
757 context, *Diuronotus aspetos* is the only Paucitubulatina known to have more than one pair of  
758 protonephridia. However, studies on the protonephridial system of *Musellifer* are needed to  
759 confirm if the presence of a single pair of protonephridia has a phylogenetic value or is a due to  
760 size dependency. Indeed, the number of pairs of protonephridia in other Gastrotricha is variable  
761 and seems to be roughly size dependent (e.g. two pairs for the ca. 250µm long *Dactylopodola*  
762 *baltica*, and 11 pairs for the ca 1mm long *Mesodasys laticaudatus* Remane, 1951 [90]) [91].

## 763 **Conclusion**

764 The present study is the first detailed anatomical description of a member of Muselliferidae, and  
765 only the second description of the nervous system within the larger clade Paucitubulitina [13]. The  
766 key phylogenetic position of *Diuronotus*, the surprising new discoveries of the nervous, muscular  
767 and ciliary system and several plausible homologies of these structures may be of significant  
768 importance for understanding the evolution of organ systems within Gastrotricha. However, as the  
769 present study showed, it is necessary to establish the position of *Neodasys* (as possible sister  
770 group to Paucitubulatina), in order to fully trace the evolution of organs systems within  
771 Paucitubulatina.

772 The musculature of *D. aspetos* presents unique traits for Paucitubulatina such as the reduction of  
773 the number of longitudinal muscles, compensated by the splitting of the ventral longitudinal

774 muscle, or the addition of dorso-ventral muscles in the transversal axis. This, in addition to many  
2  
3  
775 unique minor muscles (e.g. circular muscles of the adhesive glands, pharyngeal diagonal dorsal  
4  
5  
776 muscle) explains why the musculature of *D. aspetos* is difficult to compare to with the previously  
6  
7  
8  
777 studied Gastrotricha. However, the musculature has been shown to be phylogenetically  
9  
10  
11  
778 informative in Paucitubulatina [22] and future studies of additional species may aid to the  
12  
13  
14  
779 evolutionary reconstruction of the *D. aspetos* musculature.  
15  
16

17  
780 Although the nervous system of *D. aspetos* is in overall similar to other gastrotrichs, it presents  
18  
19  
20  
781 some additional traits such as a pair of anterior ventro-median nerves, the dorso-posterior nerves,  
21  
22  
782 and supplementary commissures, such as the pre-anal commissure. Two ganglia are described  
23  
24  
25  
783 here as well, comprising an anal ganglion, and consisting of several cells in contrast to findings in  
26  
27  
28  
784 other Chaetonotida [77]. These characters, as well as several other (e.g. details of the anterior  
29  
30  
785 nerve ring and immunoreactive perikarya) widen the diversity of nervous system traits in  
31  
32  
33  
786 Gastrotricha, showing that i) many seemingly minor nervous system components are still to be  
34  
35  
787 described in Gastrotricha, and that ii) the nervous system of *D. aspetos* is comparable to, e.g.,  
36  
37  
38  
788 *Xenotrichula*.  
39  
40

41  
789 Otherwise often overlooked organ systems were described here, such as the pharynx revealing so  
42  
43  
44  
790 far undescribed nerves, a unique system of canals, and the only finding of pharyngeal cilia in  
45  
46  
47  
791 Paucitubulatina (briefly mentioned in Ruppert 1982 [18]). Additionally, investigation of the ventral  
48  
49  
792 ciliation with CLSM reveals detailed of the cellular arrangement refining the previous description  
50  
51  
52  
793 [17]. These findings will hopefully prove to be of potential systematic value within Gastrotricha.  
53  
54

55  
794 One of the major restrictions of this study was of course the limited number of previously  
56  
57  
58  
795 conducted detailed morphological studies on Gastrotricha, but future investigation on the  
59  
60  
61  
62  
63  
64  
65

796 morphology of Paucitubulatina as *Musellifer*, *Draculiciteria*, marine *Aspidiophorus* and freshwater  
2  
3  
797 “Chaetonotidae” would vastly improve this picture.  
4  
5

## 798 **Declarations**

9

## 799 **Acknowledgements**

10  
11

12  
13  
14  
15  
16  
800 We have no competing interests.  
17  
18  
19

## 801 **Fundings**

20  
21  
22

23  
24  
802 The fieldwork on Greenland, the lab cost and the salary of the first author was supported by the  
25  
26  
803 Villum foundation (Grant no. 102544).  
27  
28  
29

## 804 **Authors’ contributions**

30  
31  
32

33  
805 NB and KW conceptualized and designed the study, collected the animals, analyzed the data, and  
34  
35  
806 wrote the manuscript. NB gathered the immunohistochemical data and made the illustrations.  
36  
37  
38  
39

## 807 **Acknowledgements**

40  
41  
42

43  
808 The Arctic Station of Qeqertarsuaq, University of Copenhagen provided an excellent working  
44  
45  
809 platform with cooling container and we are thankful to the crew of the station as well as R/V  
46  
47  
48  
810 Porsild. We also thank Christopher Laumer for his help on mining the transcriptome of *Diuronotus*  
49  
50  
51  
811 *aspetos*, Michelle Jørgensen for her help with the sequencing, Alexandra Kerbl for her help on  
52  
53  
812 proofreading the manuscript, and Laetitia Carrive for her help with the phylogenetic analysis.  
54  
55  
56  
57

## 813 **References**

58  
59  
60  
61  
62  
63  
64  
65

814 1. Edgecombe GD, Giribet G, Dunn CW, Hejnol A, Kristensen RM, Neves RC, Rouse GW, Worsaae K,  
815 Sørensen MV: **Higher-level metazoan relationships: recent progress and remaining questions.**  
816 *Organisms Diversity & Evolution* 2011, **11**(2):151-172.  
817 2. Kieneke A, Schmidt-Rhaesa A: **1. Gastrotricha.** In: *Handbook of Zoology, Gastrotricha and*  
818 *Gnathifera.* Edited by Schmidt-Rhaesa A, vol. 3: De Gruyer; 2015.  
819 3. Laumer CE, Bekkouche N, Kerb A, Goetz F, Neves RC, Sorensen MV, Kristensen RM, Hejno A, Dunn  
820 CW, Giribet G *et al*: **Spiralian Phylogeny Informs the Evolution of Microscopic Lineages.** *Current*  
821 *Biology* 2015, **25**(15):2000-2006.  
822 4. Hyman LH: **The Invertebrates. Vol. 3, Acanthocephala, aschelminthes, and entoprocta : the**  
823 **pseudocoelomate bilateria.** New York etc.: McGraw-Hill Book Company; 1951, VII, 572p.  
824 5. Bütschli O: **Untersuchungen über freilebende Nematoden und die Gattung *Chaetonotus*.** In:  
825 *Zeitschrift für wissenschaftliche Zoologie.* Edited by Engelmann W: Leipzig; 1876: 363-413.  
826 6. Rieger RM: **Monociliated epidermal cells in Gastrotricha; significance for concepts of early**  
827 **metazoan evolution.** *Zeitschrift Zool Syst Evolforsch* 1976, **14**(3):198-226.  
828 7. Zrzavý J, Mihulka S, Kepka P, Bezdek A, Tietz D: **Phylogeny of the Metazoa based on morphological**  
829 **and 18S ribosomal DNA evidence.** *Cladistics* 1998, **14**(3):249-285.  
830 8. Cavalier-Smith T: **A revised six-kingdom system of life.** *Biol Rev Camb Philos Soc* 1998, **73**(3):203-  
831 266.  
832 9. Giribet G: **Assembling the lophotrochozoan (=spiralian) tree of life.** *Philosophical Transactions of*  
833 *the Royal Society B: Biological Sciences* 2008, **363**(1496):1513-1522.  
834 10. Struck TH, Wey-Fabrizius AR, Golombek A, Hering L, Weigert A, Bleidorn C, Klebow S, Iakovenko N,  
835 Hausdorf B, Petersen M *et al*: **Platyzoan Paraphyly Based on Phylogenomic Data Supports a**  
836 **Noncoelomate Ancestry of Spiralia.** *Molecular Biology and Evolution* 2014, **31**(7):1833-1849.  
837 11. Kieneke A, Arbizu PM, Riemann O: **Body musculature of *Stylochaeta scirtetica* Brunson, 1950 and**  
838 ***Dasydytes (Setodytes) tongiorgii* (Balsamo, 1982) (Gastrotricha : Dasydytidae): A functional**  
839 **approach.** *Zoologischer Anzeiger* 2008, **247**(2):147-158.  
840 12. Rothe BH, Schmidt-Rhaesa A, Kieneke A: **The nervous system of *Neodasys chaetonotoideus***  
841 **(Gastrotricha: Neodasys) revealed by combining confocal laserscanning and transmission electron**  
842 **microscopy: evolutionary comparison of neuroanatomy within the Gastrotricha and basal**  
843 **Protostomia.** *Zoomorphology* 2011, **130**(1):51-84.  
844 13. Rothe BH, Kieneke A, Schmidt-Rhaesa A: **The nervous system of *Xenotrichula intermedia* and *X.***  
845 ***velox* (Gastrotricha: Paucitubulatina) by means of immunohistochemistry (IHC) and TEM.**  
846 *Meiofauna Marina* 2011, **19**:71-88.  
847 14. Todaro MA, Leasi F, Hochberg R: **A new species, genus and family of marine Gastrotricha from**  
848 **Jamaica, with a phylogenetic analysis of Macrodasysida based on molecular data.** *Systematics and*  
849 *Biodiversity* 2014, **12**(4):473-488.  
850 15. Todaro MA, Dal Zotto M, Leasi F: **An Integrated Morphological and Molecular Approach to the**  
851 **Description and Systematisation of a Novel Genus and Species of Macrodasysida (Gastrotricha).**  
852 *PLoS ONE* 2015, **10**(7):e0130278.  
853 16. Kolicka M, Dabert M, Dabert J, Kånneby T, Kisielewski J: ***Bifidochaetus*, a new Arctic genus of**  
854 **freshwater Chaetonotida (Gastrotricha) from Spitsbergen revealed by an integrative taxonomic**  
855 **approach.** *Invertebrates Systematics* 2016.  
856 17. Todaro MA, Balsamo M, Kristensen RM: **A new genus of marine chaetonotids (Gastrotricha), with**  
857 **a description of two new species from Greenland and Denmark.** *Journal of the Marine Biological*  
858 *Association of the United Kingdom* 2005, **85**(6):1391-1400.  
859 18. Ruppert EE: **Comparative Ultrastructure of the Gastrotrich Pharynx and the Evolution of**  
860 **Myoepithelial Foreguts in Aschelminthes.** *Zoomorphology* 1982, **99**(3):181-220.  
861 19. Ruppert EE: **Gastrotricha.** In: *Introduction to the study of meiofauna.* Smithsonian Institution Press,  
862 Washington, D.C.; 1988: 302-311.

59  
60  
61  
62  
63  
64  
65

- 863 20. Ruppert EE: **Gastrotricha**. In: *Microscopic anatomy of invertebrates Volume 4: Aschelminthes*. Edited by Harrison FW, Ruppert EE. New York, Chichester etc.: Wiley-Liss; 1991: 41-109.
- 864 21. Kieneke A: **Record of the 'Arctic' marine gastrotrich *Diuronotus aspetos* (Paucitubulatina) from the southern North Sea**. *Marine Biodiversity* 2015, **45**(4):615-616.
- 865 22. Leasi F, Todaro MA: **The muscular system of *Musellifer delamarei* (Renaud-Mornant, 1968) and other chaetonotidans with implications for the phylogeny and systematization of the Paucitubulatina (Gastrotricha)**. *Biological Journal of the Linnean Society* 2008, **94**(2):379-398.
- 866 23. Balsamo M, Guidi L, Ferraguti M, Pierboni L, Kristensen RM: ***Diuronotus aspetos* (Gastrotricha): new morphological data and description of the spermatozoon**. *Helgoland Marine Research* 2010, **64**(1):27-34.
- 867 24. D'Hondt JL: **Gastrotricha**. In: *Oceanography and Marine Biology: An Annual Review*. Edited by Barnes H, vol. 9. London: George Allen and Unwin Ltd; 1971: 141-192.
- 868 25. Hochberg R, Litvaitis MK: **Phylogeny of Gastrotricha: a morphology-based framework of gastrotrich relationships**. *Biological Bulletin* 2000, **198**(2):299-305.
- 869 26. Kånneby T, Atherton S, Hochberg R: **Two new species of *Musellifer* (Gastrotricha: Chaetonotida) from Florida and Tobago and the systematic placement of the genus within Paucitubulatina**. *Marine Biology Research* 2014, **10**(10):983-995.
- 870 27. Todaro MA, Telford MJ, Lockyer AE, Littlewood DTJ: **Interrelationships of the Gastrotricha and their place among the Metazoa inferred from 18S rRNA genes**. *Zoologica Scripta* 2006, **35**(3):251-259.
- 871 28. Paps J, Riutort M: **Molecular phylogeny of the phylum Gastrotricha: New data brings together molecules and morphology**. *Molecular Phylogenetics and Evolution* 2012, **63**(1):208-212.
- 872 29. Kieneke A, Riemann O, Ahlrichs WH: **Novel implications for the basal internal relationships of Gastrotricha revealed by an analysis of morphological characters**. *Zoologica Scripta* 2008, **37**(4):429-460.
- 873 30. Hummon WD: ***Musellifer sublitoralis* a New Genus and Species of Gastrotricha from San Juan Archipelago Washington**. *Transactions of the American Microscopical Society* 1969, **88**(2):282-286.
- 874 31. Hochberg R, Litvaitis MK: **The musculature of *Draculiciteria tessalata* (Chaetonotida, Paucitubulatina): implications for the evolution of dorsoventral muscles in Gastrotricha**. *Hydrobiologia* 2001, **452**(1-3):155-161.
- 875 32. Leasi F, Rothe BH, Schmidt-Rhaesa A, Todaro MA: **The musculature of three species of gastrotrichs surveyed with confocal laser scanning microscopy (CLSM)**. *Acta Zoologica* 2006, **87**(3):171-180.
- 876 33. Kieneke A, Ostmann A: **Structure, function and evolution of somatic musculature in Dasydytidae (Paucitubulatina, Gastrotricha)**. *Zoomorphology* 2012, **131**(2):95-114.
- 877 34. Hochberg R, Litvaitis MK: **A muscular double helix in gastrotricha**. *Zoologischer Anzeiger* 2001, **240**(1):61-68.
- 878 35. Hochberg R, Litvaitis MK: **Ultrastructural and immunocytochemical observations of the nervous systems of three macrodasyidan gastrotrichs**. *Acta Zoologica* 2003, **84**(3):171-178.
- 879 36. Rothe BH, Schmidt-Rhaesa A: **Architecture of the nervous system in two *Dactylopodola* species (Gastrotricha, Macrodasyida)**. *Zoomorphology* 2009, **128**(3):227-246.
- 880 37. Wiedermann A: **On the ultrastructure of the nervous system in *Cephalodasys maximus* (Macrodasyida, Gastrotricha)**. Zur Ultrastruktur des Nervensystems bei *Cephalodasys maximus* (Macrodasyida, Gastrotricha). *Microfauna Marina* 1995, **10**:173-233.
- 881 38. Rothe BH, Schmidt-Rhaesa A: ***Oregodasys cirratus*, a new species of Gastrotricha (Macrodasyida) from Tenerife (Canary Islands), with a description of the muscular and nervous system**. *Meiofauna Marina* 2010, **18**:49-66.
- 882 39. Hochberg R: **Comparative immunohistochemistry of the cerebral ganglion in Gastrotricha: an analysis of FMRamide-like immunoreactivity in *Neodasys cirritus* (Chaetonotida), *Xenodasys riedli* and *Turbanella cf. hyalina* (Macrodasyida)**. *Zoomorphology* 2007, **126**(4):245-264.

- 912 40. Schöpfer-Sterrer C: ***Chordodasys riedli* gen. nov. spec. nov. a macrodasyoid gastrotrich with a**  
913 **chordoid organ.** *Cahiers de Biologie Marine* 1969, **10**(4):391-404.
- 914 41. Kieneke A, Ahlrichs WH, Arbizu PM, Bartolomaeus T: **Ultrastructure of protonephridia in**  
915 ***Xenotrichula carolinensis syltensis* and *Chaetonotus maximus* (Gastrotricha : Chaetonotida):**  
916 **comparative evaluation of the gastrotrich excretory organs.** *Zoomorphology* 2008, **127**(1):1-20.
- 917 42. Kieneke A, Hochberg R: **Ultrastructural observations of the protonephridia of *Polymerurus***  
918 ***nodicaudus* (Gastrotricha: Paucitubulatina).** *Acta Zoologica* 2012, **93**(1):115-124.
- 919 43. Meyer CP: **Molecular systematics of cowries (Gastropoda: Cypraeidae) and diversification**  
920 **patterns in the tropics.** *Biological Journal of the Linnean Society* 2003, **79**(3):401-459.
- 921 44. Giribet G, Carranza S, Baguna J, Riutort M, Ribera C: **First molecular evidence for the existence of a**  
922 **Tardigrada + Arthropoda clade.** *Molecular Biology and Evolution* 1996, **13**(1):76-84.
- 923 45. Brown S, Rouse G, Hutchings P, Colgan D: **Assessing the usefulness of histone H3, U2 snRNA and**  
924 **28S rDNA in analyses of polychaete relationships.** *Australian Journal of Zoology* 1999, **47**(5):499-  
925 516.
- 926 46. Vonnemann V, Schrodli M, Klussmann-Kolb A, Wagele H: **Reconstruction of the phylogeny of the**  
927 **Opisthobranchia (Mollusca : Gastropoda) by means of 18S and 28S rRNA gene sequences.** *Journal*  
928 **of Molluscan Studies** 2005, **71**:113-125.
- 929 47. Hall TA: **BioEdit: a user-friendly biological sequence alignment editor and analysis program for**  
930 **Windows 95/98/NT.** *Nucleic Acids Symposium Series* 1999, **41**:95-98.
- 931 48. Geer LY, Marchler-Bauer A, Geer RC, Han L, He J, He S, Liu C, Shi W, Bryant SH: **The NCBI**  
932 **BioSystems database.** *Nucleic Acids Res* 2010, **38**(Database issue):D492-496.
- 933 49. Kånneby T, Todaro MA, Jondelius U: **Phylogeny of Chaetonotidae and other Paucitubulatina**  
934 **(Gastrotricha: Chaetonotida) and the colonization of aquatic ecosystems.** *Zoologica Scripta* 2013,  
935 **42**(1):88-105.
- 936 50. Kånneby T, Todaro MA: **The phylogenetic position of Neogosseidae (Gastrotricha: Chaetonotida)**  
937 **and the origin of planktonic Gastrotricha.** *Organisms Diversity & Evolution* 2015, **15**(3):459-469.
- 938 51. Todaro MA, Kånneby T, Dal Zotto M, Jondelius U: **Phylogeny of Thaumastodermatidae**  
939 **(Gastrotricha: Macrodasysida) Inferred from Nuclear and Mitochondrial Sequence Data.** *PLoS ONE*  
940 2011, **6**(3):e17892, 17891-17813.
- 941 52. Vaidya G, Lohman DJ, Meier R: **SequenceMatrix: concatenation software for the fast assembly of**  
942 **multi-gene datasets with character set and codon information.** *Cladistics* 2011, **27**(2):171-180.
- 943 53. Huelsenbeck JPR, F.: **MRBAYES: Bayesian inference of phylogeny.** *Bioinformatics* 2001, **17**:754-755.
- 944 54. **Tracer v1.6, Available from <http://beast.bio.ed.ac.uk/Tracer>**
- 945 55. Hummon WD, Balsamo M, Todaro MA: **Italian Marine Gastrotricha 1. 6 New and One Redescribed**  
946 **Species of Chaetonotida.** *Bollettino Di Zoologia* 1992, **59**(4):499-516.
- 947 56. Renaud-Mornant J: **Présence du genre *Polymerurus* en milieu marin, description de deux espèces**  
948 **nouvelles (Gastrotricha, Chaetonotoidea).** *Pubblicazioni della Stazione Zoologica di Napoli* 1968,  
949 **36**:141-151.
- 950 57. Remane A: **Die Gastrotrichen des Küstengrundwassers von Schilksee.** *Schriften des*  
951 **Naturwissenschaftlichen Vereins für Schleswig-Holstein** 1934, **20**(2):473-478.
- 952 58. Wilke U: **Mediterrane Gastrotrichen.** *Zoologische Jahrbücher* 1954, **82**(6):497-654.
- 953 59. Hochberg R: **Musculature of the primitive gastrotrich *Neodasys* (Chaetonotida): functional**  
954 **adaptations to the interstitial environment and phylogenetic significance.** *Marine Biology (Berlin)*  
955 2005, **146**(2):315-323.
- 956 60. Remane A: ***Neodasys uchdai* nov. spec., eine zwiete *Neodasys* Art (Gastrotrich Chaetoidea).** *Kieler*  
957 **Meeresforschungen** 1961, **17**:85-88.
- 958 61. Riedl R: **On the Genus *Gnathostomula* (Gnathostomulida).** *International Review of Hydrobiology*  
959 1971, **56**(3):385-496.
- 960 62. Kristeuer E: **On some species of Gnathostomulida from Bimini, Bahamas, vol. 2356; 1969, 21p.**

- 961 63. Müller MCM, Sterrer W: **Musculature and nervous system of *Gnathostomula peregrina* (Gnathostomulida) shown by phalloidin labeling, immunohistochemistry, and cLSM, and their phylogenetic significance.** *Zoomorphology (Berlin)* 2004, **123**(3):169-177.
- 962
- 963 64. Tyler S, Hooge MD: **Musculature of *Gnathostomula armata* Riedl 1971 and its ecological significance.** *Marine Ecology* 2001, **22**(1-2):71-83.
- 964
- 965
- 966 65. Leasi F, Todaro MA: **Meiofaunal cryptic species revealed by confocal microscopy: the case of *Xenotrichula intermedia* (Gastrotricha).** *Marine Biology* 2009, **156**(6):1335-1346.
- 967
- 968 66. Hochberg R, Litvaitis MK: **The muscular system of *Dactylopodola baltica* and other macrodasyidan gastrotrichs in a functional and phylogenetic perspective.** *Zoologica Scripta* 2001, **30**(4):325-336.
- 969
- 970 67. Remane A: **Morphologie und verwandtschaftsbeziehungen der aberranten gastrotrichen I.** *Zeitschrift für Morphologie und Ökologie der Tiere* 1926, **5**(4):625-754.
- 971
- 972 68. Hochberg R, Litvaitis MK: **Functional morphology of muscles in *Tetranchyroderma papii* (Gastrotricha).** *Zoomorphology* 2001, **121**(1):37-43.
- 973
- 974 69. Remane A: ***Xenotrichula velox* nov. gen. nov. spec., ein chaetonotoides Gastrotrich mit männlichen Geschlechtsorganen.** *Zoologischer Anzeiger* 1927, **71**:289-294.
- 975
- 976 70. Hochberg R, Atherton S: **A new species of *Lepidodasys* (Gastrotricha, Macrodasyida) from Panama with a description of its peptidergic nervous system using CLSM, anti-FMRamide and anti-SCPb.** *Zoologischer Anzeiger* 2011, **250**(2):111-122.
- 977
- 978 71. Rothe BH, Schmidt-Rhaesa A: **Variation in the nervous system in three species of the genus *Turbanella* (Gastrotricha, Macrodasyida).** *Meiofauna Marina* 2008, **16**:175-184.
- 979
- 980 72. Remane A: **Neue aberrante Gastrotrichen II: *Turbanella cornuta* n. sp. und *T. hyalina* M. Schultze, 1853.** *Zoologischer Anzeiger* 1925, **64**(309-314).
- 981
- 982 73. Teuchert G: **The ultrastructure of the marine gastrotrich *Turbanella cornuta* Remane (Macrodasyoidea) and its functional and phylogenetical importance.** *Zoomorphologie* 1977, **88**(3):189-246, illust.
- 983
- 984 74. Remane A: **Beiträge zur Systematik der Süßwassergastrotrichen.** *Zoologische Jahrbücher (Abteilung für Systematik, Ökologie, und Geographie der Tiere)* 1927, **53**:269-320.
- 985
- 986 75. Schultze M: **Über *Chaetonotus* und *Ichthydium* (Ehrb.) und eine neue verwandte Gattung *Turbanella*.** *Müller's Archiv für Anatomie und Physiologie* 1853, **6**:241-254.
- 987
- 988 76. Joffe BI, Wikgren M: **Immunocytochemical Distribution of 5-Ht (Serotonin) in the Nervous-System of the Gastrotrich *Turbanella cornuta*.** *Acta Zoologica* 1995, **76**(1):7-9.
- 989
- 990 77. Schmidt-Rhaesa A, Rothe BH: **Gastrotricha.** In: *Structure and Evolution of Invertebrate Nervous Systems.* Edited by Schmidt-Rhaesa A, Harzsch S, Purschke G. New York: Oxford University Press; 2016: 141-147.
- 991
- 992 78. Brusca RC, Brusca GJ: **Invertebrates. Second edition.** Sunderland: Sinauer Associates, Inc.; 2003, i-xx, 1-936p.
- 993
- 994 79. Schmidt-Rhaesa A: **The nervous system of *Nectonema munidae* and *Gordius aquaticus*, with implications for the ground pattern of the Nematomorpha.** *Zoomorphology (Berlin)* 1996, **116**(3):133-142.
- 995
- 996 80. Schmidt-Rhaesa A: **The evolution of organ systems.** Oxford & New York: Oxford University Press; 2007, i-x, 1-385p.
- 997
- 998 81. Worsaae K, Rouse GW: **Is *Diurodrilus* an annelid?** *Journal of Morphology* 2008, **269**(12):1426-1455.
- 999
- 1000 82. Worsaae K, Sterrer W, Iliffe TM: ***Longipalpa saltatrix*, a new genus and species of the meiofaunal family Nerillidae (Annelida: Polychaeta) from an anchihaline cave in Bermuda.** *Proceedings of the Biological Society of Washington* 2004, **117**(3):346-362.
- 1001
- 1002 83. Villora-Moreno S: **Ecology and distribution of the Diurodrilidae (Polychaeta), with redescription of *Diurodrilus benazzii*.** *Cahiers de Biologie Marine* 1996, **37**(1):99-108.
- 1003
- 1004 84. Todaro AM, Perissinotto R, Bownes SJ: **Neogosseidae (Gastrotricha, Chaetonotida) from the iSimangaliso Wetland Park, KwaZulu-Natal, South Africa.** *ZooKeys* 2013, **315**:77-94.
- 1005
- 1006
- 1007
- 1008
- 1009

59  
60  
61  
62  
63  
64  
65

- 1010 85. Kisielowski J: **New records of marine Gastrotricha from the French coasts of Manche and Atlantic.**  
 1011 **2. Chaetonotida, with descriptions of four new species.** *Cahiers de Biologie Marine* 1988,  
 1012 **29(2):187-213.**
- 1013 86. Kisielowski J: **Two new interesting genera of Gastrotricha (Macrodasysida and Chaetonotida) from**  
 1014 **the Brazilian freshwater psammon.** *Hydrobiologia* 1987, **153(1):23-30.**
- 1015 87. Mock H: **Chaetonotoidea (Gastrotricha) der Nordseeinsel Sylt.** *Akademie Der Wissenschaften Und*  
 1016 *Der Literatur Mainz Mathematisch-Naturwissenschaftlichen Klasse Mikrofauna Des Meeresbodens*  
 1017 1979:1-107.
- 1018 88. Ehrenberg H: **Über die Entwicklung und Lebensdauer der Infusionsthier; nebst fernerer**  
 1019 **Beiträgen zu einer Vergleichung ihrer organischen Systeme.** *Abhandlungen der Königlichen*  
 1020 *Akademie der Wissenschaften zu Berlin* 1831:1-154.
- 1021 89. Voigt M: **Über einige bisher unbekannte Süßwasserorganismen.** *Zoologischer Anzeiger* 1901,  
 1022 **24:191-195.**
- 1023 90. Remane A: **Mesodasys, ein neues Genus der Gastrotricha Macrodasysidea aus der Kieler Bucht.**  
 1024 *Kieler Meeresforschungen* 1951, **8:102-105.**
- 1025 91. Neuhaus B: **Ultrastructure of the protonephridia in *Dactylopodola baltica* and *Mesodasys***  
 1026 ***laticaudatus* (Macrodasysida): implications for the ground pattern of the Gastrotricha.** *Microfauna*  
 1027 *Marina* 1987, **3:419-438.**

## 1028 Figure legends

1029 **Figure 1: Phylogenetic position of *Diuronotus aspetos* inferred from Bayesian analysis of 18S,**  
 1030 **28S, and COI.** The analysis includes 58 taxa representing all available genera of Chaetonotida for  
 1031 molecular data on NCBI, and three Macrodasysida as outgroups. Numbers at the nodes represent  
 1032 posterior probabilities in percentages. The picture on the lower left corner is a light micrograph of  
 1033 a live specimen of *Diuronotus aspetos*.

1034 **Figure 2: CLSM of phalloidin stained muscle of *Diuronotus aspetos*.** Anterior of the specimen is  
 1035 pointing left for **A,B) and J-P),** and dorsal is pointing at the top for **D-I).** **A-N)** Muscles in green,  
 1036 nuclei in cyan **A)** Ventral view of the maximum intensity projection (MIP) of the whole specimen.  
 1037 **B)** Dorsal MIP of the pharynx. **C)** Dorsal MIP of the posterior specimen. **D- I)** CLSM virtual  
 1038 transverse section of various part of the specimen: **D)** head, **E)** posterior part of the pharynx, **F)**  
 1039 anterior of the trunk, **G)** posterior of the trunk, **H)** post-anal region of the trunk, **I)** and furca before  
 1040 bifurcation of the tubes. **J)** Dorsal MIP of a sub-stack showing details on the head musculature. **K)**

1041 Dorsal MIP of a sub-stack showing details of the furca separation. **L)** Ventral MIP of a sub-stack  
 2  
 3  
 1042 showing details of the semicircular musculature. **M)** Single section showing details of the inner  
 4  
 5  
 1043 pharynx. **N)** Dorsal MIP of a substack showing details of the helicoidal musculature. **O** And **P)**,  
 6  
 7  
 8  
 1044 isosurface reconstruction of the pharynx. **O)** Dorsal view, **P)** ventral view. **ag**, adhesive gland; **agn**,  
 9  
 10  
 11  
 1045 adhesive gland nucleus; **aps**, anterior pharyngeal sphincter; **cmag**, circular muscle of the adhesive  
 12  
 13  
 1046 gland; **dlim**, dorsal longitudinal muscle; **dvlm**, dorsal projection of the ventral longitudinal muscle;  
 14  
 15  
 16  
 1047 **dvm**, dorso-ventral muscle; **hdm**, head diagonal muscle; **hm**, helicoidal muscles; **lplm**, lateral  
 17  
 18  
 1048 pharyngeal longitudinal muscle; **lvlm**, Lateral extension of the ventral longitudinal muscle; **mn**,  
 19  
 20  
 21  
 1049 myocyte nuclei; **mvlm**, medial projection of the ventral longitudinal muscle; **pcm**, pharyngeal  
 22  
 23  
 24  
 1050 circular muscle; **pddm**, pharyngeal dorsal diagonal muscle; **pdm**, posterior diagonal muscle; **pdlm**,  
 25  
 26  
 1051 pharyngeal dorsal longitudinal muscle; **ph**, pharynx; **pps**, posterior pharyngeal sphincter; **pt**,  
 27  
 28  
 29  
 1052 primary tube; **rpm**, radial pharyngeal muscles; **scm**, semi-circular muscle; **st**, secondary tube; **tdm**,  
 30  
 31  
 1053 tube diagonal muscle; **vlm**, ventral longitudinal muscle; **vllm**, ventro-lateral longitudinal muscle;  
 32  
 33  
 34  
 1054 **vlm**, ventral longitudinal muscle.

1055 **Figure 3: Schematic drawings of the musculature of *Diuronotus aspetos*.** Anterior is pointing at  
 36  
 37  
 38  
 1056 the top for **A)** and **B)**, dorsal is pointing at the top for **C-H)**. **A)** Ventral view of the musculature, **B)**  
 39  
 40  
 41  
 1057 dorsal view of the musculature, **C-H)** cross section of the specimen **C)** in the head, **D)** posterior  
 42  
 43  
 44  
 1058 part of the pharynx, **E)** anterior of the trunk, **F)** posterior of the trunk, **G)** post-anal region of the  
 45  
 46  
 47  
 1059 trunk, **H)** and in the furca before bifurcation of the tubes. Note that in **C)** and **D)**, the helicoidal  
 48  
 49  
 50  
 1060 pharyngeal musculature is represented in dash lines due to the uncertainty of its presence, and it  
 51  
 52  
 53  
 1061 is not drawn in **A)** and **B)**. **aps**, anterior pharyngeal sphincter; **cmag**, circular muscle of the  
 54  
 55  
 56  
 1062 adhesive gland; **dlim**, dorsal longitudinal muscle; **dvlm**, dorsal projection of the ventral longitudinal  
 57  
 58  
 1063 muscle; **dvm**, dorso-ventral muscle; **hdm**, head diagonal muscle; **hm**, helicoidal muscle; **int**:

1064 intestine; **lplm**, lateral pharyngeal longitudinal muscle; **lvlm**, Lateral extention of the ventral  
2  
3  
1065 longitudinal muscle; **mvlm**, medial projection of the ventral longitudinal muscle; **ov**, ovary; **pcm**,  
4  
5  
1066 pharyngeal circular muscle; **pdm**, posterior diagonal muscle; **pddm**, pharyngeal dorsal diagonal  
6  
7  
8  
1067 muscle; **pdlm**, pharyngeal dorsal longitudinal muscle; **pps**, posterior pharyngeal sphincter; **rpm**,  
9  
10  
11  
1068 radial pharyngeal muscles; **scm**, semi-circular muscle; **tdm**, tube diagonal muscle; **vilm**, ventro  
12  
13  
1069 lateral longitudinal muscle; **vlm**, ventral longitudinal muscle.

1070 **Figure 4: Pharyngeal nervous system and canal system of *Diuronotus aspetos*. A,B)** Anterior is  
17  
18  
19  
1071 pointing at the top; **C-N** dorsal is pointing at the top. **A-H)** Schematic drawings with nerves in blue  
20  
21  
22  
1072 and pharyngeal system in yellow, nuclei in grey, glands in green and cilia in red. **A)** Dorsal section  
23  
24  
25  
1073 of the pharynx. **B)** Ventral section of the pharynx. **C-H)** Successive transverse sections of the  
26  
27  
28  
1074 pharynx from anterior to posterior. **I-N)** CLSM virtual transverse sections at the same levels as C-  
29  
30  
31  
1075 H). Acetylated  $\alpha$ -tubulin-LIR in glow and DAPI in cyan. **adpn**, anterior diagonal pharyngeal nerve;  
32  
33  
1076 **apg**, anterior pharyngeal gland; **avrc**, anterior ventro-median right pharyngeal canal; **bnr**, buccal  
34  
35  
1077 nerve ring; **dpc**, dorsal pharyngeal canal; **dpcn**, dorso-anterior pharyngeal canal nerve; **dpn**, dorsal  
36  
37  
38  
1078 pharyngeal nerve; **lpvc**, left posterior ventro-median canal; **mk**, mouth kinocilium; **pdivn**,  
39  
40  
41  
1079 pharyngeal dorso-ventral nerve; **pk**, posterior pharyngeal kinocilium; **plgn**, pharyngeal longitudinal  
42  
43  
1080 gland nerve; **plkn**, pharyngeal longitudinal kinocilium nerve; **pmdn**, paramedian dorsal pharyngeal  
44  
45  
46  
1081 nerves; **pnr**, pharyngeal nerve ring; **ppc**, posterior pharyngeal cluster; **rpvc**, right posterior ventro-  
47  
48  
49  
1082 median canal; **vlpc**, ventro-lateral pharyngeal canal; **vllpg**, ventro-lateral pharyngeal ganglion; **vpn**,  
50  
51  
1083 ventral pharyngeal nerve.

1084 **Figure 5: CLSM of the pharyngeal nervous system and canal system of *Diuronotus aspetos*. A-  
54  
55  
56  
1085 C,G,I)** anterior is pointing at the top. **D-F,H)** anterior pointing left. CLSM maximum intensity  
57  
58  
59  
60  
61  
62  
63  
64  
65

1086 projection of sub-stacks. Acetylated  $\alpha$ -tubulin-LIR in glow, DAPI in cyan. **A)** Dorso-anterior section  
 2  
 3  
 1087 of the pharynx. **B)** Dorso-anterior section of the pharynx, more ventral than B). **C)** Ventro-anterior  
 4  
 5  
 1088 section of the pharynx. **D)** Ventro-posterior section of the pharynx. **E)** Dorso-posterior section of  
 6  
 7  
 8  
 1089 the pharynx. **F)** Medio-posterior portion of the pharynx. **G)** Medio-anterior section of the pharynx.  
 9  
 10  
 1090 **H)** Details of the ventro-lateral pharyngeal ganglion. **I)** Details of the posterior pharyngeal  
 11  
 12  
 1091 ganglion. **adpn**, anterior diagonal pharyngeal nerve; **anr**, anterior nerve ring; **apg**, anterior  
 13  
 14  
 1092 pharyngeal gland; **avrc**, anterior ventro-median right pharyngeal canal; **bnr**, buccal nerve ring; **dpc**,  
 15  
 16  
 1093 dorsal pharyngeal canal; **dpcn**, dorso-anterior pharyngeal canal nerve; **dpn**, dorsal pharyngeal  
 17  
 18  
 1094 nerve; **hdpn**, head dorso-posterior nerve; **lpvc**, left posterior ventro-median canal; **mk**, mouth  
 19  
 20  
 1095 kinocilium; **np**, neuropile; **pdivn**, pharyngeal dorso-ventral nerve; **pk**, posterior pharyngeal  
 21  
 22  
 1096 kinocilium; **plgn**, pharyngeal longitudinal gland nerve; **plkn**, pharyngeal longitudinal kinocilium  
 23  
 24  
 1097 nerve; **pmdn**, paramedian dorsal pharyngeal nerves; **pnr**, pharyngeal nerve ring; **ppc**, posterior  
 25  
 26  
 1098 pharyngeal cluster; **rpvc**, right posterior ventro-median canal; **ss**, sensoria; **vlpg**, ventro-lateral  
 27  
 28  
 1099 pharyngeal ganglion; **vlpc**, ventro-lateral pharyngeal canal; **vpn**, ventral pharyngeal nerve.  
 29  
 30  
 31  
 32  
 33  
 34  
 35  
 36  
 37  
 38  
 39  
 40  
 41  
 42  
 43  
 44  
 45  
 46  
 47  
 48  
 49  
 50  
 51  
 52  
 53  
 54  
 55  
 56  
 57  
 58  
 59  
 60  
 61  
 62  
 63  
 64  
 65

**Figure 6: Drawing and CLSM of the acetylated  $\alpha$ -tubulin-LIR nervous system of *Diuronotus***  
***aspetos*.** Anterior pointing left for **A-I)**, and pointing at the top for **J)** and **K)**. **A, B)** Schematic  
 drawings of the  $\alpha$ -tubulin-LIR of the anterior part of the specimen: nerves in blue, nuclei in grey,  
 and opposite ventral or dorsal nervous system in light grey **A)** dorsal **B)** ventral. **C)** CLSM ventral  
 view of the maximum intensity projection (MIP) of the entire specimen. **D-K)** CLSM MIP sub-stacks  
 of various parts of the specimen. Acetylated  $\alpha$ -tubulin-LIR in glow, and DAPI in cyan in all CLSM  
 pictures. **D)** Ventro-anterior nervous system. **E)** Neuropil side **F)** Ventral, post pharyngeal ganglion.  
**G)** Ventral, trunk commissure. **H)** Dorso-posterior part of the head **I)** ventro-anterior part of the  
 head **J)** Dorso-anterior part of the head. **K)** Ventro posterior terminal part of the specimen. **ang**,

1109 anal ganglion; **anr**, anterior nerve ring; **avmn**, anterior ventro-median nerve; **br**, brain; **cpn**,  
2  
3  
1110 ciliated patch nerves; **dannp**, dorso-median anterior nerve projection; **dlnp**, dorso-lateral anterior  
4  
5  
1111 nerve projections; **hdpn**, head dorso-posterior nerve; **hdn**, head diagonal nerve; **hln**, head lateral  
6  
7  
8  
1112 nerve; **lgcb**, lateral gland cell of the brain; **np**, neuropile; **nppt**, nerve projection of the primary  
9  
10  
1113 tube; **pac**, pre-anal commissure; **pco**, posterior commissure; **pgg**, post-pharyngeal ganglion; **ph**,  
11  
12  
13  
1114 pharynx; **spc**, sub-pharyngeal commissure; **tt**, testis; **tv**, trunk ventral commissure; **vlnc**, ventro-  
14  
15  
16  
1115 lateral nerve cord.  
17  
18  
19

1116 **Figure 7: serotonin-LIR nervous system of *Diuronotus aspetos*.** The anterior is pointing left for all  
20  
21  
22  
1117 figures. **A, B)** Schematic drawings of the serotonin-LIR of the anterior part of the specimen: nerves  
23  
24  
25  
1118 and perikarya in green, nuclei in grey, and opposite ventral or dorsal nervous system in light grey.  
26  
27  
1119 **A)** Dorsal view, **B)** ventral view. **C-F)** CLSM images with serotonin-LIR in glow. **C)** CLSM maximum  
28  
29  
30  
1120 intensity projection (MIP) of the entire specimen. **D)** Dorsal MIP of the brain **E)** CLSM sub-stack  
31  
32  
33  
1121 MPI showing details of the brain perikarya **F)** CLSM sub-stack MPI of the ventro-posterior terminal  
34  
35  
36  
1122 part of the specimen. **br**, brain; **ph**, pharynx; **sacn**, serotonin-LI-reactive anterior commissure of  
37  
38  
1123 the neuropil; **sanr**, serotonin-LI-reactive anterior nerve ring; **sdlp**, serotonin-LI-reactive dorso-  
39  
40  
41  
1124 lateral perikaryon; **sdmp**, serotonin-LI-reactive dorso-median perikaryon; **slbn**, serotonin-LI-  
42  
43  
1125 reactive lateral brain nerve; **slnc**, serotonin-LI-reactive ventro-lateral nerve cord; **slpn**, serotonin-  
44  
45  
46  
1126 LI-reactive lateral nerves of the posterior commissure of the neuropil; **spln**, serotonin-LI-reactive  
47  
48  
1127 postero-lateral nerve node; **smbn**, serotonin-LI-reactive median-most brain nerve; **smcn**,  
49  
50  
51  
1128 serotonin-LI-reactive median commissure of the neuropil; **snp**, serotonin-LI-reactive neuropil;  
52  
53  
54  
1129 **snpt**, serotonin-LI-reactive nerve projection of the primary tube; **spag**, serotonin-LI-reactive  
55  
56  
1130 perikarya of the anal ganglion; **spbn**, serotonin-LI-reactive paramedian brain nerve; **spcn**,  
57  
58  
59  
1131 serotonin-LI-reactive posterior commissure of the neuropil; **spco**, serotonin-LI-reactive posterior  
60  
61  
62  
63  
64  
65

1132 commissure; **spog**, serotonin-LI-reactive perikarya of the post-pharyngeal ganglion; **spp**,  
2  
3  
1133 serotonin-LI-reactive neuropil patch; **sppg**, serotonin-LI-reactive para-pharyngeal cluster.  
4  
5  
6

11734 **Figure 8: FMRF-amide-LIR nervous system of *Diuronotus aspetos*.** Anterior is pointing left for **A-G)**  
8  
9  
1135 and **I-L)** and dorsal pointing at the top for **H)**. **A, B)** Schematic drawings of the FMRF-amide-LIR of  
10  
11  
1136 the anterior part of the specimen: nerves in magenta, nuclei in grey, and opposite ventral or dorsal  
12  
13  
14  
1137 nervous system in light grey. **A)** Dorsal view, **B)** ventral view. **C)** CLSM dorsal view of the maximum  
15  
16  
17  
1138 intensity projection (MIP) of the entire specimen. **D-L)** (Except H) CLSM sub-stack MIP of various  
18  
19  
2039 parts of the specimen. FMRF-amide-LIR in glow, and DAPI in cyan in all CLSM pictures. **D)** Dorsal  
21  
22  
1140 view of the whole neuropil. **E)** Ventral part of the brain. **F)** And **G)** different levels of the dorsal part  
23  
24  
25  
1141 of the neuropil. **H)** CLSM virtual transverse section of the anterior nerve ring. **I)** Ventro-anterior  
26  
27  
1142 part of the head. **J)** Ventral commissure of the anterior nerve ring. **K)** Ventral post-pharyngeal  
28  
29  
30  
1143 ganglia. **L)** ventro-posterior terminal part of the specimen. Anterior of the specimen on the left for  
31  
32  
33  
1144 **A-G)** and **I-L)** and dorsal on top for **H)**. **br**, brain; **egg**, egg; **fanr**, FMRF-amide-LI-reactive anterior  
34  
35  
1145 nerve ring; **fapn**, FMRF-amide-LI-reactive anterior perikarya of the ventro-lateral nerve cord; **fdpc**,  
36  
37  
38  
1146 FMRF-amide-LI-reactive dorso-posterior cluster of the brain; **flnc**, FMRF-amide-LI-reactive ventro-  
39  
40  
1147 lateral nerve cord; **flpb**, FMRF-amide-LI-reactive lateral perikarya of the brain; **fnp**, FMRF-amide-LI-  
41  
42  
1148 reactive neuropil; **fnpt**, FMRF-amide-LI-reactive nerve projection of the primary tube; **fpar**, FMRF-  
43  
44  
45  
1149 amide-LI-reactive dorso-median perikarya of the anterior nerve ring; **fpco**, FMRF-amide-LI-reactive  
46  
47  
48  
1150 posterior commissure; **fpp**, FMRF-amide-LI-reactive perikarya of the dorso-lateral anterior nerve  
49  
50  
51  
1151 projections; **fppg**, FMRF-amide-LI-reactive post-pharyngeal ganglion; **fspc**, FMRF-amide-LI-reactive  
52  
53  
1152 sub-pharyngeal commissure; **fvmn**, FMRF-amide-LI-reactive anterior ventro-median nerve; **fvnc**,  
54  
55  
56  
1153 FMRF-amide-LI-reactive anterior ventro-median nerve cluster; **fvpb**, FMRF-amide-LI-reactive  
57  
58  
59  
60  
61  
62  
63  
64  
65

1154 ventro-lateral perikarya of the brain; **fvpr**, FMRF-amide-LI-reactive ventral perikarya of the  
2  
3  
1155 anterior nerve ring; **ph**, pharynx.  
4  
5  
6

1156 **Figure 9: Schematic drawing of acetylated  $\alpha$ -tubulin-LIR, FMRF-amide-LIR and serotonin-LIR**  
8  
9  
1157 **nervous system of *Diuronotus aspetos***, showing the correspondences between the different  
10  
11  
12  
1158 nervous systems. Anterior pointing at the top. Acetylated  $\alpha$ -tubulin-LIR nervous system in blue,  
13  
14  
1159 FMRF-amide-LIR nervous in green, and serotonin-LIR nervous system in green. Cell nuclei in grey  
16  
17  
1160 and opposite nervous system in light grey. Legends in bold indicate structures showing-LIR for at  
18  
19  
1161 least two molecules tested. **A)** Dorsal, and **B)** ventral. **anr**, anterior nerve ring; **avmn**, anterior  
21  
22  
1162 ventro median nerve cord; **br**, brain; **cpn**, ciliated patch nerves; **danp**, dorso-median anterior  
23  
24  
1163 nerve projection; **dlnp**, dorso-lateral anterior nerve projections; **fdpc**, FMRF-amide-LI-reactive  
26  
27  
1164 postero-lateral brain cluster; **fvnc**, FMRF-amide-LI-reactive ventro-median nerve cluster; **hdn**,  
28  
29  
1165 head diagonal nerve; **hln**, head lateral nerve; **hdpn**, head dorso-posterior nerve; **hpdn**, head  
30  
31  
32  
1166 diagonal nerve; **np**, neuropile; **pgg**, post-pharyngeal ganglion; **ph**, pharynx; **spc**, sub-pharyngeal  
34  
35  
1167 commissure; **sppc**, serotonin-LI-reactive para-pharyngeal cluster; **vlnc**, ventro-lateral nerve cord.  
36  
37  
38

1168 **Figure 10: Ciliation of *Diuronotus aspetos***. Anterior pointing at the top for all figures. **A** and **B)**  
40  
41  
1169 drawings of the locomotory ciliation: **A)** dorsal view, **B)** ventral view. **C-K)** CLSM maximum  
42  
43  
1170 intensity projection (MIP) sub-stacks of the acetylated  $\alpha$ -tubulin-LIR. **C)** Ventral view of the whole  
45  
46  
1171 specimen showing the organization of the locomotory ciliation. **D)** Dorsal view of the whole  
48  
49  
1172 specimen showing parts of the locomotory ciliation and the position of the protonephridia. **E)** And  
50  
51  
1173 **F)**, dorsal head ciliation. **E)** Is more dorsal than **F)**. **G-I)** Ventral head and pharyngeal ciliation: **G)** is  
53  
54  
1174 more dorsal than **H)** which is more dorsal than **I)**. **J)** And **K)** details of, respectively, the anterior  
55  
56  
1175 and the posterior pairs of protonephridia. **acp**, anterior ciliated patch; **apn**, anterior proto-  
58  
59  
60  
61  
62  
63  
64  
65

1176 nephridia; **br**, brain; **c**, **c'**, cilia of the proto-nephridia; **hacc**, head dorso-anterior ciliated cells; **hlc**,  
 2  
 3  
 1177 head lateral ciliation; **hlcc**, head lateral ciliated cells; **hmcc**, head dorso-median ciliated cell; **hpcc**,  
 4  
 5  
 1178 head postero-lateral dorsal ciliated cell; **hvc**, head ventral ciliation; **hvlm**, head ventral lateral-most  
 6  
 7  
 8  
 1179 row of ciliated cells; **hvmm**, head ventral median-most row of ciliated cells; **hvpl**, head ventral  
 9  
 10  
 1180 para-lateral row of ciliated cells; **hvpm**, head ventral paramedian row of ciliated cells; **mz**, muzzle;  
 11  
 12  
 13  
 1181 **pc**, pharyngeal ciliation; **pcp**, posterior ciliated patch; **ph**, pharynx; **pk**, posterior pharyngeal  
 14  
 15  
 1182 kinocilium; **plcc**, pharyngeal lateral ciliated cells; **pmcc**, pharyngeal median ciliated cell; **ppn**,  
 16  
 17  
 18  
 1183 posterior proto-nephridia; **ss**, sensoria; **tc**, trunk ciliation; **tcc**, trunk ciliated cells; **tt**, testis.  
 19  
 20  
 21  
 22

## 1184 Figure abbreviations

23  
 24  
 25  
 1185 **acp**, anterior ciliated patch;  
 26  
 27  
 1186 **adpn**, anterior diagonal pharyngeal nerve;  
 28  
 29  
 1187 **ag**, adhesive gland;  
 30  
 31  
 1188 **agn**, adhesive gland nucleus;  
 32  
 33  
 1189 **ang**, anal ganglion;  
 34  
 35  
 1190 **anr**, anterior nerve ring;  
 36  
 37  
 1191 **apg**, anterior pharyngeal gland;  
 38  
 39  
 1192 **apn**, anterior proto-nephridia;  
 40  
 41  
 1193 **aps**, anterior pharyngeal sphincter;  
 42  
 43  
 1194 **avmn**, anterior ventro-median nerve;  
 44  
 45  
 1195 **avrc**, anterior ventro-median right pharyngeal canal;  
 46  
 47  
 48  
 49  
 1196 **bnr**, buccal nerve ring;  
 50  
 51  
 1197 **br**, brain;  
 52  
 53  
 1198 **c**, **c'**, cilia of the proto-nephridia;  
 54  
 55  
 1199 **cmag**, circular muscle of the adhesive gland;  
 56  
 57  
 1200 **cpn**, ciliated patch nerves;  
 58  
 59  
 60  
 61  
 62  
 63  
 64  
 65

1201 **danp**, dorso-median anterior nerve projection;  
2

1202 **dlim**: dorsal longitudinal muscle;  
4

1203 **dlnp**, dorso-lateral anterior nerve projections;  
6

1204 **dpc**, dorsal pharyngeal canal;  
8

1205 **dpcn**, dorso-anterior pharyngeal canal nerve;  
10

1206 **dpn**, dorsal pharyngeal nerve;  
12

1207 **dvlm**, dorsal projection of the ventral longitudinal muscle;  
14

1208 **dvm**, dorso-ventral muscle;  
16

1209 **egg**, egg;  
18

1210 **fanr**, FMRF-amide-LI-reactive anterior nerve ring;  
20

1211 **fapn**, FMRF-amide-LI-reactive anterior perikarya of the ventro-lateral nerve cord;  
22

1212 **fdpc**, FMRF-amide-LI-reactive dorso-posterior cluster of the brain;  
24

1213 **flnc**, FMRF-amide-LI-reactive ventro-lateral nerve cord;  
26

1214 **flpb**, FMRF-amide-LI-reactive lateral perikarya of the brain;  
28

1215 **fnp**, FMRF-amide-LI-reactive neuropil;  
30

1216 **fnpt**, FMRF-amide-LI-reactive nerve projection of the primary tube;  
32

1217 **fpar**, FMRF-amide-LI-reactive dorso-median perikarya of the anterior nerve ring;  
34

1218 **fpc**, FMRF-amide-LI-reactive posterior commissure;  
36

1219 **fpp**, FMRF-amide-LI-reactive perikarya of the dorso-lateral anterior nerve projections;  
38

1220 **fppg**, FMRF-amide-LI-reactive post-pharyngeal ganglion;  
40

1221 **fspc**, FMRF-amide-LI-reactive sub-pharyngeal commissure;  
42

1222 **fvmn**, FMRF-amide-LI-reactive anterior ventro-median nerve;  
44

1223 **fvnc**, FMRF-amide-LI-reactive anterior ventro-median nerve cluster;  
46

1224 **fvpb**, FMRF-amide-LI-reactive ventro-lateral perikarya of the brain;  
48

1225 **fvpr**, FMRF-amide-LI-reactive ventral perikarya of the anterior nerve ring;  
50

1226 **hacc**, head dorso-anterior ciliated cells;  
52

1227 **hdm**, head diagonal muscle;  
54

1228 **hdn**, head diagonal nerve;  
2

1229 **hdpn**, head dorso-posterior nerve;  
3  
4

1230 **hlc**, head lateral ciliation;  
5  
6

1231 **hlcc**, head lateral ciliated cells;  
7  
8

1232 **hm**, helicoidal muscles;  
9

1233 **hln**, head lateral nerve;  
11

1234 **hmcc**, head dorso-median ciliated cell;  
13

1235 **hpcc**, head postero-lateral dorsal ciliated cell;  
14  
15

1236 **hvc**, head ventral ciliation;  
16  
17

1237 **hvlm**, head ventral lateral-most row of ciliated cells;  
18  
19

1238 **hvmm**, head ventral median-most row of ciliated cells;  
20  
21

1239 **hvpl**, head ventral para-lateral row of ciliated cells;  
22  
23

1240 **hvpm**, head ventral paramedian row of ciliated cells;  
24  
25

1241 **int**, intestine;  
26  
27

1242 **lgcb**, lateral gland cell of the brain;  
28  
29

1243 **lplm**, lateral pharyngeal longitudinal muscle;  
30  
31

1244 **lpvc**, left posterior ventro-median canal;  
32  
33

1245 **lvlm**, lateral extension of the ventral longitudinal muscle;  
34  
35

1246 **mk**, mouth kinocilium;  
36  
37

1247 **mn**, myocyte nuclei;  
38  
39

1248 **mvlm**, medial projection of the ventral longitudinal muscle;  
40  
41

1249 **mz**, muzzle;  
42  
43

1250 **np**, neuropile;  
44  
45

1251 **nppt**, nerve projection of the primary tube;  
46  
47

1252 **ov**, ovary;  
48  
49

1253 **pac**, pre-anal commissure;  
50  
51

1254 **pc**, pharyngeal ciliation;  
52  
53

1255 **pcm**, pharyngeal circular muscle;  
2

1256 **pco**, posterior commissure;  
4

1257 **pcp**, posterior ciliated patch;  
6

1258 **pddm**, pharyngeal dorsal diagonal muscle;  
8

1259 **pdm**, posterior diagonal muscle;  
10

1260 **pdlm**, pharyngeal dorsal longitudinal muscle;  
12

1261 **pdvn**, pharyngeal dorso-ventral nerve;  
14

1262 **pgg**, post-pharyngeal ganglion;  
16

1263 **ph**, pharynx;  
18

1264 **pk**, posterior pharyngeal kinocilium;  
20

1265 **plcc**, pharyngeal lateral ciliated cells;  
22

1266 **plgn**, pharyngeal longitudinal gland nerve;  
24

1267 **plkn**, pharyngeal longitudinal kinocilium nerve;  
26

1268 **pmcc**, pharyngeal median ciliated cell;  
28

1269 **pmdn**, paramedian dorsal pharyngeal nerves;  
30

1270 **pnr**, pharyngeal nerve ring;  
32

1271 **ppc**, posterior pharyngeal cluster;  
34

1272 **ppn**, posterior proto-nephridia;  
36

1273 **pps**, posterior pharyngeal sphincter;  
38

1274 **pt**, primary tube;  
40

1275 **rpm**: radial pharyngeal muscles;  
42

1276 **rpvc**, right posterior ventro-median canal;  
44

1277 **sacn**, serotonin-LI-reactive anterior commissure of the neuropil;  
46

1278 **sanr**, serotonin-LI-reactive anterior nerve ring;  
48

1279 **scm**, semi-circular muscle;  
50

1280 **sdlp**, serotonin-LI-reactive dorso-lateral perikaryon;  
52

1281 **sdmp**, serotonin-LI-reactive dorso-median perikaryon;  
54

1282 **slbn**, serotonin-LI-reactive lateral brain nerve;  
2

1283 **slnc**, serotonin-LI-reactive ventro-lateral nerve cord;  
3  
4

1284 **spc**, sub-pharyngeal commissure;  
5  
6

1285 **slpn**, serotonin-LI-reactive lateral nerves of the posterior commissure of the neuropil;  
7  
8

1286 **spln**, serotonin-LI-reactive postero-lateral nerve node;  
9  
10

1287 **smbn**, serotonin-LI-reactive median-most brain nerve;  
11  
12

1288 **smcn**, serotonin-LI-reactive median commissure of the neuropil;  
13  
14

1289 **snp**, serotonin-LI-reactive neuropil;  
15  
16  
17

1290 **snpt**, serotonin-LI-reactive nerve projection of the primary tube;  
18  
19

1291 **spag**, serotonin-LI-reactive perikarya of the anal ganglion;  
20  
21

1292 **spbn**, serotonin-LI-reactive paramedian brain nerve;  
22  
23

1293 **spcn**, serotonin-LI-reactive posterior commissure of the neuropil;  
24  
25

1294 **spco**, serotonin-LI-reactive posterior commissure;  
26  
27

1295 **spog**, serotonin-LI-reactive perikarya of the post-pharyngeal ganglion;  
28  
29  
30

1296 **spp**, serotonin-LI-reactive neuropil patch;  
31  
32

1297 **sppg**, serotonin-LI-reactive para-pharyngeal cluster;  
33  
34

1298 **ss**, sensoria;  
35  
36

1299 **st**: secondary tube;  
37  
38

1300 **tc**, trunk ciliation;  
39  
40  
41

1301 **tcc**, trunk ciliated cells;  
42  
43

1302 **tdm**: tube diagonal muscle;  
44  
45

1303 **tt**, testis;  
46  
47

1304 **tvc**, trunk ventral commissure;  
48  
49

1305 **vllm**: ventro-lateral longitudinal muscle;  
50  
51

1306 **vlm**, ventral longitudinal muscle;  
52  
53  
54

1307 **vlpc**, ventro-lateral pharyngeal canal;  
55  
56

1308 **vlpg**, ventro-lateral pharyngeal ganglion;  
57  
58

59  
60  
61  
62  
63  
64  
65

1309 **vpn**, ventral pharyngeal nerve;

1310 **Table 1: sequences used for the phylogenetic reconstruction**

Species name	18S	28S	COI
<i>Arenotus strixinoi</i>	JQ798537.1	JQ798608.1	JQ798677.1
<i>Aspidiophorus kw654</i>	NB#####	NB#####	No
<i>Aspidiophorus ophiodermus</i>	JN185463.1	JN185510.1	JN185544.1
<i>Aspidiophorus paramediterraneus</i>	JQ798538.1	JQ798609.1	JQ798678.1
<i>Aspidiophorus polystictos</i> TK76	JQ798598.1	JQ798665.1	JQ798727.1
<i>Aspidiophorus polystictos</i> TK75	JQ798597.1	JQ798664.1	JQ798726.1
<i>Aspidiophorus</i> sp.3	JQ798559.1	JQ798629.1	JQ798694.1
<i>Aspidiophorus tentaculatus</i> TK120	JQ798553.1	JQ798625.1	JQ798690.1
<i>Aspidiophorus tentaculatus</i> TK228	JQ798591.1	JQ798659.1	JQ798721.1
<i>Aspidiophorus tetrachaetus</i>	JN185505.1	JN185540.1	JN185576.1
<i>Chaetonotus laroides</i>	JQ798580.1	No	JQ798712.1
<i>Chaetonotus</i> cf. <i>sphagnophilus</i>	JQ798604.1	JQ798671.1	JQ798733.1
<i>Chaetonotus</i> cf. <i>dispar</i>	JQ798561.1	JQ798631.1	JQ798696.1
<i>Chaetonotus</i> cf. <i>hystrix</i>	JQ798603.1	Q798670.1	JQ798732.1
<i>Chaetonotus</i> cf. <i>laroides</i> TK86	JQ798602.1	JQ798669.1	JQ798731.1
<i>Chaetonotus</i> cf. <i>maximus</i> TK186	JQ798574.1	JQ798646.1	JQ798706.1
<i>Chaetonotus heterocanthus</i> TK100	JQ798543.1	JQ798615.1	JQ798681.1
<i>Chaetonotus mariae</i>	JQ798558.1	JQ798628.1	No
<i>Chaetonotus neptuni</i> MT61	JQ798539.1	JQ798610.1	JQ798679.1
<i>Chaetonotus uncinus</i>	JQ798540.1	JQ798611.1	No
<i>Chaetonotus</i> cf. <i>novenarius</i>	JQ798566.1	JQ798636.1	JQ798699.1
<i>Dactylopodola mesotyphle</i>	JF357651.1	JF357699.1	JF432036.1
<i>Dasydytes papaveroi</i> TK157	JQ798571.1	JQ798640.1	JQ798703.1
<i>Diuronotus aspetos</i>	NB##### and	SRX1121926	SRX1121926

1  
2  
3  
4  
5  
6  
7  
8  
9  
10  
11  
12  
13  
14  
15  
16  
17  
18  
19  
20  
21  
22  
23  
24  
25  
26  
27  
28  
29  
30  
31  
32  
33  
34  
35  
36  
37  
38  
39  
40  
41  
42  
43  
44  
45  
46  
47  
48  
49  
50  
51  
52  
53  
54  
55  
56  
57  
58  
59  
60  
61  
62  
63  
64  
65

	SRX1121926		
<i>Draculiciteria tesellata</i> MT63	JN185457.1	JN185506.1	JN185541.1
<i>Draculiciteria tesellata</i> TK142	JN185470.1	JN185516.1	JN185549.1
<i>Halichaetonotus aculifer</i>	JQ798550.1	JQ798622.1	JQ798688.1
<i>Halichaetonotus euromarinus</i>	JQ798551.1	JQ798623.1	No
<i>Haltidytes squamosus</i>	JQ798567.1	JQ798637.1	No
<i>Heterolepidoderma macrops</i>	JN185469.1	JN185515.1	JN185548.1
<i>Heterolepidoderma</i> sp.2	JN185485.1	JQ798644.1	JN185563.1
<i>Heteroxenotrichula squamosa</i>	JQ798542.1	JQ798613.1	No
<i>Ichthyidium skandicum</i> TK182	JQ798573.1	JQ798645.1	JQ798705.1
<i>Ichthyidium squamigerum</i>	JQ798607.1	JQ798674.1	JQ798736.1
<i>Kijanebalola devestiva</i> TK240	KR822112.1	KR822117.1	KR822120.1
<i>Lepidochaetus brasilense</i> TK223	JN185495.1	JQ798658.1	JN185568.1
<i>Lepidochaetus zelinkai</i> TK94	JN185503.1	JN185538.1	JN185574.1
<i>Lepidodermella squamata</i> TK97	JN185504.1	JN185539.1	JN185575.1
<i>Macrodasys</i> sp.1	JF357654.1	JF357702.1	JF432040.1
<i>Megadasys</i> sp.1	JF357656.1	JF357704.1	JF432042.1
<i>Musellifer delamarei</i>	AM231775.1	No	No
<i>Musellifer reichardtii</i>	KF578503.1	No	No
<i>Neodasys chaetonotoideus</i>	JQ798535.1	No	JQ798675.1
<i>Neodasys uchidai</i>	JQ798536.1	No	JQ798676.1
<i>Neogossesea acanthocolla</i>	KR822114.1	KR822119.1	KR822121
<i>Neogossesea antennigera</i> TK232	KR822110.1	KR822115.1	No
<i>Ornamentula paraensis</i> TK147	JQ798562.1	JQ798632.1	JQ798697.1
<i>Polymerurus nodicaudus</i> TK165	JN185502.1	JN185537.1	JN185573.1
<i>Polymerurus rhomboides</i> TK217	JN185493.1	JN185533.1	JN185567.1
<i>Stylochaeta fusiformis</i>	JN185471.1	JN185517.1	JN185550.1
<i>Xenotrichula cf. intermedia</i>	JN185461.1	No	No

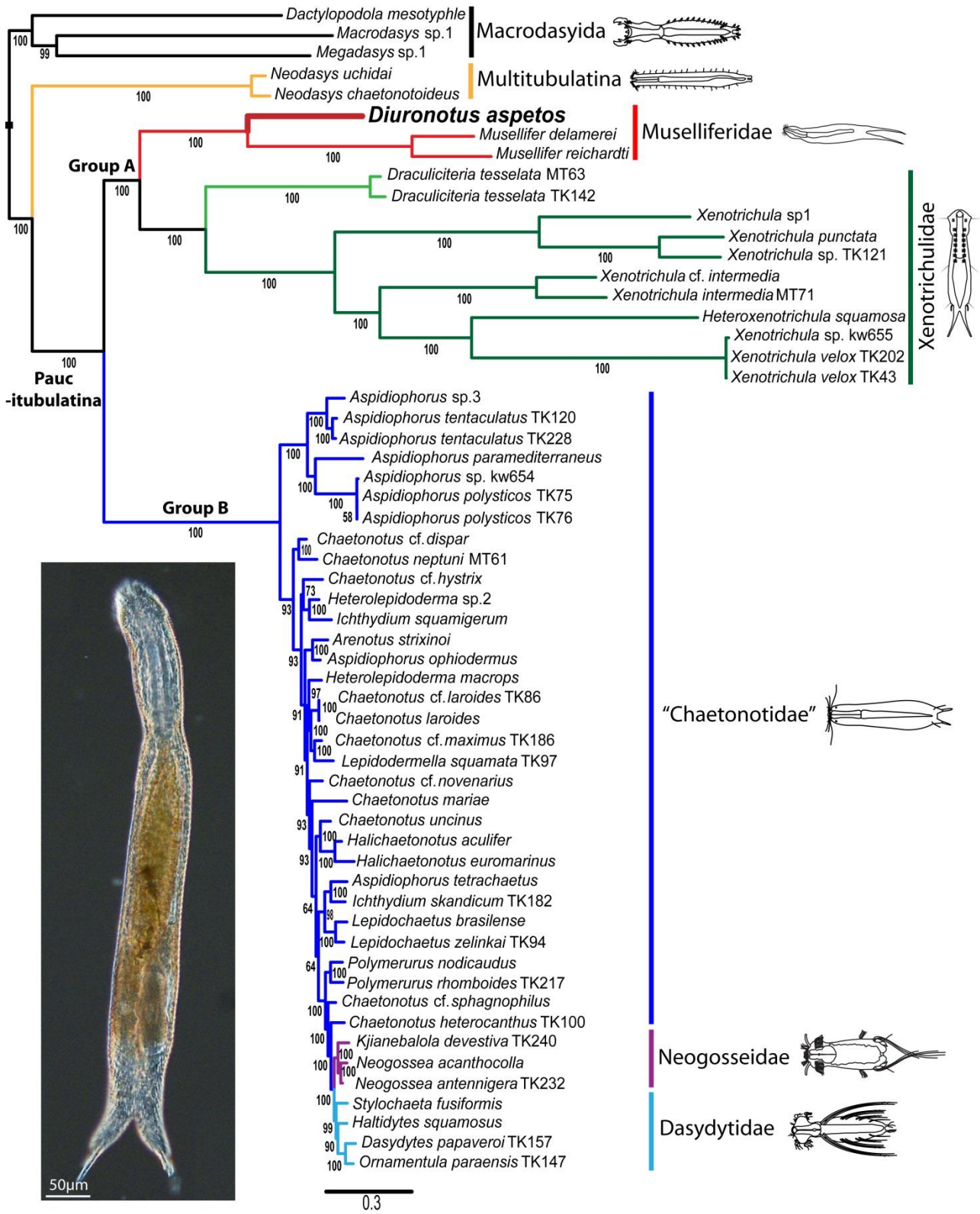
1  
2  
3  
4  
5  
6  
7  
8  
9  
10  
11  
12  
13  
14  
15  
16  
17  
18  
19  
20  
21  
22  
23  
24  
25  
26  
27  
28  
29  
30  
31  
32  
33  
34  
35  
36  
37  
38  
39  
40  
41  
42  
43  
44  
45  
46  
47  
48  
49  
50  
51  
52  
53  
54  
55  
56  
57  
58  
59  
60  
61  
62  
63  
64  
65

<i>Xenotrichula intermedia</i> MT71	JF357664.1	JF357712.1	No
<i>Xenotrichula</i> sp. kw655	NB#####	NB#####	No
<i>Xenotrichula punctata</i>	JN185464.1	JN185511.1	No
<i>Xenotrichula</i> sp. TK121	JF970234.1	No	No
<i>Xenotrichula</i> sp.1	JN185466.1	No	JN185545.1
<i>Xenotrichula velox</i> TK202	JN185488.1	JQ798652	No
<i>Xenotrichula velox</i> TK43	JN185499.1	No	No



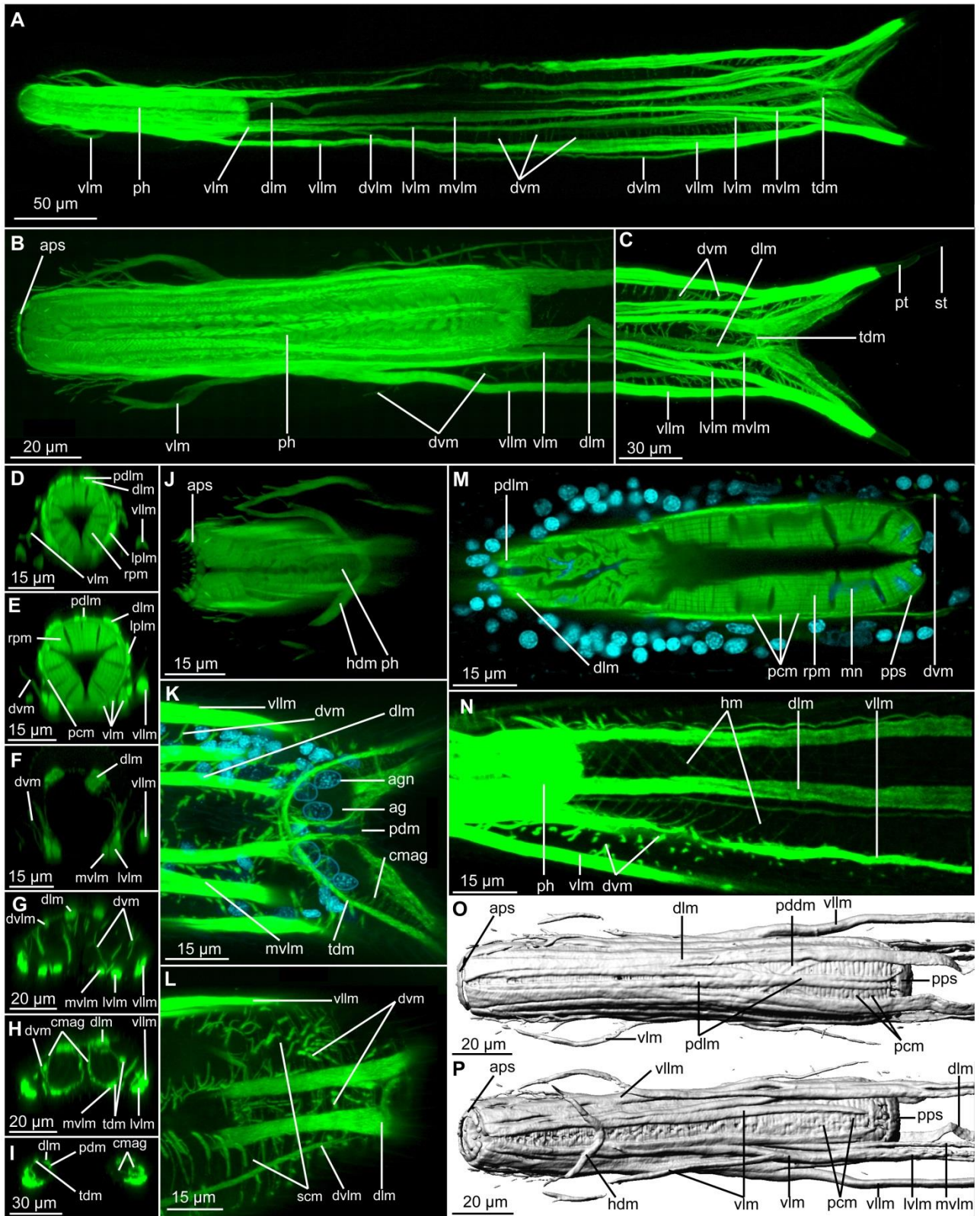
**Figure 1: Phylogenetic position of *Diuronotus aspetos* inferred from Bayesian analysis of 18S, 28S, and COI.** The analysis includes 58 taxa representing all available genera of Chaetonotida for molecular data on NCBI, and three Macrodasyida as outgroups. Numbers at the nodes represent posterior probabilities in percentages. The picture on the lower left corner is a light micrograph of a live specimen of *Diuronotus aspetos*.

Figure 1



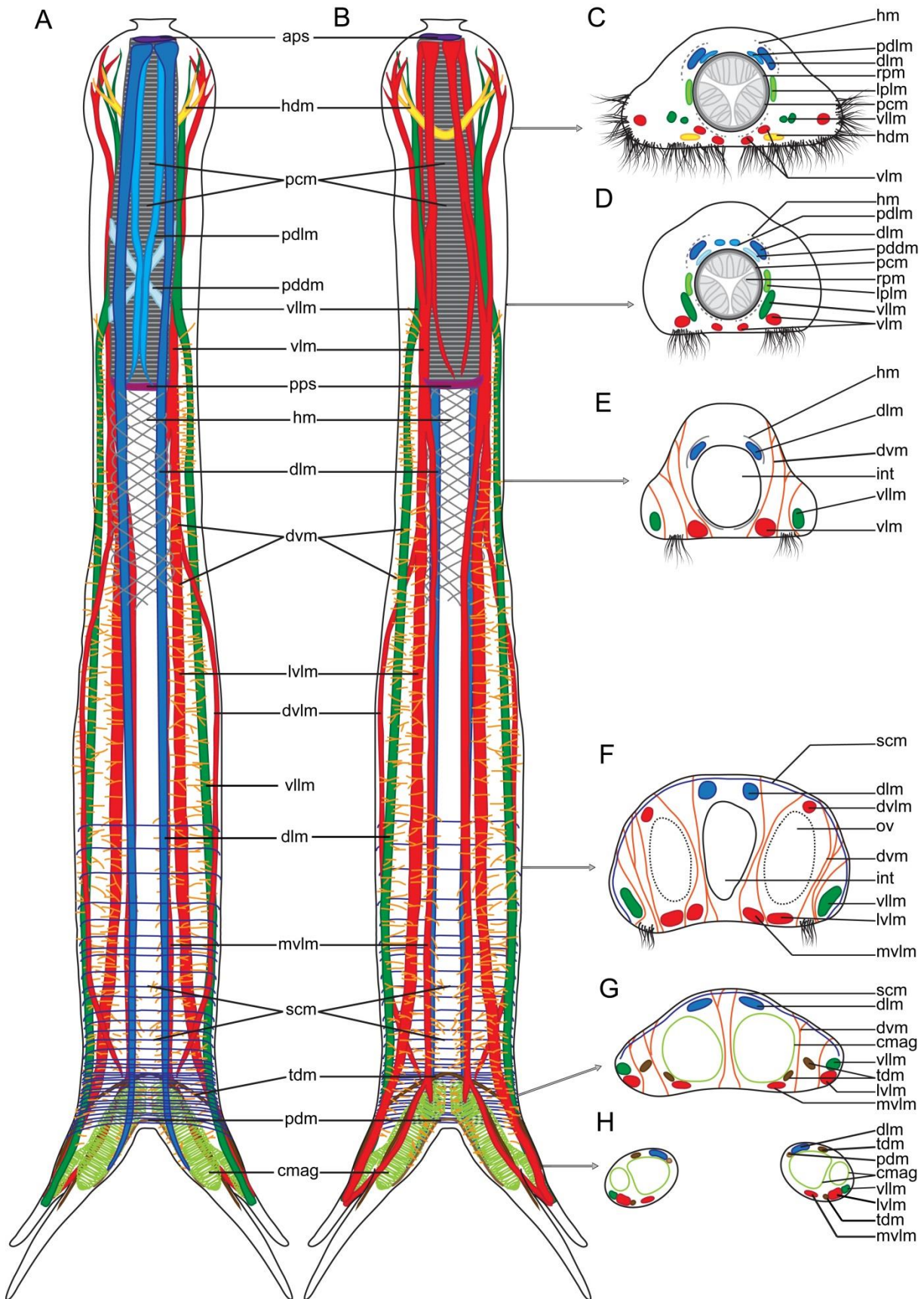
**Figure 2: CLSM of phalloidin stained muscle of *Diuronotus aspetos*.** Anterior of the specimen is pointing left for **A,B)** and **J-P)**, and dorsal is pointing at the top for **D-I)**. **A-N)** Muscles in green, nuclei in cyan **A)** Ventral view of the maximum intensity projection (MIP) of the whole specimen. **B)** Dorsal MIP of the pharynx. **C)** Dorsal MIP of the posterior specimen. **D- I)** CLSM virtual transverse section of various part of the specimen: **D)** head, **E)** posterior part of the pharynx, **F)** anterior of the trunk, **G)** posterior of the trunk, **H)** post-anal region of the trunk, **I)** and furca before bifurcation of the tubes. **J)** Dorsal MIP of a sub-stack showing details on the head musculature. **K)** Dorsal MIP of a sub-stack showing details of the furca separation. **L)** Ventral MIP of a sub-stack showing details of the semicircular musculature. **M)** Single section showing details of the inner pharynx. **N)** Dorsal MIP of a substack showing details of the helicoidal musculature. **O** And **P)**, isosurface reconstruction of the pharynx. **O)** Dorsal view, **P)** ventral view. **ag**, adhesive gland; **agn**, adhesive gland nucleus; **aps**, anterior pharyngeal sphincter; **cmag**, circular muscle of the adhesive gland; **dIm**, dorsal longitudinal muscle; **dvIm**, dorsal projection of the ventral longitudinal muscle; **dvm**, dorso-ventral muscle; **hdm**, head diagonal muscle; **hm**, helicoidal muscles; **lplm**, lateral pharyngeal longitudinal muscle; **lvIm**, Lateral extension of the ventral longitudinal muscle; **mn**, myocyte nuclei; **mvIm**, medial projection of the ventral longitudinal muscle; **pcm**, pharyngeal circular muscle; **pddm**, pharyngeal dorsal diagonal muscle; **pdm**, posterior diagonal muscle; **pdlm**, pharyngeal dorsal longitudinal muscle; **ph**, pharynx; **pps**, posterior pharyngeal sphincter; **pt**, primary tube; **rpm**, radial pharyngeal muscles; **scm**, semi-circular muscle; **st**, secondary tube; **tdm**, tube diagonal muscle; **vIm**, ventral longitudinal muscle; **vllm**, ventro-lateral longitudinal muscle; **vIm**, ventral longitudinal muscle.

Figure 2



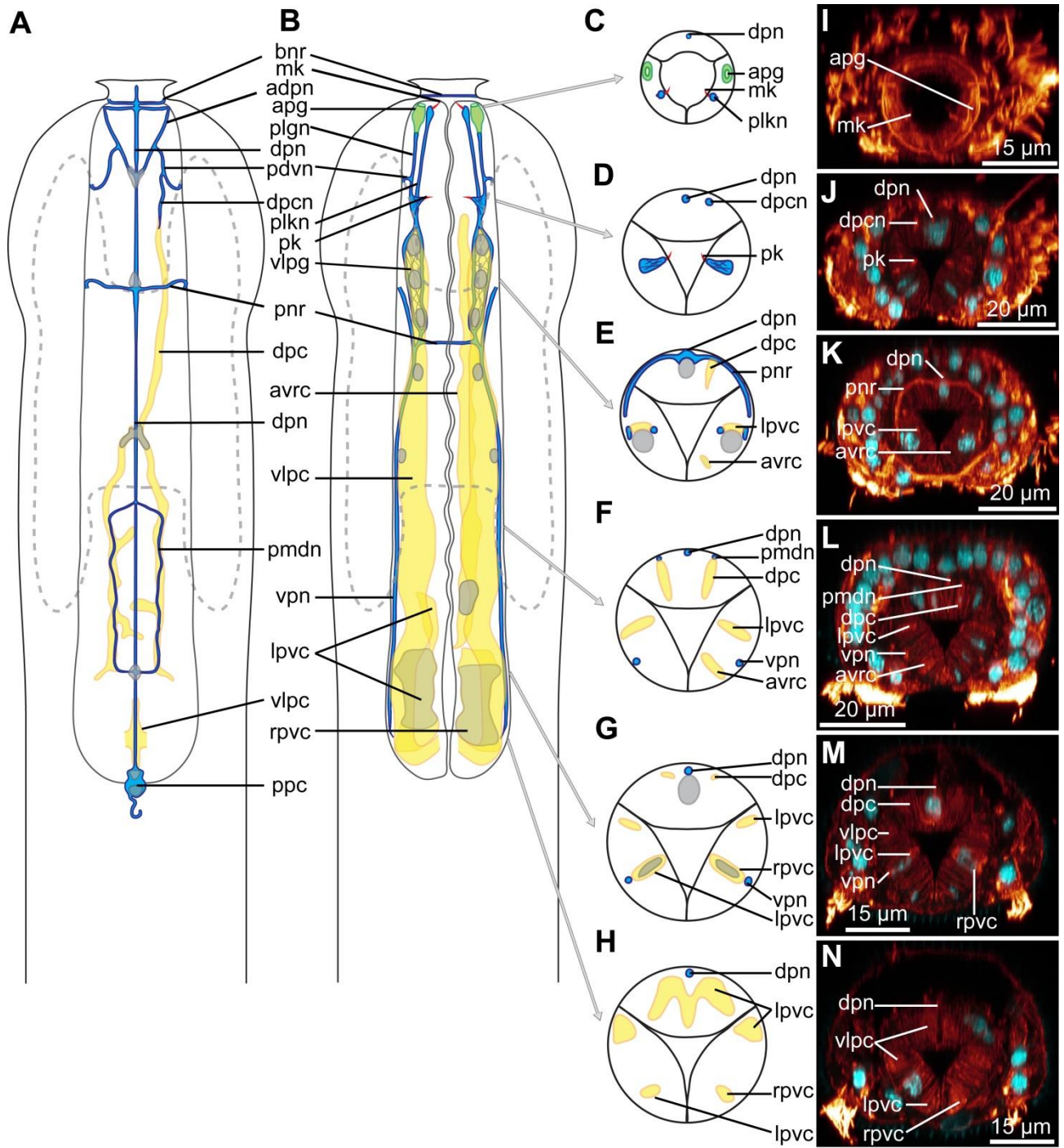
**Figure 3: Schematic drawings of the musculature of *Diuronotus aspetos*.** Anterior is pointing at the top for **A)** and **B)**, dorsal is pointing at the top for **C-H)**. **A)** Ventral view of the musculature, **B)** dorsal view of the musculature, **C-H)** cross section of the specimen **C)** in the head, **D)** posterior part of the pharynx, **E)** anterior of the trunk, **F)** posterior of the trunk, **G)** post-anal region of the trunk, **H)** and in the furca before bifurcation of the tubes. Note that in **C)** and **D)**, the helicoidal pharyngeal musculature is represented in dash lines due to the uncertainty of its presence, and it is not drawn in **A)** and **B)**. **aps**, anterior pharyngeal sphincter; **cmag**, circular muscle of the adhesive gland; **dlim**, dorsal longitudinal muscle; **dvlm**, dorsal projection of the ventral longitudinal muscle; **dvm**, dorso-ventral muscle; **hdm**, head diagonal muscle; **hm**, helicoidal muscle; **int**: intestine; **lplm**, lateral pharyngeal longitudinal muscle; **lvlm**, Lateral extension of the ventral longitudinal muscle; **mvlm**, medial projection of the ventral longitudinal muscle; **ov**, ovary; **pcm**, pharyngeal circular muscle; **pdm**, posterior diagonal muscle; **pddm**, pharyngeal dorsal diagonal muscle; **pdlm**, pharyngeal dorsal longitudinal muscle; **pps**, posterior pharyngeal sphincter; **rpm**, radial pharyngeal muscles; **scm**, semi-circular muscle; **tdm**, tube diagonal muscle; **vllm**, ventro lateral longitudinal muscle; **vlm**, ventral longitudinal muscle.

Figure 3



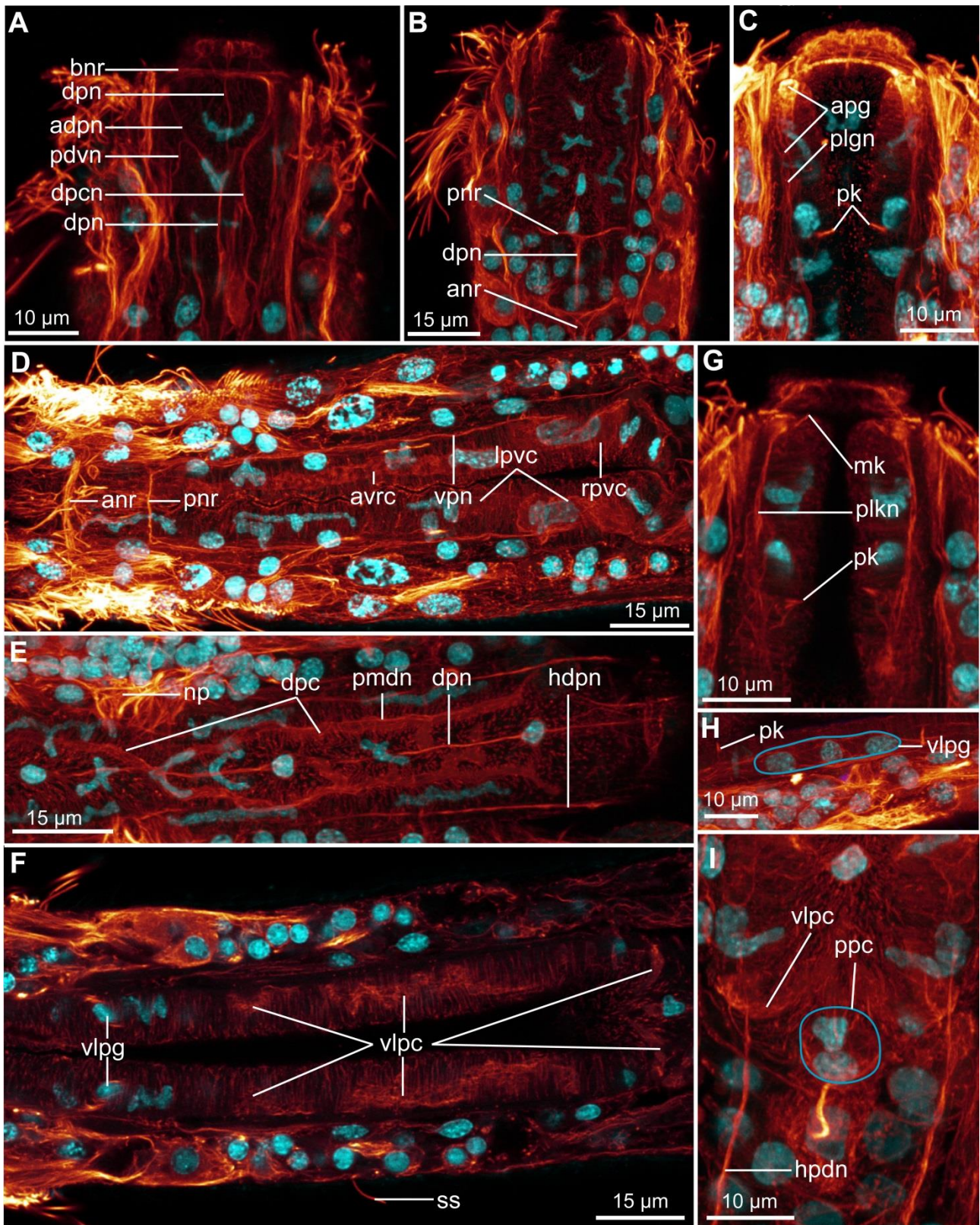
**Figure 4: Pharyngeal nervous system and canal system of *Diuronotus aspetos*. A,B)** Anterior is pointing at the top; **C-N** dorsal is pointing at the top. **A-H)** Schematic drawings with nerves in blue and pharyngeal system in yellow, nuclei in grey, glands in green and cilia in red. **A)** Dorsal section of the pharynx. **B)** Ventral section of the pharynx. **C-H)** Successive transverse sections of the pharynx from anterior to posterior. **I-N)** CLSM virtual transverse sections at the same levels as C-H). Acetylated  $\alpha$ -tubulin-LIR in glow and DAPI in cyan. **adpn**, anterior diagonal pharyngeal nerve; **apg**, anterior pharyngeal gland; **avrc**, anterior ventro-median right pharyngeal canal; **bnr**, buccal nerve ring; **dpc**, dorsal pharyngeal canal; **dpcn**, dorso-anterior pharyngeal canal nerve; **dpn**, dorsal pharyngeal nerve; **lpvc**, left posterior ventro-median canal; **mk**, mouth kinocilium; **pdivn**, pharyngeal dorso-ventral nerve; **pk**, posterior pharyngeal kinocilium; **plgn**, pharyngeal longitudinal gland nerve; **plkn**, pharyngeal longitudinal kinocilium nerve; **pmdn**, paramedian dorsal pharyngeal nerves; **pnr**, pharyngeal nerve ring; **ppc**, posterior pharyngeal cluster; **rpvc**, right posterior ventro-median canal; **vlpc**, ventro-lateral pharyngeal canal; **vlpq**, ventro-lateral pharyngeal ganglion; **vpn**, ventral pharyngeal nerve.

**Figure 4**



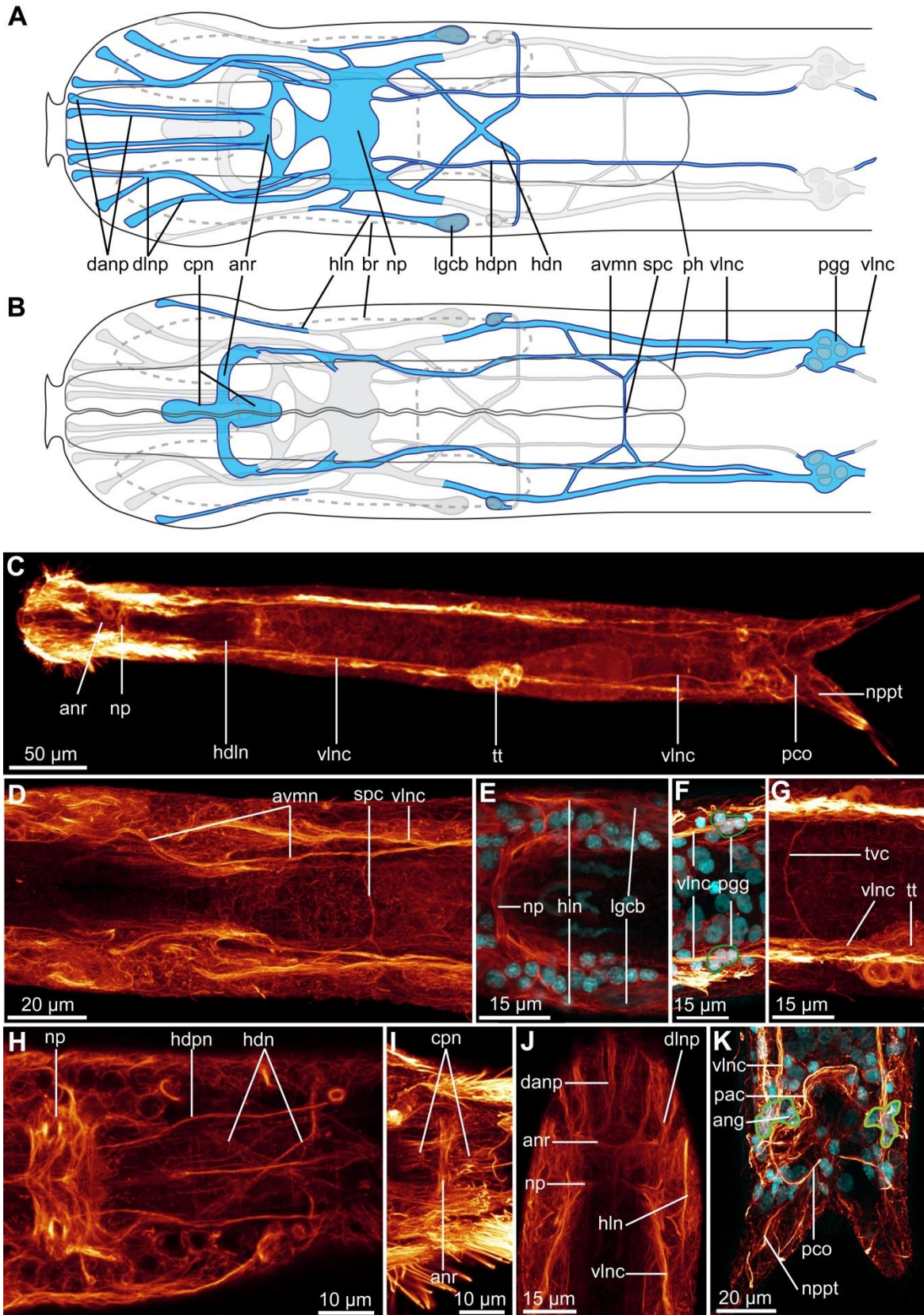
**Figure 5: CLSM of the pharyngeal nervous system and canal system of *Diuronotus aspetos*. A-C,G,I) anterior is pointing at the top. D-F,H) anterior pointing left. CLSM maximum intensity projection of sub-stacks. Acetylated  $\alpha$ -tubulin-LIR in glow, DAPI in cyan. A) Dorso-anterior section of the pharynx. B) Dorso-anterior section of the pharynx, more ventral than B). C) Ventro-anterior section of the pharynx. D) Ventro-posterior section of the pharynx. E) Dorso-posterior section of the pharynx. F) Medio-posterior portion of the pharynx. G) Medio-anterior section of the pharynx. H) Details of the ventro-lateral pharyngeal ganglion. I) Details of the posterior pharyngeal ganglion. **adpn**, anterior diagonal pharyngeal nerve; **anr**, anterior nerve ring; **apg**, anterior pharyngeal gland; **avrc**, anterior ventro-median right pharyngeal canal; **bnr**, buccal nerve ring; **dpc**, dorsal pharyngeal canal; **dpcn**, dorso-anterior pharyngeal canal nerve; **dpn**, dorsal pharyngeal nerve; **hdpn**, head dorso-posterior nerve; **lpvc**, left posterior ventro-median canal; **mk**, mouth kinocilium; **np**, neuropile; **pdvn**, pharyngeal dorso-ventral nerve; **pk**, posterior pharyngeal kinocilium; **plgn**, pharyngeal longitudinal gland nerve; **plkn**, pharyngeal longitudinal kinocilium nerve; **pmdn**, paramedian dorsal pharyngeal nerves; **pnr**, pharyngeal nerve ring; **ppc**, posterior pharyngeal cluster; **rpvc**, right posterior ventro-median canal; **ss**, sensoria; **vlpg**, ventro-lateral pharyngeal ganglion; **vlpc**, ventro-lateral pharyngeal canal; **vpn**, ventral pharyngeal nerve.**

Figure 5



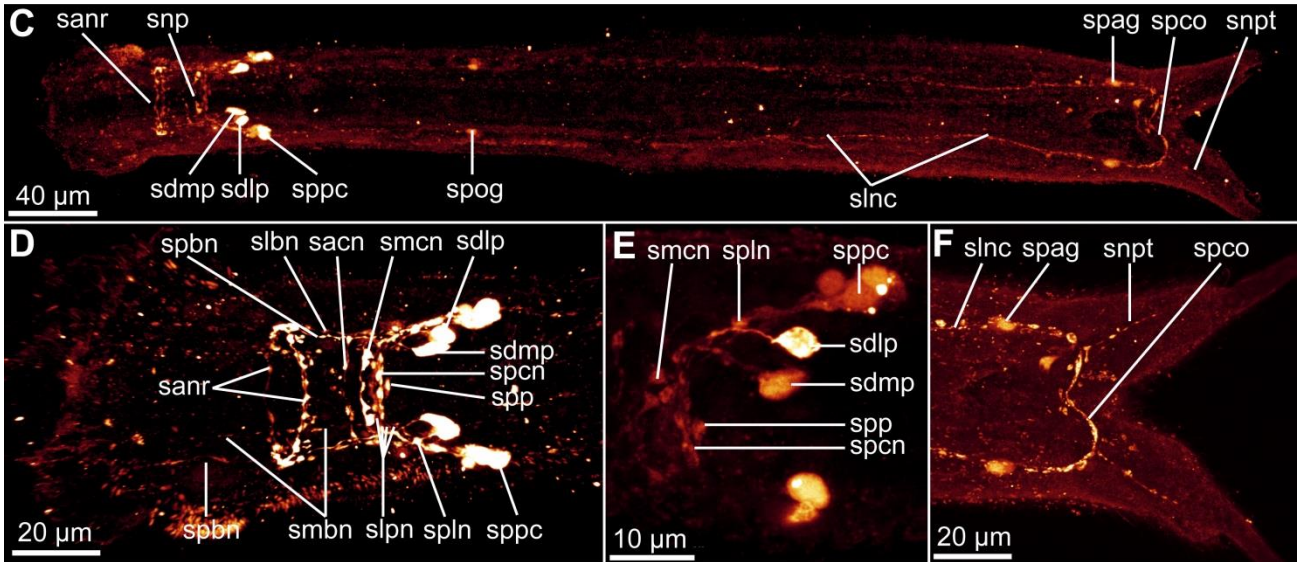
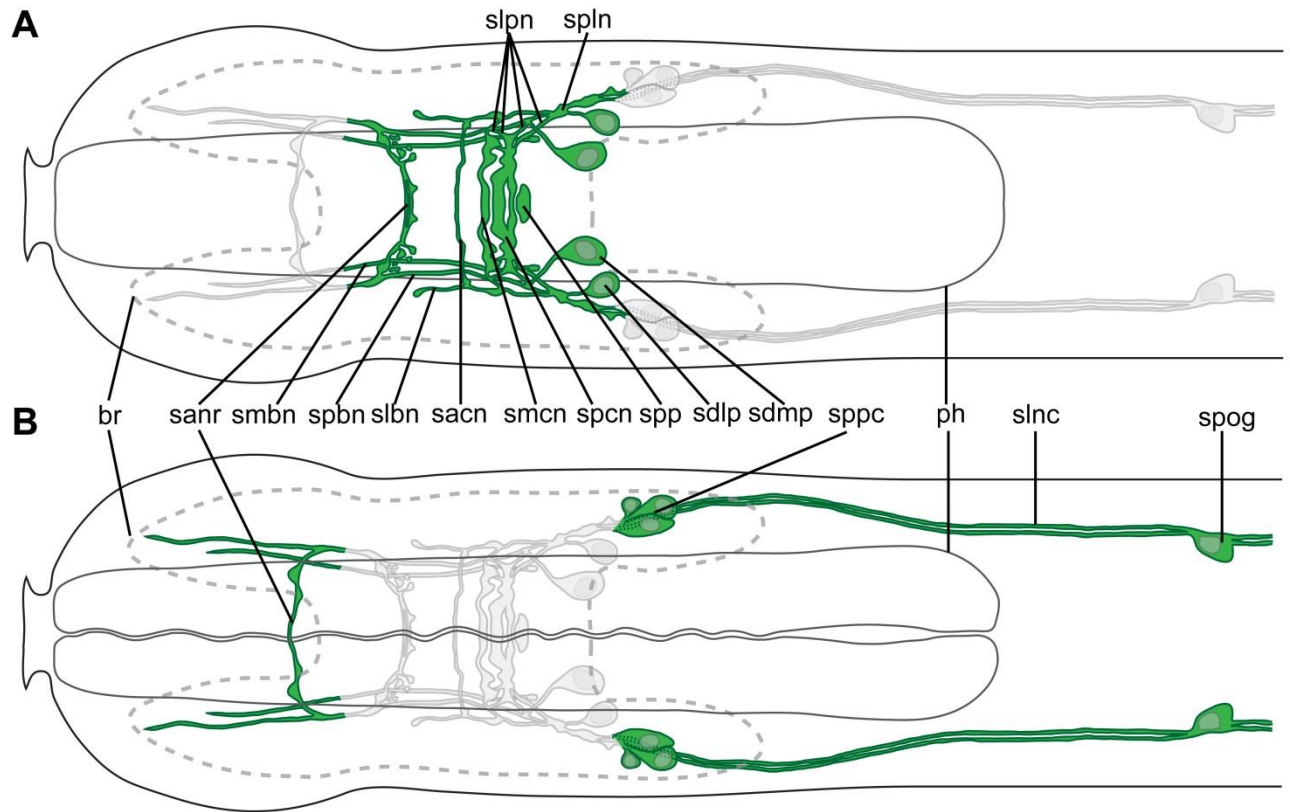
**Figure 6: Drawing and CLSM of the acetylated  $\alpha$ -tubulin-LIR nervous system of *Diuronotus aspetos*.** Anterior pointing left for **A-I**), and pointing at the top for **J**) and **K**). **A, B**) Schematic drawings of the  $\alpha$ -tubulin-LIR of the anterior part of the specimen: nerves in blue, nuclei in grey, and opposite ventral or dorsal nervous system in light grey **A**) dorsal **B**) ventral. **C**) CLSM ventral view of the maximum intensity projection (MIP) of the entire specimen. **D-K**) CLSM MIP sub-stacks of various parts of the specimen. Acetylated  $\alpha$ -tubulin-LIR in glow, and DAPI in cyan in all CLSM pictures. **D**) Ventro-anterior nervous system. **E**) Neuropil side **F**) Ventral, post pharyngeal ganglion. **G**) Ventral, trunk commissure. **H**) Dorso-posterior part of the head **I**) ventro-anterior part of the head **J**) Dorso-anterior part of the head. **K**) Ventro posterior terminal part of the specimen. **ang**, anal ganglion; **anr**, anterior nerve ring; **avmn**, anterior ventro-median nerve; **br**, brain; **cpn**, ciliated patch nerves; **dannp**, dorso-median anterior nerve projection; **dlnp**, dorso-lateral anterior nerve projections; **hdpn**, head dorso-posterior nerve; **hdn**, head diagonal nerve; **hln**, head lateral nerve; **lgcb**, lateral gland cell of the brain; **np**, neuropile; **nppt**, nerve projection of the primary tube; **pac**, pre-anal commissure; **pco**, posterior commissure; **pgg**, post-pharyngeal ganglion; **ph**, pharynx; **spc**, sub-pharyngeal commissure; **tt**, testis; **tvc**, trunk ventral commissure; **vlnc**, ventro-lateral nerve cord.

Figure 6



**Figure 7: serotonin-LIR nervous system of *Diuronotus aspetos*.** The anterior is pointing left for all figures. **A, B)** Schematic drawings of the serotonin-LIR of the anterior part of the specimen: nerves and perikarya in green, nuclei in grey, and opposite ventral or dorsal nervous system in light grey. **A)** Dorsal view, **B)** ventral view. **C-F)** CLSM images with serotonin-LIR in glow. **C)** CLSM maximum intensity projection (MIP) of the entire specimen. **D)** Dorsal MIP of the brain **E)** CLSM sub-stack MPI showing details of the brain perikarya **F)** CLSM sub-stack MPI of the ventro-posterior terminal part of the specimen. **br**, brain; **ph**, pharynx; **sacn**, serotonin-LI-reactive anterior commissure of the neuropil; **sanr**, serotonin-LI-reactive anterior nerve ring; **sdlp**, serotonin-LI-reactive dorso-lateral perikaryon; **sdmp**, serotonin-LI-reactive dorso-median perikaryon; **slbn**, serotonin-LI-reactive lateral brain nerve; **slnc**, serotonin-LI-reactive ventro-lateral nerve cord; **slpn**, serotonin-LI-reactive lateral nerves of the posterior commissure of the neuropil; **spln**, serotonin-LI-reactive postero-lateral nerve node; **smbn**, serotonin-LI-reactive median-most brain nerve; **smcn**, serotonin-LI-reactive median commissure of the neuropil; **snp**, serotonin-LI-reactive neuropil; **snpt**, serotonin-LI-reactive nerve projection of the primary tube; **spag**, serotonin-LI-reactive perikarya of the anal ganglion; **spbn**, serotonin-LI-reactive paramedian brain nerve; **spcn**, serotonin-LI-reactive posterior commissure of the neuropil; **spco**, serotonin-LI-reactive posterior commissure; **spog**, serotonin-LI-reactive perikarya of the post-pharyngeal ganglion; **spp**, serotonin-LI-reactive neuropil patch; **sppg**, serotonin-LI-reactive para-pharyngeal cluster.

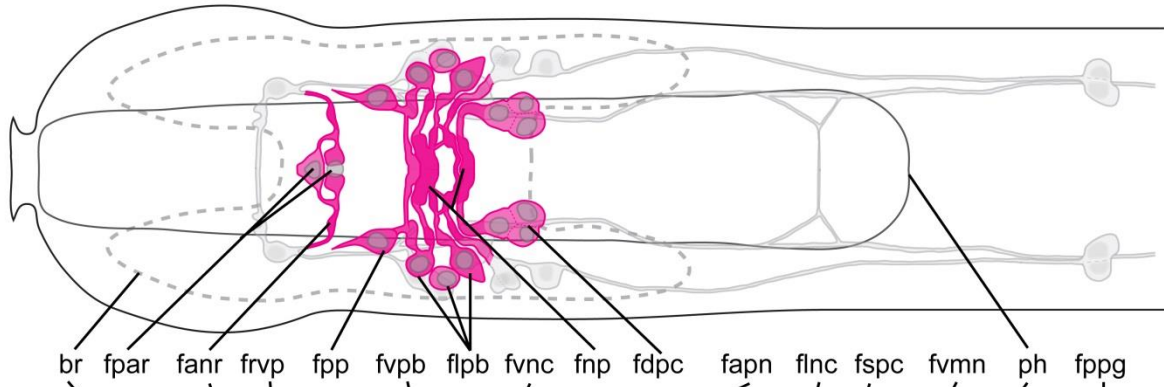
**Figure 7**



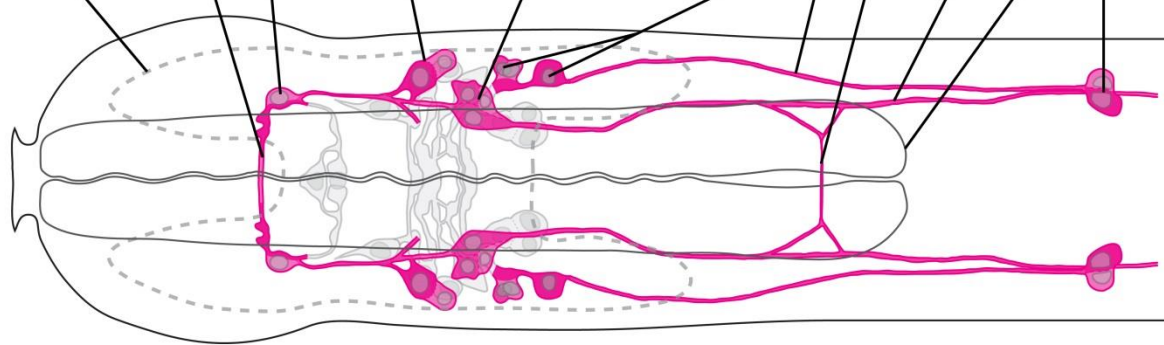
**Figure 8: FMRF-amide-LIR nervous system of *Diuronotus aspetos*.** Anterior is pointing left for **A-G)** and **I-L)** and dorsal pointing at the top for **H)**. **A, B)** Schematic drawings of the FMRF-amide-LIR of the anterior part of the specimen: nerves in magenta, nuclei in grey, and opposite ventral or dorsal nervous system in light grey. **A)** Dorsal view, **B)** ventral view. **C)** CLSM dorsal view of the maximum intensity projection (MIP) of the entire specimen. **D-L)** (Except H) CLSM sub-stack MIP of various parts of the specimen. FMRF-amide-LIR in glow, and DAPI in cyan in all CLSM pictures. **D)** Dorsal view of the whole neuropil. **E)** Ventral part of the brain. **F)** And **G)** different levels of the dorsal part of the neuropil. **H)** CLSM virtual transverse section of the anterior nerve ring. **I)** Ventro-anterior part of the head. **J)** Ventral commissure of the anterior nerve ring. **K)** Ventral post-pharyngeal ganglia. **L)** ventro-posterior terminal part of the specimen. Anterior of the specimen on the left for **A-G)** and **I-L)** and dorsal on top for **H)**. **br**, brain; **egg**, egg; **fanr**, FMRF-amide-LI-reactive anterior nerve ring; **fapn**, FMRF-amide-LI-reactive anterior perikarya of the ventro-lateral nerve cord; **fdpc**, FMRF-amide-LI-reactive dorso-posterior cluster of the brain; **flnc**, FMRF-amide-LI-reactive ventro-lateral nerve cord; **flpb**, FMRF-amide-LI-reactive lateral perikarya of the brain; **fnp**, FMRF-amide-LI-reactive neuropil; **fnpt**, FMRF-amide-LI-reactive nerve projection of the primary tube; **fpar**, FMRF-amide-LI-reactive dorso-median perikarya of the anterior nerve ring; **fpc**, FMRF-amide-LI-reactive posterior commissure; **fpp**, FMRF-amide-LI-reactive perikarya of the dorso-lateral anterior nerve projections; **fppg**, FMRF-amide-LI-reactive post-pharyngeal ganglion; **fspc**, FMRF-amide-LI-reactive sub-pharyngeal commissure; **fvmn**, FMRF-amide-LI-reactive anterior ventro-median nerve; **fvnc**, FMRF-amide-LI-reactive anterior ventro-median nerve cluster; **fvpb**, FMRF-amide-LI-reactive ventro-lateral perikarya of the brain; **fvpr**, FMRF-amide-LI-reactive ventral perikarya of the anterior nerve ring; **ph**, pharynx.

Figure 8

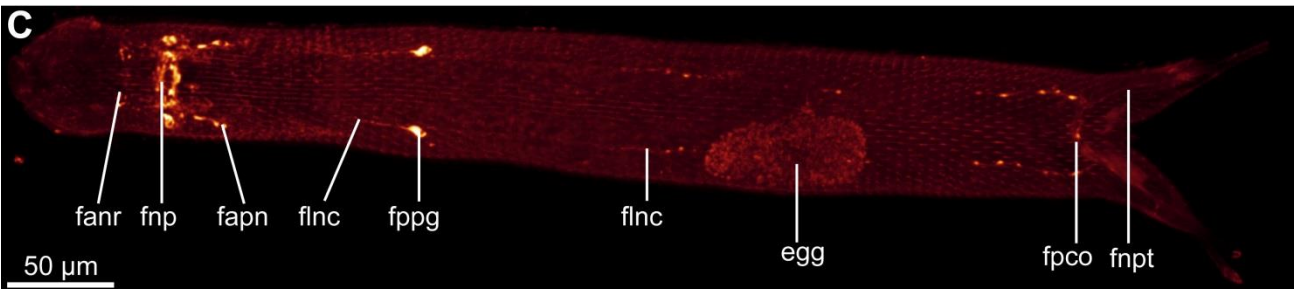
A



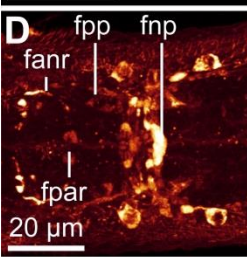
B



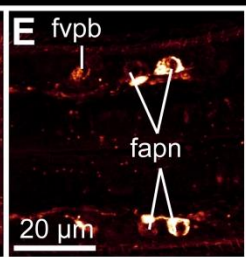
C



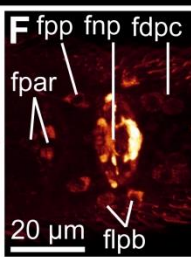
D



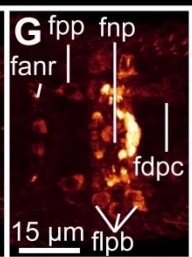
E



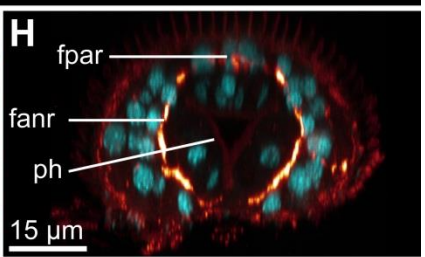
F



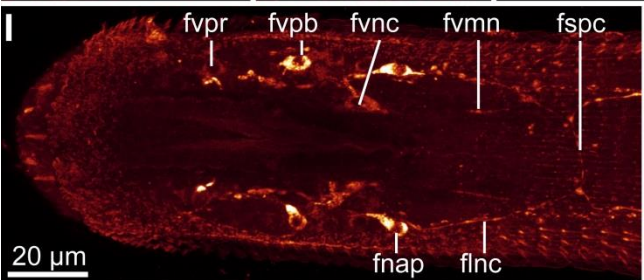
G



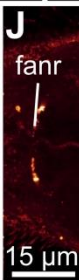
H



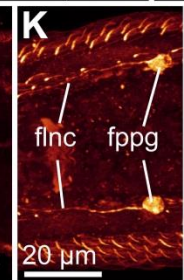
I



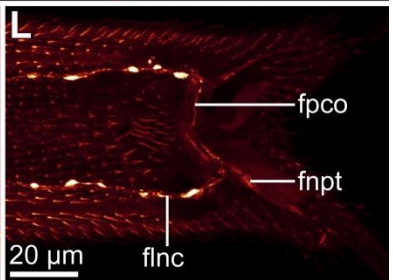
J



K



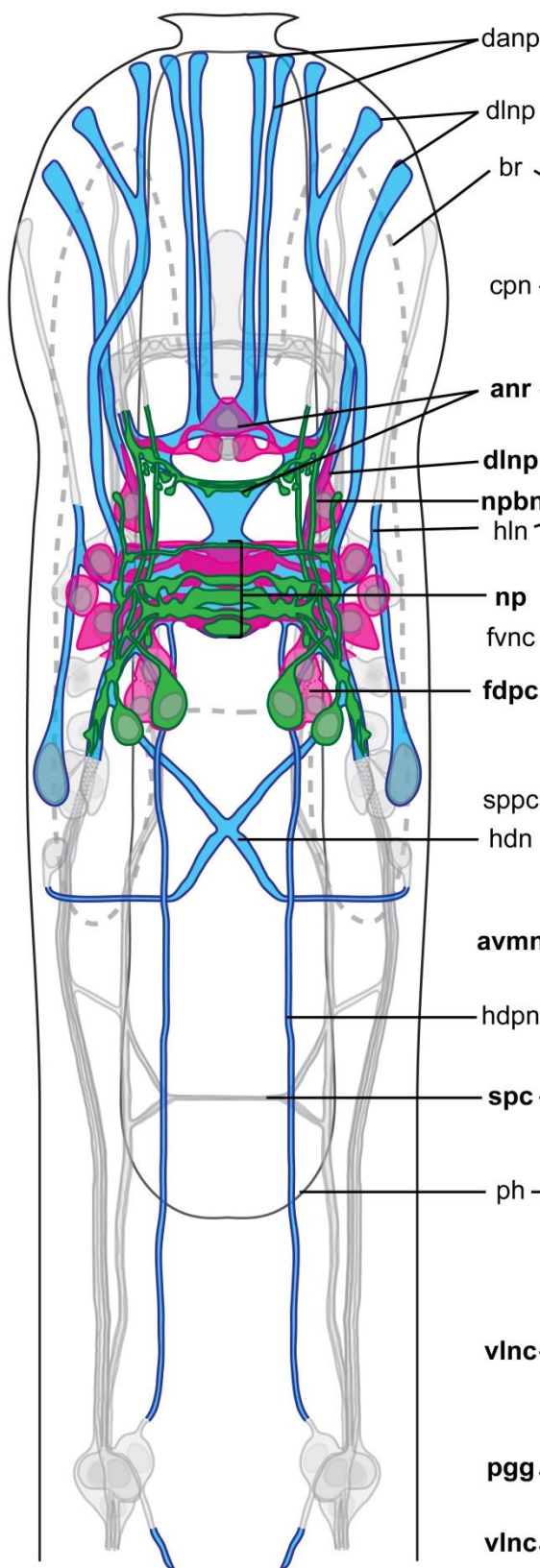
L



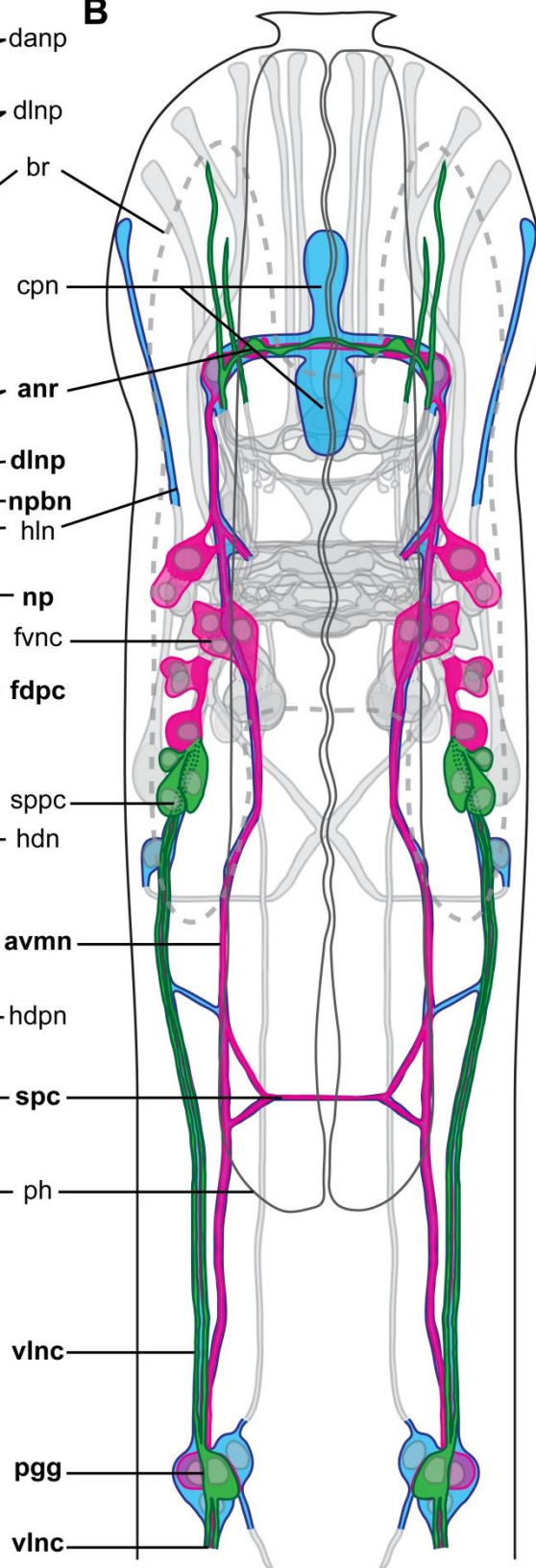
**Figure 9: Schematic drawing of acetylated  $\alpha$ -tubulin-LIR, FMRF-amide-LIR and serotonin-LIR nervous system of *Diuronotus aspetos*, showing the correspondences between the different nervous systems. Anterior pointing at the top. Acetylated  $\alpha$ -tubulin-LIR nervous system in blue, FMRF-amide-LIR nervous in green, and serotonin-LIR nervous system in green. Cell nuclei in grey and opposite nervous system in light grey. Legends in bold indicate structures showing-LIR for at least two molecules tested. **A)** Dorsal, and **B)** ventral. **anr**, anterior nerve ring; **avmn**, anterior ventro median nerve cord; **br**, brain; **cpn**, ciliated patch nerves; **dantp**, dorso-median anterior nerve projection; **dlap**, dorso-lateral anterior nerve projections; **fdpc**, FMRF-amide-LI-reactive postero-lateral brain cluster; **fvnc**, FMRF-amide-LI-reactive ventro-median nerve cluster; **hdn**, head diagonal nerve; **hln**, head lateral nerve; **hdpn**, head dorso-posterior nerve; **hpdn**, head diagonal nerve; **np**, neuropile; **pgg**, post-pharyngeal ganglion; **ph**, pharynx; **spc**, sub-pharyngeal commissure; **sppc**, serotonin-LI-reactive para-pharyngeal cluster; **vlnc**, ventro-lateral nerve cord.**

Figure 9

**A**



**B**



**Figure 10: Ciliation of *Diuronotus aspetos*.** Anterior pointing at the top for all figures. **A** and **B**) drawings of the locomotory ciliation: **A**) dorsal view, **B**) ventral view. **C-K**) CLSM maximum intensity projection (MIP) sub-stacks of the acetylated  $\alpha$ -tubulin-LIR. **C**) Ventral view of the whole specimen showing the organization of the locomotory ciliation. **D**) Dorsal view of the whole specimen showing parts of the locomotory ciliation and the position of the protonephridia. **E**) and **F**), dorsal head ciliation. **E**) is more dorsal than **F**). **G-I**) Ventral head and pharyngeal ciliation: **G**) is more dorsal than **H**) which is more dorsal than **I**). **J**) and **K**) details of, respectively, the anterior and the posterior pairs of protonephridia. **acp**, anterior ciliated patch; **apn**, anterior protonephridia; **br**, brain; **c**, **c'**, cilia of the proto-nephridia; **hacc**, head dorso-anterior ciliated cells; **hlc**, head lateral ciliation; **hlcc**, head lateral ciliated cells; **hmcc**, head dorso-median ciliated cell; **hpcc**, head postero-lateral dorsal ciliated cell; **hvc**, head ventral ciliation; **hvlm**, head ventral lateral-most row of ciliated cells; **hvmm**, head ventral median-most row of ciliated cells; **hvpl**, head ventral para-lateral row of ciliated cells; **hvpm**, head ventral paramedian row of ciliated cells; **mz**, muzzle; **pc**, pharyngeal ciliation; **pcp**, posterior ciliated patch; **ph**, pharynx; **pk**, posterior pharyngeal kinocilium; **plcc**, pharyngeal lateral ciliated cells; **pmcc**, pharyngeal median ciliated cell; **ppn**, posterior proto-nephridia; **ss**, sensoria; **tc**, trunk ciliation; **tcc**, trunk ciliated cells; **tt**, testis.

**Figure 10**

